

24.8.78

Vehicle Traffic Monitoring

by

Kamran Eshraghian, B.Tech.

A Thesis Submitted to the Department of
Electrical Engineering The University of
Adelaide for the Degree of MASTER
of ENGINEERING SCIENCE.

THE UNIVERSITY OF ADELAIDE

This thesis embodies the results of supervised project work which made up two-thirds of the work for the degree.

September, 1977

CONTENTS

Summary	v
List of Principal Symbols	ix
Chapter 1 TRAFFIC CONTROL	1
1.1 Introduction	1
1.2 Traffic Control Systems	2
1.3 Fundamentals of Traffic Movement on Freeways	4
1.4 Traffic Models	7
1.5 Identification	9
1.6 System Implementation	9
Chapter 2 REVIEW OF VEHICLE SENSORS	12
2.1 Introduction	12
2.2 Behaviour of a Coil in Proximity of a Conducting Surface	16
2.3 Inductive Loop Detectors	19
2.3.1 The Bridge-Balance Detector	22
2.3.2 Self-Tuning Loop Detector	22
2.3.3 Phase Shift Loop Detector	24
2.4 Speed Measurement	27
2.4.1 Single Loop Technique	27
2.4.2 Double Loop Technique	32
2.5 Discrimination	35
2.6 Classification	37
2.7 Conclusions	37
Chapter 3 COUPLED COILS DETECTION TECHNIQUE	40
3.1 Introduction	40
3.2 Derivation of the Induced Voltage in the Receiver Coil in the Proximity of a Conducting Surface	42
3.3 Behaviour of Image Voltage as a Function of Coil Spacing and Interface Height	47
3.4 The Effect of Finite Conductivity of the Interface on the Image Voltage	47

3.5	Experimental Evaluation	51
3.5.1	Magnitude of Image Voltage	51
3.5.2	Ratio Test	56
3.6	Conclusions	58
Chapter 4	IMAGE VOLTAGE BEHAVIOUR AS A FUNCTION OF DISTANCE FROM A MOVING PLATE	59
4.1	Experimental Hardware	59
4.2	Experimental Observation	63
4.2.1	Derivation of P using Linear Regression Technique	63
4.3	Modelling Technique	66
4.4	Phase Characteristics	66
Chapter 5	EVALUATION OF PARAMETER P	67
5.1	Introduction	67
5.1.1	Horizontal Plate	67
5.1.2	Vertical Plate	69
5.1.3	L - Shaped Plate	69
5.1.4	Image Voltage Characteristics in the Presence of Brine Solution	94
5.1.5	Other Considerations	94
5.2	Discussions of the Results	94
5.3	Derivation of P Using Vehicles	96
5.4	Conclusions	99
Chapter 6	SPEED ESTIMATION	106
6.1	Modelling Technique	106
6.2	Identification of the Peak Values of the Image Voltage	111
6.3	Circuit Realization	113
6.3.1	Receiver Amplifier	113
6.3.2	Demodulator	116
6.3.3	Difference Signal Generator	117
6.3.4	Differentiator	117
6.3.5	Divider	117
6.3.6	Time Generator	122
6.4	Experimental Results	122
6.5	Conclusions	138

Chapter 7	VEHICLE IDENTIFICATION	139
7.1	Introduction	139
7.2	Vehicle Length Measurements	140
7.3	Vehicle Signature	148
7.4	Identification Process	154
7.5	Discussions	156
Chapter 8	CONCLUSIONS AND THE FUTURE DEVELOPMENTS	158
8.1	Introduction	158
8.2	Acceleration Measurement	159
8.3	Conclusions	160
Appendices		161
Publications		185
Patents		186
Bibilography		187

SUMMARY

The research activity has been primarily directed towards the development of a vehicle sensor to obtain traffic parameters such as vehicle count, speed and vehicle identification. In order to have an appreciation of the technique adopted, a review of the more prominent approaches in traffic monitoring and control systems are made in Chapter 1. Chapter 2 provides an appraisal of the various vehicle detectors in terms of their ability to meet the requirements of the more advanced traffic control systems.

The vehicle sensor selected for the investigation consists of two coils spaced apart with a common axis and located in the road surface, orthogonal to the direction of travel of the vehicle. The operating principle is based on the fact that if one coil is energised by an alternating current source then as a vehicle approaches the sensor, eddy currents are induced in the undercarriage.* The magnetic field created by these currents result in a change in the induced voltage in the second coil.

Experimental observations have indicated that a constant parameter can be obtained in terms of the change in the induced voltage and the distance of the vehicle from the sensor. This parameter has been found to be independent of the normal variables expected in traffic situations, and is used to construct a mathematical model for determination of the vehicle speed. Through the analysis of actual data collected from several vehicles, it has further been

* usage of this term includes the whole of the underside of the vehicle

demonstrated that good speed prediction is possible using the output of this single sensor.

The report also embodies an identification technique based on the length and the characteristic signature of a vehicle derived from the sensor output.

The economies associated with many traffic control and surveillance systems are generally determined by vehicle sensors. The concept presented in this report represents an attempt to solve some of the known problems and provide an economical solution for speed measurements, count and vehicle identification (in terms of vehicle grouping)*using a single vehicle sensor.

* by vehicle group it is meant vehicles of the same make and model

ACKNOWLEDGEMENTS

The Author is indebted to Professor R.E. Bogner under whose supervision the research was carried out. He is also grateful to the Management of Philips Allied Industries - R.G. Menzies Research and Development Group for their technical support during the course of the project. He would like to thank the Electrical Engineering Staff of the University whose help has also been invaluable.

This thesis contains no material which has been accepted for the award of any other degree or diploma in any University and, to the best of my knowledge and belief, contains no material previously written or published by another person except where due reference is made in the text of the thesis.

K. ESHRAGHIAN.

September, 1977.

LIST OF PRINCIPLE SYMBOLS

- a = radius of a circular coil (m)
 A_c = cross sectional area of a circular coil (m^2)
 \bar{A} = magnetic vector potential
 A_\emptyset = \emptyset - component of the magnetic vector potential
 \bar{B} = magnetic flux density
 B_ρ, B_\emptyset, B_z = cylindrical components of the magnetic flux density
 $B_r, B_\theta, B_\emptyset$ = spherical components of the magnetic flux density
 d_c = displacement of conducting surface from centre of sensor
 d_s = vehicle lateral displacement
 D = distance between vehicle sensor and vehicle
 D_e = effective distance of sensor
 f = frequency (Hz)
 h = coil to conducting surface spacing (cm)
 \bar{H} = magnetic field intensity
 $H_r, H_\theta, H_\emptyset$ = spherical components of the magnetic field intensity
 H_x, H_y, H_z = rectangular components of the magnetic field intensity
 H_{xi} = x component of the magnetic field at the receiver due to the image
 H_{xt} = x component of the magnetic field at the receiver due to the transmitter
 I = current in coil
 $k = \sqrt{\frac{4a(a-r_w)}{(2a-r_w)^2}}$
 $K_i = NA_c W \mu_o m$
 l_d = inductive loop vehicle detector length
 $l_e = (l_p - l_d)$
 l_m = vehicle length
 l_{me} = "Electrical" length of vehicle
 \bar{l}_m = assigned average vehicle length
 l_p = effective electrical length of inductive loop
 l_s = length of ferrite rod
 l_{sd} = separation between two inductive loops

- L_c = inductance of a coil in the presence of a conducting surface
 L_L = loop detector inductance
 L_o = self inductance of a coil
 M = mutual inductance between two coils
 N = number of turns
 N_v = number of vehicles
 p = density (vehicles per kilometre)
 P = speed constant
 q = volume (vehicles per hour)
 r = radial distance from origin (metre)
 r_c = correlation coefficient
 r_w = radius of wire
 R_s = surface resistivity
 S = speed (kilometres per hour)
 S_v = vehicle speed
 S_{dl} = vehicle speed using double loops
 S_{sl} = vehicle speed using single inductive loop
 \bar{S}_{sl} = estimated speed using single inductive loop
 t_s = time to travel distance D_s
 t_w = time the inductive loop is occupied
 V = voltage across a coil
 V_p = induced voltage change in a receiver coil
 V_R = resultant induced voltage in a coil in the presence of a conducting surface
 V_{p_m} = maximum value of V_p
 V_{R_x} = peak to peak induced voltage in receiver coil
 V_{T_x} = peak to peak transmitter voltage
 W_p = total sensor length
 w = angular frequency (rad./sec.)
 x = spacing between transmitter and receiver coils
 x_p = simulated plate length
 X_{L_r} = reflected reactance (ohms)

- y_p = simulated plate width
 Z_t = load impedance
 X, Y, Z = rectangular co-ordinates
 r, θ, ϕ = spherical co-ordinates
 ρ, ϕ, z = cylindrical co-ordinates
 μ = permeability of a material
 μ_0 = permeability of a free space
 μ_r = **effective** permeability of material
 σ = conductivity of material
 δ = approach angle
 δ_s = skin depth
 ∇ = gradient operator
 Δ = incremental change
 α = slope
 α_m = modified slope
 σ_d^2 = variance of D
 σ_v^2 = variance of V_p
 θ_p = angle of incline
 γ_e = length constant



CHAPTER 1

TRAFFIC CONTROL

1.1 INTRODUCTION

In recent years reports on traffic control systems have been numerous. ¹⁻²⁰ The objectives of many of the investigations have been to evaluate not only the behaviour of the systems according to some performance criteria, but also provide justification in terms of reliability, maintenance and economics.

The present research has been primarily concerned with the development of a vehicle sensor to obtain traffic parameters such as vehicle count, speed, length and classification. However, in order to have an appreciation of this approach, it is considered useful to review the more prominent approaches in traffic control and monitoring systems.

1.2 TRAFFIC CONTROL SYSTEMS

There are two basic types of traffic control systems: pretimed and traffic-actuated.²¹⁻²⁴ The pretimed systems are primarily used for downtown urban-area streets, where the daily traffic patterns are well known. Such systems are gradually being replaced by the traffic-actuated controls, the operation of which, depends on traffic parameters obtained from vehicle detectors.

Consequently, many researchers have directed their activities towards the development of traffic actuated control systems in terms of feedback path and have followed two directions.

The first looks for car-borne equipment in the form of an information system whereby traffic and safety information is conveyed to the motorists by radio and by variable signal panels in the vehicle.²⁵⁻²⁶ The complexities and problems with such systems are well known and various proposals are being evaluated.

The second approach is the traffic responsive control system and surveillance.²⁷⁻²⁸ To improve the traffic situation, the driver is required to make educated decisions based on the information displayed by variable message signs. Fig 1.1 shows a typical system currently under investigation by N.V. Philips Gloeilampenfabrieken for the Dutch Government.

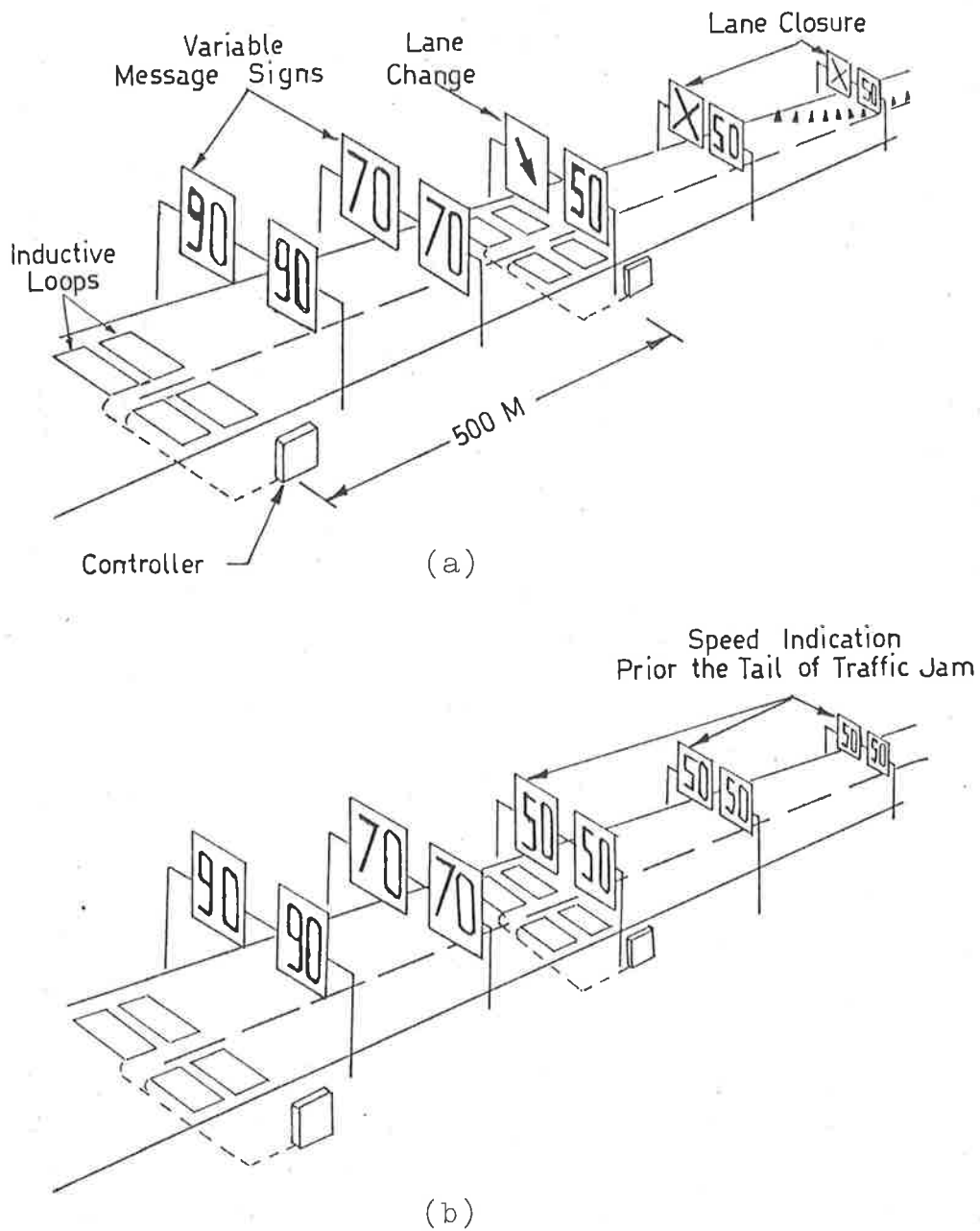


Fig 1.1 Signalling Plan

- (a) Variable message sign indicating lane change.
- (b) Variable message sign indicating the tail of traffic jam.

In this system for example, the lane change is indicated by an arrow, followed by a signal indicating lane closure. Alternatively, in the case of a traffic jam, the tail of the jam is indicated by the allowable speed limit. As the traffic jam grows, the image moves to the left. The visual information conveyed to the driver provides an early warning of a possible traffic jam. The driver, (considered as part of a feed-back loop) is required to take the necessary corrective measures in accordance with the displayed signal, to maintain the smooth flow.

Such systems in general are based on those parameters which reflect the overall flow characteristics, such as volume (vehicles per hour per lane), density (vehicles per lane per Kilometre) and mean speed (Kilometres per hour).

1.3 FUNDAMENTALS OF TRAFFIC MOVEMENT ON FREEWAYS

The traffic on freeways under uniform conditions, i.e. all vehicles in a section travelling at the same speed and equal spacing, can be described in terms of continuum variables associated with fluid mechanics flow. Lighthill and Whitham in 1954, developed a model on this basis and proposed the identity

$$q = p \cdot S \quad \dots(1.1)$$

where

q = volume

p = density

S = speed.

30-31

A typical volume-density curve which reflects many of the properties of road traffic is shown in Fig 1.2. For example if the observed volume is q_1 , then the density may be either at p_1 or p_2 which represents two different traffic conditions. The capacity of the freeway (the maximum sustained volume of vehicles which can pass a point) is determined by the turning point represented by C_p . Since density gives the true measure of the state of freeway at a given time, it is a vital element for traffic control.

An additional factor which contributes in the understanding of the traffic flow on a freeway is the speed-volume characteristics as shown in Fig 1.3. Empirical and theoretical studies have indicated that for normal flow, traffic volume decreases with increasing speeds. At a point of maximum volume, flow becomes unstable and eventually turns into a forced flow. This results in the simultaneous decrease of the volume and speed.

32-33

The identity given in Eq. 1.1 is the basic criteria from which many of the traffic models have been derived.

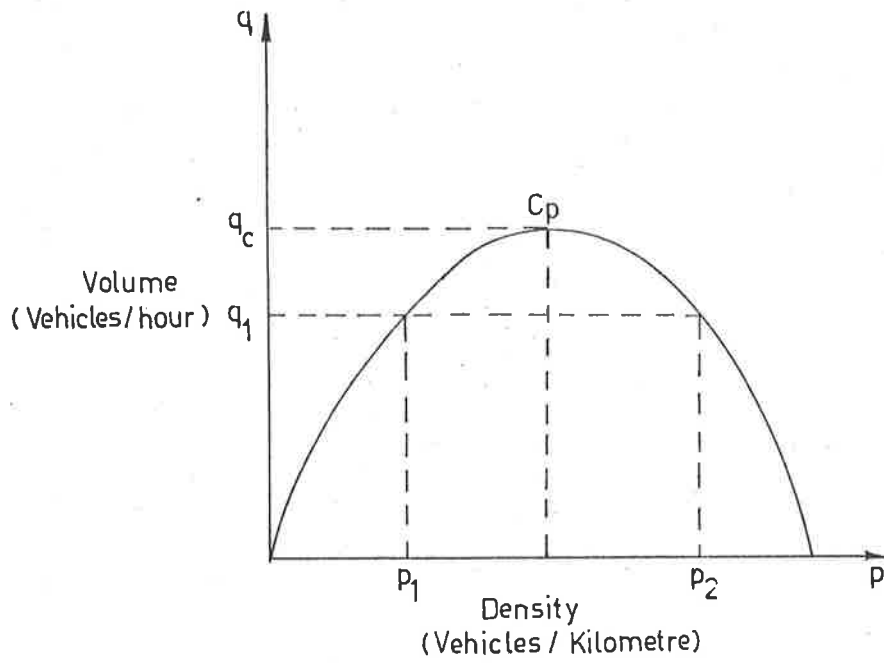


Fig. 1.2 Fundamental diagram of traffic flow

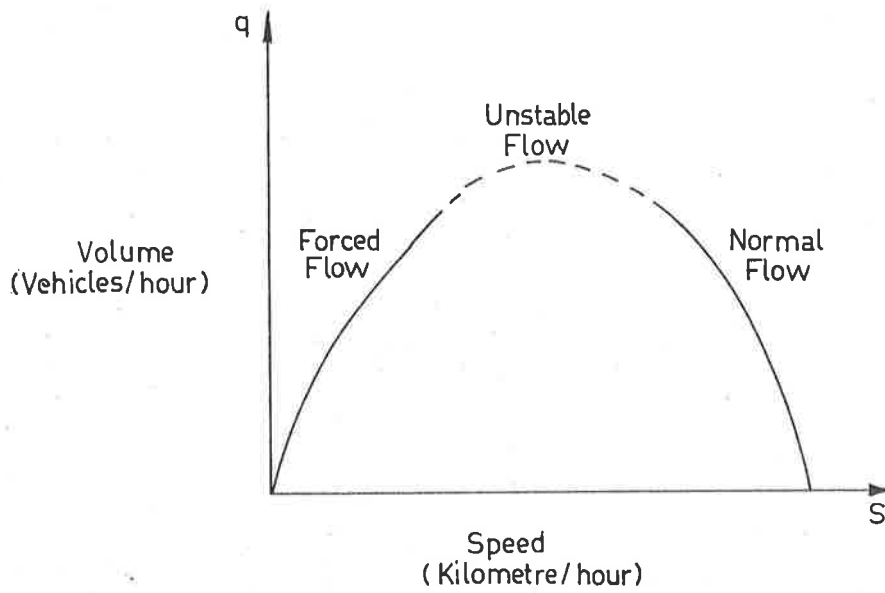


Fig. 1.3 Speed - Volume Characteristics

1.4 TRAFFIC MODELS

The traffic on a freeway is generally characterized in terms of macroscopic or microscopic models.³⁴⁻³⁵ In developing a representation of traffic on a freeway segment, several Kilometres in length for several hours, the main objective is concerned with gross features of traffic such as volume, density, speed, and average travel time. Models developed with this objective in mind need only provide an accurate representation of these parameters and are generally termed macroscopic models.

Although accurate measurements of traffic parameters over the entire length of the freeway and knowledge of the proper control action for any given set of traffic conditions are still relatively limited, several authors have formulated various schemes on the data obtained from vehicle detectors placed at regular intervals on the freeway.

Gazis and Knapp³⁶ developed a modelling technique for estimating the number of vehicles on a section of freeway from speed and flow measurements at the entrance and exit points of a section. From the estimate of the travel time a rough measure of density was obtained. An alternative approach was taken by Mikhalkin³⁷ where the occupancy (the percentage of time the detector is activated by the vehicle during a given period) was utilized in

place of section density. Although the approach was simple and the technique could readily be implemented, the resultant speed estimates were highly unreliable.³⁸ Nahi and Trivedi³⁹ applied the modern estimation theory concept and presented an improved modelling technique which provides simultaneous estimation of traffic parameters such as section density and speed based on various averages over the freeway section.

The above techniques provide a means to accomplish two objectives:

- (a) predict traffic conditions
- (b) indicate congestion.

However there are situations, particularly in incident detection, identification and tracking schemes, where detailed representation of traffic flow down to the level where individual vehicles are concerned, is required. These models are known as microscopic models and are extremely useful tools in studying problems concerned with relatively short lengths of the freeway and for relatively short periods of time.

1.5 IDENTIFICATION

Considerable effort has also been expended in recent years to develop automatic vehicle identification and classification systems.⁴⁰⁻⁴⁸ The main purpose has been the individual detection of a selected vehicle. A common requirement of such systems is that the vehicle requiring identification be equipped with a transponder which may be either a passive coded or an active⁴⁹ unit capable of sending out a coded signal. When the vehicle comes within the range of an interrogator, the code is read and the vehicle identification is obtained.

1.6 SYSTEM IMPLEMENTATION

Since vehicle detectors are slow speed devices the information obtained from detectors at the entrance and exits of a section is processed initially by a local processor, before being transmitted to a central processor for the overall coordination plan. A typical approach to the implementation of a traffic controller is shown by the block diagram of Fig. 1.4. In such arrangements the variable message sign can take various forms, the simplest being the conventional traffic signal lights.

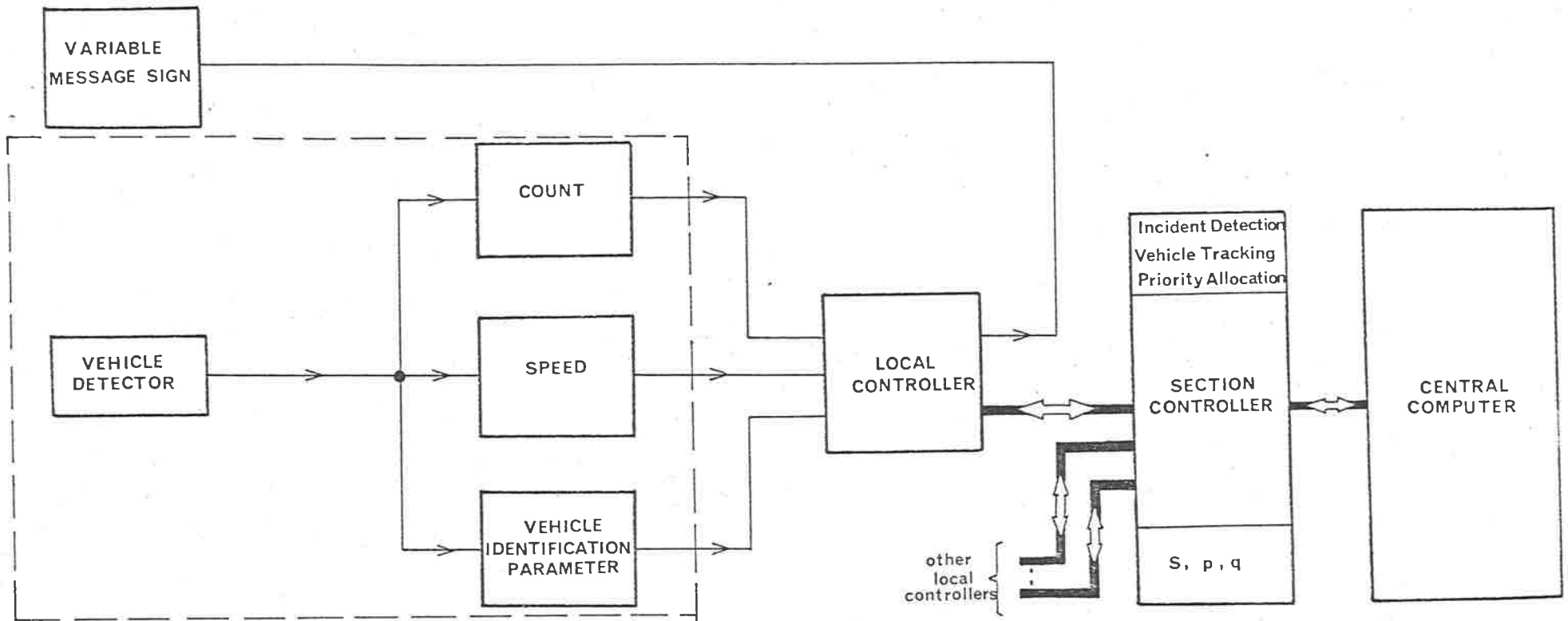


Fig. 1.4 A Typical Representation of A Traffic Monitoring and Control System

The success and the performance of the system is dependant on the accuracy of data obtained from vehicle detectors. Therefore vehicle detectors are the essential link between the vehicle and the control system.

The blocks within the dotted lines of Fig. 1.4 are the subject of the current study.

CHAPTER 2

REVIEW OF VEHICLE SENSORS

2.1 INTRODUCTION

A vehicle sensor can be defined as a special detector which not only provides information regarding the status (presence or passage) of a vehicle, but also gives an indication regarding its speed and classification.

The basic requirements⁵⁰ and the desired accuracies of vehicle sensors are shown in Table 2.1.

⁵¹⁻⁵² Barker made a detailed comparative study of various detectors such as magnetic, magnetometer, pressure, inductive loop, sonic and radar.⁵³⁻⁵⁴

⁵⁵ Ziolkowski and Tsao investigated an alternative scheme using near-field (freq. 300KHz) and directional (freq. 3 GHz) antennae buried in the road surface. The results of these investigations are shown in Table 2.2. This is an extension of Barker's findings and indicate the performance of the detectors in terms of the relative acceptance criteria defined by: good (G), satisfactory (S), marginal (M), and unsatisfactory (U).

	Parameter	Tolerance
i	Passage	2% error for 90% of the time
ii	Direction	Zero error
iii	Stationary (vehicle stopped)	2% error for 90% of the time
iv	Vehicle length	5% error
v	Speed (0-110Km/h)	5% error
vi	Density	5% error for 90% of the time
vii	Volume	5% error
viii	Queue length	5% error
ix	Acceleration	5% error

(a)

	Parameter	Tolerance
i	Temperature	-40°C to 75°C
ii	Humidity	0 to 100%
iii	Snow depth	200 mm
iv	Snow-ice mixture depth	150 mm
v	Ice depth	25 mm
vi	Water depth	25 mm
vii	Soil depth	25 mm
viii	Grease-oil depth	1.5 mm

(b)

Table 2.1 Basic Requirements of Vehicle Sensor
 (a) Accuracy requirements in terms of traffic parameters
 (b) Environmental conditions

NOTE: This information was prepared by the Bureau of Public Roads and Federal Highway Administration -
 Contract No. FH -11-6973

	Count Accuracy	Single Lane Coverage Definition	Speed	Status	Relative Installation Cost	Installation Time (hr.)	Maintenance	Environment	Relative (Hardware) Detector Cost	Identification	Reliability
Pressure	S	G	U	M	2	48-64	G	S	1.8	U	S
Magnetic	S	S	U	S	0.7-0.9	4-12	G	G	1.2	M	G
Magnetometer	G	G	U	S	0.8	0.5	G	G	1	M	G
Radar	S	S	G	S	0.5-2	2	S	G	3	U	S
Sonic	S	S	S	S	0.5-2	2	S	S	3	U	S
Inductive Loop	G	G	M	S	1	2-4	G	G	1	M	S
Antenna f ≐ 300 KHz	G	S	S	S	0.9	2-3	G	G	1	S	G
Antenna f ≐ 3GHz	G	S	M	G	0.8	1	S	M	1.2	G	G

Table 2.2(a) A Comparative Study of Vehicle Detectors

DETECTORS	INSTALLATION
Pressure	Installed flush with the road surface in a 2 metre by 45cm by 30cm excavated trench sealed with concrete
Magnetic	Mounted flush with road surface in 5cm by 50cm slot or slid into a 5cm diameter nonmetallic conduit in a bored hole from roadside not more than 30cm below the pavement surface
Magnetometer	Installed in a 5cm diameter by 25cm deep hole in pavement surface with 30 metre nominal lead length
Radar	Mounted on a pole in overhead or sidefire position
Sonic	Mounted on a pole in overhead or sidefire position
Inductive Loop	1-5 turn of insulated no. 14 gauge wire installed in a rectangular slot 0.5cm wide by 0.5-5cm deep cut into the pavement surface. Loop size varies from 1 metre sq. to 2 metre by 30 metre, with 200 metre maximum lead
Antenna f \approx 300 KHz (HED)	The near-field Horizontal Electric dipole (HED) is constructed from a coaxial cable and installed in a slot 2cm by 10cm deep cut in the lane
Antenna f \approx 3GHz	The antenna is seated in a pod of 10cm by 20cm and 2cm deep

Table 2.2(b) Installation Technique for the Various Vehicle Detectors

Although this type of assessment depends on the users' judgement, the technique provides a basis for the development of a figure of merit which can be used as a guide for comparison.

From the various vehicle detectors developed, no single detector is available which fulfills all the requirements of the modern traffic monitoring system. However one of these, the inductive loop, has been accepted as an interim solution because of its reliability and economic advantage. Therefore, the following section outlines the basic concepts associated with this approach and reviews the relative merits and the limitations in terms of vehicle detection, speed measurement and classification.

2.2 BEHAVIOUR OF A COIL IN PROXIMITY OF A CONDUCTING SURFACE

When a coil carrying a time-varying current is placed in the proximity of a conducting surface, eddy currents are induced in that surface. Subsequently, a pronounced change in the impedance of the coil is observed.

The self inductance L_0 of a loop conductor of finite cross section is given by

$$L_0 = \mu(2a-r_w) \left[\left(1 - \frac{k^2}{2} \right) K(k) - E(k) \right] \dots (2.1)$$

where

$$k^2 = \frac{4a(a-r_w)}{(2a-r_w)^2}$$

a = radius of loop

r_w = radius of wire

$K(k)$ = complete elliptic integral of the first kind

$E(k)$ = complete elliptic integral of the second kind

When the coil is placed near a conducting surface, its impedance is modified. This change can be thought to be caused by the presence of an image coil as shown in Fig. 2.1. The modified inductance can be obtained by applying Newman's equation⁶² for mutual inductance.

$$M = \frac{\mu}{4\pi} \iint \iint \frac{d\bar{l}_1 \cdot d\bar{l}_2}{r} \quad \dots (2.2)$$

Where $d\bar{l}_1$ and $d\bar{l}_2$ are differential elements of length about the actual and the image loops respectively.

The inductance of the coil may be written as

$$L_c = L_o - \sqrt{a(a-r_w)} \left[\left(\frac{2}{k} - k \right) K(k) - \frac{2}{k} E(k) \right] \quad \dots (2.3)$$

where

$$k = \sqrt{\frac{4a(a-r_w)}{(2a-r_w)^2 + (2h)^2}}$$

and

h = spacing between the coil and the conducting surface.

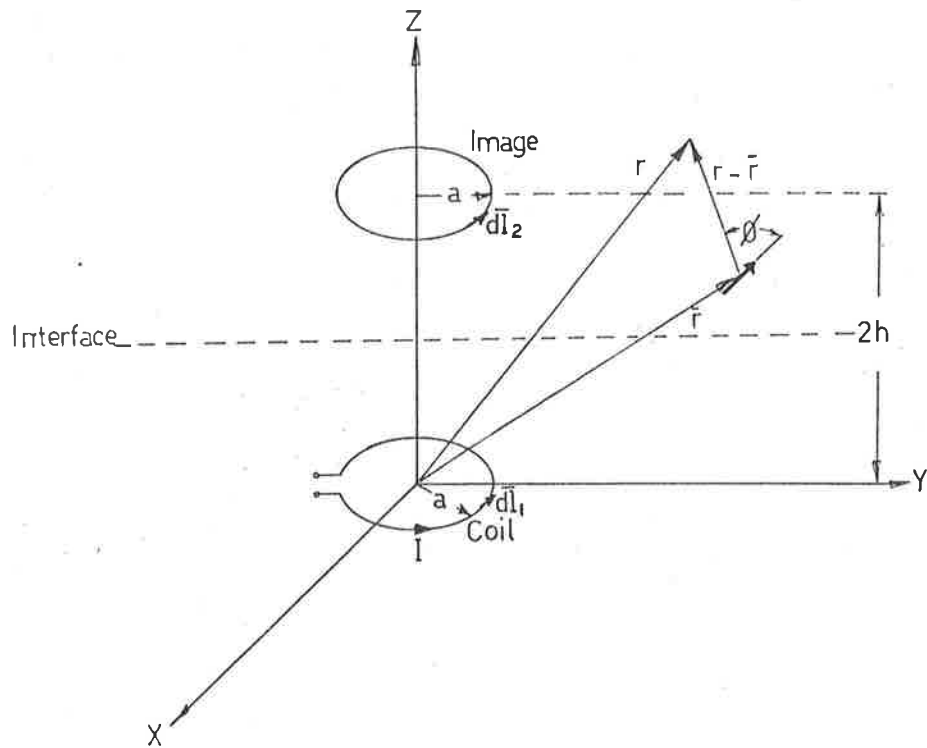


Fig. 2.1 Geometry of the coil and its image with respect to a conducting plane.

The second term in Eq. (2.3) is the change in inductance of the coil caused by the proximity of a conducting surface. This is illustrated in Fig. 2.2 as a function of the spacing h , for a given frequency and coil size.

The negative sign in Eq. (2.3) implies that the reflected reactance becomes more capacitive as the spacing h is reduced.

The impedance bridge shown in Fig. 2.3 was used for the measurement of the coil inductance. For values of $h > 5\text{cm}$ good correlation was obtained between the computed and the experimental results.

2.3 INDUCTIVE LOOP DETECTORS

The change in the inductance of the loop due to the presence of a vehicle has been implemented in several designs.⁶³ The various configurations such as the bridge balance, self-tuning and phase shift systems consist of a loop of one or two turns of wire and approximately 1-2 metres square, located horizontally in the road surface. The loop is energized by an oscillator having a frequency in the range of 40KHz-100KHz.

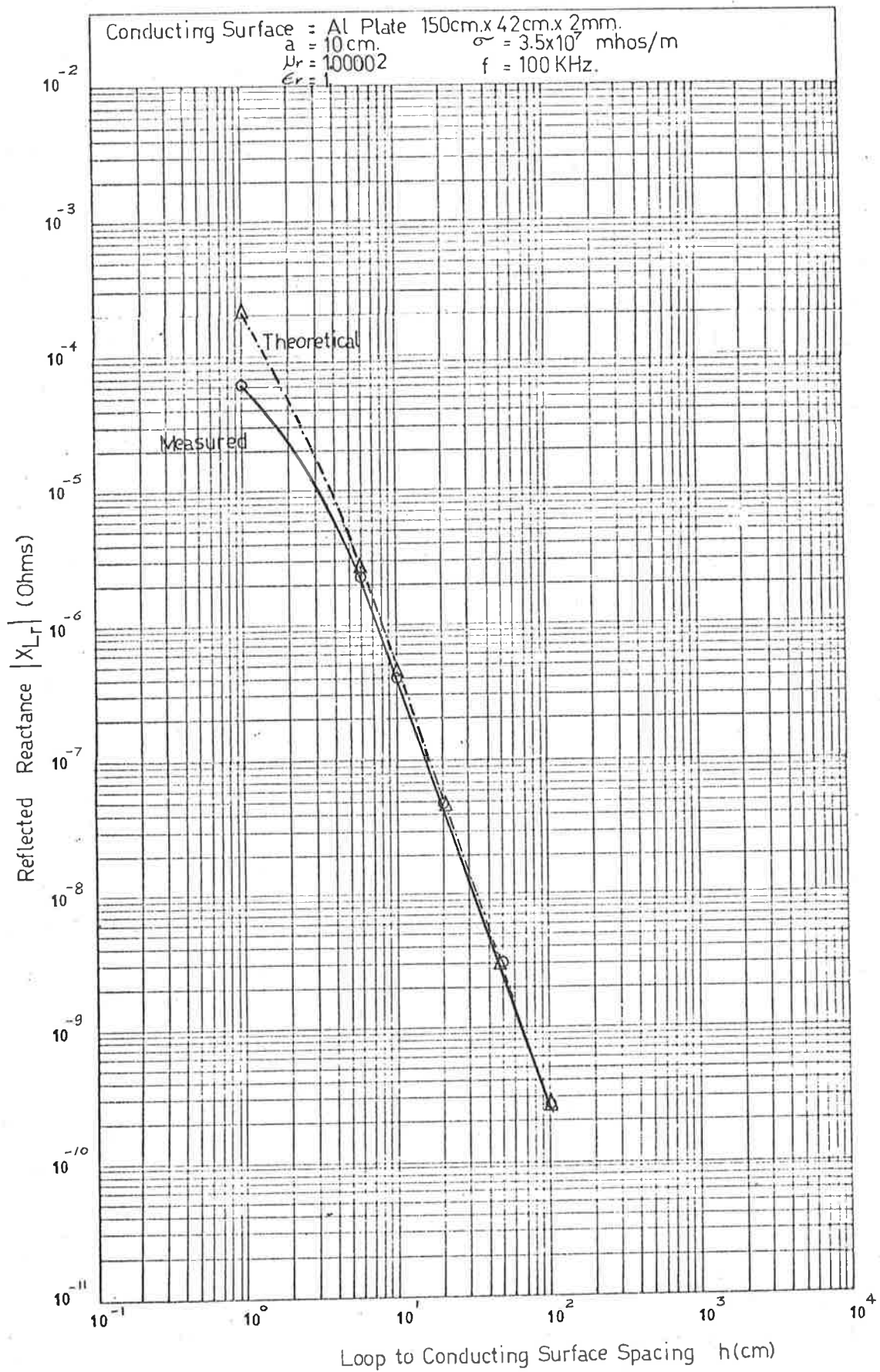
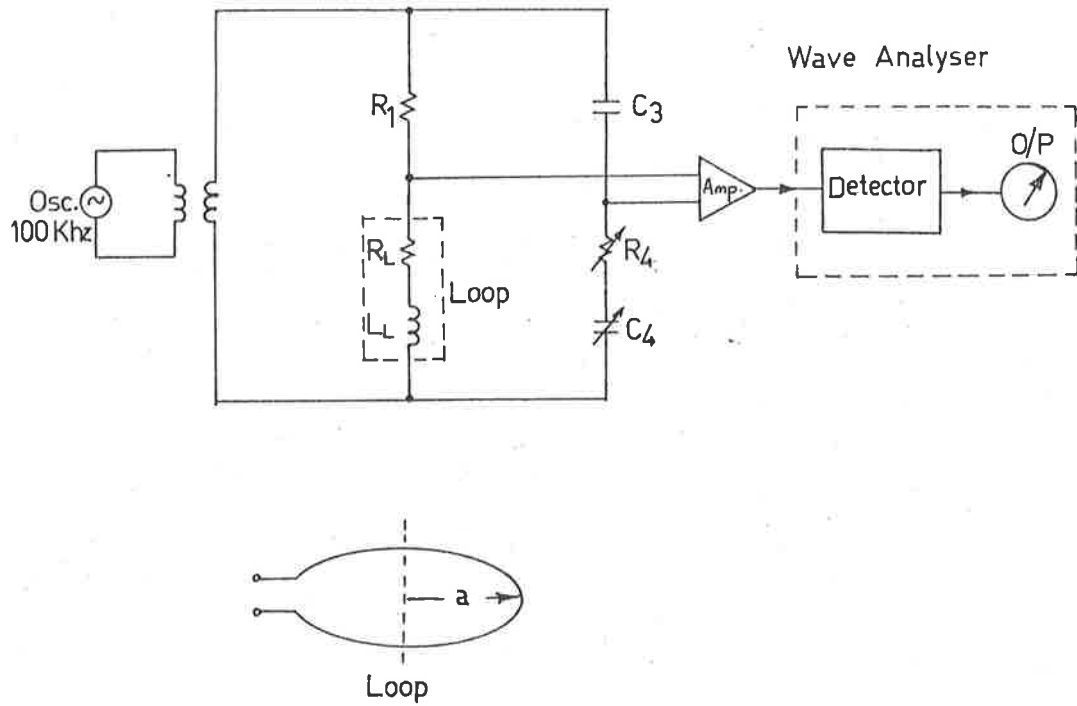


Fig. 2.2 Plot of Change in Reflected Reactance of a Coil as a Function of Spacing h , in the proximity of a Conducting Surface



R_L = Loop Resistance
 L_L = Loop Inductance
 a = 10 cm.

Fig. 2.3 Impedance Bridge for Measurement of the Loop Parameters

2.3.1 The Bridge - Balance Detector

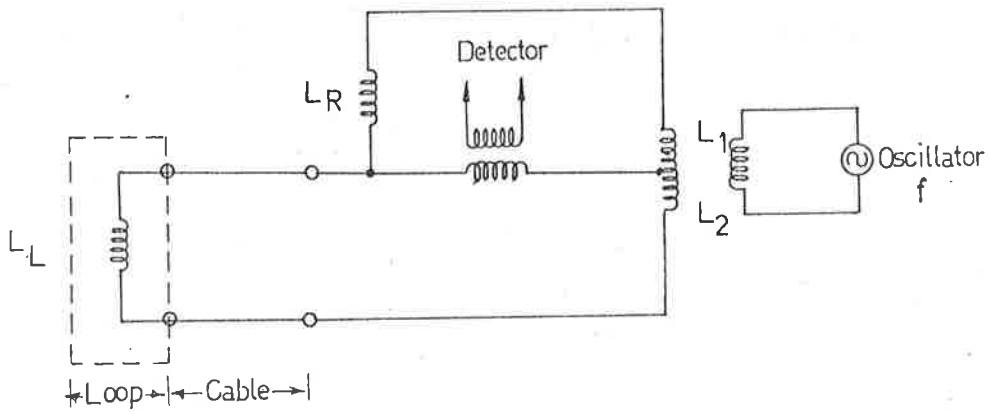
A typical configuration for a bridge - balance loop detector is shown in Fig. 2.4. The combined inductance of the loop L_1 and the lead-in cable L_d form one leg of the bridge while the other leg is comprised of a fixed reference inductor L_R having similar characteristics as the loop-cable combination. Presence of a vehicle causes a decrease in the inductance of the loop which results in an unbalanced voltage being generated. Subsequently, this is detected and processed.

The main advantage of this arrangement is its insensitivity to changes in the frequency of the excitation source.

The major drawback is the inability of the reference inductor to follow the changes in inductances of the loop and the lead-in cable, caused by temperature and humidity variations.

2.3.2 Self-Tuning Loop Detector

This technique uses the loop as part of a parallel resonant tank circuit which automatically adjusts a voltage-controlled oscillator (VCO) to a predetermined frequency relative to resonant frequency of a tank circuit. A vehicle in the proximity of the loop causes a reduction in the



$$50\mu\text{H} < L_L < 500\mu\text{H}$$

$$40\text{ KHz} < f < 100\text{ KHz}$$

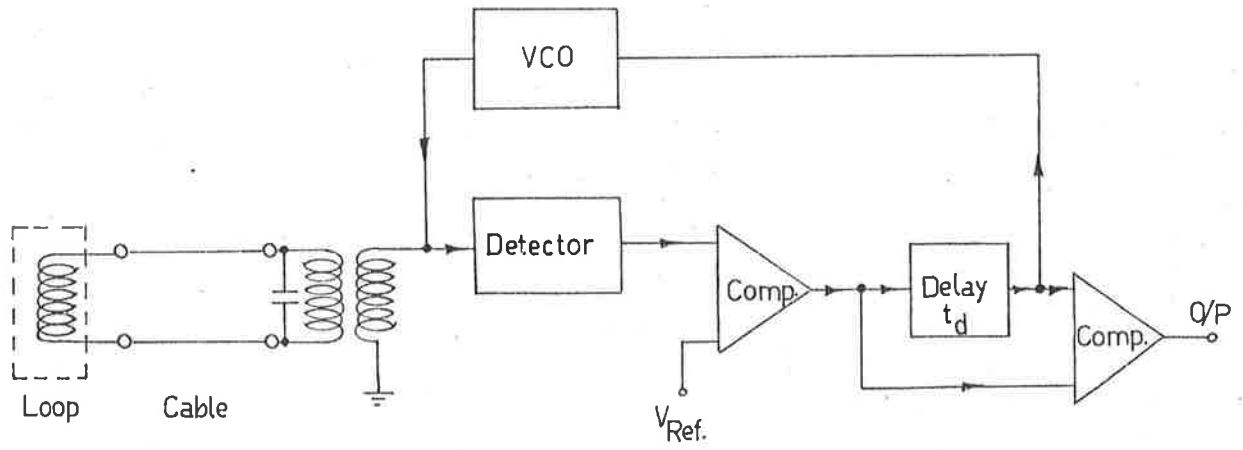
Fig. 2.4 Vehicle Detector Using Bridge-Balance Technique.

inductance of the loop, which in turn changes the frequency of the tank from f_1 to f_2 . This is reflected as a voltage change in the tank circuit, a delayed version of which is applied to the VCO. The delay circuit compensates for slow changes in the characteristics of the loop and the lead-in cable resulting from variations in temperature and humidity. This arrangement is shown in Fig. 2.5.

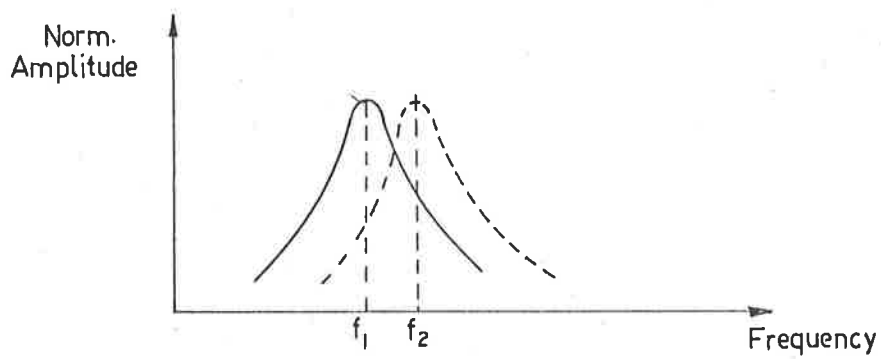
The main advantage of this configuration is that no field adjustments are necessary during the installation phase.

2.3.3 Phase Shift Loop Detector

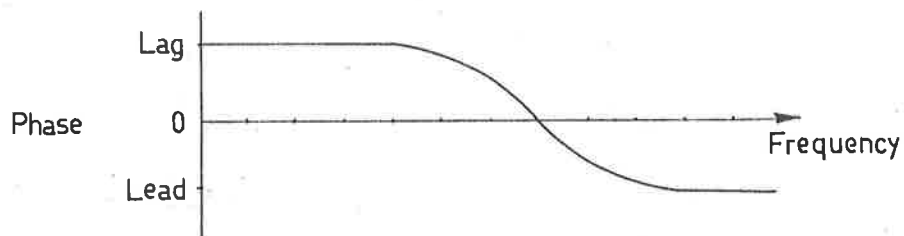
In this configuration the loop and the lead-in cable in conjunction with a tuning capacitor form a resonant tank circuit. The phase of the voltage in the loop tank circuit is being continually compared with the phase of the signal derived from the oscillator. Presence of a vehicle detunes the circuit which causes a change in phase of voltage appearing across the tank circuit. Fig. 2.6 shows the circuit arrangement for the phase shift loop vehicle detector.



(a)



(b)



(c)

Fig. 2.5 Self Tuning Loop Detector

(a) Circuit Configuration

(b) Resonant curves

(c) Phase characteristics

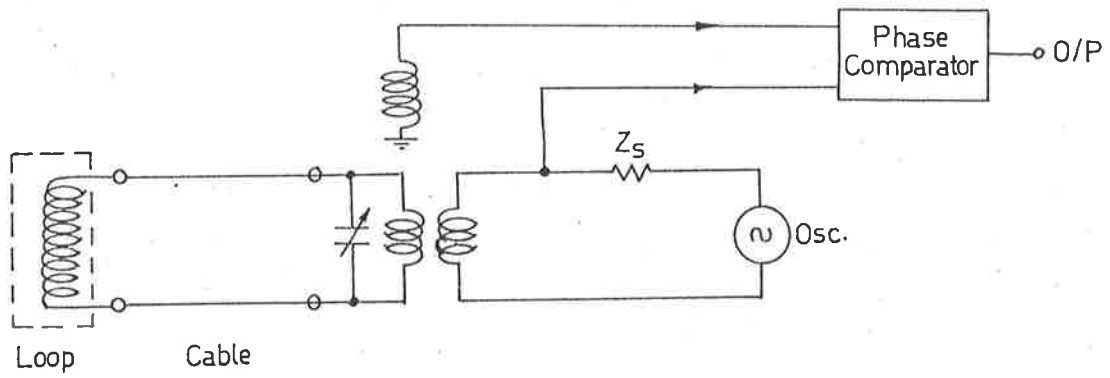


Fig. 2.6 Phase Shift Loop Detector

2.4 SPEED MEASUREMENT

The vehicle speed S_v is given by the fundamental relationship

$$S_v = \frac{D_s}{t_s} \quad \dots(2.4)$$

where

D_s = distance between two points

t_s = time to travel the distance D_s

In a number of traffic monitoring systems inductive loops are used for speed measurements.

2.4.1 Single Loop Technique

In systems where the accuracy of the speed information is non critical, a single inductive loop detector is implemented for speed estimations.

The expression defining the speed in terms of loop length l_d and vehicle length l_m as shown in Fig 2.8, is given by

$$S_{sl} = \frac{l_m + l_d}{t_w} \quad \dots(2.5)$$

where

t_w = period the loop is occupied.

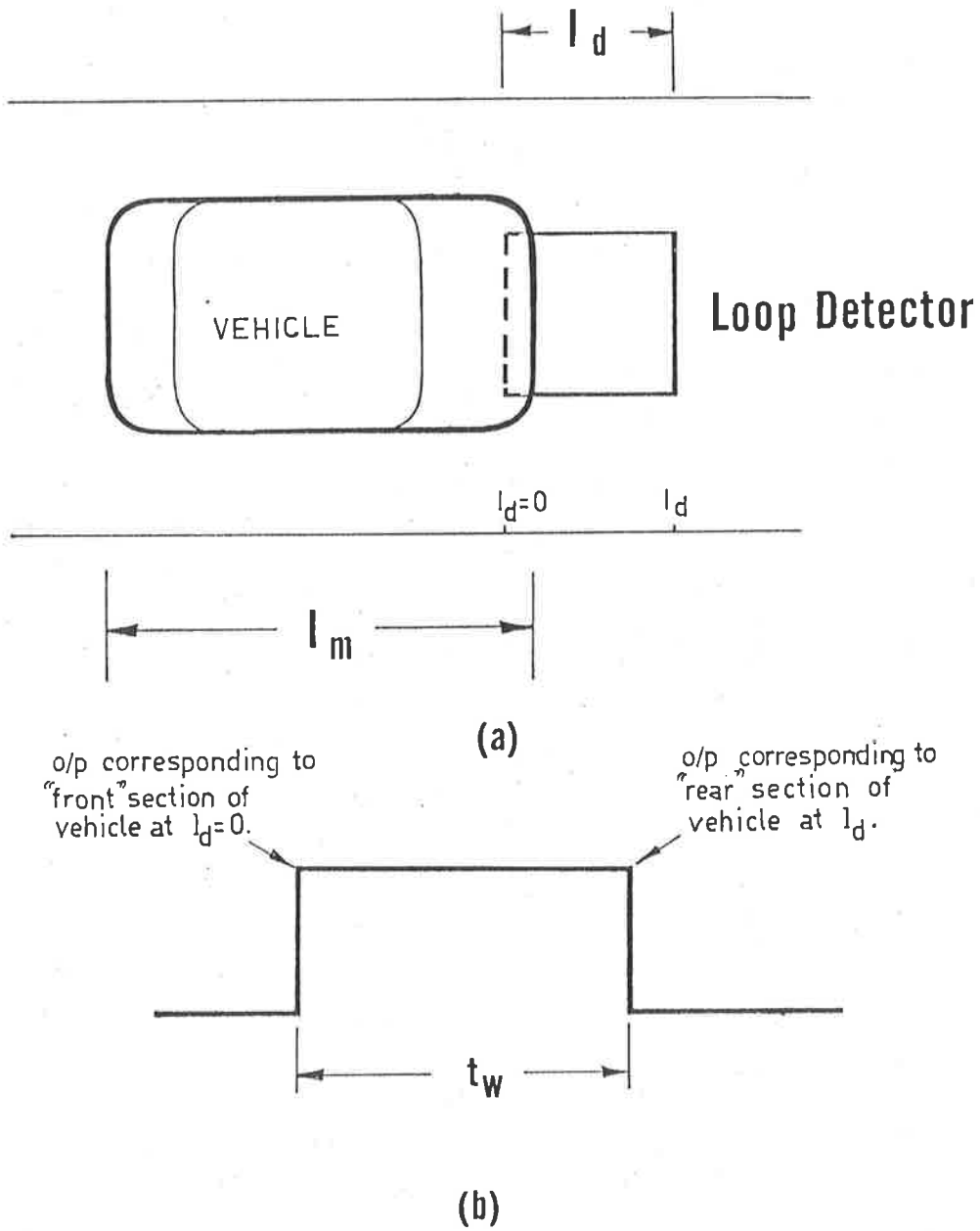


FIG 2.8 (a) Physical Layout for Single Loop Vehicle Detection.
 (b) Detector Output.

Eq. (2.5) assumes that the length of the vehicle is known. To overcome this limitation, an average length \bar{l}_m which is determined experimentally, is assigned to the vehicle. It is found that \bar{l}_m is dependent on the highway, location of the detector, and time of the day.

A typical characteristic associated with a particular section of the highway in terms of vehicle count and length is shown in Fig. 2.9. The average length \bar{l}_m can be expressed as

$$\bar{l}_m = \frac{1}{N_v} \sum_{i=1}^{N_v} l_{m_i} \quad \dots(2.6)$$

where

N_v = number of vehicles

l_{m_i} = length associated with the i^{th} vehicle.

The modified expression in terms of the average vehicle length is

$$\bar{S}_{sl} = \frac{\bar{l}_m + l_d}{t_w} \quad \dots(2.7)$$

To obtain an indication of the speed error when \bar{l}_m is used in place of l_m , we differentiate Eq. (2.5)

to obtain

$$\frac{\Delta S_{sl}}{S_{sl}} = \frac{\Delta l_m}{l_m + l_d} \quad \dots(2.8)$$

where

$$\Delta l_m = l_m - \bar{l}_m \quad \dots(2.9)$$

This is plotted in Fig. 2.10 as a function of the assigned average length \bar{l}_m .

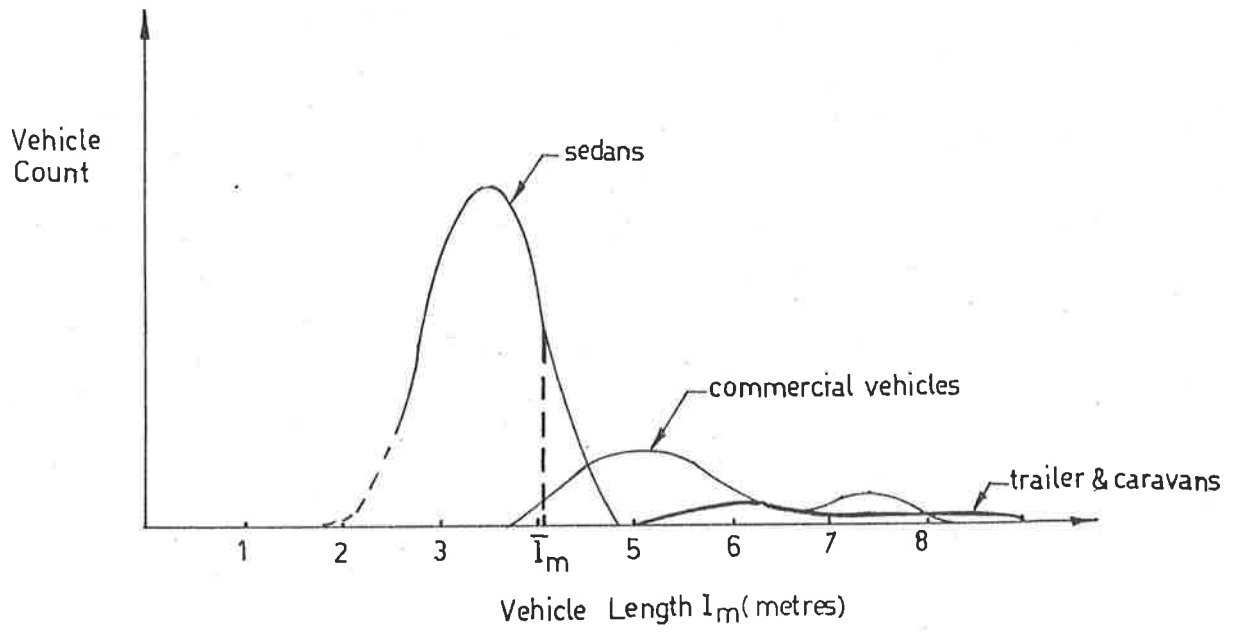


Fig. 2.9 Typical Characteristics of Vehicle Count as a Function of Vehicle Length

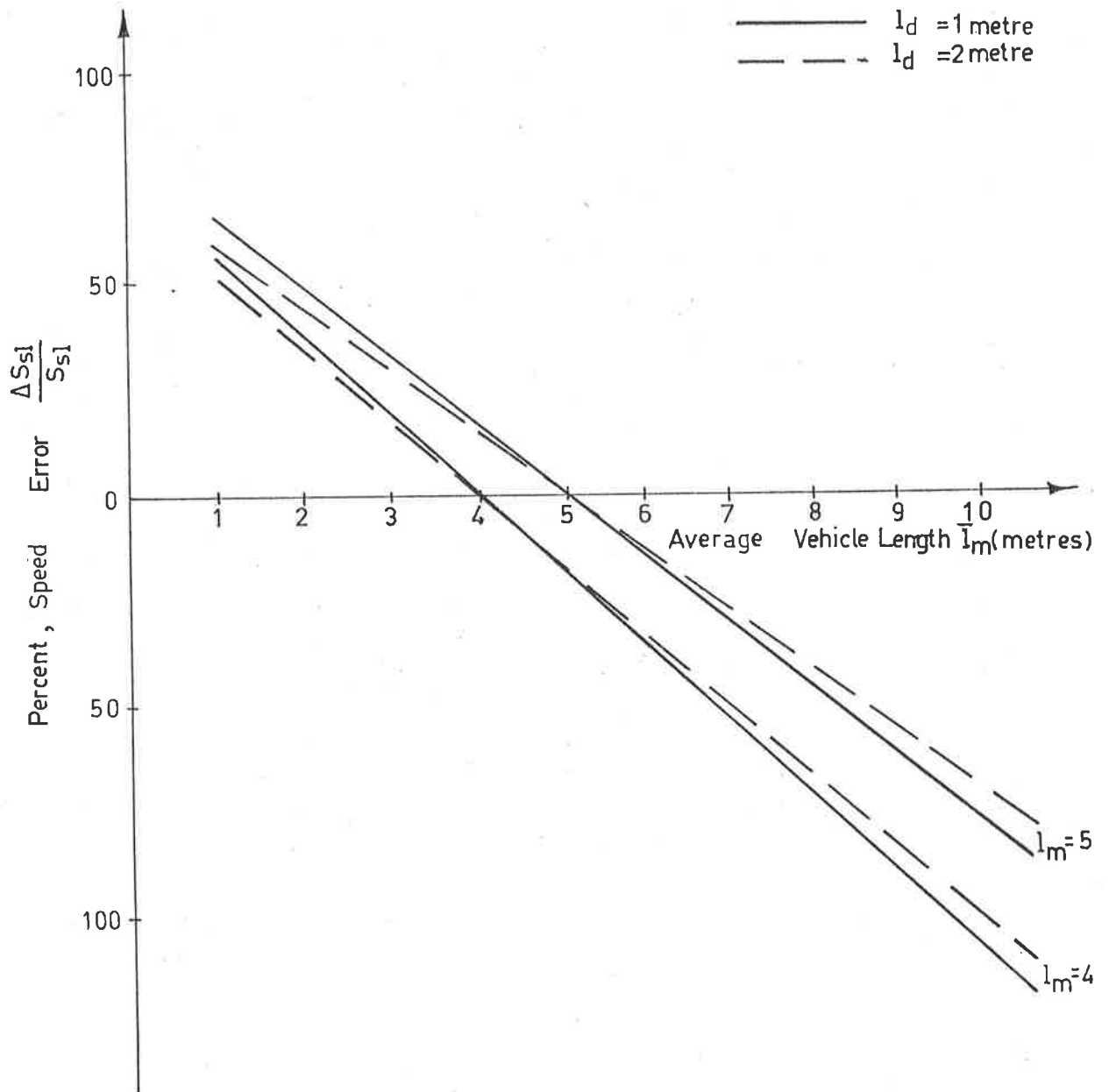


Fig. 2.10 Percent, Speed Error as a function of Average Vehicle Length \bar{l}_m for two Loops and Vehicle Dimensions

2.4.2 Double Loop Technique

The vehicle speed derived using Eq. (2.7) is highly unreliable for most traffic monitoring applications. The accuracy is improved by using two loops spaced a distance l_{sd} apart. This configuration is shown in Fig. 2.11.

The speed S_{dl} for double loops is given by

$$S_{dl} = \frac{l_{sd}}{t_s} \quad \dots(2.10)$$

where

l_{sd} = Separation between the loops

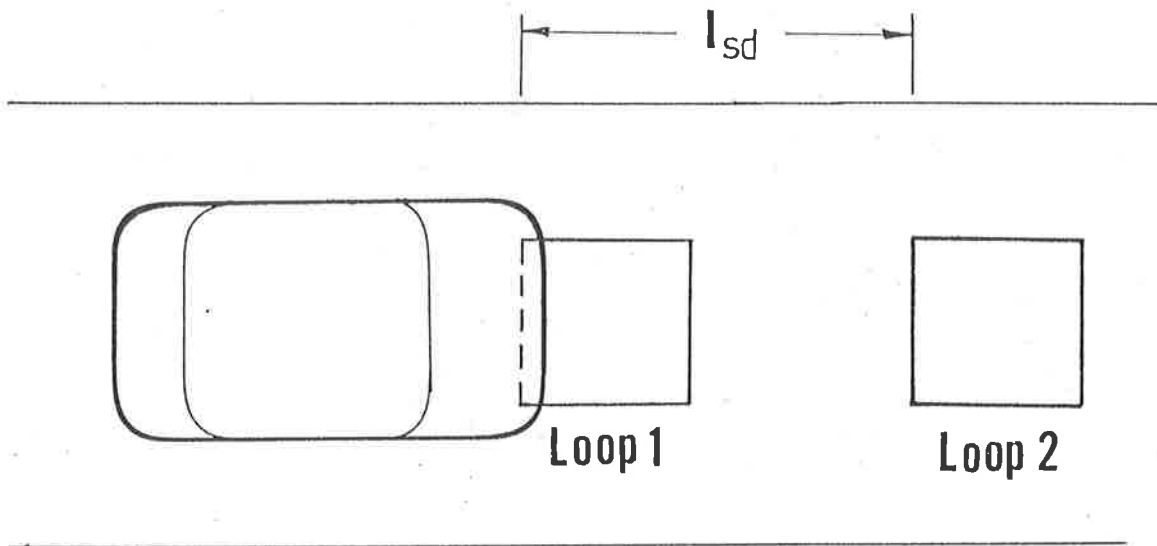
and

t_s = Time difference between the leading edges of the outputs of the loops.

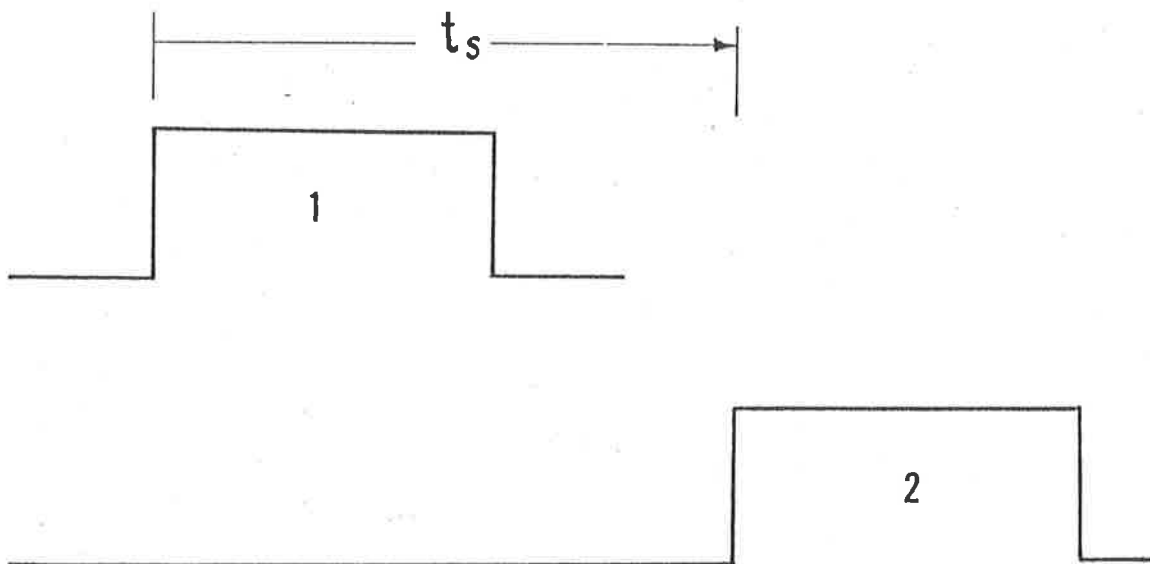
A number of systems avoid duplication of the equipment by using double loops at strategic locations for calibration purposes, followed by single loops. ¹⁹ By equating expressions (2.5) and (2.10) the length of the vehicle is

$$l_m = l_{sd} \cdot \left(\frac{t_w}{t_s} \right) - l_d \quad \dots(2.11)$$

This information is then used by the single loop detectors for speed measurement. A typical arrangement is shown in Fig. 2.12.



(a)



(b)

Fig 2.11 (a) Physical Layout for Double Loop System.
 (b) Inductive Loop Outputs.

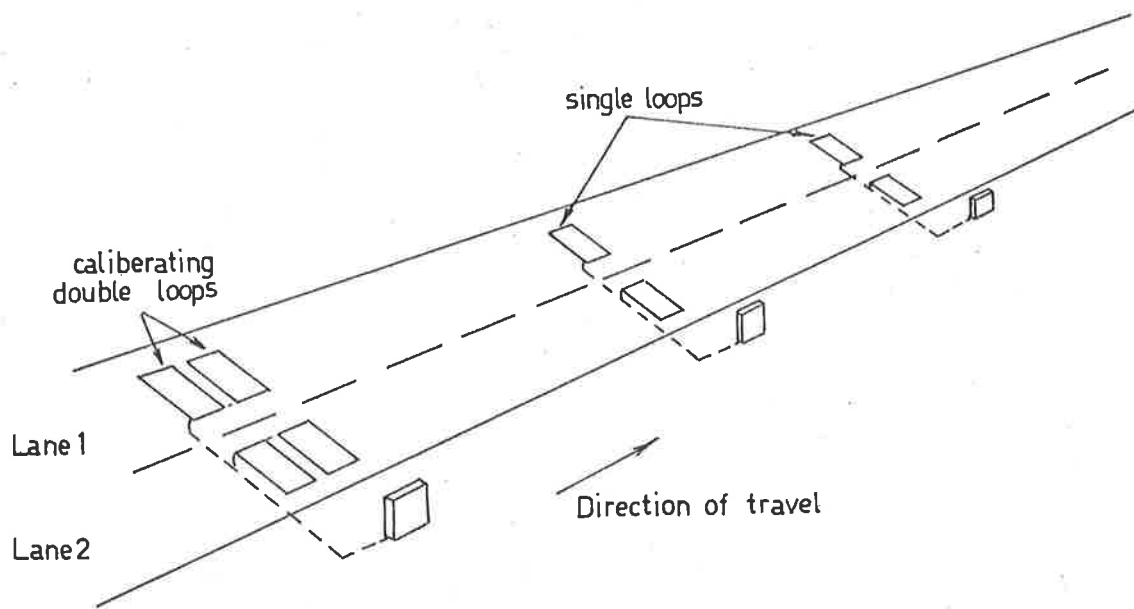


Fig. 2.12 Physical Layout of Double Calibrating Loops followed by Single Loops for Speed and Length Measurements

The main difficulty encountered with this approach is that of vehicles changing lane after the calibration points.

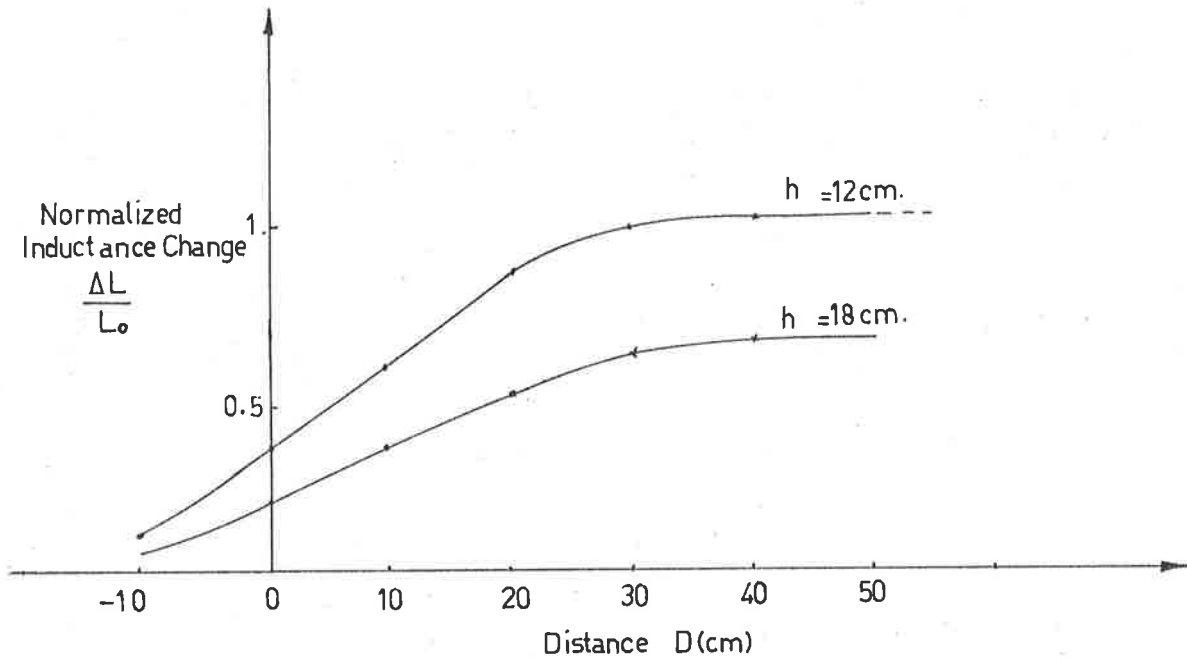
2.5 DISCRIMINATION

The sinusoidal signal associated with the inductive loop produces a magnetic field, the effective size of which is slightly larger than the loop length l_d . This is demonstrated in Fig. 2.13 where the change in inductance L_c is plotted as a function of the distance (D) of a steel plate from the inductive loop. The modified loop length l_p can be expressed as

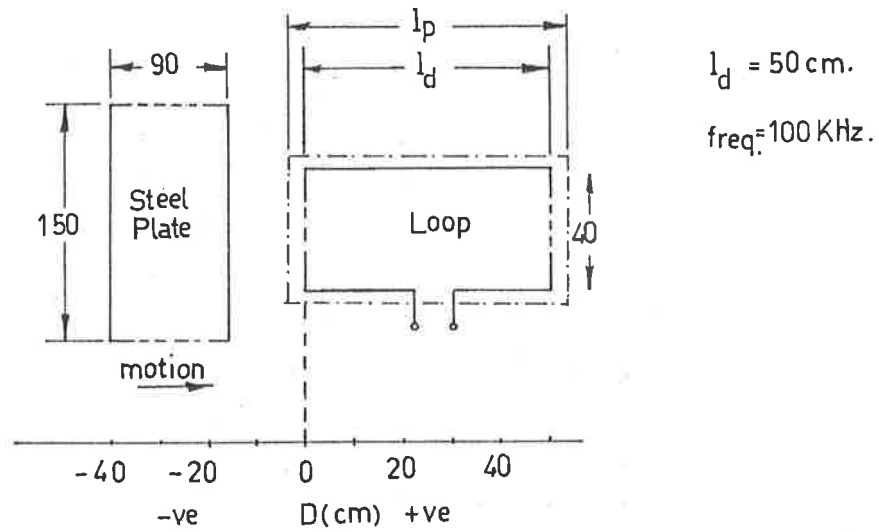
$$l_p = l_d + l_e \quad \dots(2.12)$$

where l_e is found to be in the range of 20cm - 80cm, and is dependant on such factors as the number of turns, height and vehicle characteristics.⁵⁰

The vehicle spacing (expressed in terms of time) is variable with volume and in 90 percent of the cases, is greater than one second.⁶⁵ Therefore, the output of the inductive loop provides an accurate indication of the vehicle count for most of the traffic conditions. However during a traffic jam, the spacing between vehicles becomes comparable with the modified loop length l_p which may result in the loop being occupied by two vehicles simultaneously, thus giving an incorrect count output.



(a)



(b)

Fig. 2.13 Inductive Loop Characteristics

(a) Normalized impedance change as a function of approach distance D

(b) Physical Layout

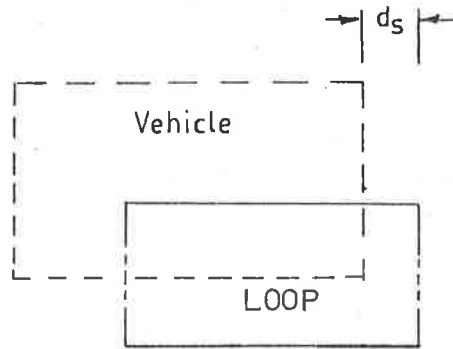
2.6 CLASSIFICATION

Thilo and Drebing⁶⁴ used the vehicle length and the undercarriage height as the criteria for vehicle classification. The length was measured using double loops, while the undercarriage height was estimated from measurement of the maximum value of the change in the inductance of the loop. In this way they were able to provide a rough indication of the classification, such as sedans, trucks or commercial vehicles.

The main drawback is with vehicles which cover only part of the loop. Fig. 2.14 indicates⁶⁴ a typical inductance change of a loop as a function of height for several vehicle displacement values. Thus partial coverage of the loop results in inaccurate height estimation which leads to wrong classification. Problems are also encountered when magnitude of transmitted signal is varied due to environmental changes.

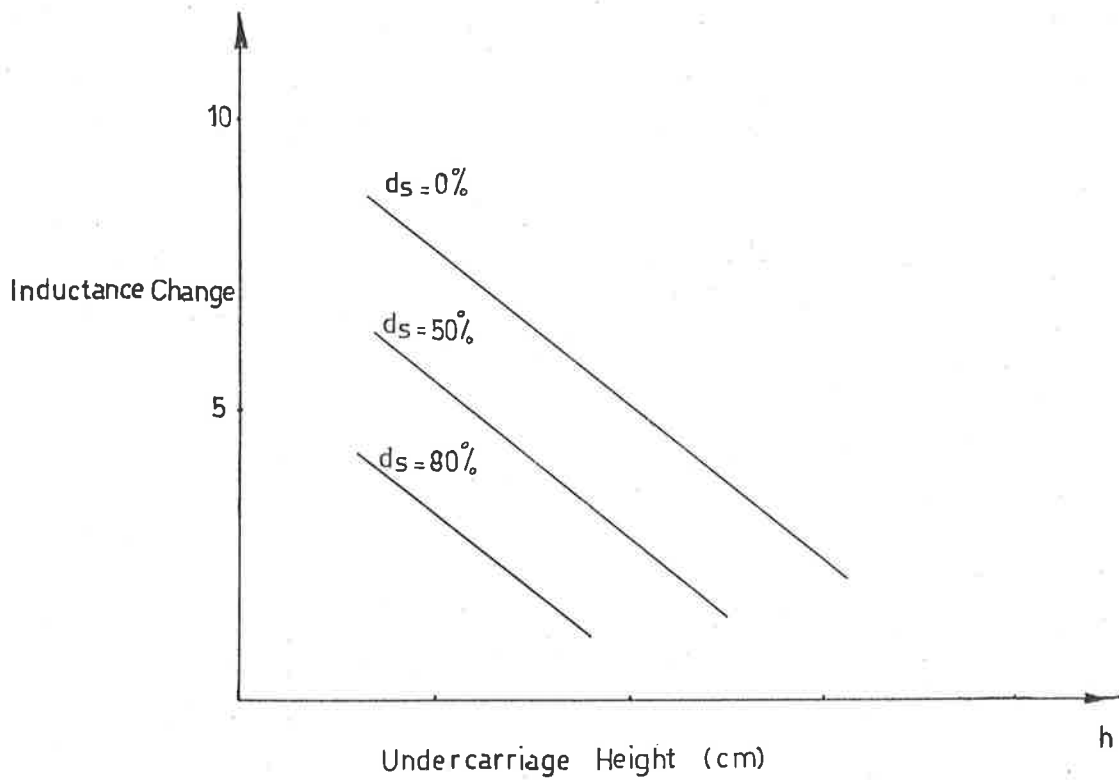
2.7 CONCLUSIONS

From the discussions so far, it is apparent that the vehicle detectors available commercially do not fulfil the requirements of the modern traffic monitoring systems specified in Table 2.1. The obvious installation problems associated with the overhead vehicle sensors make their application less attractive than



d_s = Vehicle lateral displacement

(a)



(b)

Fig. 2.14 Typical Inductance Change as a Function of Undercarriage Height h for several Values of Vehicle Lateral Displacement

(a) Physical Layout

(b) Characteristics

those installed in the road surface. The ability of a detector to discriminate between closely following vehicles and vehicles in the adjacent lanes is also an essential factor which requires careful consideration. The dimensions of the sensor also need attention in order to avoid the weakening of the road surface structure.

Finally, from economics consideration of traffic systems, it is desirable to have only one sensor per lane to obtain the relevant traffic data such as count, status, speed and identification.

CHAPTER 3

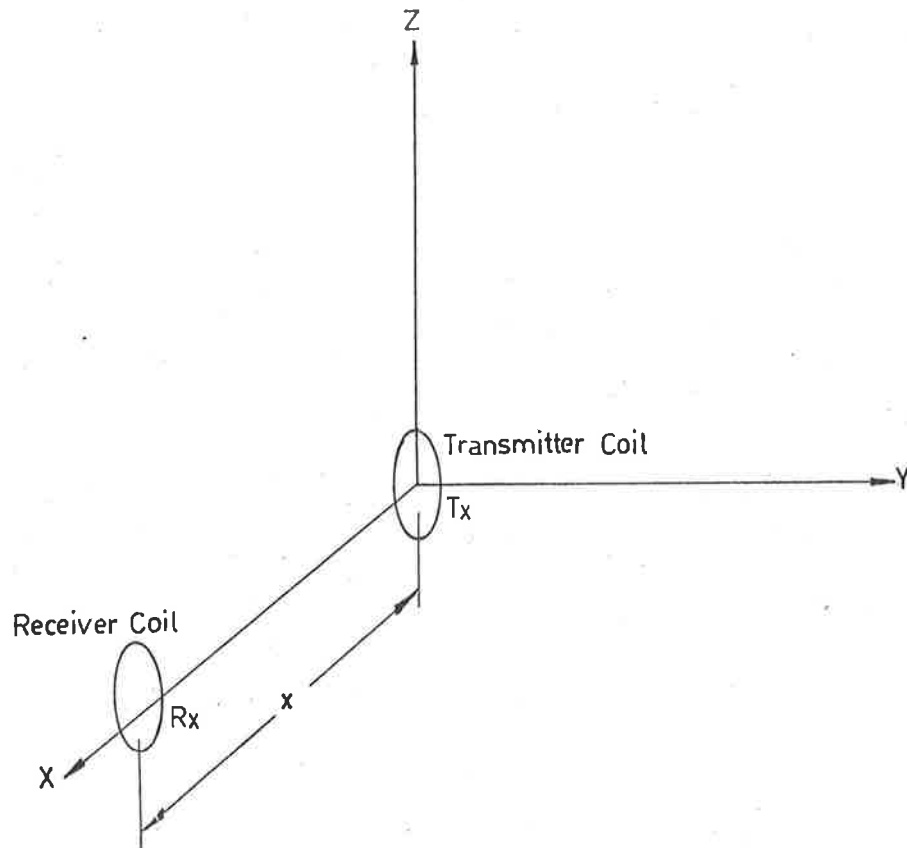
COUPLED COILS DETECTION TECHNIQUE

3.1 INTRODUCTION

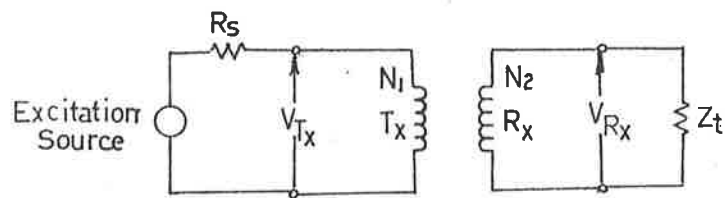
The requirements of the modern traffic monitoring systems in conjunction with analysis of the various vehicle detectors, as discussed in previous chapters, provided the basis for the development of a vehicle sensor using coupled coils.⁶⁶⁻⁶⁷ This technique was adopted because of the simplicity of construction.

In this arrangement two coils are spaced apart with a common axis. One coil (T_x) is energized by a time-varying current source, resulting in an induced voltage in the second coil (R_x). The geometry of the coils and the equivalent circuit is shown in Fig. 3.1.

When the coils are placed in the proximity of a conducting material, eddy currents are induced in that material.^{65,68} The magnetic field created by these currents is in opposition to the applied field and hence the average field in the conductor can be approximated to the value of the applied magnetic field. This results in a change in the induced voltage in the receiver, an analytical solution to which may be obtained using the method of images.



(a)



(b)

Fig. 3.1 Coupled Coils Detector
 (a) Co-ordinate system definition
 (b) Equivalent circuit

3.2 DERIVATION OF THE INDUCED VOLTAGE IN THE RECEIVER COIL IN THE PROXIMITY OF A CONDUCTING SURFACE⁶⁹

The induced voltage in the receiver coil R_x in the presence of an interface, can be derived by considering the interface as an infinite conducting plane. The change in the induced voltage can then be represented in terms of an image coil situated at $Z = 2h$. The geometry of the co-ordinate system used is shown in Fig. 3.2.

The components of the magnetic flux density⁷⁰ from Appendix I is found from the magnetic vector potential \bar{A} . Thus

$$\nabla \times \bar{A} = \bar{B} \quad \dots(3.1)$$

giving

$$B_r = \left(\frac{\mu N I A_c}{2 \pi r^3} \right) \cos \theta \quad \dots(3.2)$$

$$B_\theta = \left(\frac{\mu N I A_c}{4 \pi r^3} \right) \sin \theta \quad \dots(3.3)$$

$$B_\phi = 0 \quad \dots(3.4)$$

Now we can obtain directly the magnetic field components H_r and H_θ from the relation

$$\bar{B} = \mu \bar{H} \quad \dots(3.5)$$

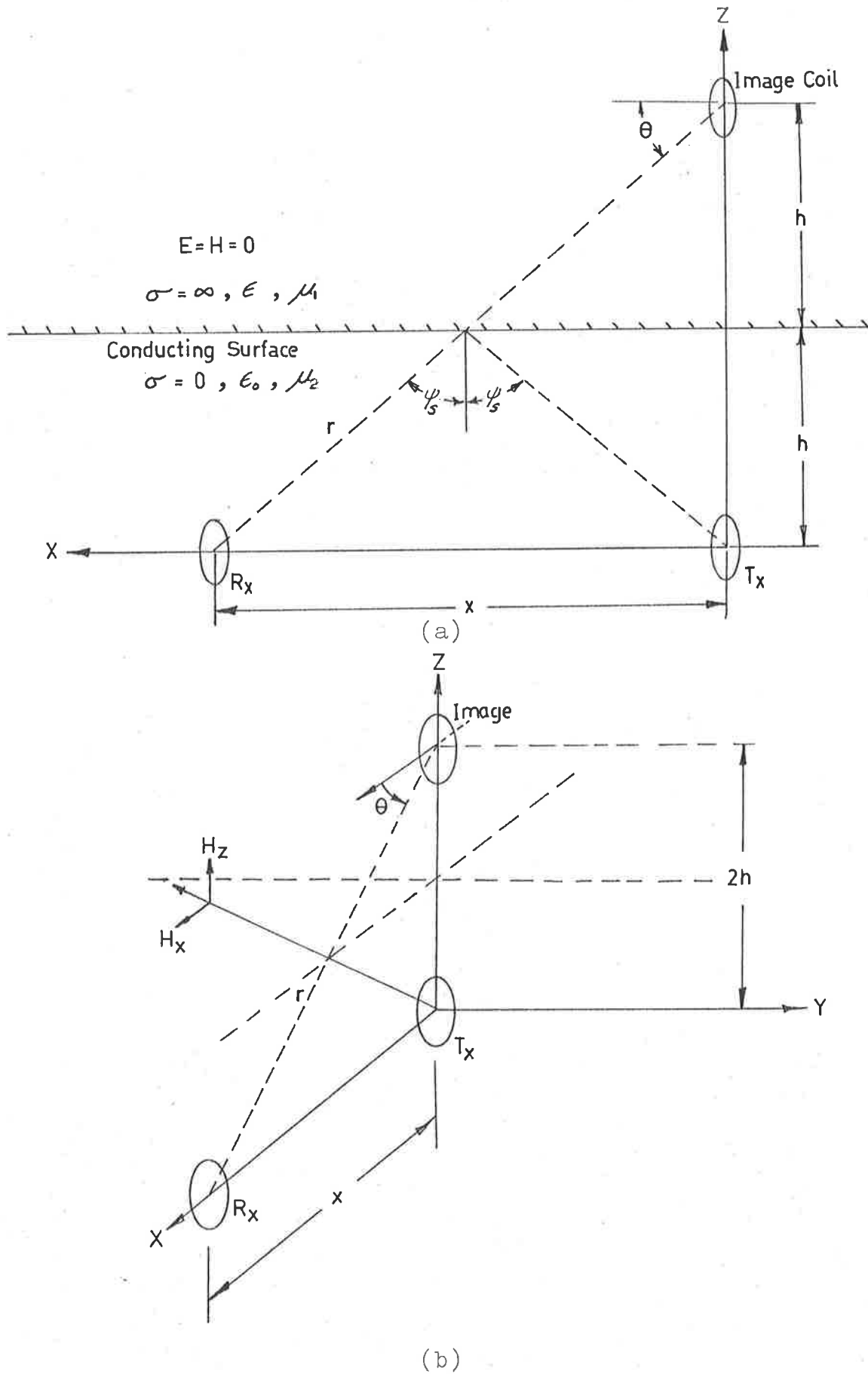


Fig. 3.2 Geometry of Co-ordinate System
 (a) in terms of XZ plane
 (b) in terms of XYZ axis

The x component of the magnetic field as shown in Fig. 3.2 can be written as

$$H_x = H_r \cos \theta - H_\theta \sin \theta \quad \dots(3.6)$$

Substituting equations (3.2), (3.3) and (3.5) in equation (3.6) we obtain the magnetic field at the receiver coil, written as

$$H_x = \frac{m}{4\pi r^3} (3\cos^2 \theta - 1) \quad \dots(3.7)$$

where

$$m = NIA_c \mu_r \quad \dots(3.8)$$

A_c = area of coil with radius a

Here μ_r is used as an effective permeability when a ferrite rod is introduced into the coil. The value of μ_r depends on the material, geometry and permeability. For coils of ellipsoidal shape it can be obtained using the theory of demagnetization factor⁸⁹. For practical geometry empirical determination is more appropriate.

From Fig. 3.2

$$\cos \theta = \frac{x}{r} \quad \dots(3.9)$$

and

$$r = \sqrt{(4h^2 + x^2)} \quad \dots(3.10)$$

Thus, the magnetic field H_{xt} due to the transmitter coil is

$$H_{xt} = \frac{m}{2\pi x^3} \quad \dots(3.11)$$

Here we have assumed that

$$a \ll x \quad \dots(3.12)$$

where

a = radius of coil

Similarly, the field H_{xi} at the receiver coil due to the image is

$$H_{xi} = \frac{m}{2\pi} \cdot \frac{x^2 - 2h^2}{[4h^2 + x^2]^{\frac{5}{2}}} \quad \dots(3.13)$$

The induced voltage V in a coil in terms of the magnetic vector \vec{A} is defined by

$$V = -\frac{\partial}{\partial t} \oint_C \vec{A} \cdot d\vec{l} \quad \dots(3.14)$$

$$= -\frac{\partial}{\partial t} \oint_S \vec{B} \cdot d\vec{S} \quad \dots(3.15)$$

$$= -j\omega A_c \mu H \quad \dots(3.16)$$

where S is any surface with C as its boundary and element $d\vec{l}$.

For a loop having N turns, Eq. (3.16) is modified to

$$V = -j\omega N A_c \mu H \quad \dots(3.17)$$

Therefore from Eq. (3.11) and Eq. (3.17) the induced voltage in the receiver coil due to the transmitter coil is

$$V_{R_x} = \frac{K_i}{2\pi} \left(\frac{1}{x^3} \right) \quad \dots(3.18)$$

where

$$K_i = N A_c w \mu_m \dots(3.19)$$

and

μ_o = permeability of free space

Similarly the induced voltage V_p in the receiver coil due to the image coil from Eq. (3.13) and Eq. (3.17) can be expressed as

$$V_p = \frac{K_i}{2\pi} \left(\frac{x^2 - 2h^2}{[4h^2 + x^2]^{5/2}} \right) \dots(3.20)$$

The resultant induced voltage V_R in the receiver coil is given by

$$V_R = V_{R_x} + V_p \dots(3.21)$$

$$= \frac{K_i}{2\pi} \left(\frac{1}{x^3} + \frac{(x^2 - 2h^2)}{[4h^2 + x^2]^{5/2}} \right) \dots(3.22)$$

The important factor associated with Eq. (3.21) is that only V_p in the expression conveys any useful information. Therefore the main task is to examine the behaviour of V_p as a function of various external parameters such as coil spacing x , interface height h , induced voltage V_{R_x} and the effect of interface conductivity.

3.3 BEHAVIOUR OF IMAGE VOLTAGE AS A FUNCTION OF COIL SPACING AND INTERFACE HEIGHT

The change V_p in the induced voltage V_R in the receiver coil due to the presence of a conducting plate defined by Eq. (3.20) is shown in Fig. 3.3, as a function of interface height h for several values of coil separation x . The numerator of Eq.(3.20) provides the basis for an important relationship between x and h which can be written in terms of an inequality

$$x > (2)^{\frac{1}{2}} \cdot h \quad \dots(3.23)$$

The constraint defined by Eq. (3.23) ensures that the magnitude of the image voltage V_p is positive for ease of processing.

3.4 THE EFFECT OF FINITE CONDUCTIVITY OF THE INTERFACE ON THE IMAGE VOLTAGE

The model defined by Eq. (3.20) to describe the change in the induced voltage V_p in the receiver coil is based on the assumption that the interface is a perfect electrical conductor, (i.e. $\sigma = \infty$). However in practice we do not have perfect conductors, but the materials we are concerned with such as aluminium and steel have large conductivities, so that at relatively high frequencies, negligible error is made if the dimensions of the conductors are made large,

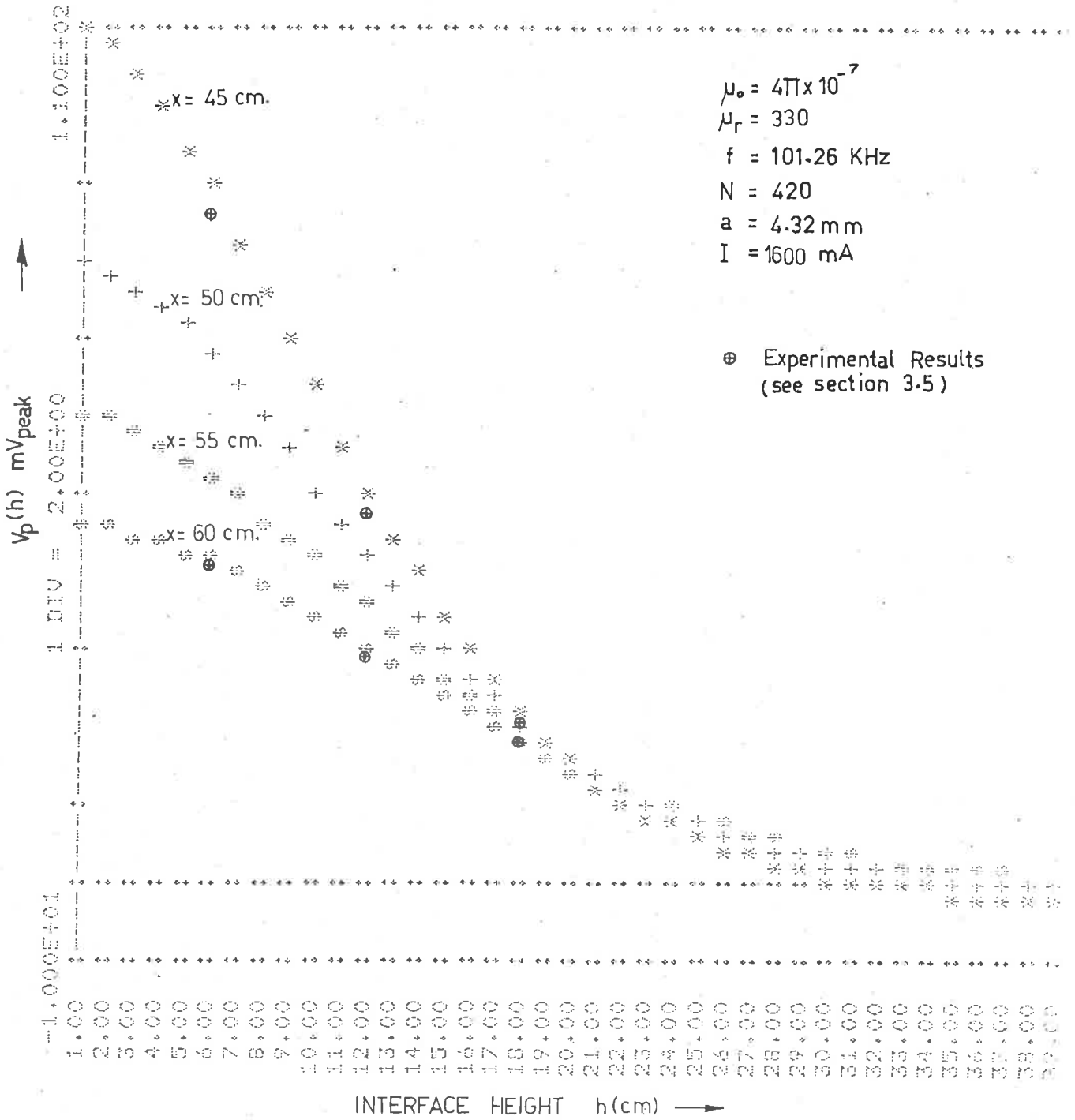


Fig. 3.3 Change in the Induced Voltage $V_p(h)$ in the receiver coil R_x as a Function of Height 'h' for various coil spacings 'x'.

compared with the skin depth δ_s . Here by high frequency we mean one that yields a value of skin depth that is small compared with the conductor dimensions. The skin depth⁵⁴ can be expressed as

$$\delta_s = \left[\frac{1}{\pi \sigma \mu f} \right]^{\frac{1}{2}} \quad (\text{meter}) \quad \dots(3.24)$$

where

σ = conductivity of material (mohs/meter)

μ = permeability of material

and can be defined as the distance the wave propagates in order to decay by an amount e^{-1} . Therefore as σ tends to infinity, δ_s approaches zero. This implies that the time-varying electromagnetic field decays infinitely fast and cannot penetrate the conductor. Fig. 3.4 shows the skin depths δ_s for steel and aluminium as a function of frequency. The conductor can be shown to be characterised as a boundary surface exhibiting a surface impedance the resistive⁶² part of which is given by

$$R_s = \frac{1}{\delta_s \sigma} \text{ ohm/square} \quad \dots(3.25)$$

For aluminium and steel (304) at 100KHz the values are 9.3×10^{-5} ohm and 4.8×10^{-4} ohm respectively. For reasonably good conductor, R_s is small and for all practical purposes the field in front of the conductor is the same as would exist if σ were infinite.

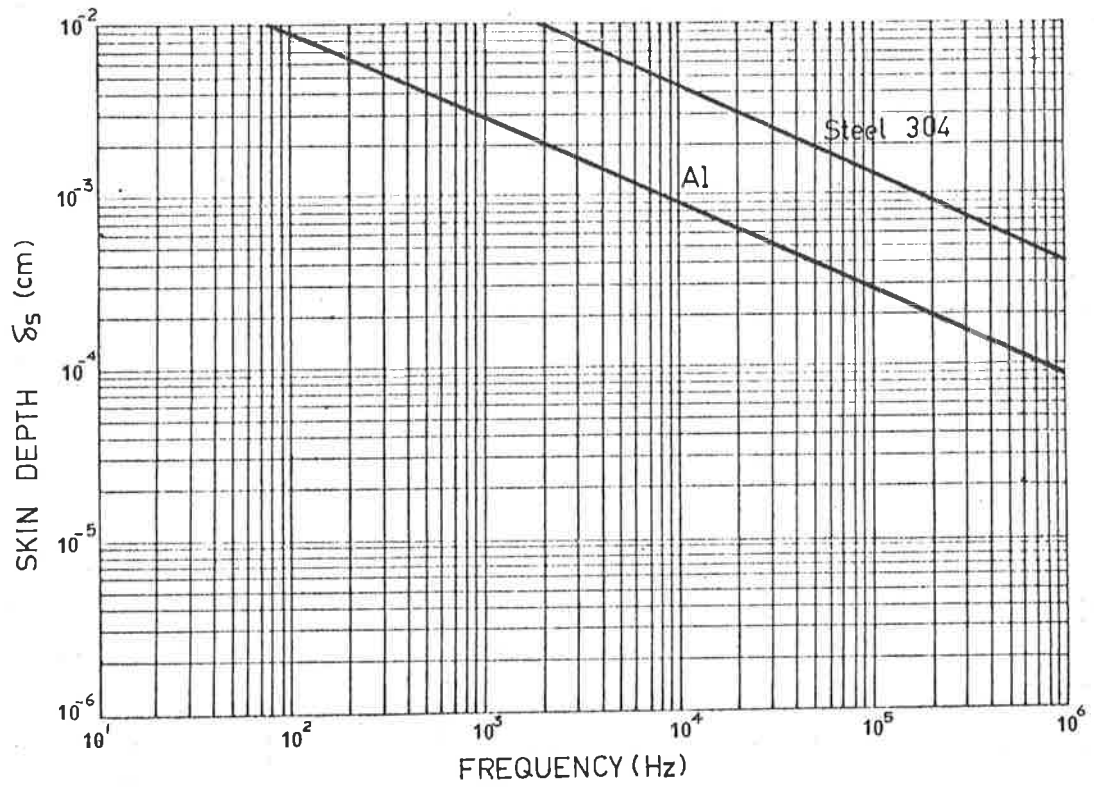


Fig. 3.4 Skin Depth for Aluminium and Steel Plate Conductors

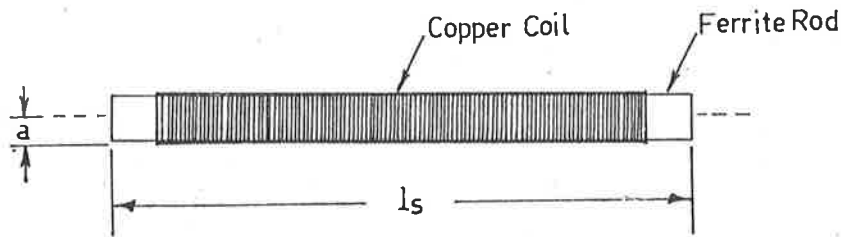
3.5 EXPERIMENTAL EVALUATION

To substantiate the theoretical approximations under the assumed ideal conditions, an experimental sensor as illustrated in Fig. 3.5, was developed. A test set-up, which consisted of a wooden frame with adjustable guide rails as shown in Fig. 3.6, was constructed. Two metal plates (aluminium and steel) having different conductivities were used. The resultant characteristics of the plates are shown in Table 3.1.

3.5.1 Magnitude of Image Voltage

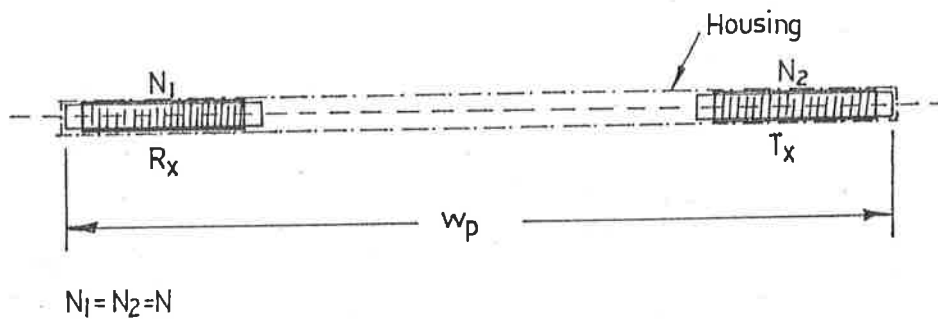
The induced voltage V_{R_x} was initially set to a predetermined value by controlling the current in the transmitter coil. A horizontal plate was then introduced above the sensor and the value of V_p (mV) was noted as a function of height h (cm) for three values of induced voltage V_{R_x} (mV). The experimental results are shown in Table 3.2 for two values of coil spacing x .

The computed results for $V_{R_x} = 500\text{mV}$ obtained from Fig. 3.3 are also included for comparison. The computed values are in agreement with those obtained experimentally for both aluminium and steel plates.



Ferrite	:	4302 020 35401 (Philips Elcoma)
μ_r	:	330
N	:	420 turns polyester wire 206-170
a	:	4.32 mm
r_w	:	0.2 mm

(a)



(b)

Fig. 3.5 Sensor

(a) Coil

(b) Relationship between T_x and R_x

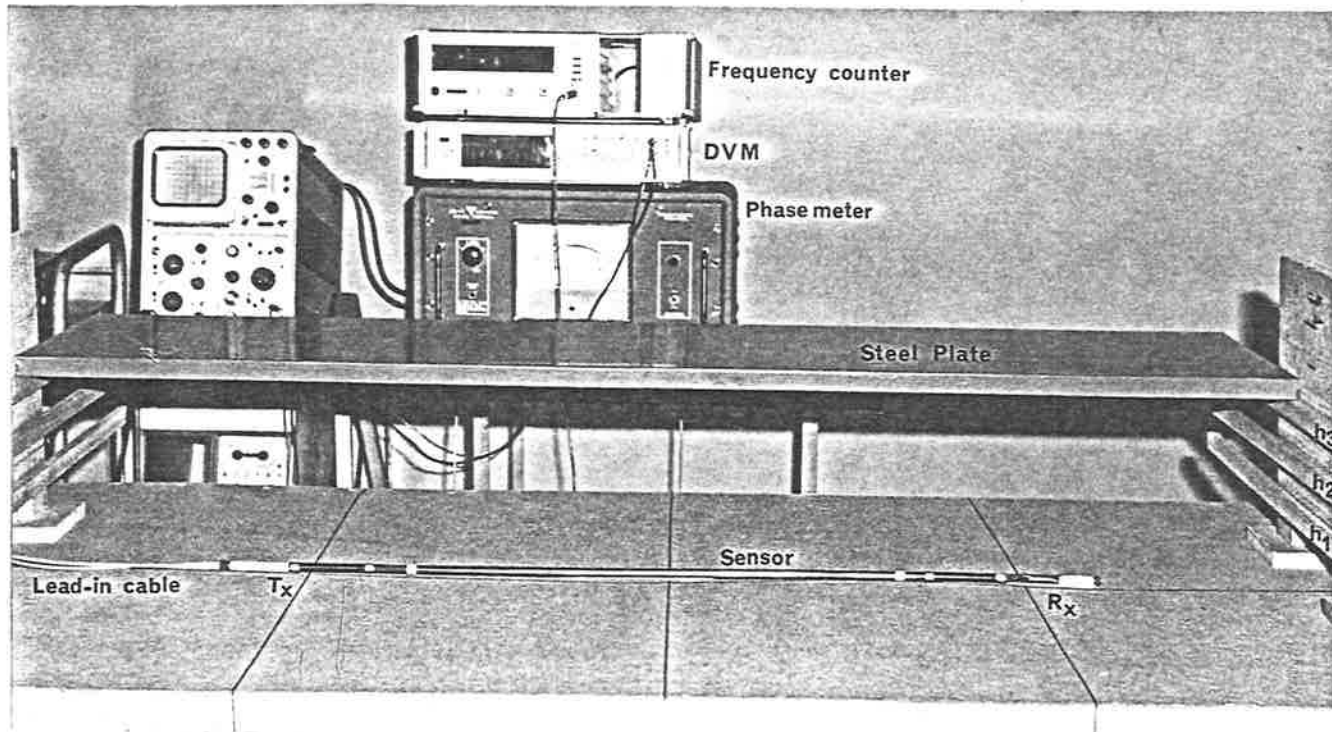


Fig. 3.6 Test Set-up for Measurement of V_p

	μ_r	σ (moh/m)	δ_s (metre)
Al	1.00002	3.72×10^7	2.9×10^{-4}
304 Steel	1.02	1.39×10^6	1.5×10^{-3}

(a)

	x_p cm	y_p cm	t_h mm
Al	150	42	2.5
304 Steel	150	42	2.0

(b)

	x_p cm	y_p cm	t_h mm
Al	90	42	2.5
304 Steel	90	42	2.0

(c)

Table 3.1 Plate Characteristics

- (a) Electrical and magnetic characteristics
- (b) Dimensions of set a
- (c) Dimensions of set b

V_{R_x} (mV) h (cm)	100	250	500		
			Experiment	Computed	Error *
6	18.7	46.2	86.7	90.0	3.30
12	9.3	25.0	47.7	50.8	3.60
18	3.8	11.7	20.4	21.9	1.50

(a)

V_{R_x} (mV) h (cm)	100	250	500		
			Experiment	Computed	Error *
6	7.9	21.6	40.1	41.5	1.40
12	5.7	14.7	28.1	29.7	1.60
18	3.1	8.6	16.8	17.8	1.00

(b)

Table 3.2 Image Voltage Characteristics V_p as a function of h (cm) V_{R_x} (mV)

(a) $x = 45$ cm(b) $x = 60$ cm

* Error = (Computed - Experimental)

3.5.2 Ratio Test

The values of V_p obtained experimentally as shown in Table 3.2 are used to obtain a ratio $R_{h_{1,n}}$ defined by

$$R_{h_{1,n}} = \frac{V_{p_1}}{V_{p_{n+1}}} \quad n = 1, 2, 3, \dots (3.26)$$

where

V_{p_1} = image voltage with interface height set to h_1

$V_{p_{n+1}}$ = image voltage with interface height set to h_{n+1}

Values for $R_{h_{1,n}}$ are illustrated in Table 3.3 for three values of V_{R_x} and two coil spacings. The experimental and computed results are in close agreement for V_{R_x} set at 500mV.

The notable feature of $R_{h_{1,n}}$ is its constancy with variations of V_{R_x} which is consistent with Eq.(3.20) when different values of h are used.

$h_{1,n} \backslash V_{R_x} \text{ (mV)}$	100	250	500		
			Experiment	Computed	Error *
$n = 2$	2.01	1.85	1.82	1.77	-0.05
$n = 3$	4.92	3.95	4.15	4.11	-0.04

(a)

$h_{1,n} \backslash V_{R_x} \text{ (mV)}$	100	250	500		
			Experiment	Computed	Error *
$n = 2$	1.39	1.47	1.43	1.40	-0.03
$n = 3$	2.55	2.51	2.39	2.33	-0.06

(b)

Table 3.3 Values $R_{h_{m,n}}$ as a Function of V_{R_x} (a) $x = 45\text{cm}$ (b) $x = 60\text{cm}$

* Error = (Computed - Experimental)

3.6 CONCLUSIONS

The modelling technique adopted for the representation of the change in the induced voltage in the receiver coil due to the presence of a conducting surface has provided results which are in agreement with those obtained experimentally. The model has further provided a suitable means for establishing a relationship between the sensor length and the sensor to interface spacing. This is an important factor when variations in the undercarriage of the various vehicles are considered.*

The similarity of the experimental results obtained when using aluminium and steel plates having different conductivities, is not surprising. This is mainly due to the surface resistivity of the two materials which are in the same order.

Although at first sight the flat conducting surface shows little resemblance to the complex nature of the vehicle's undercarriage, the assumption serves as a suitable means to explore the behaviour of the change in induced voltage in terms of the changes in the various parameters encountered in practice.

* Examination of the undercarriage associated with 76 different vehicles indicated a range of 15cm to 65cm. Only 10% of the vehicles considered had values which exceeded 30cm.

CHAPTER 4

IMAGE VOLTAGE BEHAVIOUR AS A FUNCTION OF DISTANCE FROM A MOVING PLATE

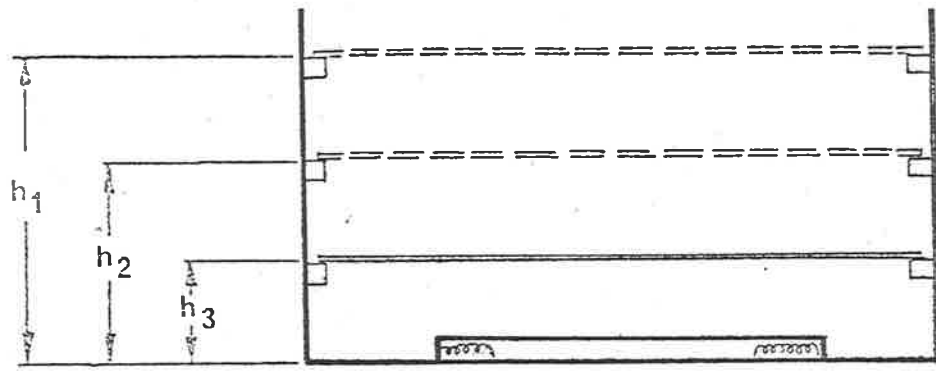
4.1 EXPERIMENTAL HARDWARE

To explore the existence of any notable feature associated with the image voltage V_p , the test set up described in section 3.5 was modified such that the motion of a plate over the sensor could be controlled in both the horizontal and the vertical planes.

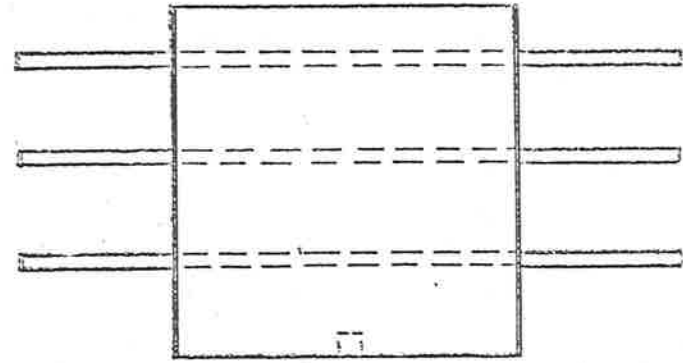
The distance D between the sensor and the plate as shown in Fig. 4.1 was assigned a negative value for an approaching plate while a receding plate was given a positive value.

The transmitter coil T_x was energized by a 100KHz time-varying current source, while the output of the receiver was monitored as a steel plate approached the sensor.

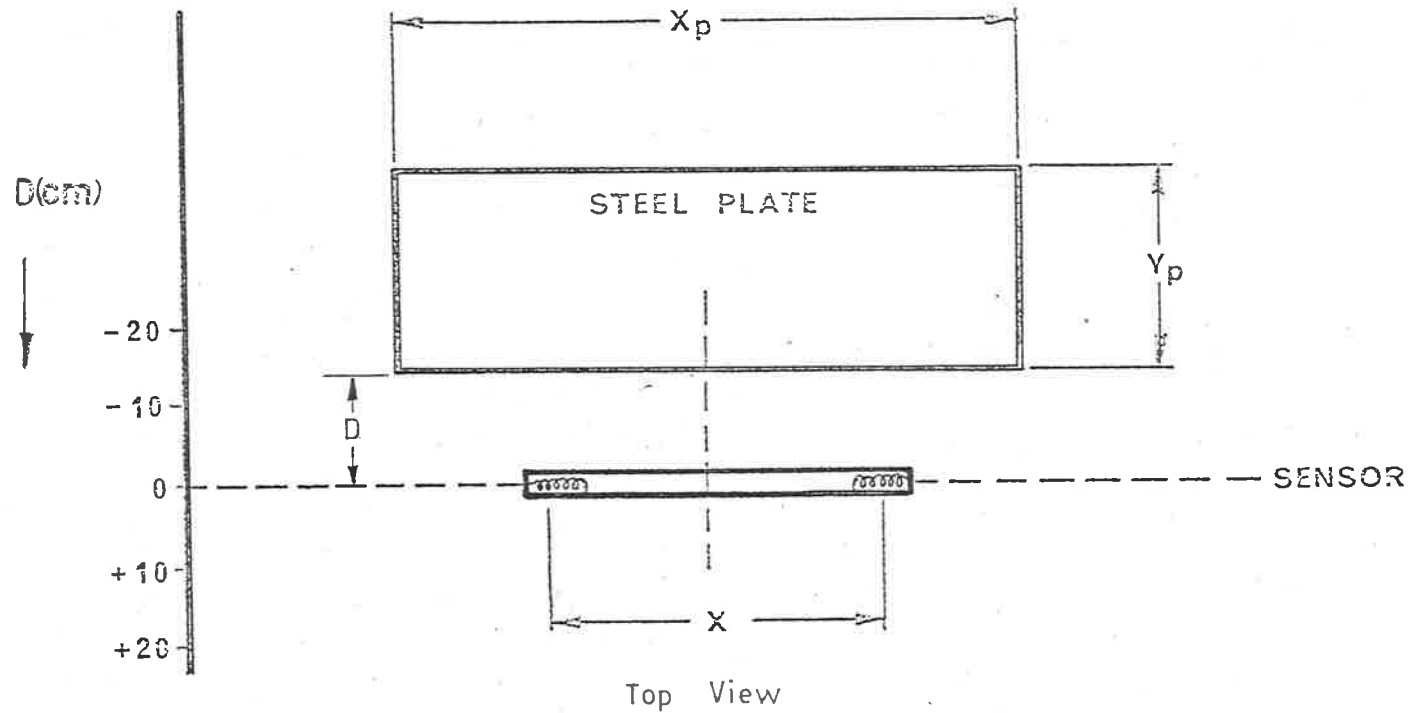
Fig. 4.2 shows the image voltage characteristics V_p as a function of the distance $D(\text{cm})$ for a horizontal steel plate, for several values of plate height $h(\text{cm})$ and initial induced voltage (V_{R_x}).



Front View

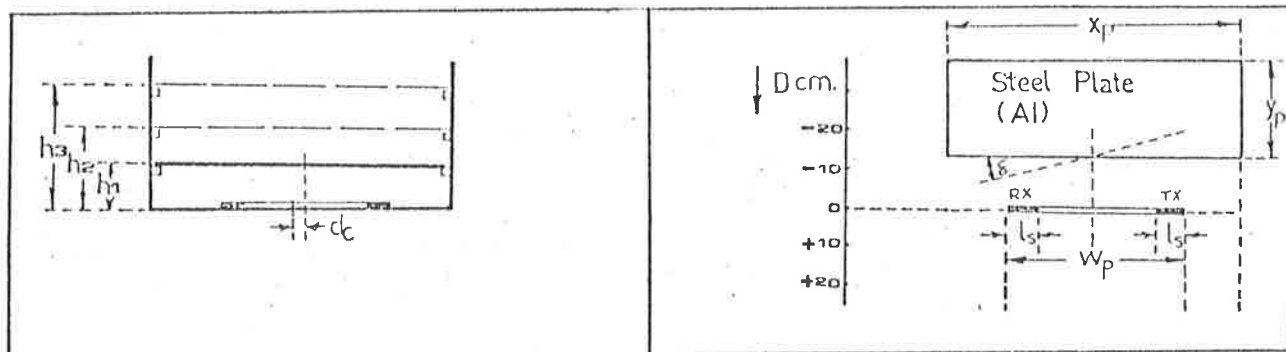


Side View



Top View

Fig. 4.1 Relationship between the Sensor and the Steel Plate



TEST CONDITION		Ref:		Freq. = 100 khz.		
$h_1 = 6$ cm.	$d_c = 0$ cm.	$X_p = 150$ cm.	V _{RX} = 250 V _{pp} Sine			
$h_2 = 12$ cm.	$\xi = 0$ deg.	$Y_p = 42$ cm.	P ₁	P ₂	P ₃	
$h_3 = 18$ cm.	$W_p = 55$ cm.		22.34	23.07	23.40	
	$l_s = 10$ cm.		V _{p_{m1}} = 46.2	V _{p_{m2}} = 25.0	V _{p_{m3}} = 11.7	
			$\alpha_1 = 2.06$	$\alpha_2 = 1.08$	$\alpha_3 = 0.50$	

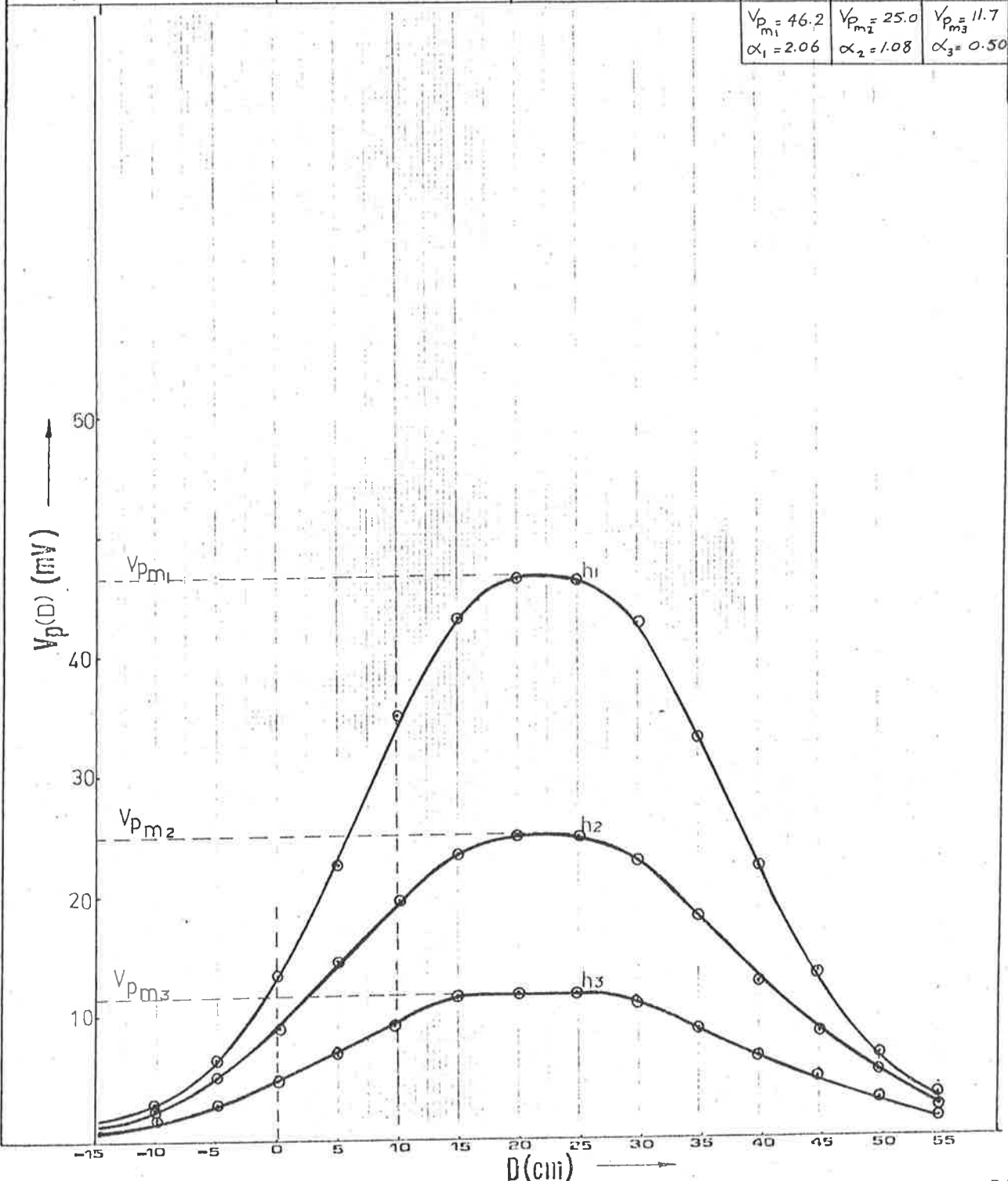
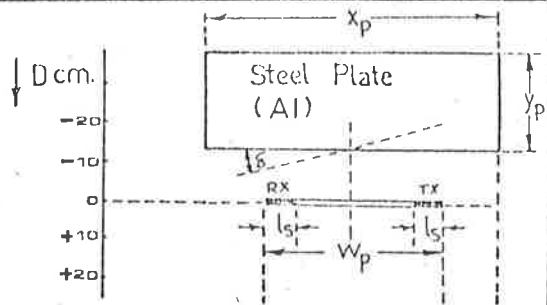
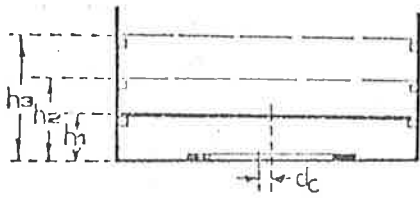


Fig. 4.2(a) Behaviour of the Image Voltage V_p (mV) as a Function of Distance D (cm) for several Values of Height h (cm) with $V_{Dx} = 250$ mV.



TEST CONDITION

Ref:

$h_1 = 6$ cm.
 $h_2 = 12$ cm.
 $h_3 = 18$ cm.

$d_c = 0$ cm.
 $\xi = 0$ deg.
 $w_p = 55$ cm.
 $l_s = 10$ cm.

$X_p = 150$ cm.
 $Y_p = 42$ cm.

Freq. = 100 kHz.
 $V_{RX} = 500 mV_{pp}$ Sine

P_1	P_2	P_3
21.96	24.37	24.70
$V_{P_{m1}} = 86.7$ $\alpha_1 = 3.94$	$V_{P_{m2}} = 47.7$ $\alpha_2 = 1.95$	$V_{P_{m3}} = 20.4$ $\alpha_3 = 0.83$

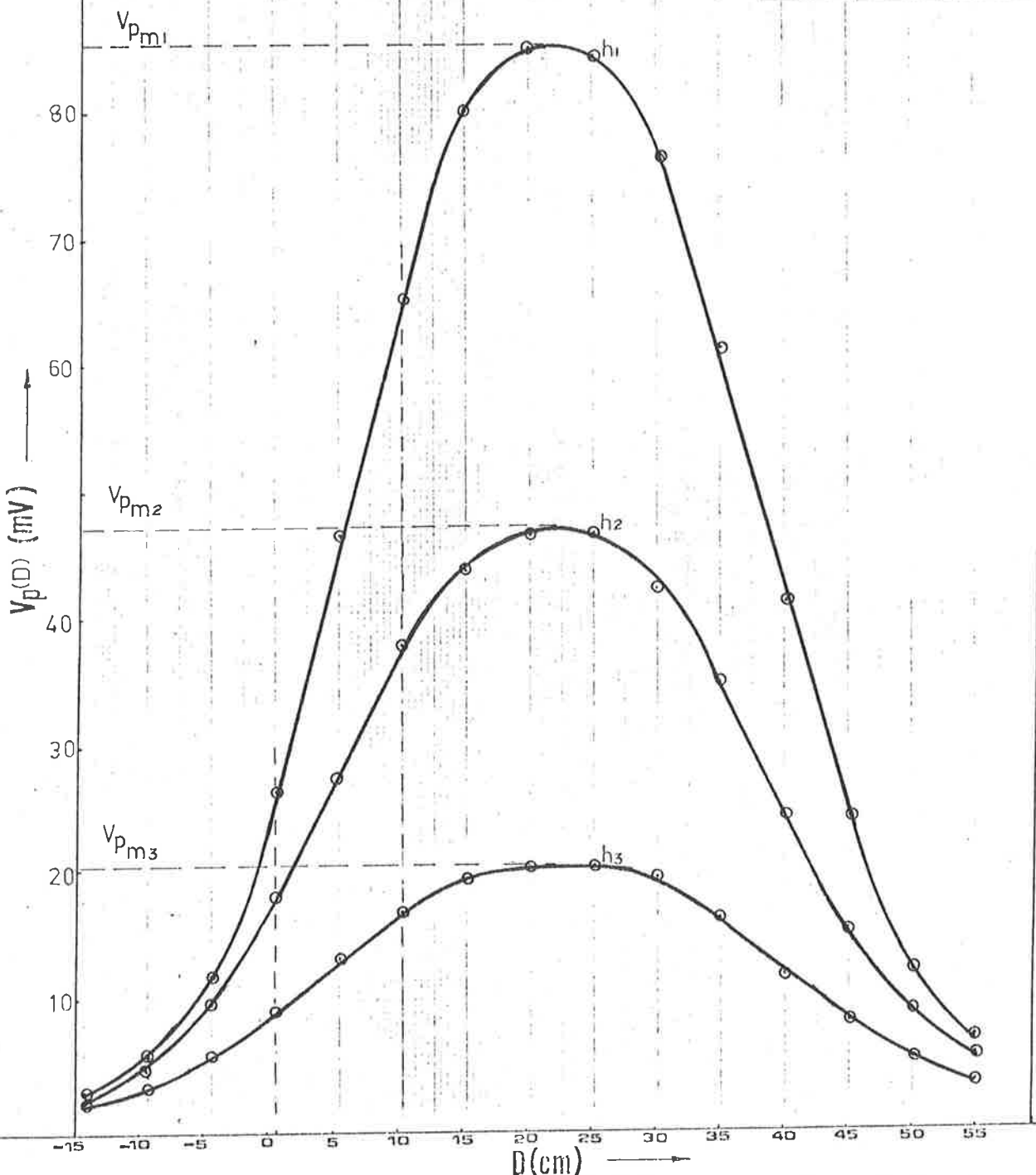


Fig. 4.2(b) Behaviour of the Image Voltage V_p (mV) as a Function of Distance D (cm) for several Values of Height h (cm) with $V_{R_v} = 500 mV$.

4.2 EXPERIMENTAL OBSERVATION

The image voltage characteristics shown in Fig. 4.2 were examined against several criteria. The similarity of the shape of the V_p and D curves shown in Fig. 4.2 provided the basis for the derivation of a parameter, the value of which was found to be independent of interface height h and the initial induced voltage V_{R_x} . This parameter is designated by P and is defined as

$$P = \frac{V_{p_m}}{\alpha} \quad \dots (4.1)$$

where

V_{p_m} = maximum value of image voltage

α = slope of the linear region of the V_p v D curves.

4.2.1 Derivation of P Using Linear Regression Technique

To obtain a straight line of best fit for the linear region of V_p versus D curves, the least-squares linear regression analysis was used.⁷¹ The modified slope α_m based on this method is given by

$$\alpha_m = r_c \left[\frac{\sigma_v}{\sigma_d} \right] \quad \dots (4.2)$$

where

r_c = correlation coefficient

and

σ_v^2 = variance of the V_p values

σ_d^2 = variance of the D values.

The value of P using the modified value of slope is

$$P = V_{p_m} \cdot \left[\frac{\sigma_d}{\sigma_v} \right] \cdot \frac{1}{r_c} \quad \dots(4.3)$$

Derivation of Eq. (4.2) and Eq. (4.3) are given in Appendix II.

Eq. (4.3) was used to obtain values of P as shown in Table 4.1 for several values of plate height h and induced voltage V_{R_x} , using the V_p versus D characteristics of Fig. 4.2

V_{R_x} (mV) h (cm)	250	500
6	22.34	21.96
12	23.07	24.37
18	23.40	24.70

Table 4.1 Values of P as a Function of Plate Height h(cm) and Induced Voltage V_{R_x} (mV).

4.3 MODELLING TECHNIQUE

Although several authors have provided various techniques for the derivation of the magnetic field associated with a coil carrying a time-varying current in the proximity of a conducting surface,⁷²⁻⁷³ no reporting has been noted regarding the characteristics of the magnetic field as a function of distance D. In the absence of such an analysis, a very primitive modelling technique based on a moving image concept, was developed. Due to the obvious short comings of the model, it is included in Appendix III purely as a possible guide for future work.

4.4 PHASE CHARACTERISTICS

The phase relationship between the transmitter and the receiver coils was also examined and found to be in quadrature. Since no new information was obtained from this examination, the phase characteristics were subsequently neglected

CHAPTER 5

EVALUATION OF PARAMETER P

5.1 INTRODUCTION

The experimental procedure developed in Chapter 4 was extended such that the behaviour of the image voltage V_p could be evaluated as a function of the approach angle θ_p and incline angle δ as illustrated in Fig. 5.1 for three different plates. The following structures in addition to actual vehicles, were considered.

- (i) horizontal aluminium and steel plates
- (ii) vertical aluminium and steel plates
- (iii) L-shaped aluminium and steel plates.

5.1.1 Horizontal Plate

The behaviour of the image voltage as a function of the distance for several parameter changes using a horizontal steel plate is as follows

- (i) Approach Angle δ

The V_p versus D characteristics as a function of distance D for three values of approach angle δ and

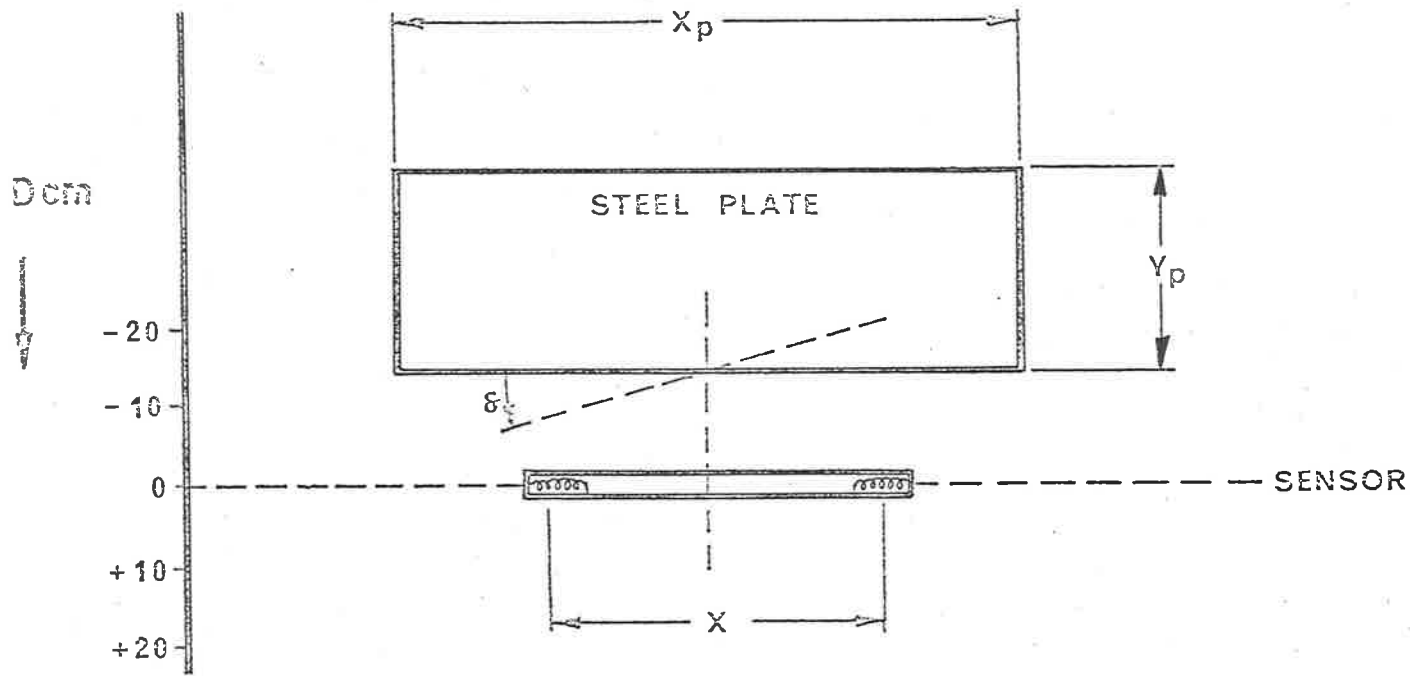
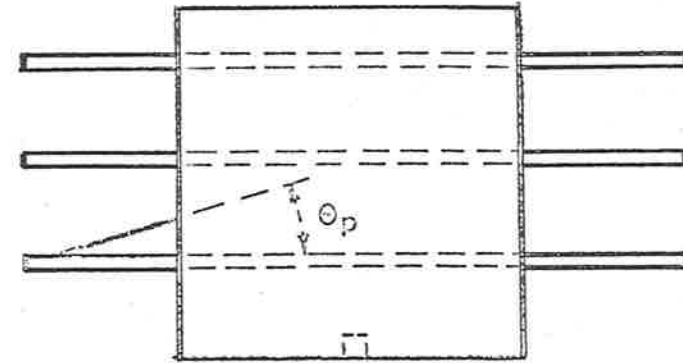
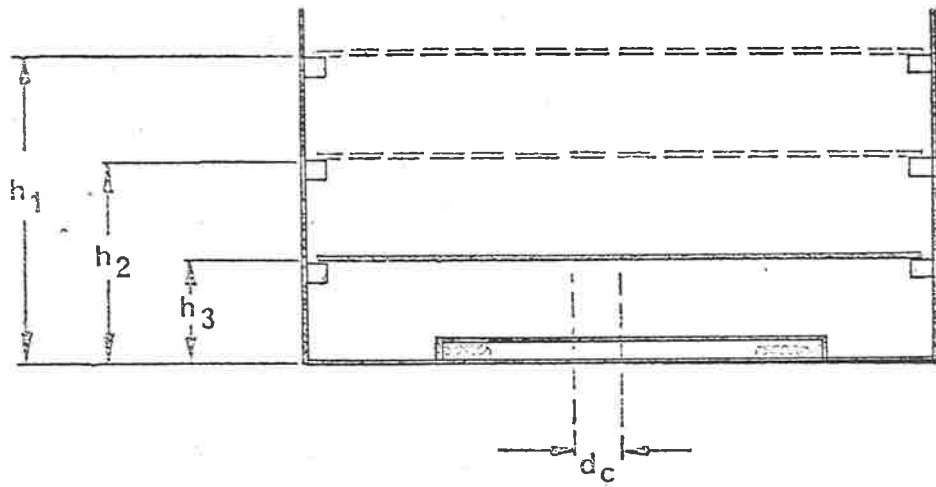


Fig. 5.1 Approach Angle δ and Incline Angle θ_p of Steel Plate in Relation to the Position of the Sensor

two values of induced voltage V_{R_x} are shown in Figures 5.2, 5.3 and 5.4. The respective values of P are indicated in Table 5.1.

(ii) Incline Angle θ_p

The V_p versus D characteristics as a function of distance D for three values of incline angle θ_p are shown in Figures 5.5, 5.6, 5.7 and 5.8. The respective values of P are tabulated in Table 5.2.

5.1.2 Vertical Plate

The image voltage V_p as a function of distance D for a vertical plate is shown in Fig. 5.9. The notable feature is that the magnitude of V_p is considerably smaller than that obtained using a horizontal plate. The value for V_p was found to be in the order of 15% of that obtained for a horizontal plate.

5.1.3 L - Shaped Plate

The V_p versus D characteristics as a function of approach angle δ for several values of induced voltage V_{R_x} are shown in Figures 5.10, 5.11, 5.12 and 5.13. Table 5.3 indicates the values of P for four values of V_{R_x} . Table 5.4 shows P as a function of approach angle δ .

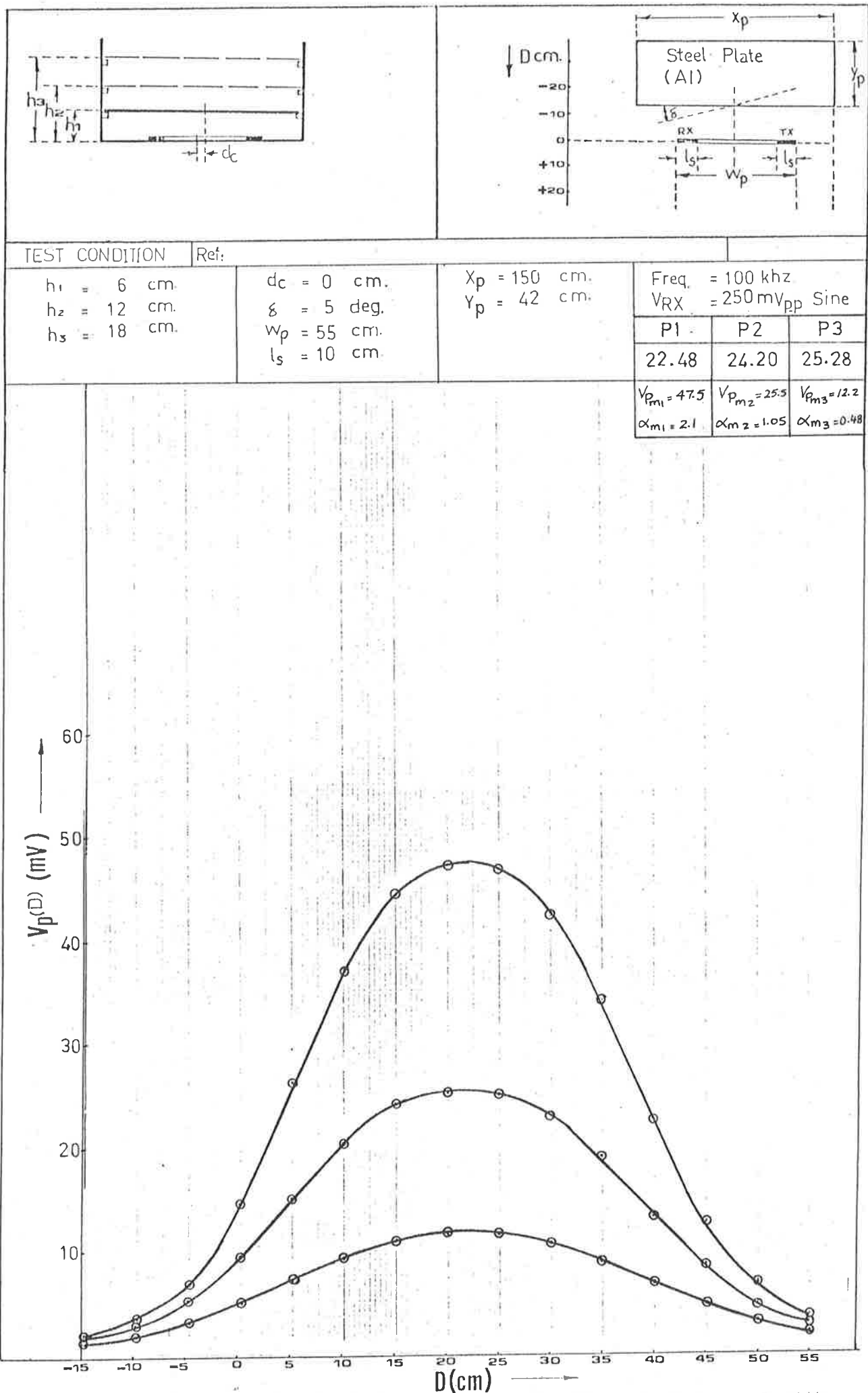


Fig. 5.2(a) Image Voltage Characteristic as a function of distance D with approach angle $\xi = 5$ deg. and $V_{RX} = 250$ mV.

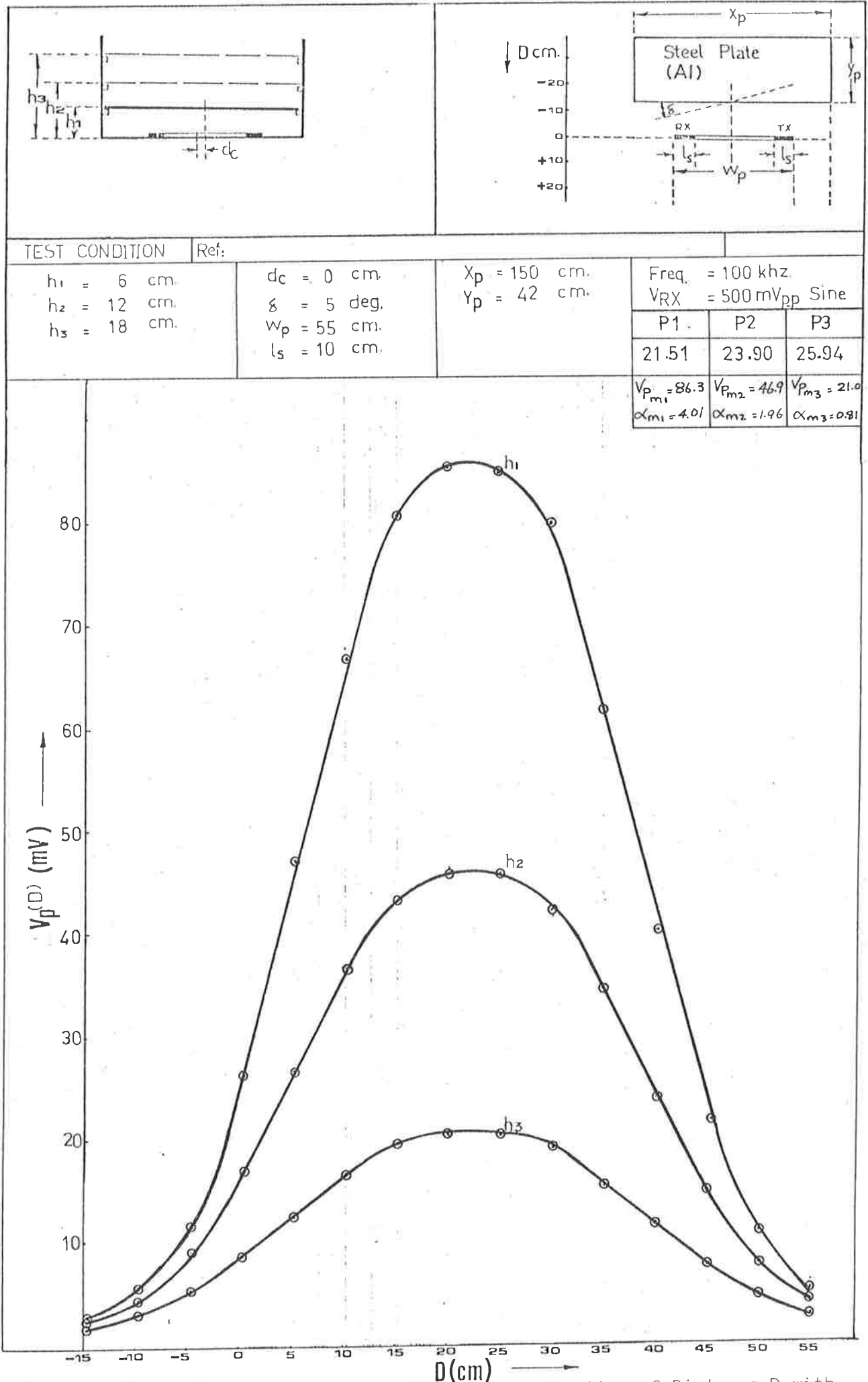
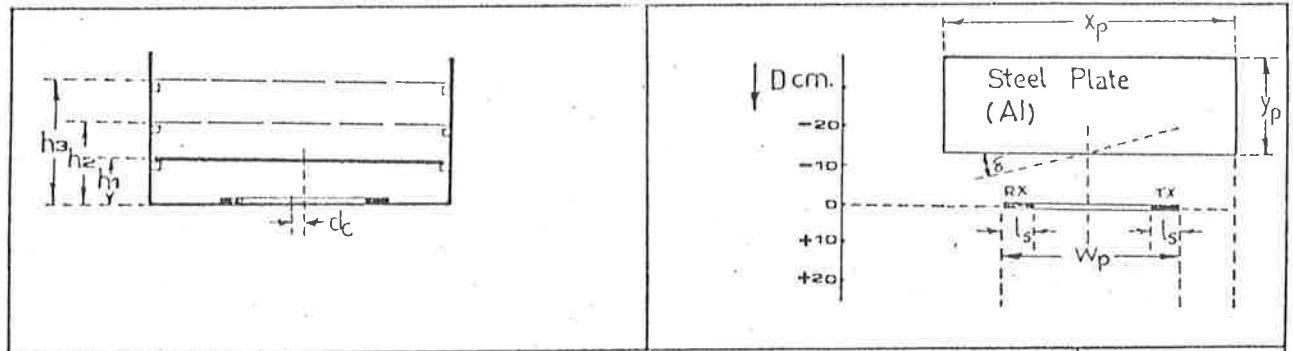


Fig. 5.2(b) Image Voltage Characteristics as a function of Distance D with Approach Angle $\delta = 5$ deg. and $V_{RX} = 500$ mV.



TEST CONDITION		Ref:			
$h_1 = 6$ cm.	$d_c = 0$ cm.	$X_p = 150$ cm.	Freq. = 100 kHz.		
$h_2 = 12$ cm.	$\delta = 10$ deg.	$Y_p = 42$ cm.	$V_{RX} = 250$ mV _{pp} Sine		
$h_3 = 18$ cm.	$W_p = 55$ cm.		P_1	P_2	P_3
	$l_s = 10$ cm.		20.96	22.80	26.20

$V_{P_{m1}} = 48.5$	$V_{P_{m2}} = 26.5$	$V_{P_{m3}} = 12.4$
$\alpha_{m1} = 2.31$	$\alpha_{m2} = 1.16$	$\alpha_{m3} = 0.47$

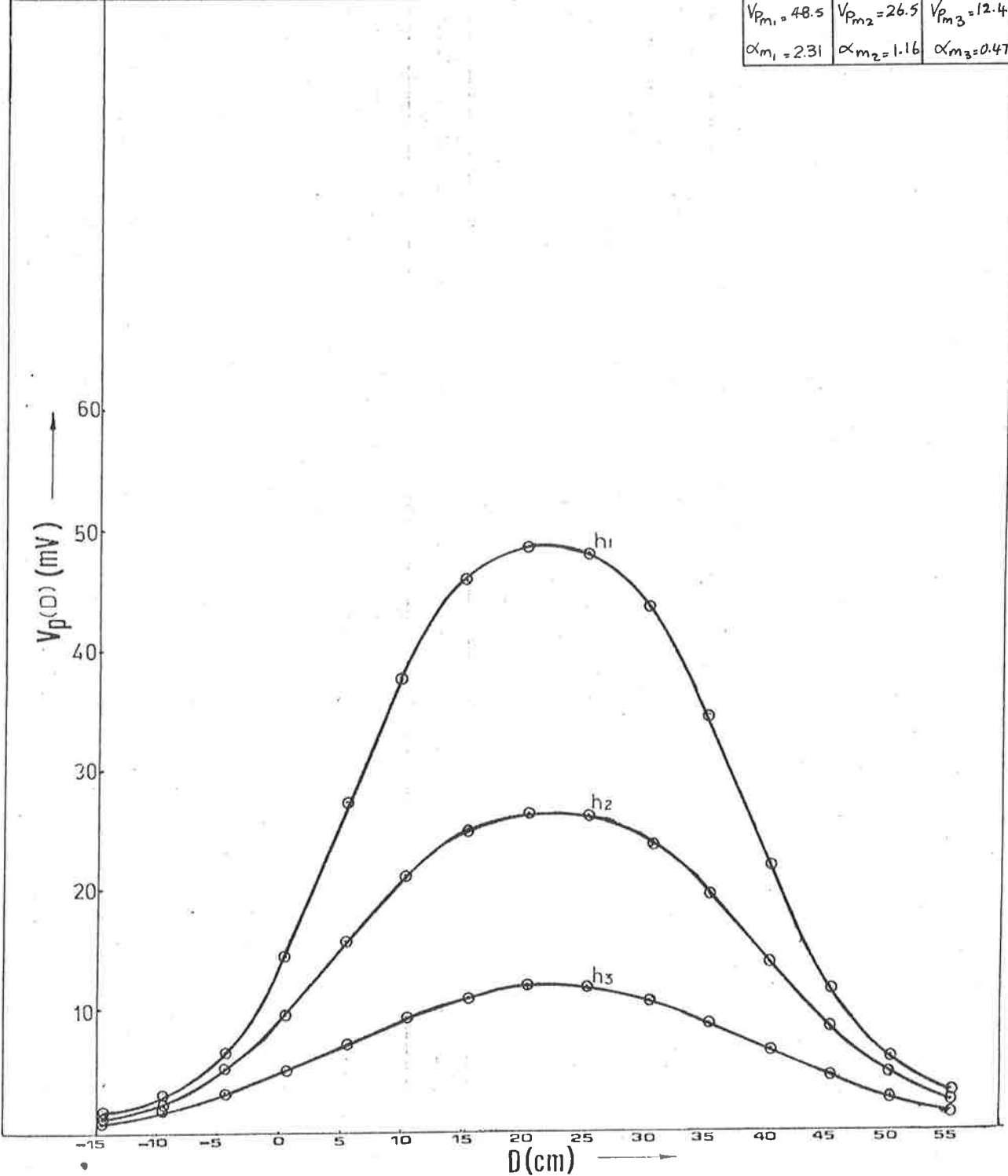
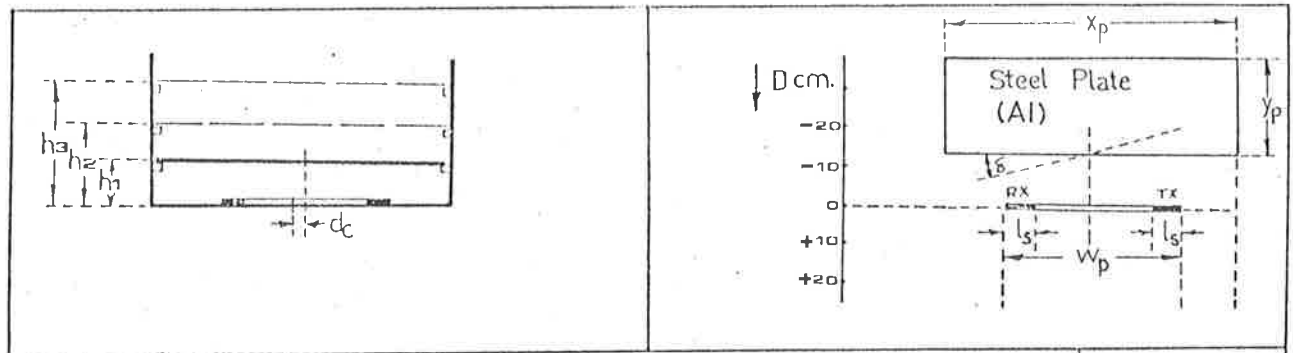


Fig. 5.3(a) Image Voltage Characteristics as a function of Distance D with Approach Angle $\delta = 10$ deg. and $V_{RX} = 250$ mV.



TEST CONDITION		Ref:			
$h_1 = 6$ cm.	$h_2 = 12$ cm.	$h_3 = 18$ cm.	$d_c = 0$ cm.	$\delta = 10$ deg.	$W_p = 55$ cm.
			$l_s = 10$ cm.	$X_p = 150$ cm.	$Y_p = 42$ cm.
			Freq. = 100 kHz.		$V_{RX} = 500$ mV _{pp} Sine
P1		P2		P3	
20.98		22.69		25.36	

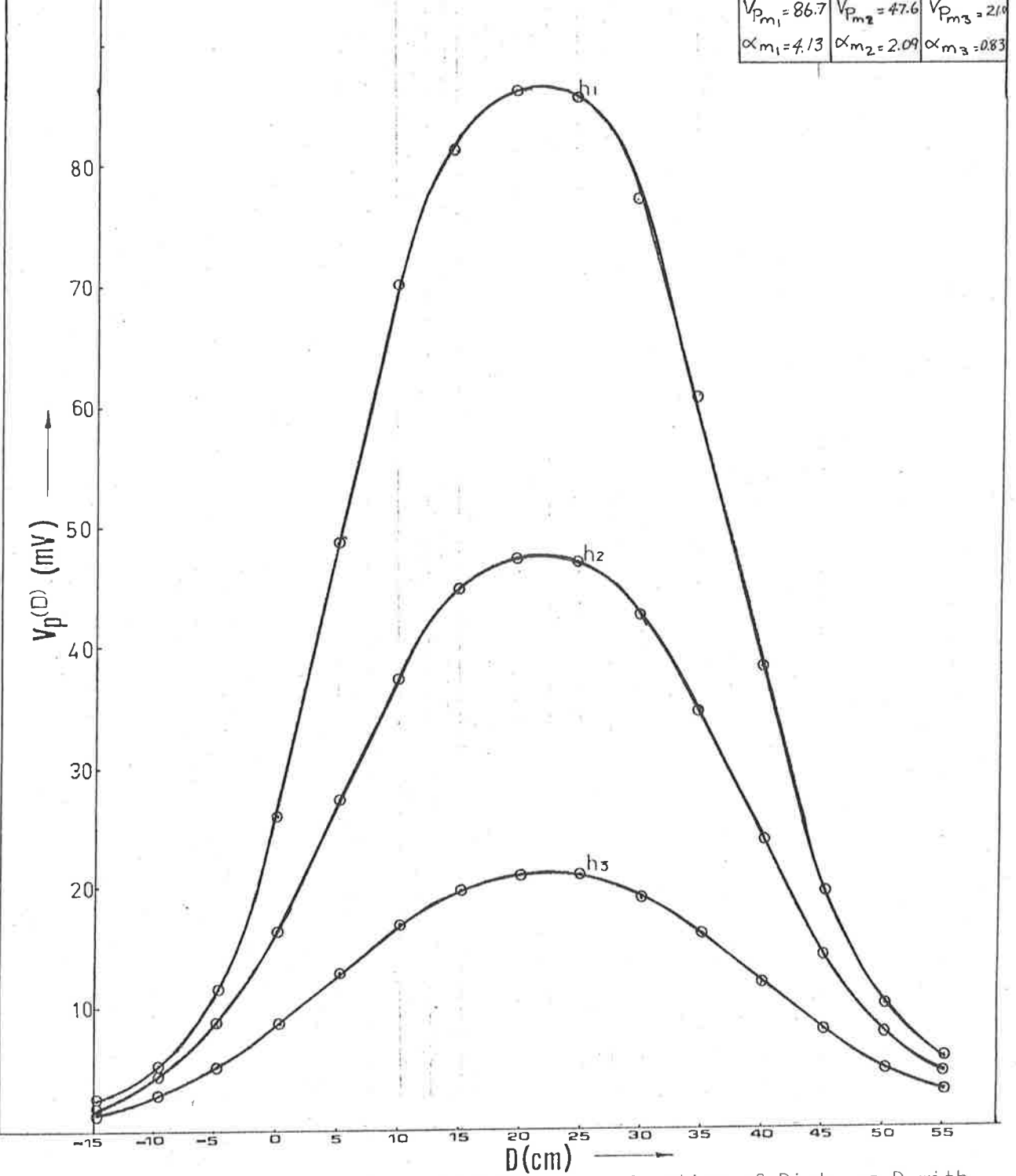
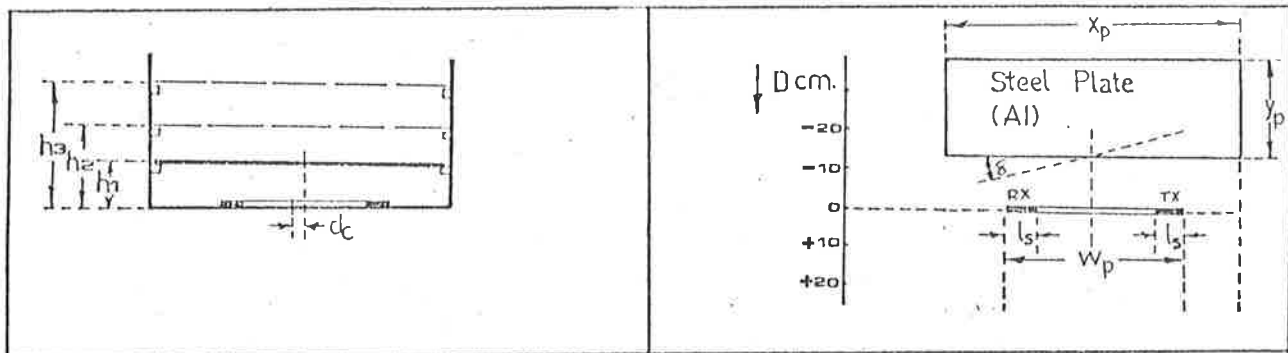


Fig. 5.3(b) Image Voltage Characteristics as a function of Distance D with Approach Angle $\delta = 10$ deg. and $V_{RX} = 500$ mV.



TEST CONDITION		Ref:			
$h_1 = 6$ cm.	$d_c = 0$ cm.	$X_p = 150$ cm.	Freq. = 100 kHz.		
$h_2 = 12$ cm.	$\delta = 20$ deg.	$Y_p = 42$ cm.	$V_{RX} = 250$ mV _{pp} Sine		
$h_3 = 18$ cm.	$w = 55$ cm.		P_1	P_2	P_3
	$l_s = 10$ cm.		20.24	22.95	25.50

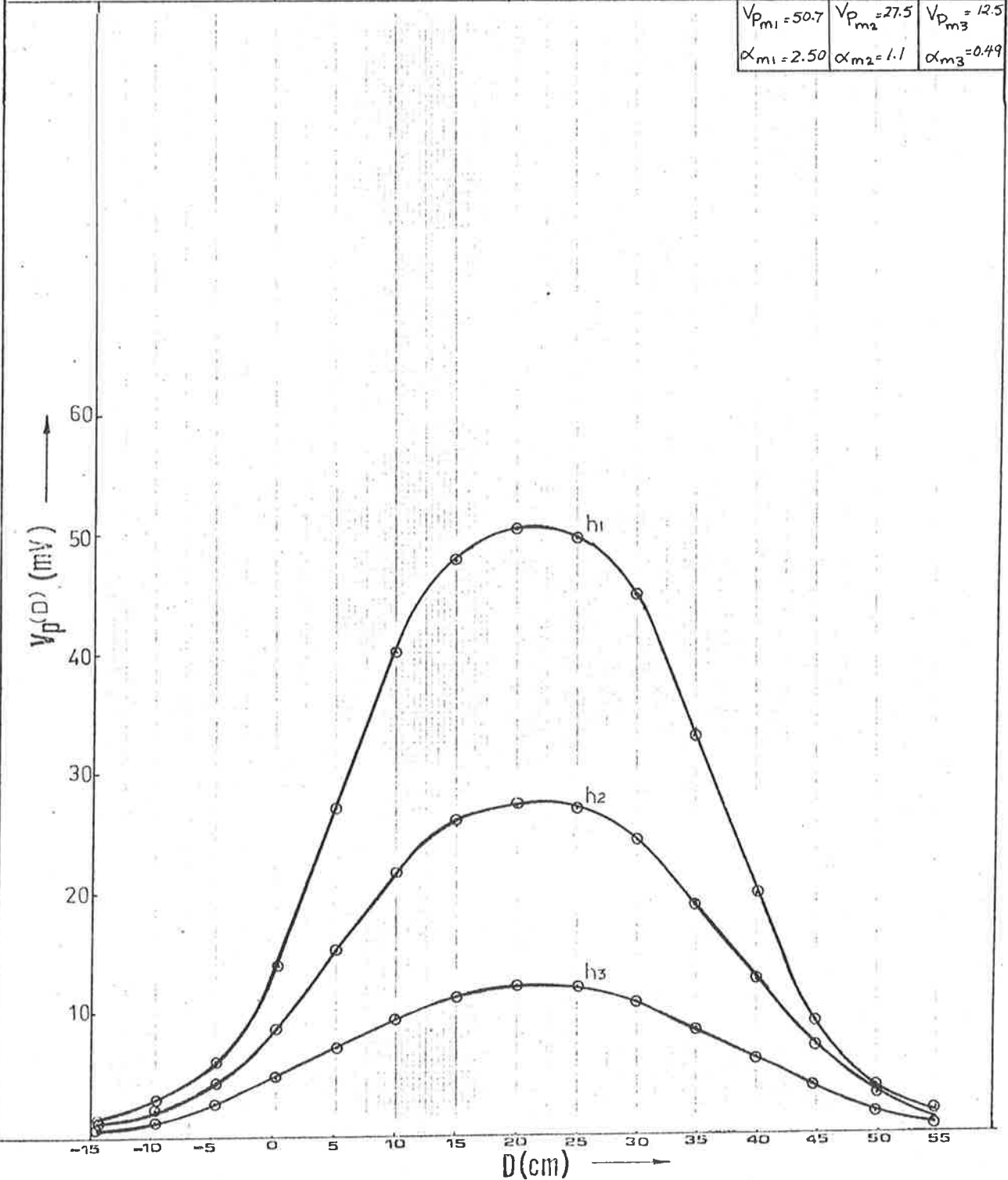
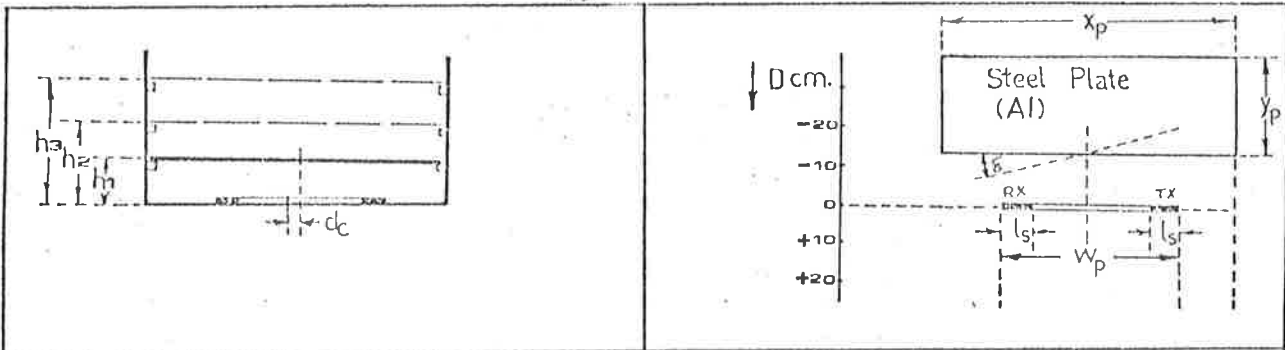


Fig. 5.4(a) Image Voltage Characteristics as a function of Distance D with Approach Angle $\delta = 20$ deg. and $V_{R_x} = 250$ mV.



TEST CONDITION		Ref:				
$h_1 = 6$ cm.	$dc = 0$ cm.	$X_p = 150$ cm.	Freq. = 100 khz.			
$h_2 = 12$ cm.	$\delta = 20$ deg.	$Y_p = 42$ cm.	$V_{RX} = 500$ mV _{pp} Sine			
$h_3 = 18$ cm.	$W_p = 55$ cm.		P_1	P_2	P_3	
	$l_s = 10$ cm.		20.94	23.68	25.83	

$V_{p_{m1}} = 91.5$	$V_{p_{m2}} = 49.5$	$V_{p_{m3}} = 22.1$
$\alpha_{m1} = 4.37$	$\alpha_{m2} = 2.09$	$\alpha_{m3} = 0.86$

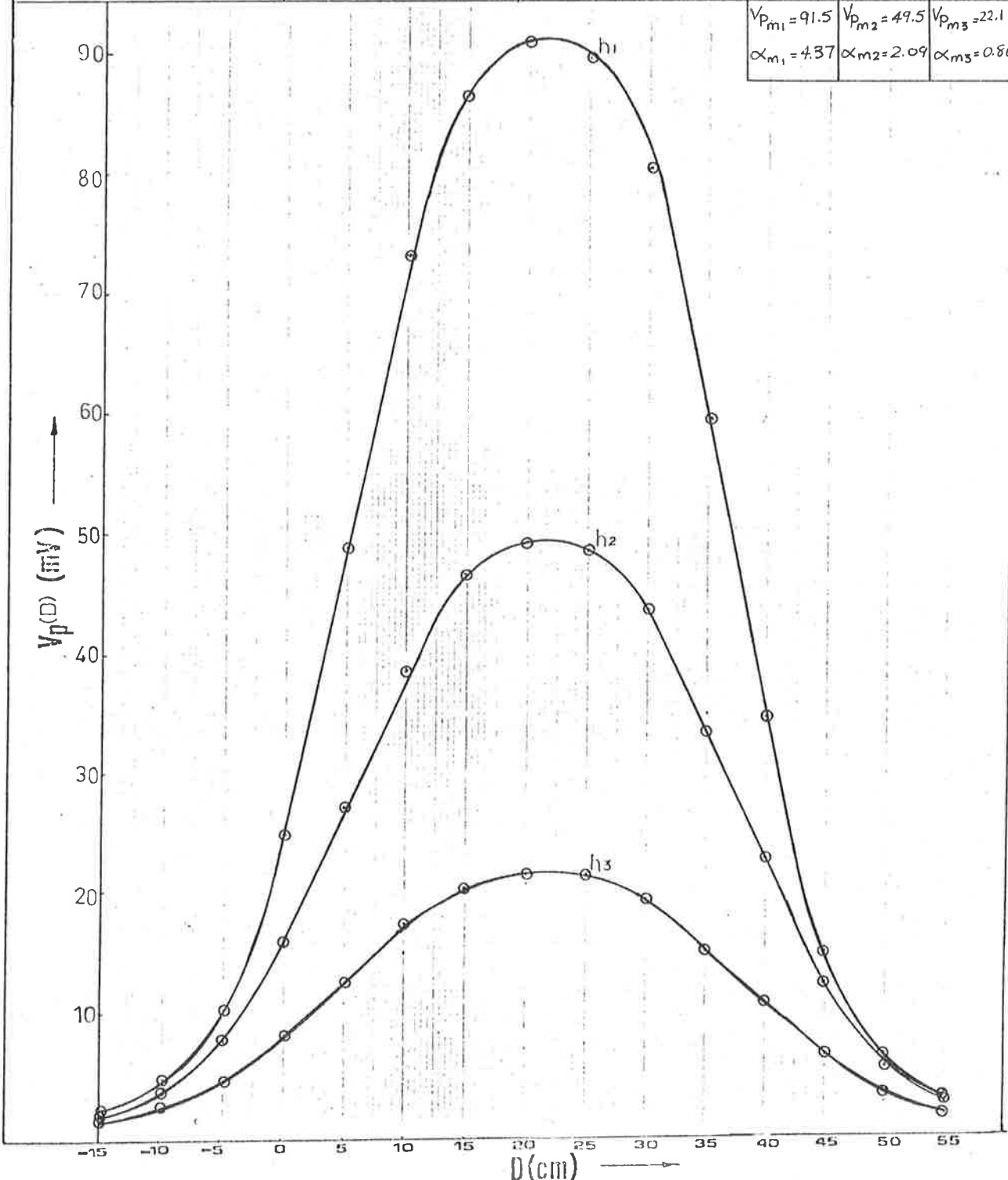


Fig. 5.4(b) Image Voltage Characteristics as a function of Distance D with Approach Angle $\delta = 20$ deg. and $V_{RX} = 500$ mV.

δ degs h(cm)	0	5	10	20
6	22.34	22.48	20.96	20.24
12	23.07	24.20	22.80	22.95
18	23.40	25.28	26.20	25.50

(a)

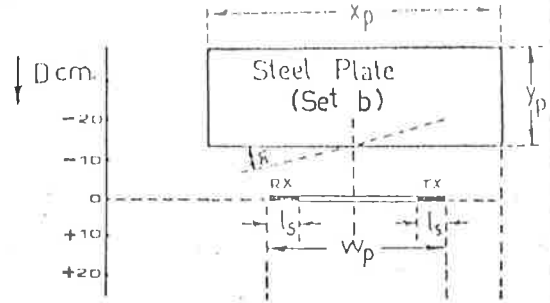
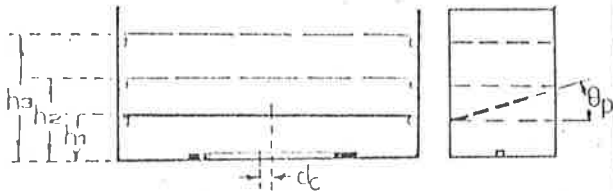
δ degs. h(cm)	0	5	10	20
6	21.96	21.51	20.98	20.94
12	24.37	23.90	22.69	23.68
18	24.70	25.94	25.36	25.83

(b)

Table 5.1 Value of P as a Function of Plate Height h(cm) and Approach Angle δ for

(a) $V_{R_x} = 250\text{mV}$

(b) $V_{R_x} = 500\text{mV}$.



TEST CONDITION

Ref:

$h_1 = 6 \text{ cm}$
 $h_2 = 12 \text{ cm.}$
 $h_3 = 18 \text{ cm.}$

$d_c = 0 \text{ cm.}$
 $\delta = 0 \text{ deg.}$
 $w_p = 55 \text{ cm.}$
 $l_s = 10 \text{ cm}$
 $\theta_p = 0 \text{ deg.}$

$x_p = 90 \text{ cm.}$
 $y_p = 42 \text{ cm.}$

Freq. = 100 kHz
 $V_{RX} = 500 \text{ mV}_{pp} \text{ Sine}$

P1	P2	P3
23.01	23.74	26.76
$V_{Pm1} = 73.5$ $\alpha_{m1} = 3.19$	$V_{Pm2} = 42.25$ $\alpha_{m2} = 1.79$	$V_{Pm3} = 17.45$ $\alpha_{m3} = 0.65$

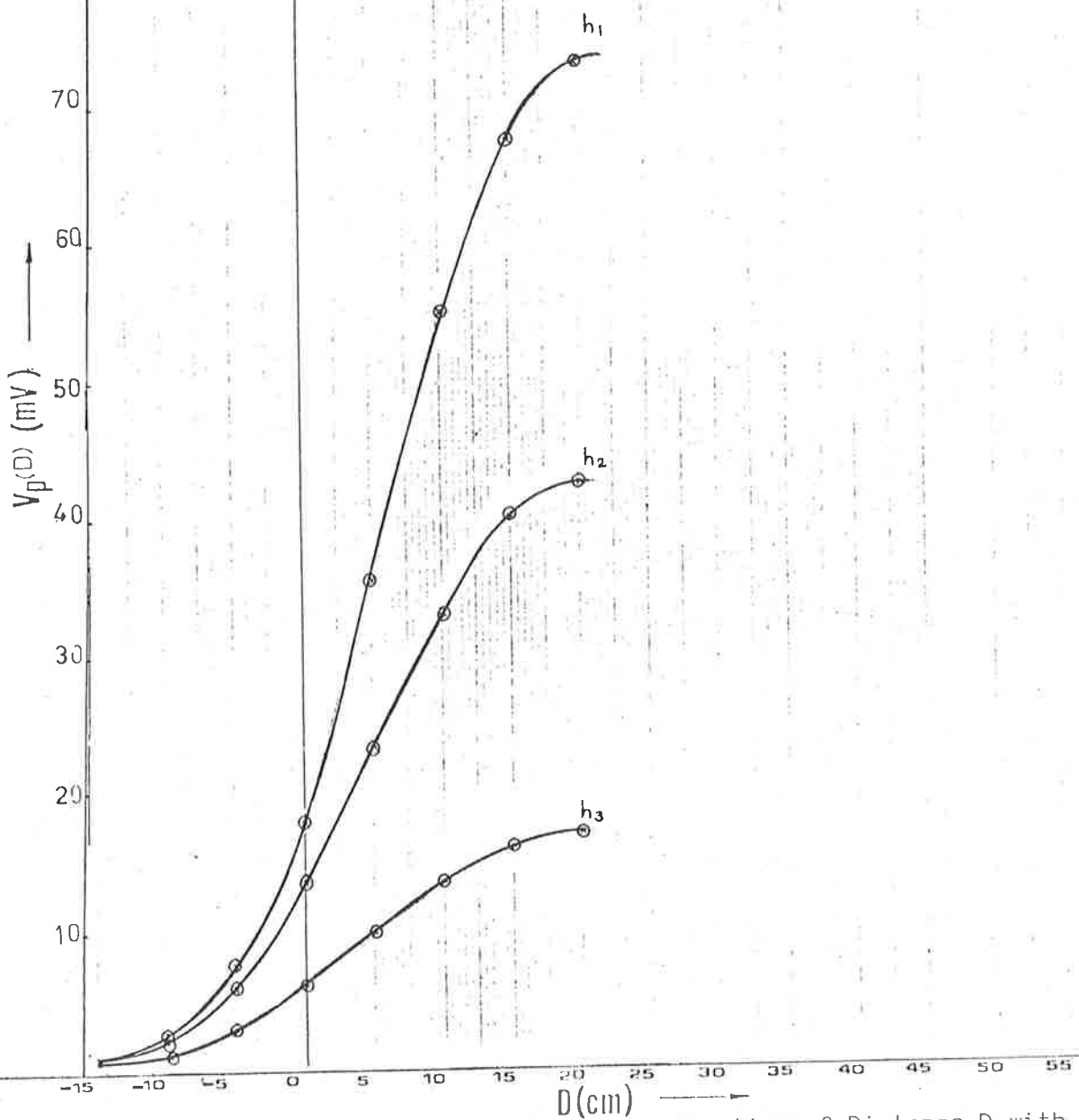
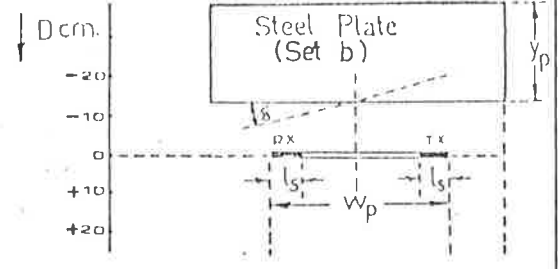
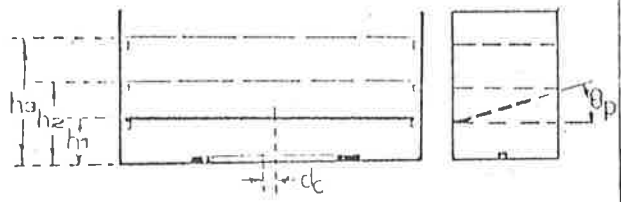


Fig. 5.5. Image Voltage Characteristics as a function of Distance D with Incline Angle $\theta_p = 0 \text{ deg.}$



TEST CONDITION

Ref:

$h_1 = 6 \text{ cm}$
 $h_2 = 12 \text{ cm}$
 $h_3 = 18 \text{ cm}$

$d_c = 0 \text{ cm}$
 $\delta = 0 \text{ deg}$
 $w_p = 55 \text{ cm}$
 $l_s = 10 \text{ cm}$
 $\theta_p = 5 \text{ deg}$

$x_p = 9.0 \text{ cm}$
 $y_p = 42 \text{ cm}$

Freq. = 100 kHz
 $V_{RX} = 500 \text{ mV}_{pp}$ Sine

P1	P2	P3
23.05	23.91	25.90
$V_{p_{m1}} = 66.6$ $\alpha_{m1} = 2.89$	$V_{p_{m2}} = 34.4$ $\alpha_{m2} = 1.44$	$V_{p_{m3}} = 14.6$ $\alpha_{m3} = 0.56$

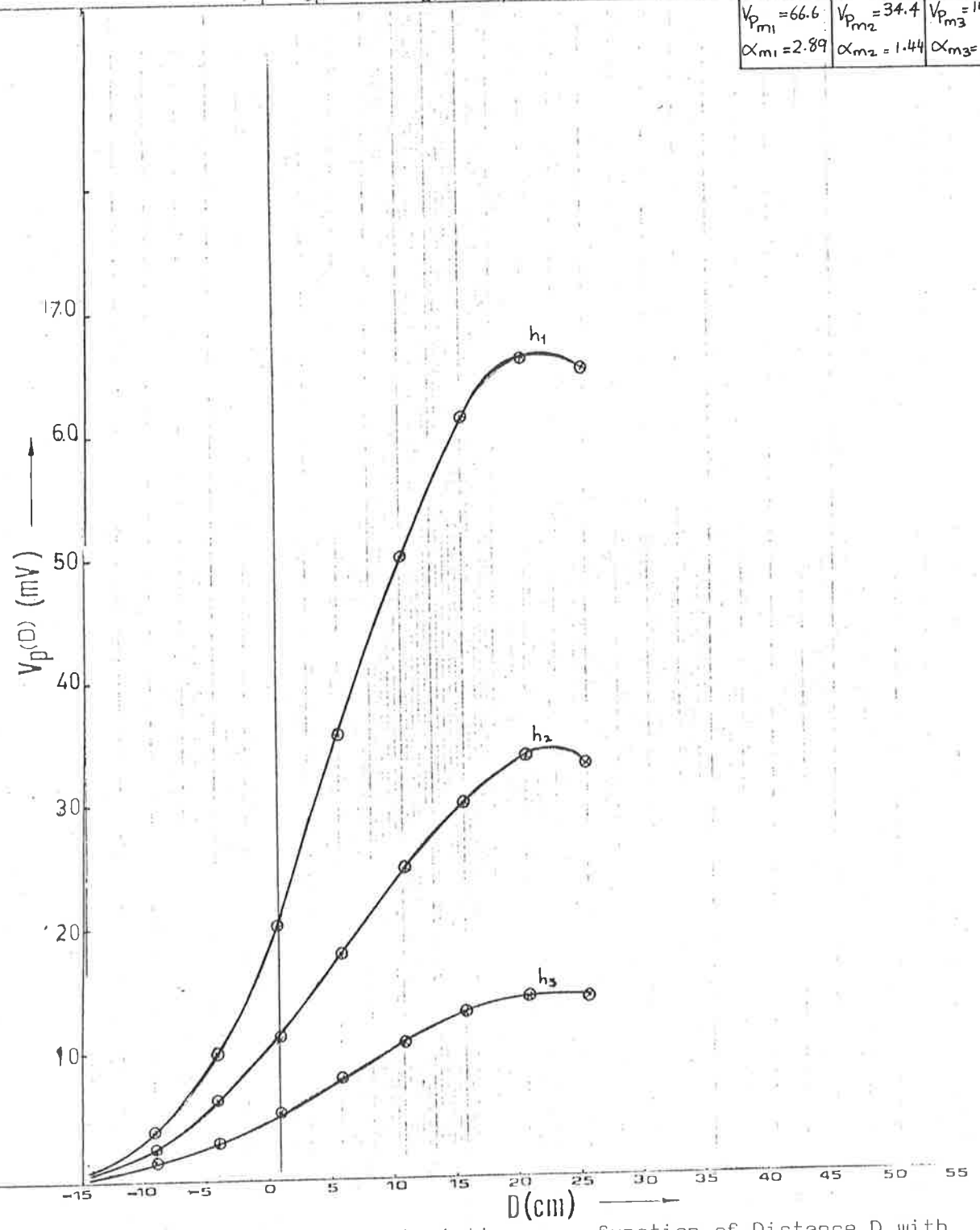
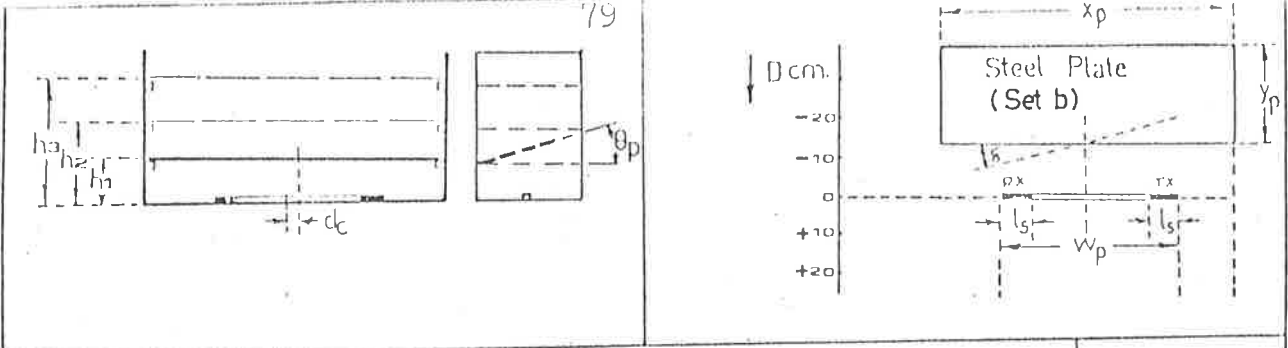


Fig. 5.6. Image Voltage Characteristics as a function of Distance D with Incline Angle $\theta_p = 5 \text{ deg}$.



TEST CONDITION		Ref:			
$h_1 = 6$ cm	$dc = 0$ cm.	$X_p = 90$ cm.	Freq. = 100 kHz		
$h_2 = 12$ cm.	$\delta = 0$ deg.	$Y_p = 42$ cm.	$V_{RX} = 500$ mV _{pp} Sine		
$h_3 = 18$ cm.	$w_p = 55$ cm.		P1	P2	P3
	$l_s = 10$ cm		24.02	24.40	24.20
	$\theta_p = 10$ deg.				

$V_{p,m1} = 63.2$	$V_{p,m2} = 28.4$	$V_{p,m3} = 11.8$
$\alpha_{m1} = 2.63$	$\alpha_{m2} = 1.16$	$\alpha_{m3} = 0.49$

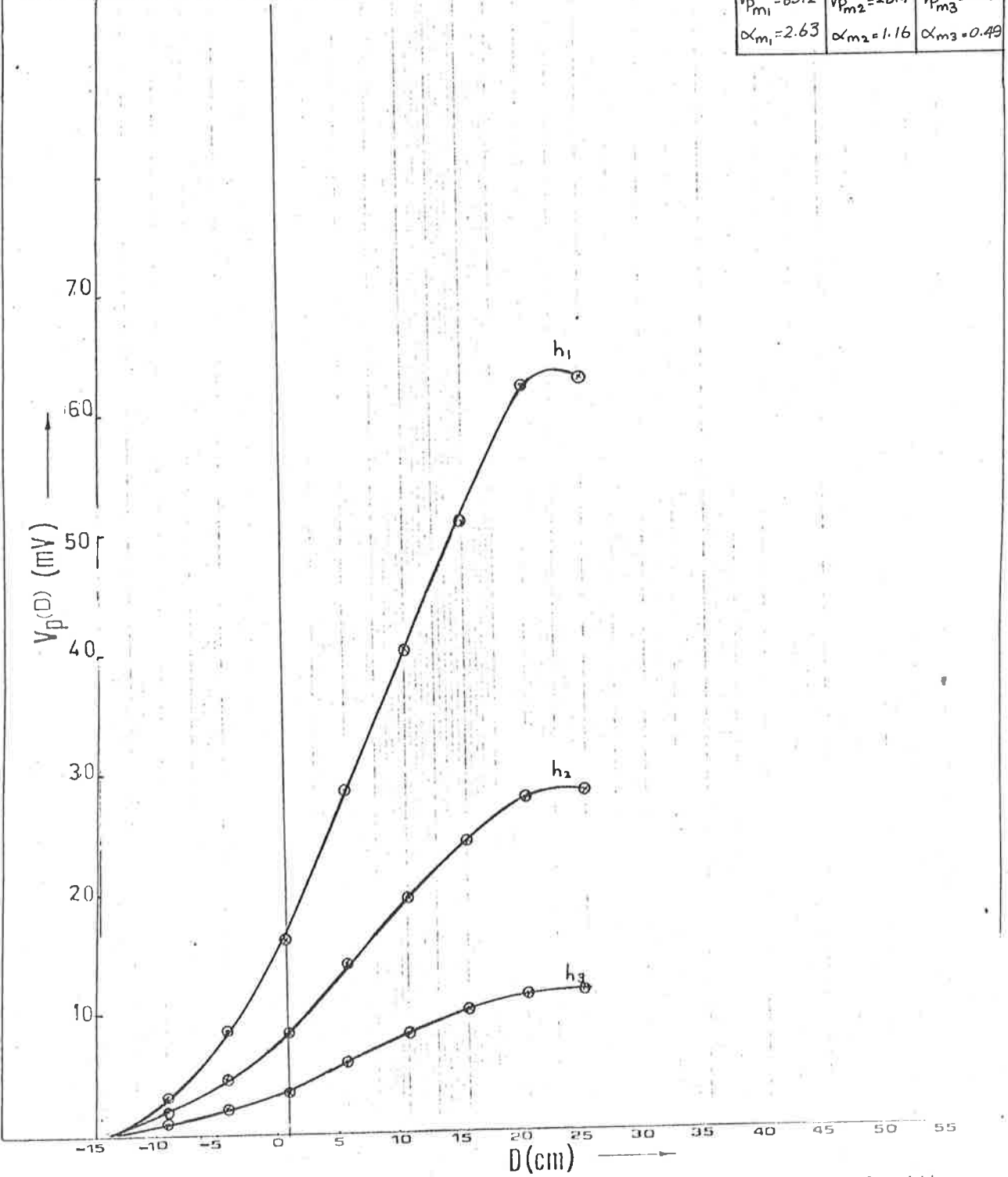
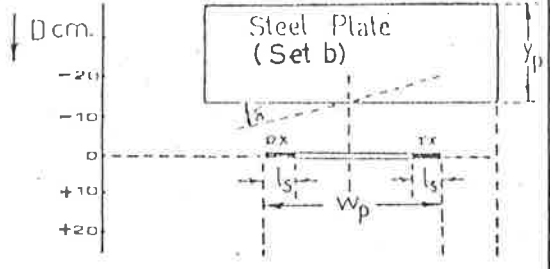
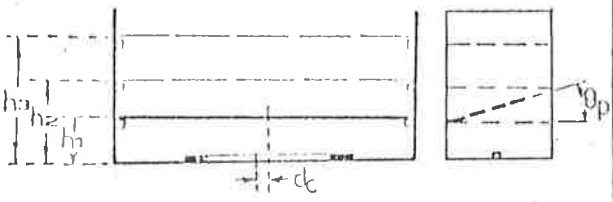


Fig. 5.7 Image Voltage Characteristics as a function of Distance D with Incline Angle $\theta_p = 10$ deg.



TEST CONDITION		Ref:		Freq. = 100 kHz		V _{RX} = 500 mV _{rms} Sine		
$h_1 = 6$ cm	$dc = 0$ cm.	$x_p = 90$ cm.	$y_p = 42$ cm.	P1	P2	P3		
$h_2 = 12$ cm.	$\delta = 0$ deg.			26.30	27.02	26.70		
$h_3 = 18$ cm.	$w_p = 55$ cm.			$V_{P_{m1}} = 50.1$	$V_{P_{m2}} = 21$	$V_{P_{m3}} = 10.1$		
	$l_s = 10$ cm			$\alpha_{m1} = 1.90$	$\alpha_{m2} = 0.78$	$\alpha_{m3} = 0.38$		
	$\theta_p = 15$ deg.							

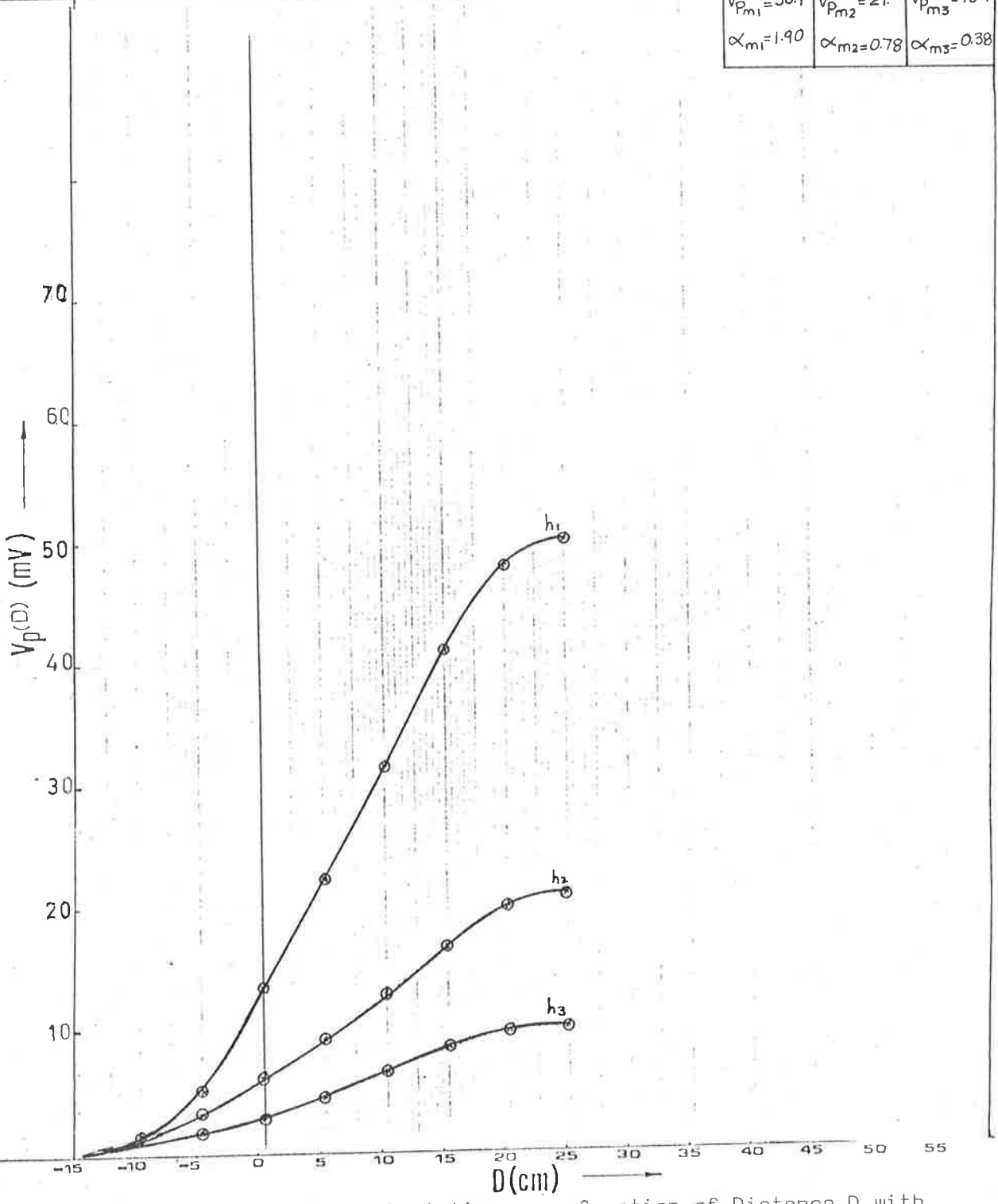
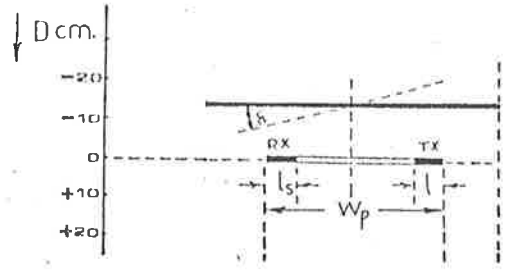
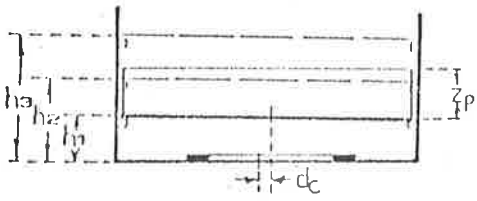


Fig. 5.8 Image Voltage Characteristics as a function of Distance D with Incline Angle $\theta_p = 15$ deg.

θ_p (deg) h (cm)	0	5	10	15
6	23.01	23.05	24.02	26.30
12	23.74	23.91	24.40	27.02
18	26.76	25.90	24.20	26.70

Table 5.2 Value of P as a Function of Plate Height h(cm) and Slope θ_p (degrees) for $V_{R_x} = 500\text{mV}$.



TEST CONDITION		Ref:	
$h_1 = 6 \text{ cm}$	$d_c = 0 \text{ cm.}$	$Z_p = 42 \text{ cm}$	Freq. = 100 kHz. $V_{RX} = 500 \text{ mV}_{pp}$ Sine
$h_2 = 12 \text{ cm.}$	$\delta = 0 \text{ deg.}$		
$h_3 = 18 \text{ cm.}$	$W_p = 55 \text{ cm.}$ $l_s = 10 \text{ cm.}$		

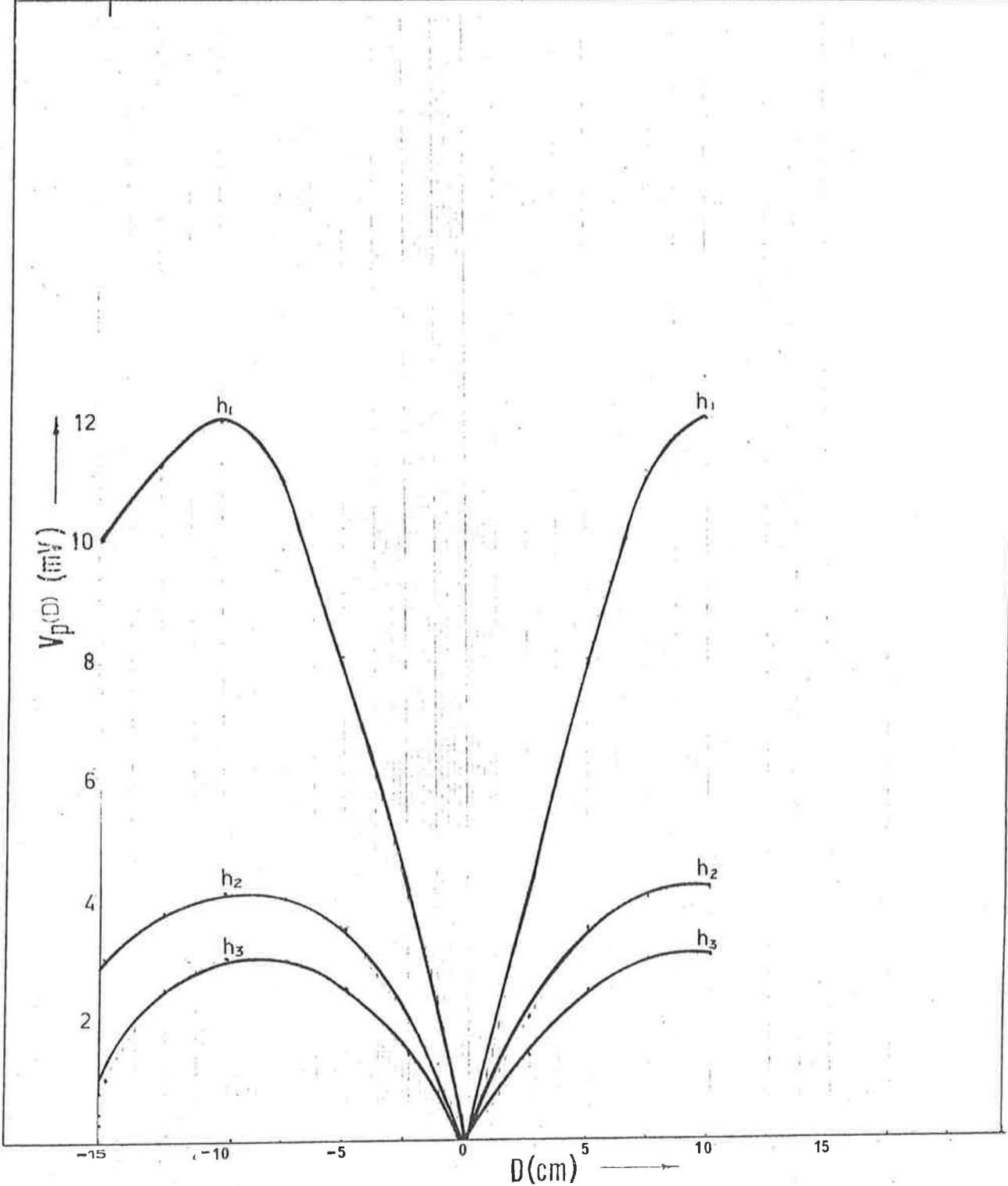
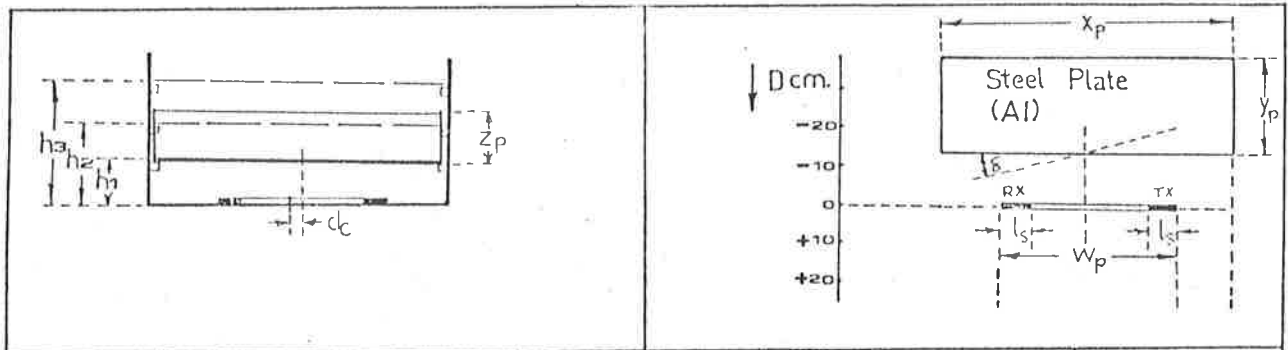


Fig. 5.9 Image Voltage Characteristics for a Vertical Steel Plate.



TEST CONDITION		Ref:		Freq. = 100 kHz		
$h_1 = 6$ cm.	$d_c = 0$	$X_p = 150$ cm.	$V_{RX} = 250mV_{pp}$ Sine	P1	P2	P3
$h_2 = 12$ cm.	$\delta = 0$ deg.	$Y_p = 42$ cm.		24.63	25.02	26.12
$h_3 = 18$ cm.	$W_p = 55$ cm.	$Z_p = 42$ cm.		$V_{Pm1} = 109.3$	$V_{Pm2} = 58.2$	$V_{Pm3} = 25.7$
	$l_s = 10$ cm.			$\alpha_{m1} = 4.44$	$\alpha_{m2} = 2.33$	$\alpha_{m3} = 0.96$

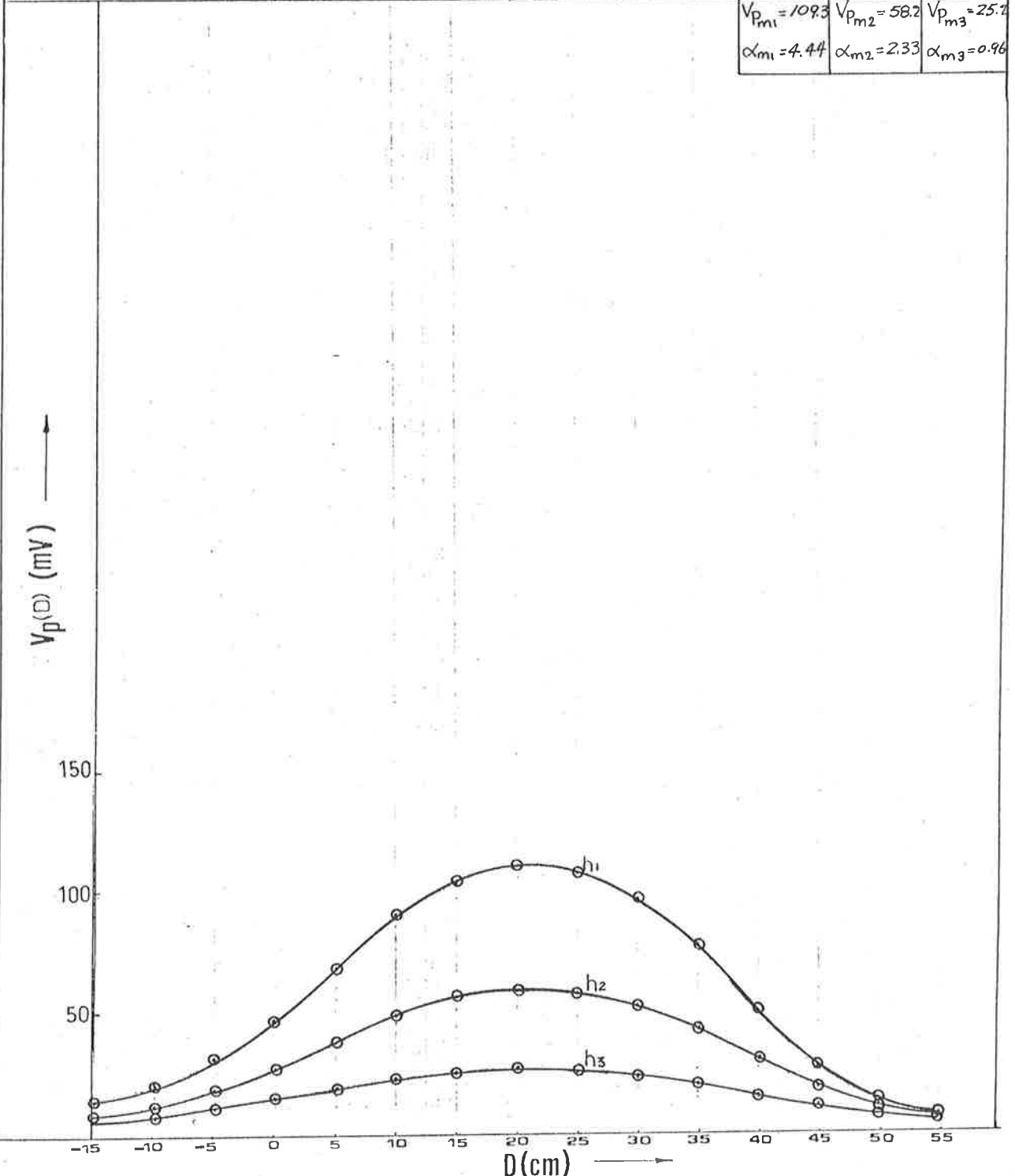
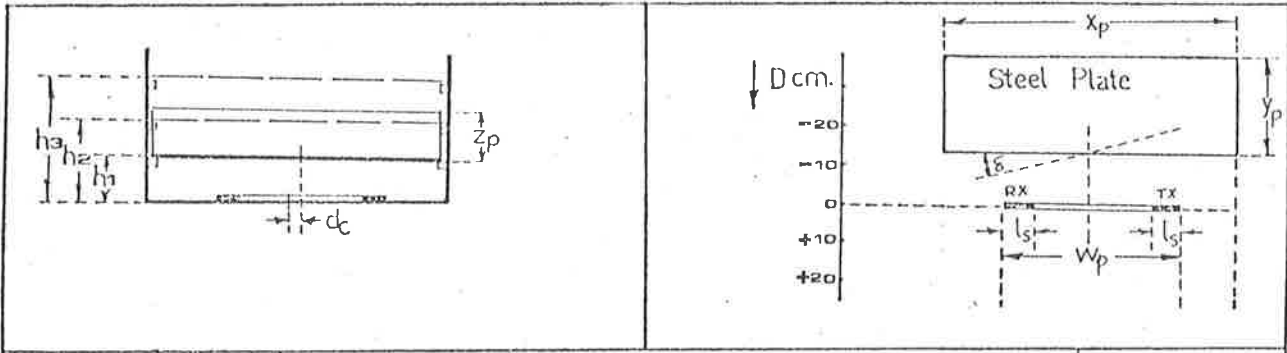


Fig. 5.10(a) Image Voltage Characteristics for an L-shaped Plate as a function of Approach Angle $\delta = 0$ deg. with $V_R = 250mV$.



TEST CONDITION	Ref:								
$h_1 = 6 \text{ cm.}$ $h_2 = 12 \text{ cm.}$ $h_3 = 18 \text{ cm.}$	$d_c = 0 \text{ cm.}$ $\delta = 0 \text{ deg.}$ $w_p = 55 \text{ cm.}$ $l_s = 10 \text{ cm.}$	$x_p = 150 \text{ cm.}$ $y_p = 42 \text{ cm.}$ $z_p = 42 \text{ cm.}$	Freq. = 100 kHz. $V_{RX} = 500mV_{pp}$ Sine						
			<table border="1"> <tr> <th>P₁</th> <th>P₂</th> <th>P₃</th> </tr> <tr> <td>25.19</td> <td>26.47</td> <td>26.52</td> </tr> </table>	P ₁	P ₂	P ₃	25.19	26.47	26.52
P ₁	P ₂	P ₃							
25.19	26.47	26.52							

$V_{p_{m1}} = 189.5$	$V_{p_{m2}} = 102.7$	$V_{p_{m3}} = 44.9$
$\alpha_{m1} = 7.52$	$\alpha_{m2} = 3.86$	$\alpha_{m3} = 1.69$

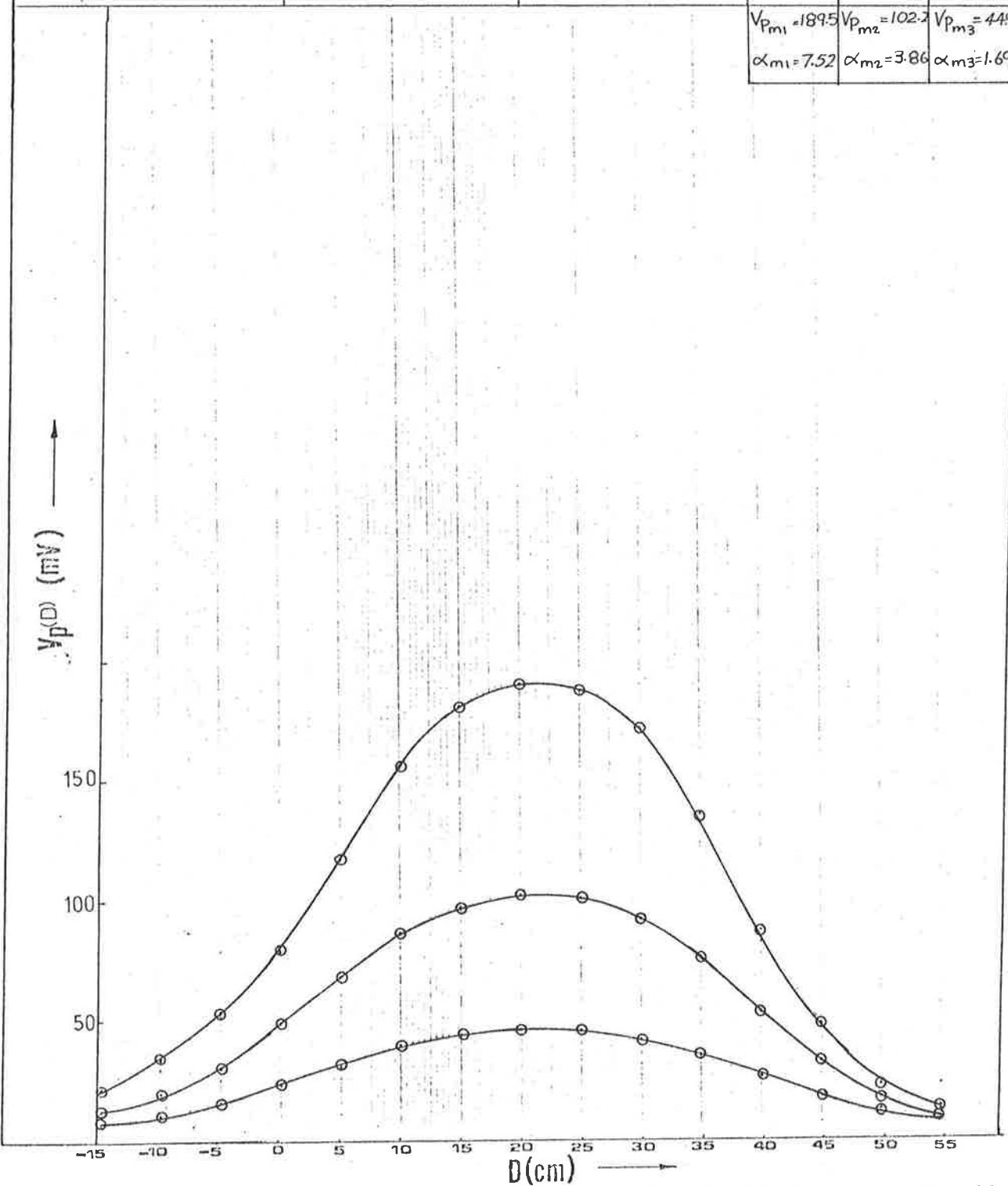
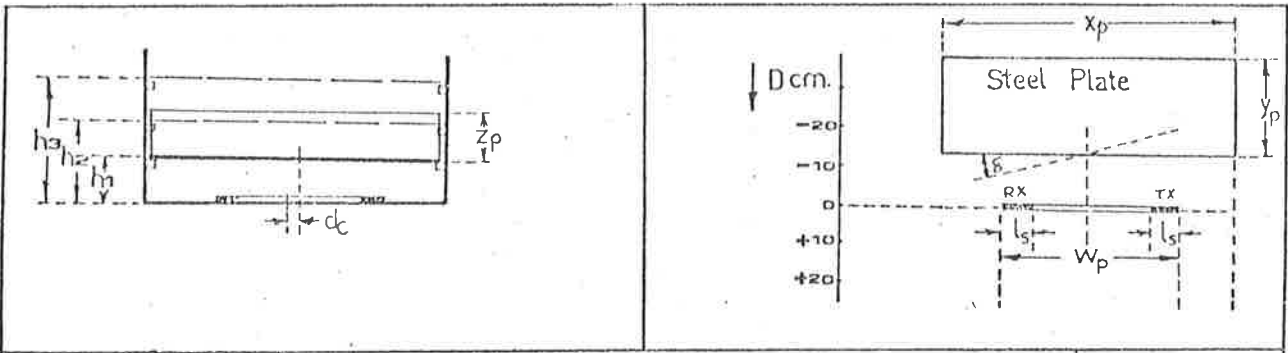


Fig. 5.10(b) Image Voltage Characteristics for an L-shaped Plate as a function of Approach Angle $\delta = 0 \text{ deg.}$ with $V_{R_v} = 500mV$.



TEST CONDITION		Ref:			
$h_1 = 6$ cm.	$dc = 0$ cm.	$X_p = 150$ cm.	Freq. = 100 khz.		
$h_2 = 12$ cm.	$\xi = 0$ deg.	$Y_p = 42$ cm.	VRX = 1 Vpp Sine		
$h_3 = 18$ cm.	$W_p = 55$ cm.	$Z_p = 42$ cm.	P ₁	P ₂	P ₃
	$l_s = 10$ cm.		25.78	26.59	27.82

$V_{p_{m1}} = 248$	$V_{p_{m2}} = 157$	$V_{p_{m3}} = 72$
$\alpha_{m1} = 9.61$	$\alpha_{m2} = 5.9$	$\alpha_{m3} = 2.59$

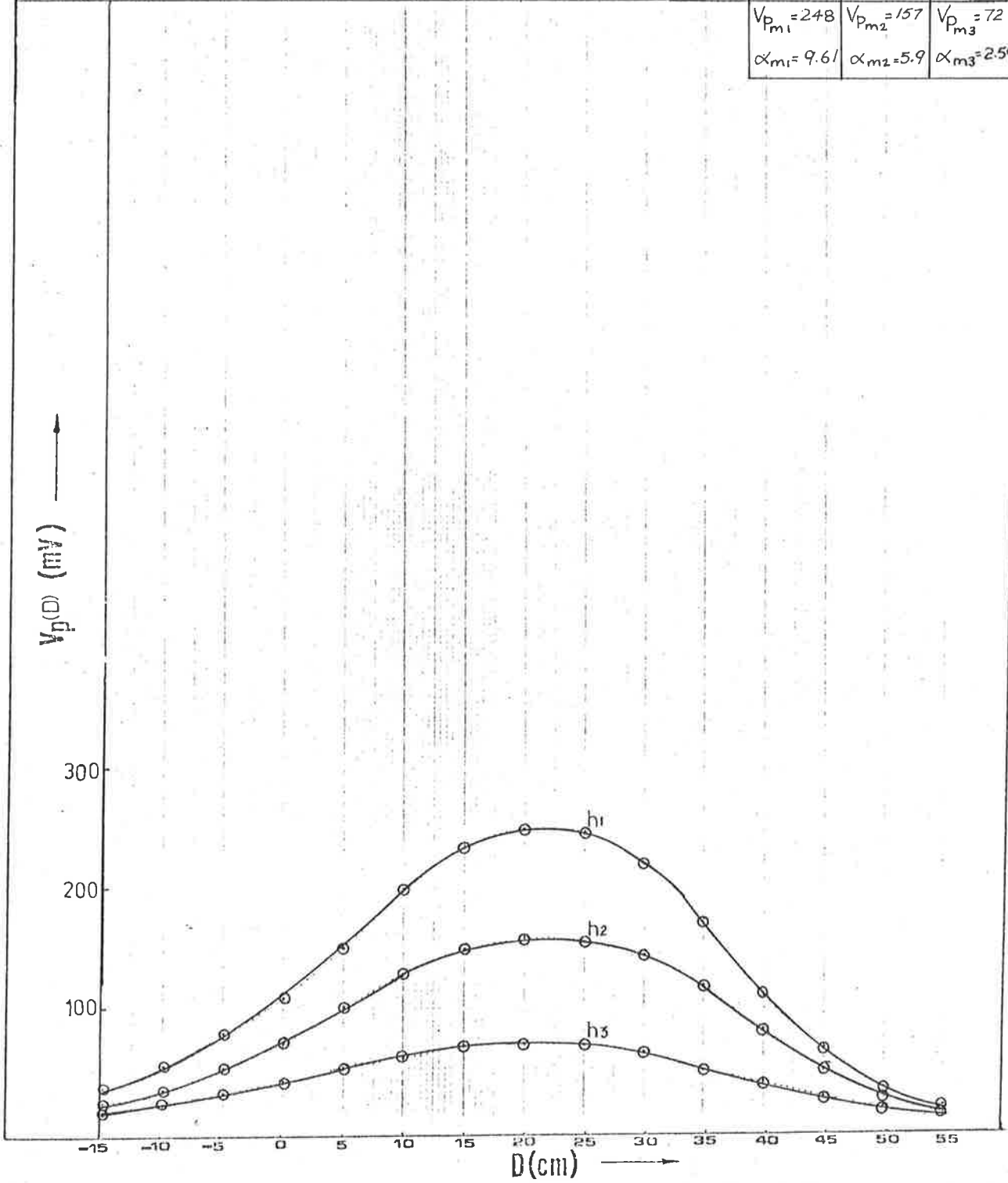
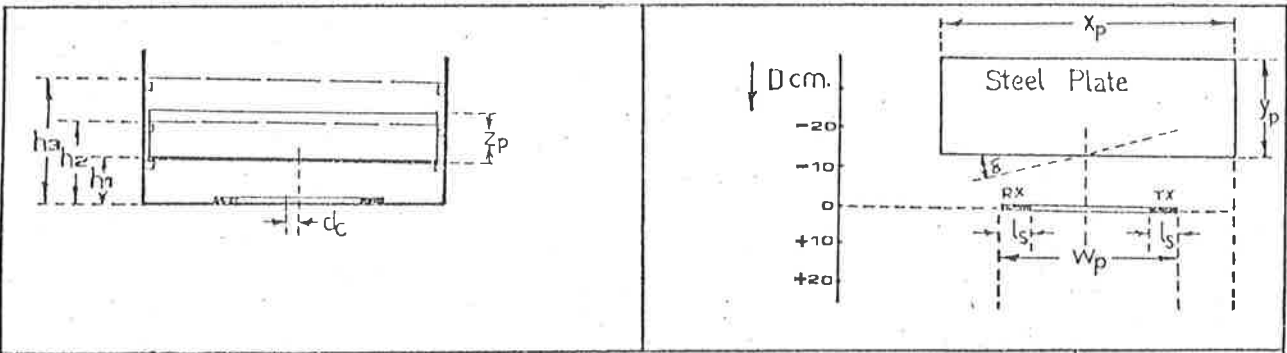


Fig. 5.10(c) Image Voltage Characteristics for an L-shaped Plate as a function of Approach Angle $\xi = 0$ deg. with $V_R = 1000$ mV.



TEST CONDITION	Ref:		
$h_1 = 6 \text{ cm.}$ $h_2 = 12 \text{ cm.}$ $h_3 = 18 \text{ cm.}$	$d_c = 0 \text{ cm.}$ $\xi = 0 \text{ deg.}$ $w_p = 55 \text{ cm.}$ $l_s = 10 \text{ cm.}$	$x_p = 150 \text{ cm.}$ $y_p = 42 \text{ cm.}$ $z_p = 42 \text{ cm.}$	Freq. = 100 khz. $V_{RX} = 2 V_{pp} \text{ Sine}$

P_1	P_2	P_3
26.53	26.02	27.60
$V_{p_{m1}} = 486$ $\alpha_{m1} = 18.31$	$V_{p_{m2}} = 323$ $\alpha_{m2} = 12.41$	$V_{p_{m3}} = 144$ $\alpha_{m3} = 5.22$

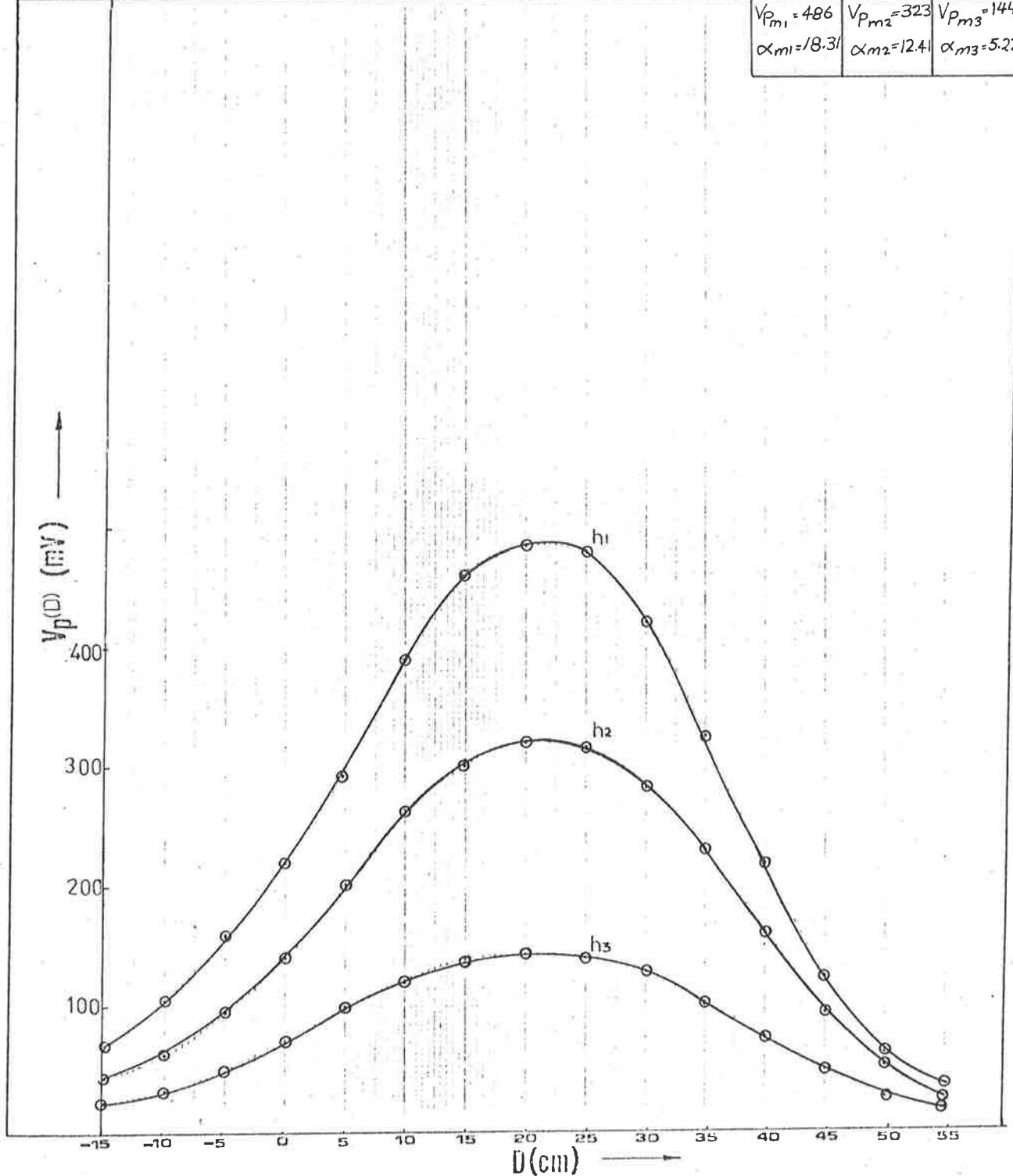
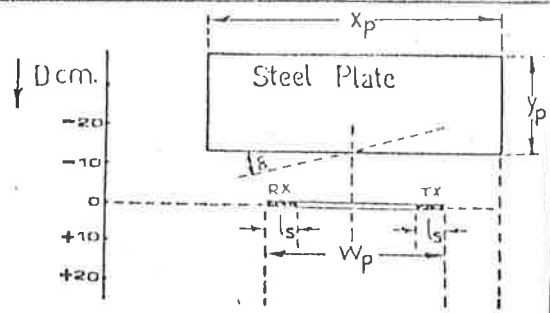
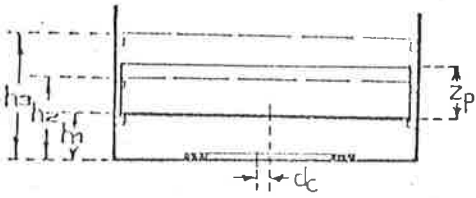


Fig. 5.10(d) Image Voltage Characteristics for an L-shaped Plate as a function of Approach Angle $\xi = 0 \text{ deg.}$ with $V_R = 2000\text{mV.}$



TEST CONDITION

Ref:

$h_1 = 6$ cm.
 $h_2 = 12$ cm.
 $h_3 = 18$ cm.

$dc = 0$ cm.
 $\delta = 5$ deg.
 $W_p = 55$ cm.
 $l_s = 10$ cm.

$X_p = 150$ cm.
 $Y_p = 42$ cm.
 $Z_p = 42$ cm.

Freq. = 100 kHz.
 $V_{RX} = 250$ mV_{pp} Sine

P_1	P_2	P_3
24.93	26.13	27.75
$V_{P_{m1}} = 110.8$	$V_{P_{m2}} = 59.1$	$V_{P_{m3}} = 25$
$\alpha_{m1} = 4.44$	$\alpha_{m2} = 2.26$	$\alpha_{m3} = 0.9$

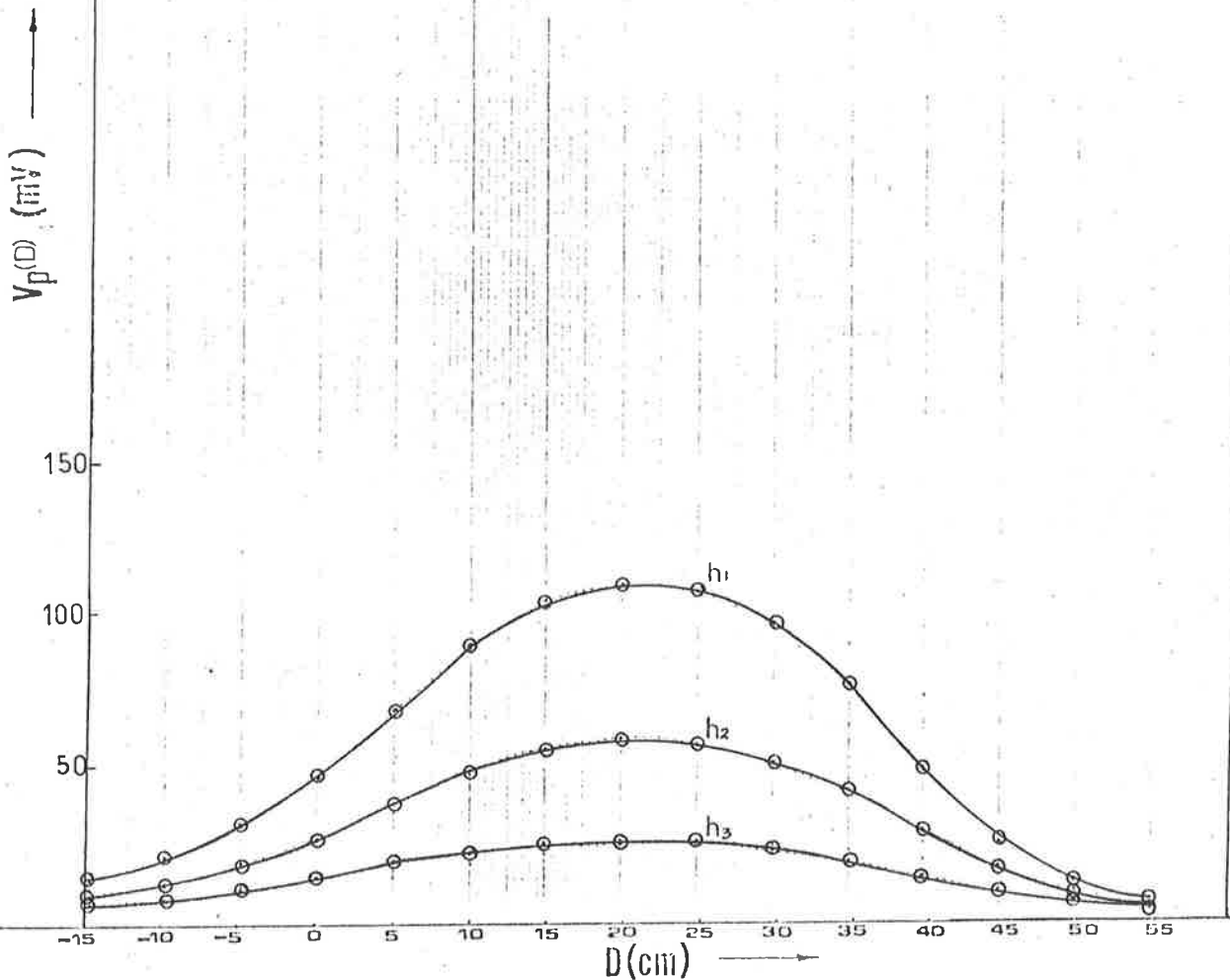
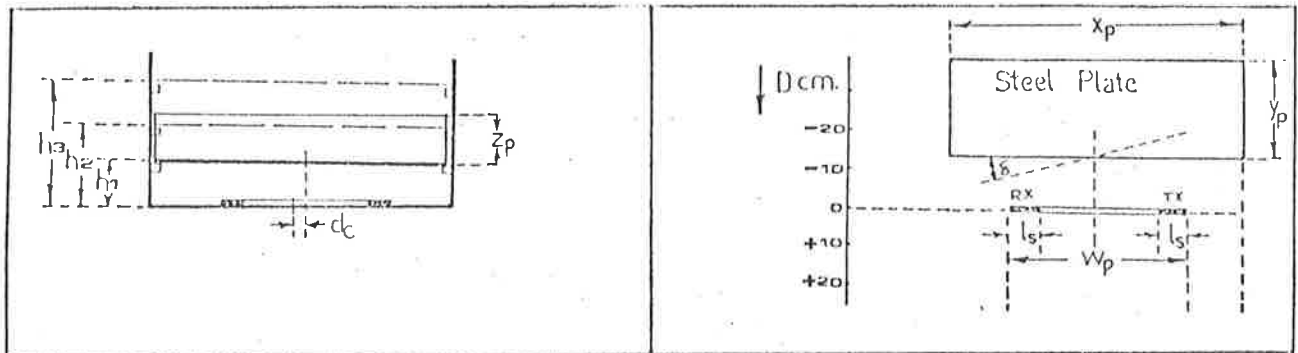


Fig. 5.11(a) Image Voltage Characteristics for an L-shaped Plate as a function of Approach Angle $\delta = 5$ deg. with $V_R = 250$ mV.



TEST CONDITION		Ref:				
$h_1 = 6$ cm.	$dc = 0$ cm.	$X_p = 150$ cm.	Freq. = 100 kHz.			
$h_2 = 12$ cm.	$\delta = 5$ deg.	$Y_p = 42$ cm.	$V_{RX} = 500 mV_{pp}$ Sine			
$h_3 = 18$ cm.	$w_p = 55$ cm.	$Z_p = 42$ cm.	P_1	P_2	P_3	
	$l_s = 10$ cm.		24.88	26.70	27.37	
			$V_{P_{m1}} = 181$	$V_{P_{m2}} = 102$	$V_{P_{m3}} = 45.8$	
			$\alpha_{m1} = 7.27$	$\alpha_{m2} = 3.82$	$\alpha_{m3} = 1.67$	

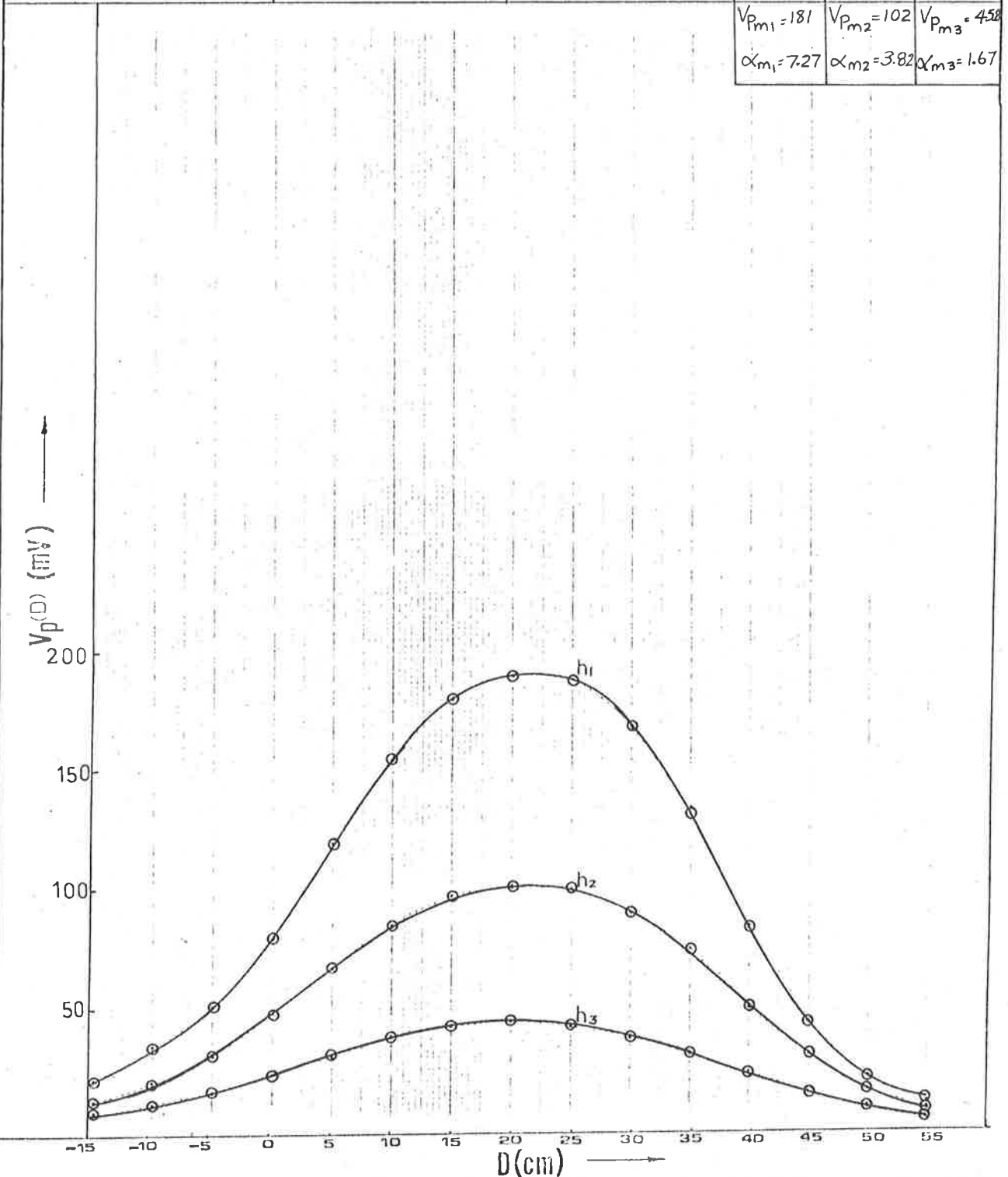
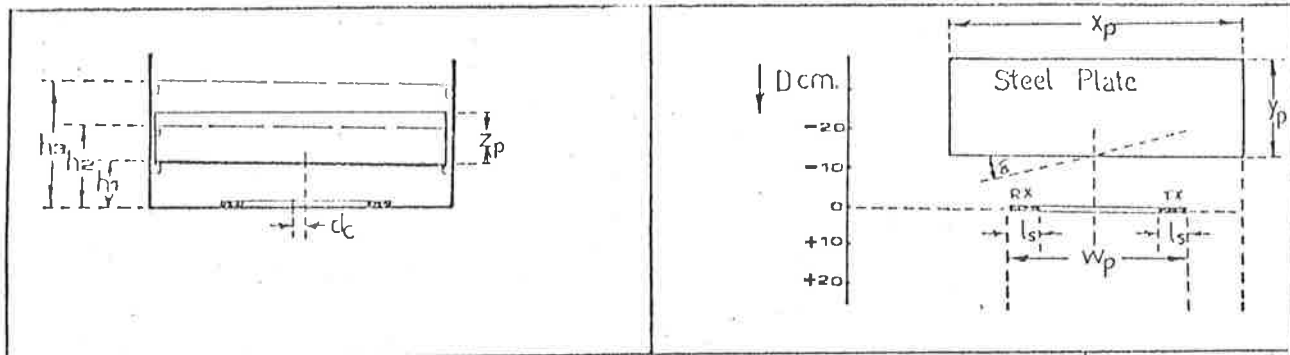


Fig. 5.11(b) Image Voltage Characteristic for an L-shaped Plate as a function of Approach Angle $\delta = 5$ deg. with $V_{R_x} = 500 mV$.



TEST CONDITION		Ref:				
$h_1 = 6$ cm.	$dc = 0$ cm.	$X_p = 150$ cm.	Freq. = 100 khz.			
$h_2 = 12$ cm.	$\delta = 10$ deg.	$Y_p = 42$ cm.	$V_{RX} = 250$ mV _{pp} Sine			
$h_3 = 18$ cm.	$W_p = 55$ cm.	$Z_p = 42$ cm.	P_1	P_2	P_3	
	$l_s = 10$ cm.		24.44	25.93	27.65	
			$V_{P_{m1}} = 110.3$	$V_{P_{m2}} = 58$	$V_{P_{m3}} = 25.1$	
			$\alpha_{m1} = 4.51$	$\alpha_{m2} = 2.24$	$\alpha_{m3} = 0.91$	

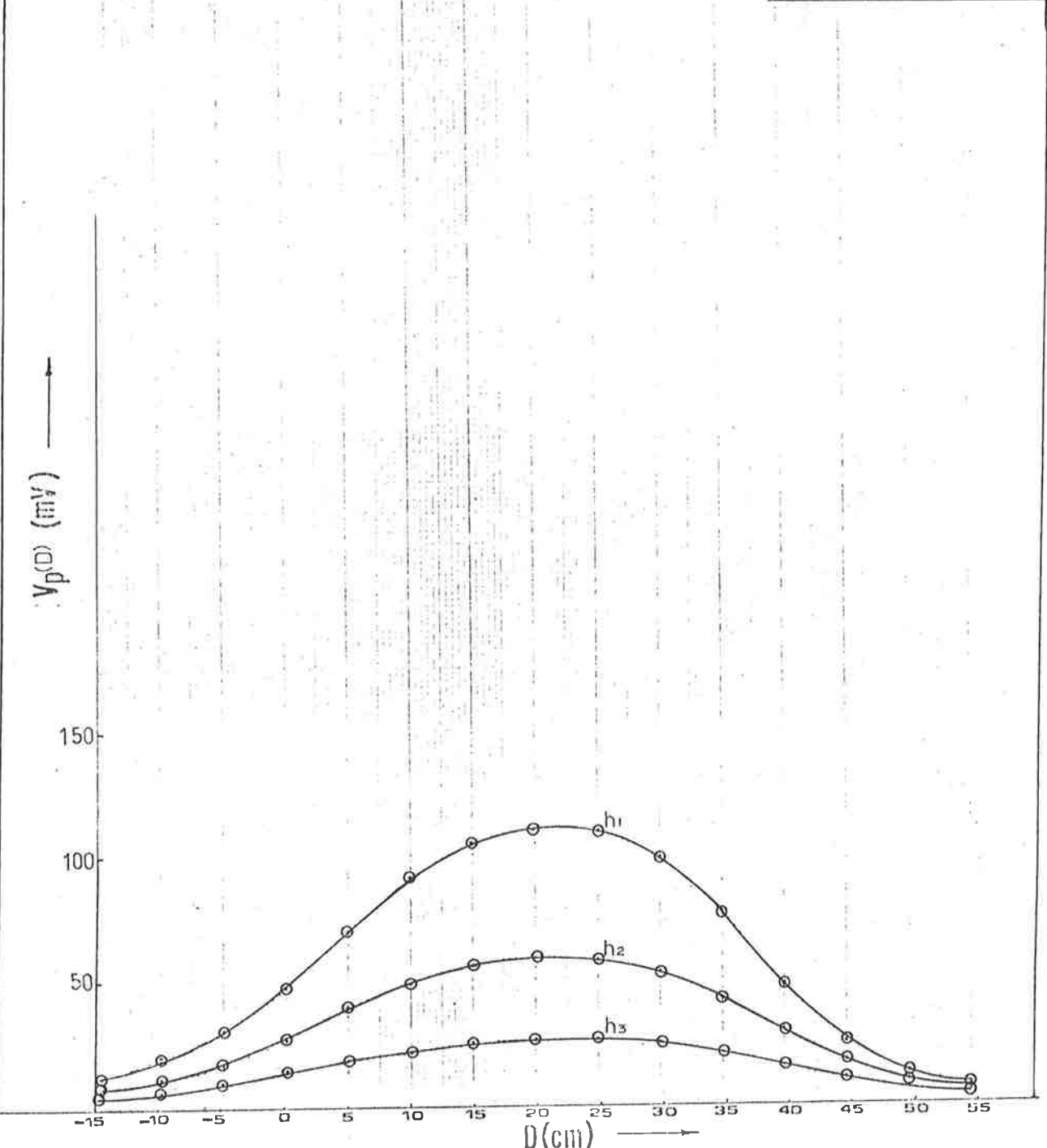
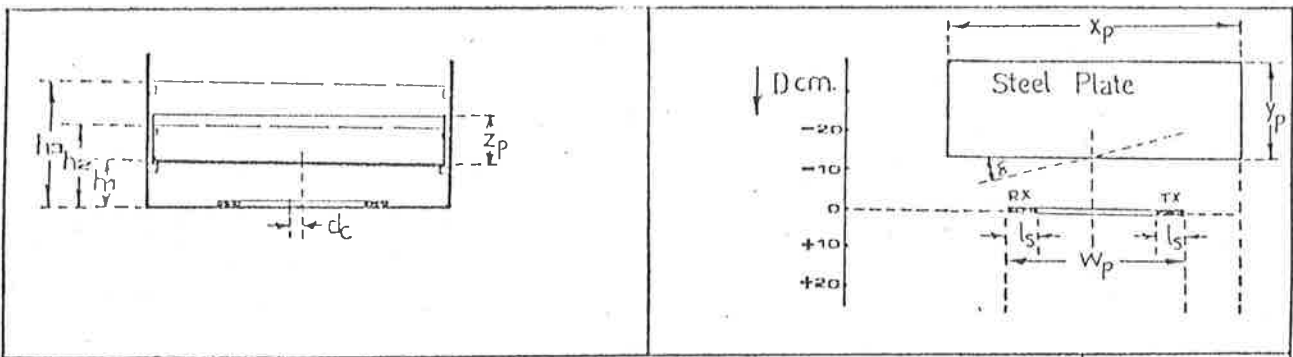


Fig. 5.12(a) Image Voltage Characteristics for an L-shaped Plate as a function of Approach Angle $\delta = 10$ deg. with $V_{R_x} = 250$ mV.



TEST CONDITION		Ref:				
$h_1 = 6$ cm.	$dc = 0$ cm.	$X_p = 150$ cm.	Freq. = 100 khz.			
$h_2 = 12$ cm.	$\delta = 20$ deg.	$Y_p = 42$ cm.	$V_{RX} = 250$ mV _{pp} Sine			
$h_3 = 18$ cm.	$W_p = 55$ cm.	$Z_p = 42$ cm.	P_1	P_2	P_3	
	$l_s = 10$ cm.		24.84	24.98	26.50	
			$V_{Pm1} = 115$	$V_{Pm2} = 64$	$V_{Pm3} = 25.6$	
			$\alpha_{m1} = 4.62$	$\alpha_{m2} = 2.56$	$\alpha_{m3} = 0.97$	

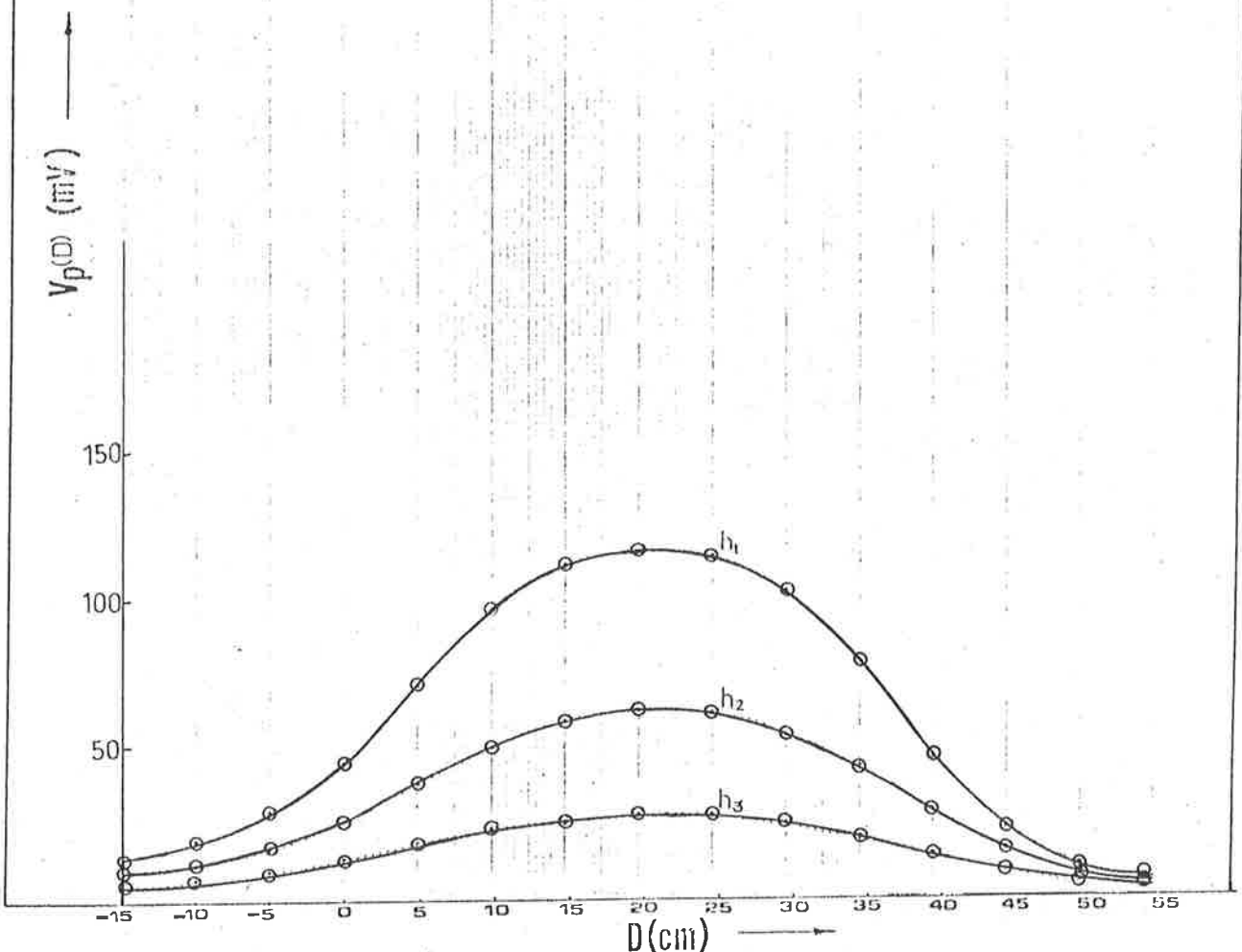
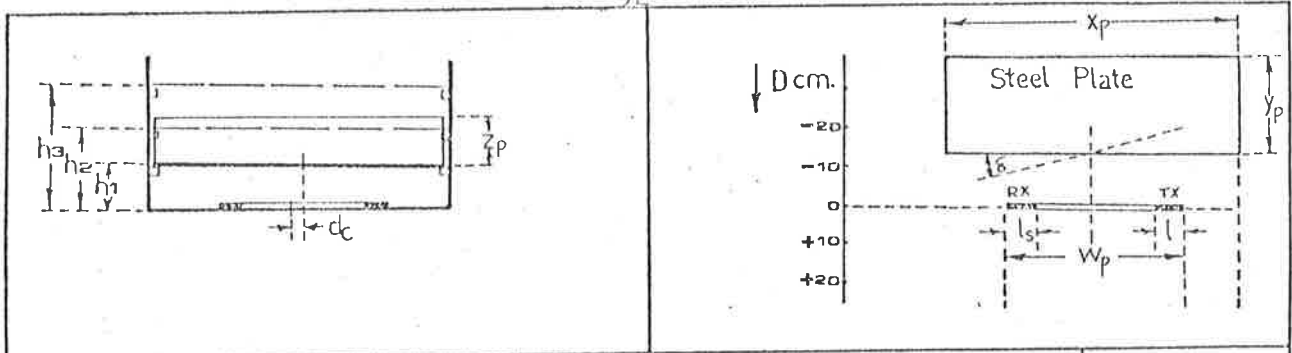


Fig. 5.13(a) Image Voltage Characteristics for an L-shaped Plate as a function of Approach Angle $\delta = 20$ deg. with $V_{RX} = 250$ mV.



TEST CONDITION		Ref:				
$h_1 = 6$ cm.	$dc = 0$ cm.	$X_p = 150$ cm.	Freq. = 100 kHz.			
$h_2 = 12$ cm.	$\delta = 20$ deg.	$Y_p = 42$ cm.	$V_{RX} = 500$ mV _{pp} Sine			
$h_3 = 18$ cm.	$W_p = 55$ cm.	$Z_p = 42$ cm.	P_1	P_2	P_3	
	$l_s = 10$ cm.		23.84	24.97	25.82	
			$V_{Pm1} = 201.2$	$V_{Pm2} = 111.6$	$V_{Pm3} = 50.6$	
			$\alpha_{m1} = 8.44$	$\alpha_{m2} = 4.47$	$\alpha_{m3} = 1.96$	

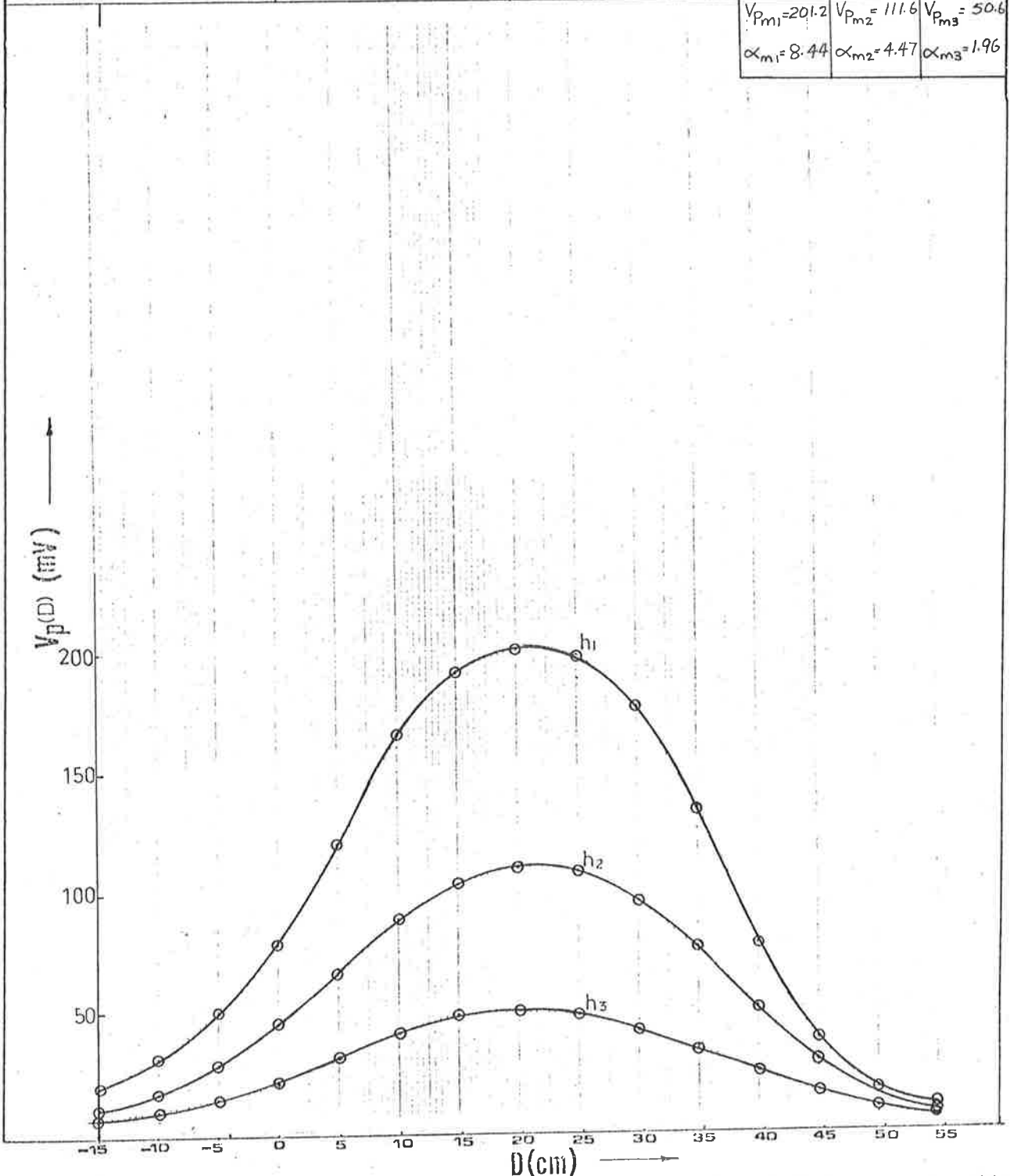


Fig. 5.13(b) Image Voltage Characteristics for an L-shaped Plate as a function of Approach Angle $\delta = 20$ deg. with $V_{R_x} = 500$ mV.

V_{R_x} (mV) \ h (cm)	250	500	1000	2000
6	24.63	25.19	25.78	26.53
12	25.92	26.47	26.59	26.02
18	26.12	26.52	27.82	27.60

Table 5.3 Value of P as a function of Plate Height h (cm) and Initial Induced Voltage V_{R_x} (mV) in the Receiver Coil R_x for an L-Shaped Steel Plate.

δ (deg) \ h (cm)	5	10	20
6	24.93	24.44	24.84
12	26.13	25.93	24.98
18	27.75	27.65	26.50

(a)

δ (deg) \ h (cm)	5	10	20
6	24.88	24.65	23.84
12	26.70	26.07	24.97
18	27.37	26.87	25.82

(b)

Table 5.4 Value of P as a Function of Approach Angle δ (deg) for an L-shaped Steel Plate

(a) $V_{R_x} = 250\text{mV}$

(b) $V_{R_x} = 500\text{mV}$.

5.1.4 Image Voltage Characteristics in the Presence of Brine Solution.

The behaviour of the image voltage was also examined with the sensor immersed in a layer of brine solution. Although this test was rather severe, it provided the basis for the representation of "slush" which exists on the road surface. Fig. 5.14 shows the image voltage characteristics as a function of distance for several values of height h . The notable feature demonstrated was that the change in the image voltage was very marginal. In fact for values of $h > 12\text{cm}$ no change was noted.

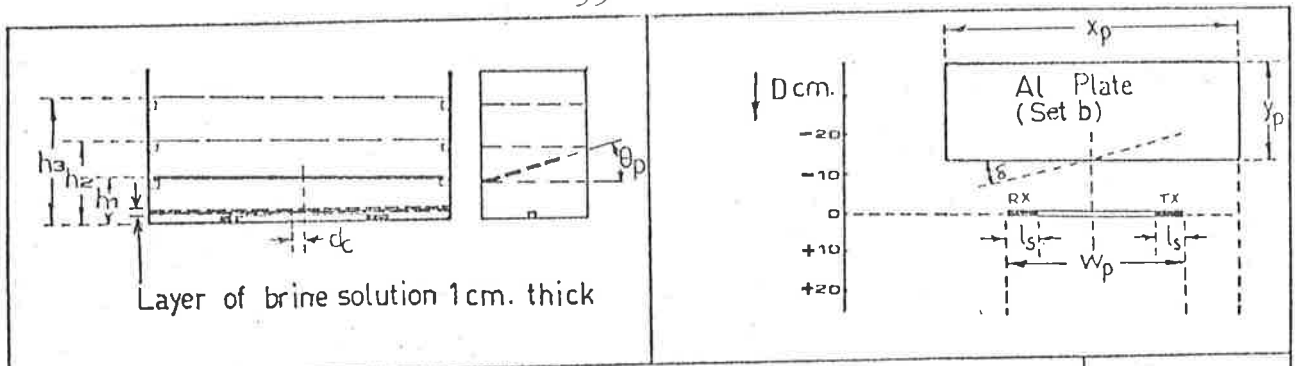
5.1.5 Other Considerations

The value of P was also noted for several displacement values d_c of the sensor from the centre position and for larger values of h . Since the values were within the range shown in Tables 5.2 - 5.4, the graphical representations have been omitted.

5.2 DISCUSSIONS OF THE RESULTS

The range of the values obtained for P with the imposed variations in the external parameters were rather remarkable. If we further consider the under-carriage heights encountered in practice, we can neglect the results for $h < 12\text{cm}$. Thus we obtain a range of values for P given by

$$28 > P > 23 \quad \dots(5.1)$$



TEST CONDITION		Ref:		
$h_1 = 6$ cm.	$dc = 0$ cm.	$x_p = 90$ cm.	Freq. = 100 kHz	
$h_2 = 12$ cm.	$\delta = 0$ deg.	$y_p = 42$ cm.	$V_{RX} = 500$ mV _{pp} Sine	
$h_3 = 18$ cm.	$w_p = 55$ cm.		P1	P2
	$l_s = 10$ cm.		20.2	22.6
	$\theta_p = 0$ deg.			P3
				24.4

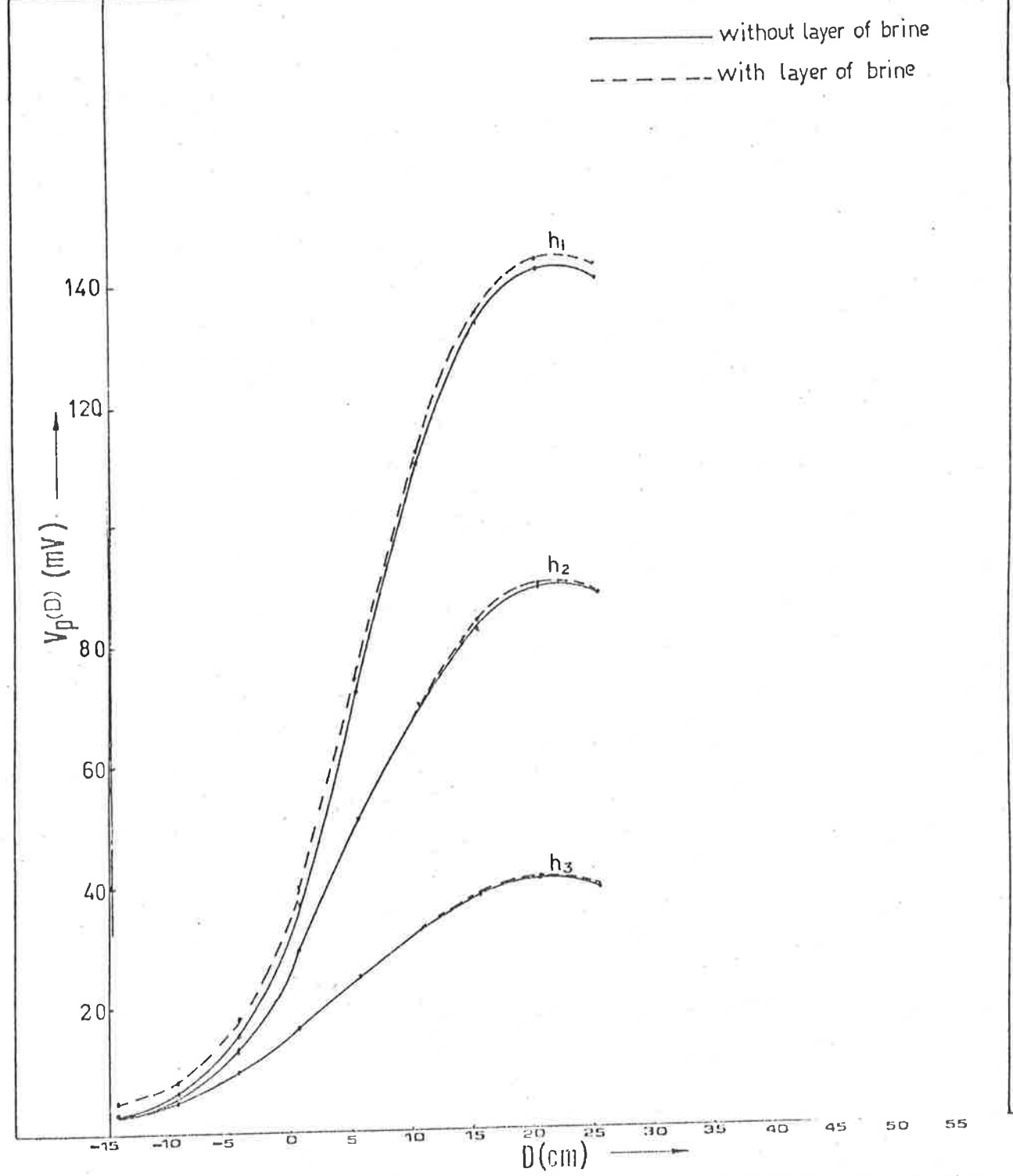


Fig. 5.14 Image Voltage Characteristics as a Function of Distance D with the Sensor Immersed in Brine Solution.

If we consider the L-shaped plate to resemble the front section of the vehicle, and neglect values of P obtained for $h < 12\text{cm}$, we obtain a new range of values from Table 5.3 which are well defined. Therefore P can be assigned a value of 27 with a tolerance of $\pm 4\%$.

5.3 DERIVATION OF P USING ACTUAL VEHICLES

The experimental procedure discussed in Chapter 4 was repeated using three different makes of vehicles. The vehicles considered were

- (i) 1972 Ford Futura
- (ii) 1976 Chrysler Centura
- (iii) 1976 Datsun 180B

The above choices were made on the basis that the "front" sections of these vehicles were sufficiently different to allow satisfactory method of testing the model defined by Eq.(4.3)

The sensor was located on the road surface and the output of the receiver coil was recorded as a function of distance D , as a vehicle approached the sensor. Measurement of D was in accordance with our definition of section 4.1. The experimental set up is shown in Fig. 5.15. To have some degree of uniformity of the measurements between the three vehicles, D was referenced with respect to the centre of the front bumper bar as shown in Fig. 5.16. The approach was made on the basis of the regularity of "front" section associated with most vehicles.

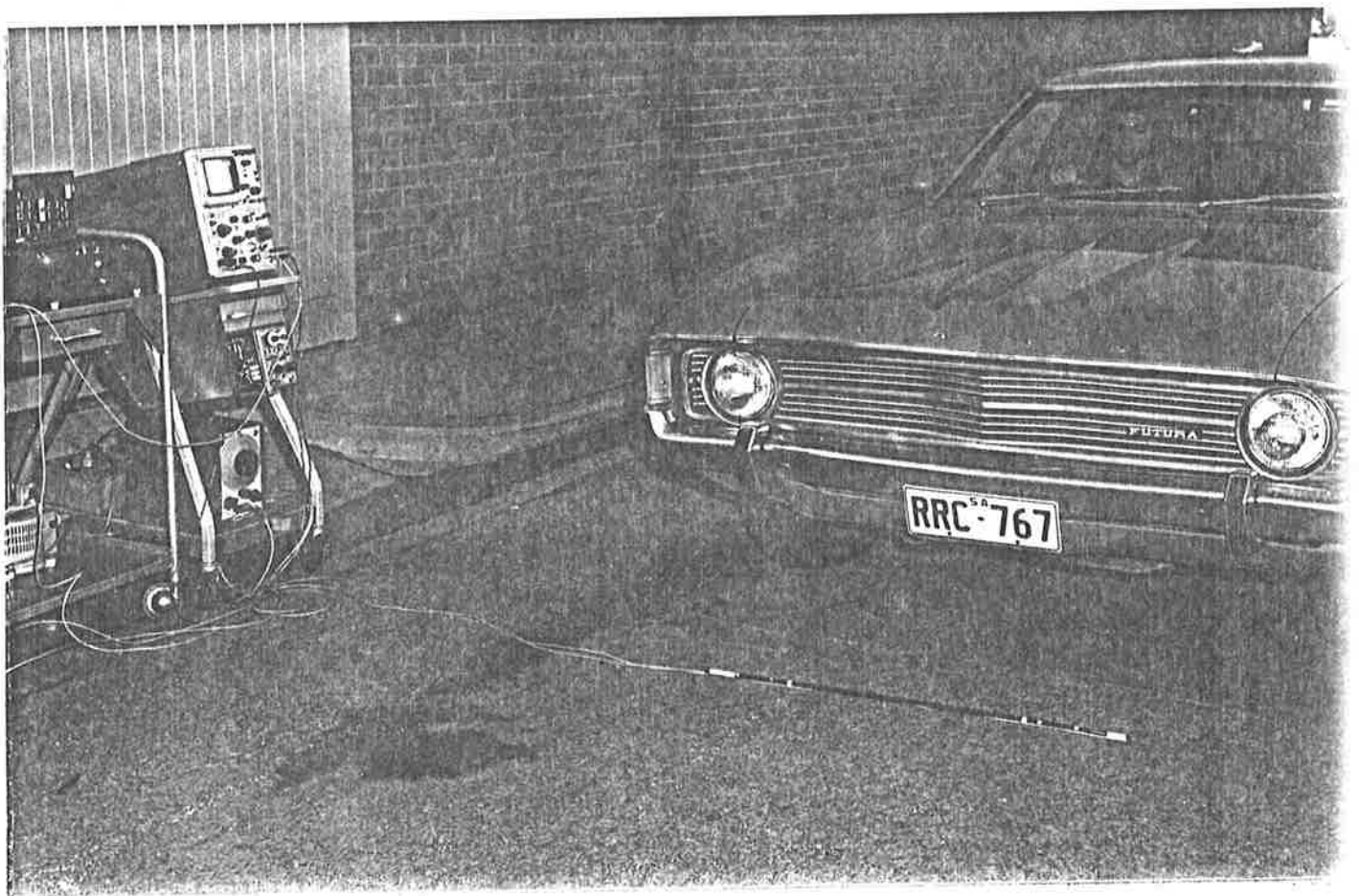


Fig. 5.15 Experimental set up Showing Position of Sensor Relative to the Vehicle

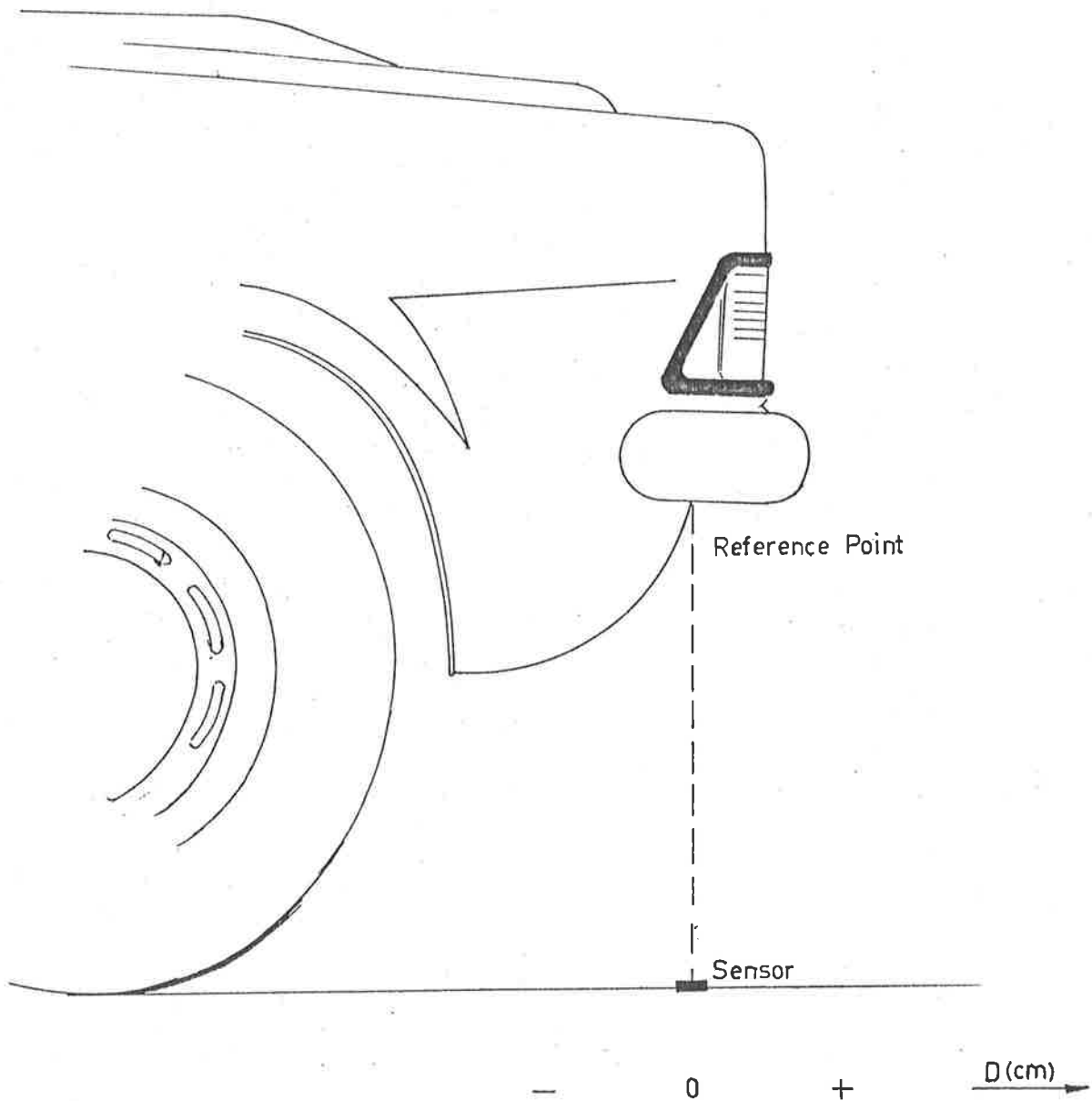


Fig. 5.16 Relationship Between the Sensor and the "Front" Bumper Bar of the Vehicle

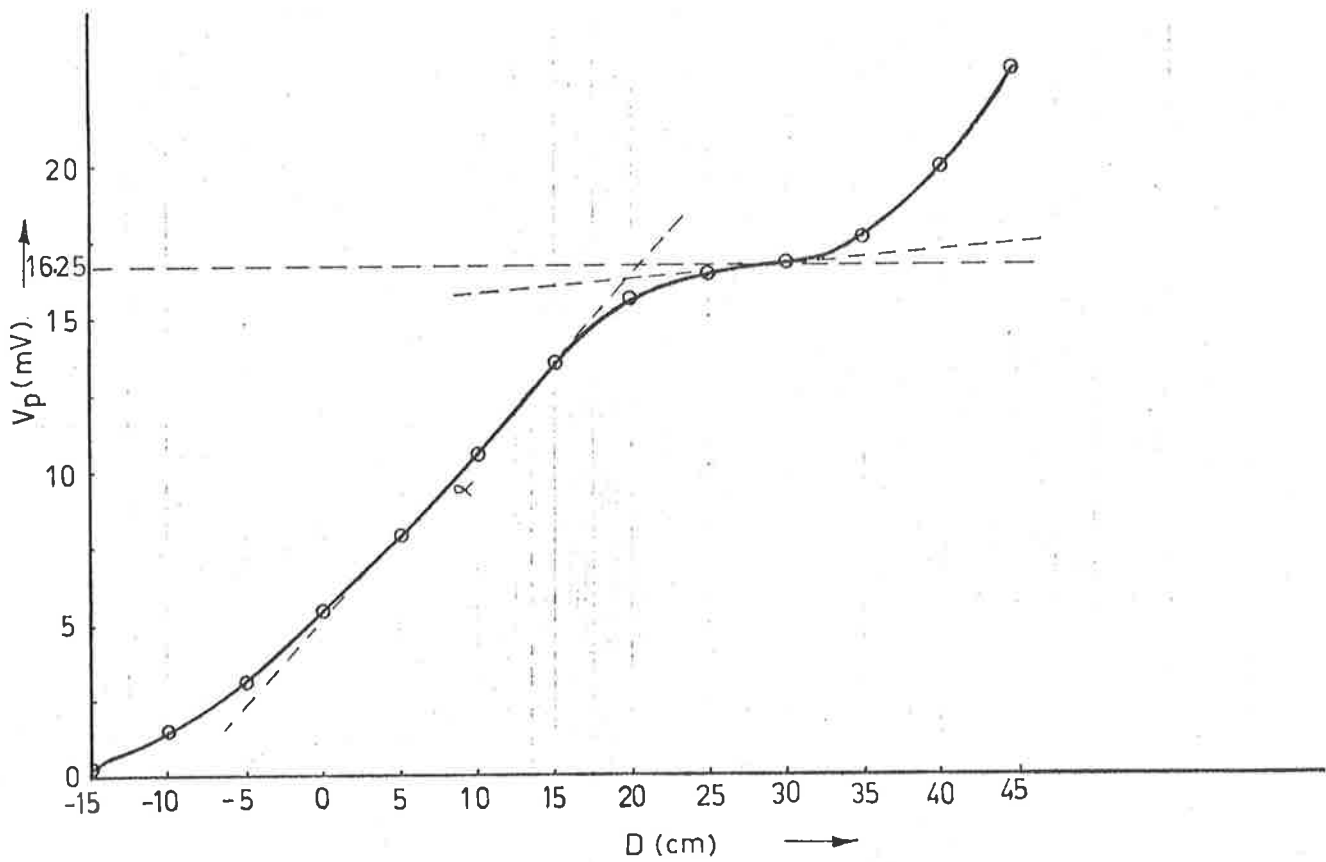
The magnitude of the image voltage as a function of distance are shown in Fig. 5.17, Fig. 5.18 and Fig. 5.19. The values of P for the Ford, the Centura and the Datsun are shown in Table 5.5. A similar characteristic was also plotted for the "rear" section of the Datsun as illustrated in Fig. 5.20. The value of P in this case was found to be 26.54.

Two important features in the behaviour of the image voltage characterised by the "front" section of the vehicle are noted:

- (i) The image voltage rises to its peak and then levelling occurs before it rises again. The Ford and Centura gave this effect.
- (ii) the image voltage rises to its peak and then decays. This effect was noted with the Datsun and is mainly due to the flat cover-plate used in the undercarriage.

5.4 CONCLUSIONS

The L-shaped plate adopted in the experimental procedure, resulted in a value of P which was found to be substantially constant for values of $h > 12\text{cm}$. The value assigned to P is 27 having a tolerance of $\pm 4\%$. This is consistent with the observed range. If the results of the horizontal plate are also included, the tolerance can be extended to $+4\%$, -15% .

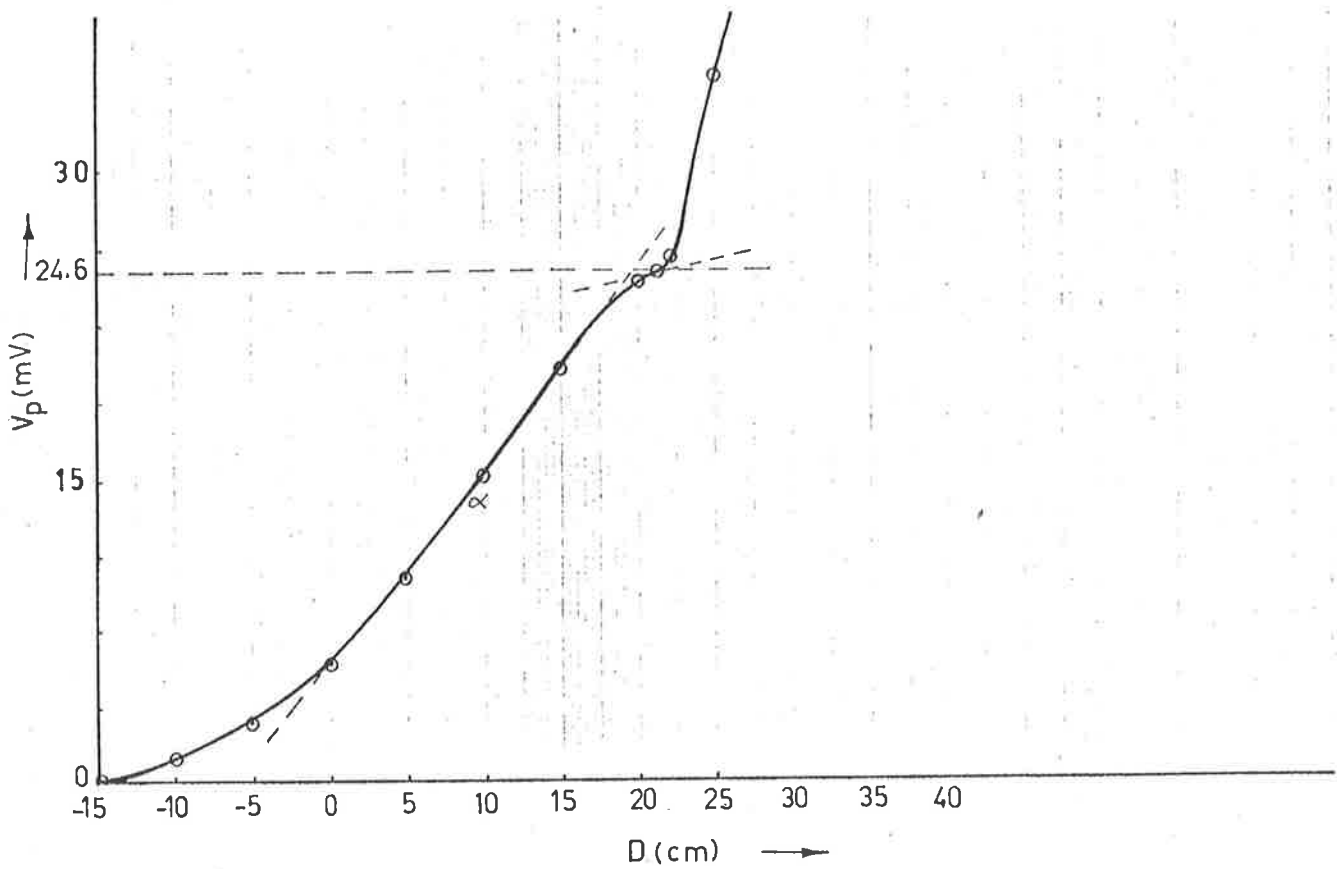


$$V_{p_m} = 16.25 \text{ mV}$$

$$\alpha = 0.60$$

$$P = 27.01$$

Fig. 5.17 Image Voltage Characteristics as a function of distance for "Front" Section of a 1972 Ford Futura

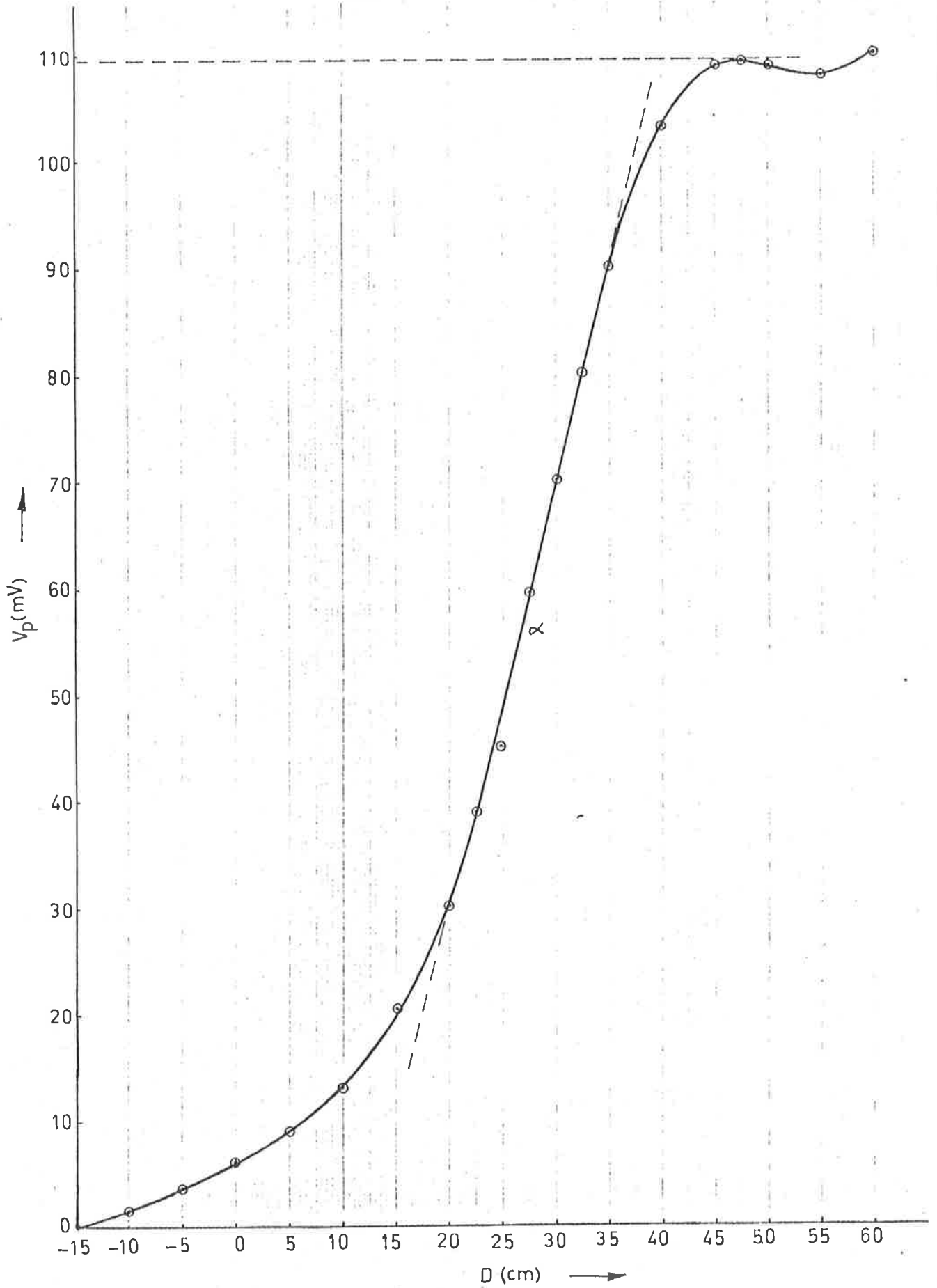


$$V_{pm} = 24.6 \text{ mV}$$

$$\alpha = 0.93$$

$$P = 26.45$$

Fig. 5.18 Image Voltage Characteristic as a function of distance for the "Front" Section of a 1976 Chrysler Centura.

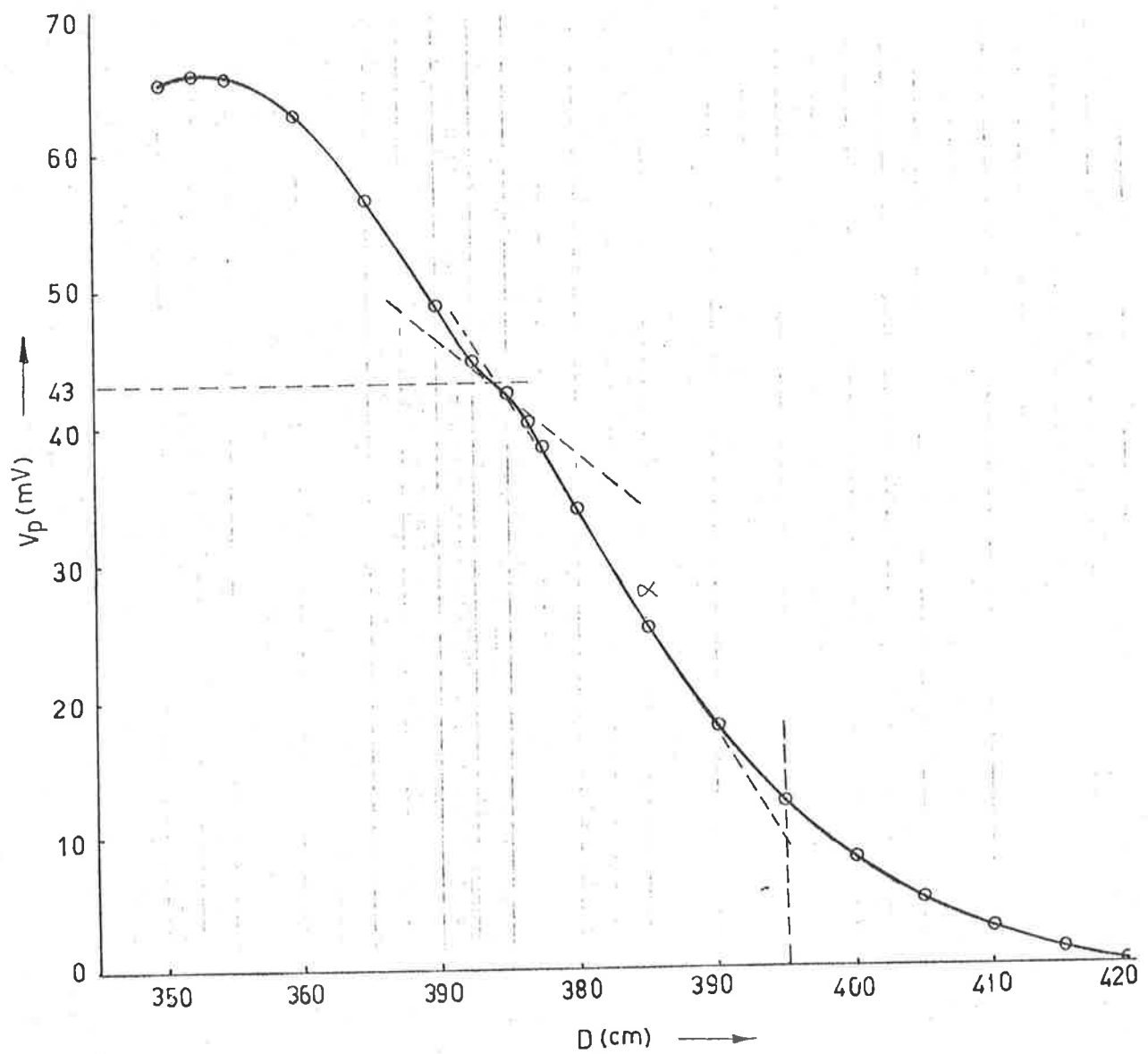


$$V_{Pm} = 109.5 \text{ mV}$$

$$\alpha = 4.01$$

$$P = 27.37$$

Fig. 5.19 Image Voltage Characteristics as a function of distance for the "Front" Section of a Datsun 180B



$$V_{P_m} = 43.0 \text{ mV}$$

$$\alpha = 1.62$$

$$p = 26.54$$

Fig. 5.20 Image Voltage Characteristics as a function of distance for the "Rear" Section of a Datsun 180B

Vehicle \ Parameters	α_m	V_{p_m}	r_c	P
FORD	0.60	16.25	0.981	27.01
CENTURA	0.93	24.60	0.991	26.45
DATSUN	4.01	109.5	0.983	2 737

Table 5.5 Value of P for the Front Section of Three Different Vehicles using the Parameters of the Speed Model

The values of P derived using the V_p versus D characteristics of the "front" sections of the three vehicles were within the expected range and corresponded closely to the values obtained for an L-shaped plate. The recognition and the subsequent identification process associated with either the first turning point or the point of inflection, provide the basis for establishing the value of V_{p_m} . It should be noted that it is possible other structures associated with the "front" bumper-bar may be encountered in practice where the value of P may be outside the expected range. However limitations of the approach can only be assessed through further experimental studies focused on a variety of vehicles and traffic conditions which are beyond the scope of this thesis.

CHAPTER 6

SPEED ESTIMATION

6.1 MODELLING TECHNIQUE

In order to estimate the speed of a vehicle using the output of the sensor described in Chapter 3, it is necessary to redefine the parameters of the fundamental speed equation (2.4) in terms of the output characteristics of the receiver coil R_x . Referring to Eq. 4.1, the effective distance D_e observed by the sensor is given by

$$D_e = \frac{(V_2 - V_1)}{V_{P_m}} \cdot P \quad \dots(6.1)$$

where

$$D_e = (D_2 - D_1)$$

This results from the similarity of the shapes of the V_p vs D graphs on which the constancy of P is based. This is illustrated in Fig. 6.1(a).

The interval corresponding to D_e is determined by measuring the transition period of $V_p(t)$ from V_1 to V_2 , as shown in Fig. 6.1(b).

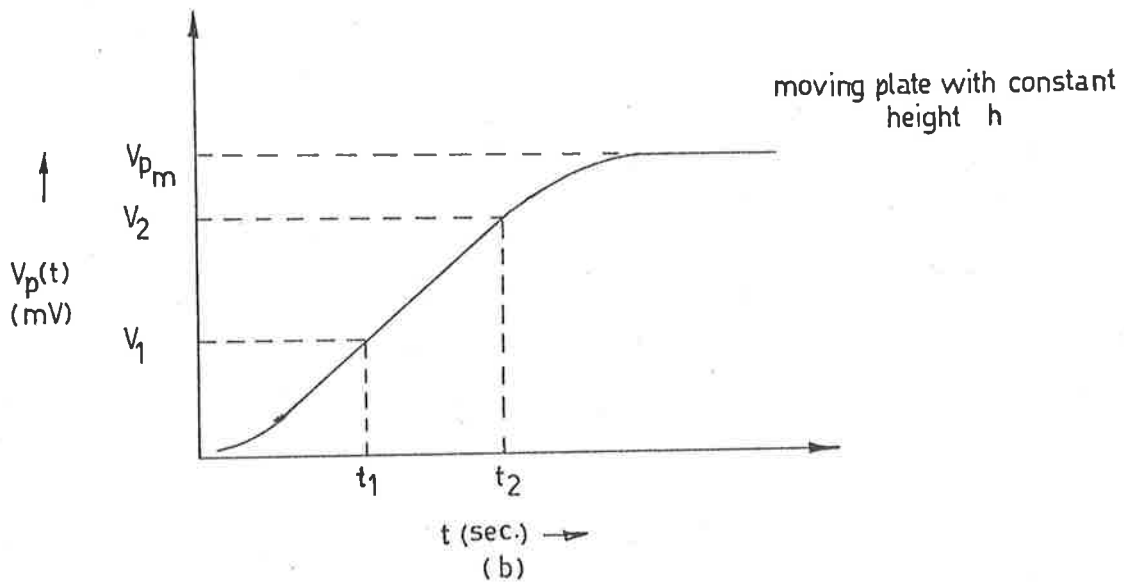
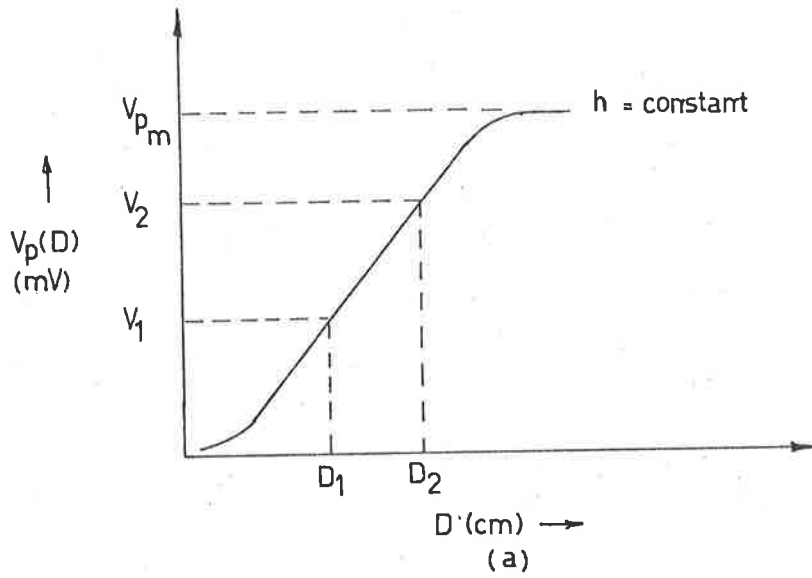


FIG 6.1 (a) Change in induced voltage in receiver coil as a function of distance D .
 (b) Change in induced voltage in receiver coil as a function of time with change in D .

The speed S can be expressed as

$$S = \frac{D_e}{(t_2 - t_1)} \quad \dots (6.2)$$

which can be rewritten in terms of the measurable output parameters of the sensor. Thus

$$S = \frac{(V_2 - V_1)}{(t_2 - t_1)} \cdot \frac{P}{V_{p_m}} \quad \dots (6.3)$$

Since units for distance and time in Eq. (6.3) are cm and seconds respectively, a conversion factor of 0.036 is incorporated to change to Kilometres per hour (Kph). The modified expression becomes

$$S = \left(\frac{\Delta V_p}{\Delta t_e} \right) \cdot \left(\frac{P}{V_{p_m}} \right) 0.036 \quad \dots (6.4)$$

where

$$\Delta V_p = (V_2 - V_1) \quad \dots (6.5)$$

and

$$\Delta t_e = (t_2 - t_1) \quad \dots (6.6)$$

The resolution to which the speed can be estimated, however, will depend on the relative contribution of the constant P and the accuracy with which V_{p_m} and $\frac{\Delta V_p}{\Delta t_e}$ are determined.

The accuracy of the procedure due to the slight uncertainty associated with the value of P is determined by differentiating Eq.(6.4) to obtain

$$\left| \frac{\Delta S}{S} \right| = \left| \frac{\Delta P}{P} \right| \quad \dots(6.7)$$

This is plotted in Fig. 6.2 in terms of percentage speed error as a function of an incremental change ΔP .

Similarly the error associated with determination of V_{p_m} is given by

$$\left| \frac{\Delta S}{S} \right| = \left| - \frac{\Delta V_{p_m}}{V_{p_m}} \right| \quad \dots(6.8)$$

The percentage speed error is plotted in Fig. 6.3 for several values of V_{p_m} as a function of an incremental change ΔV_{p_m} .

If $\frac{\Delta V_p}{\Delta t_e}$ is denoted by α_t then upon differentiation we obtain

$$\left| \frac{\Delta S}{S} \right| = \frac{\Delta \alpha_t}{\alpha_t} \quad \dots(6.9)$$

The behaviour of the error is similar to the previous cases and is mainly circuit orientated.

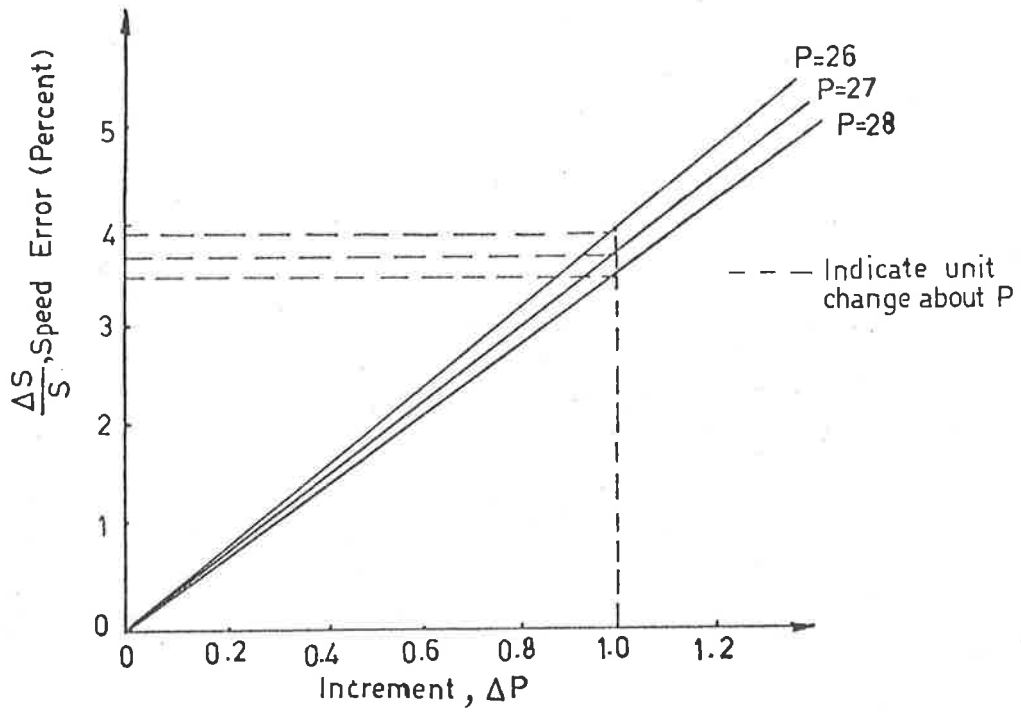


Fig. 6.2 Percentage Speed Error in Terms of the Deviations About P .

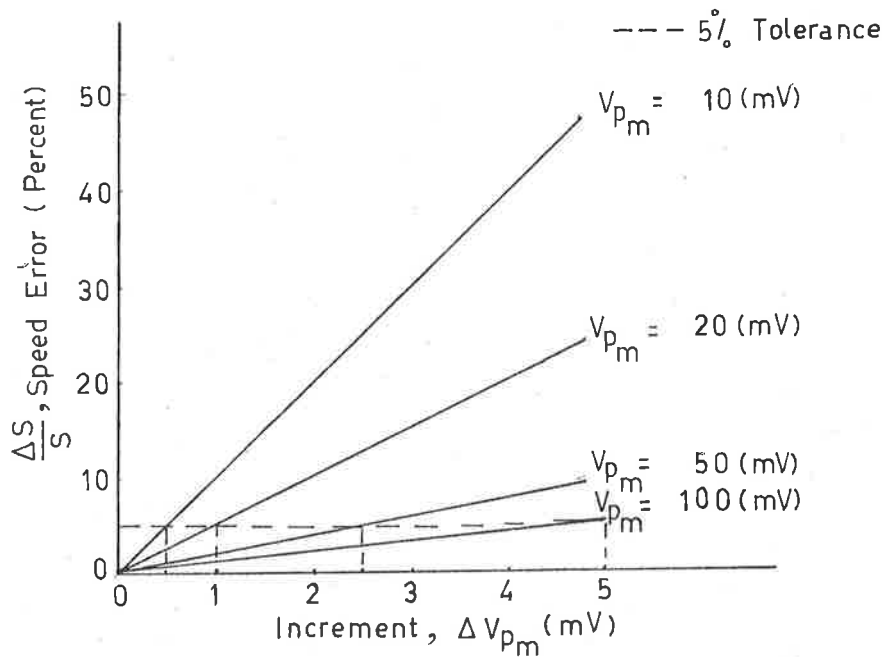


Fig. 6.3 Percent Speed Error in Terms of the Deviations About V_{p_m} .

6.2 IDENTIFICATION OF THE PEAK VALUE OF THE IMAGE VOLTAGE

The model defined by Eq.(6.4) for speed measurements requires identification of V_{p_m} .

To define a suitable criteria for detection of V_{p_m} in real time the properties of V_{p_m} prior to, and in the vicinity of, the peak must be examined. Observations of the change in image voltage resulting from an approaching vehicle as described in Section 5.3 provided us with two cases of interest.

(i) $V_p(t)$ rises to its peak and then drops.

This is illustrated in Fig. 6.4(a).

(ii) $V_p(t)$ rises to its peak and then levelling occurs before it rises again.

This is shown in Fig. 6.4(b).

In case (i) the peak of $V_p(t)$ may be defined as the first point at which

$$\frac{dV_p(t)}{dt} = 0 \quad \dots(6.10)$$

$$\frac{d^2V_p(t)}{dt^2} < 0 \quad \dots(6.11)$$

and may be identified some time Δt after its occurrence.

In case (ii), the curve passes from below the tangent as shown in Fig. 6.4(b) to a point above it.

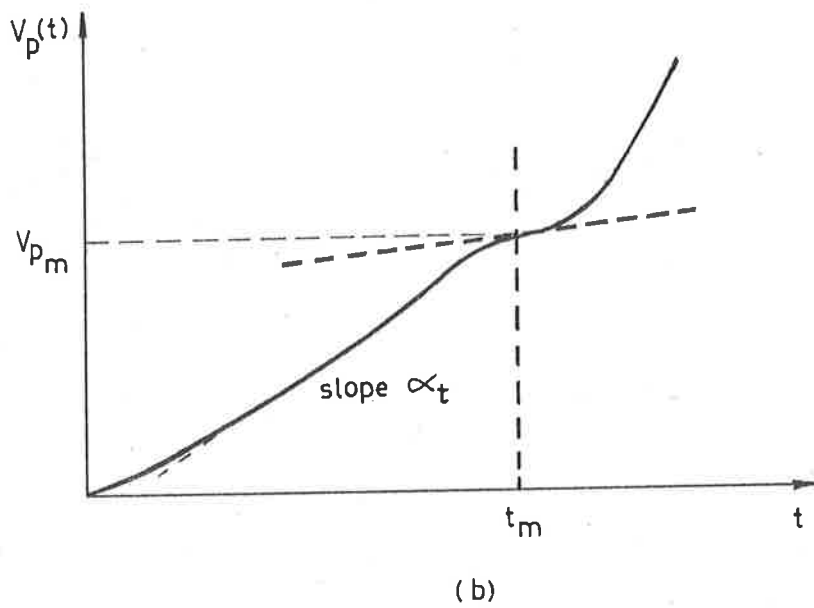
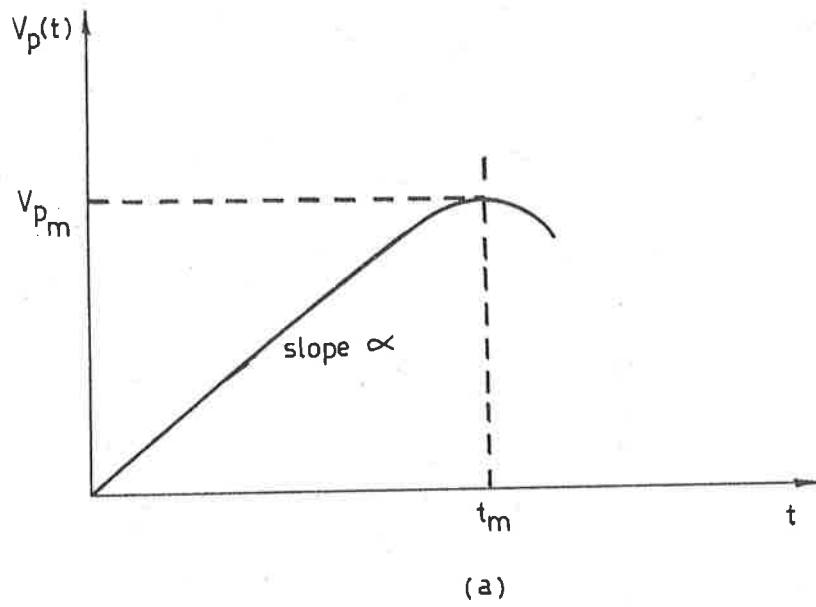


Fig. 6.4 Behaviour of $V_p(t)$ Prior to and in the Vicinity of the Peak

- (a) $V_p(t)$ rises as a non decreasing function to its peak before decaying
- (b) $V_p(t)$ having a point of inflection.

The second derivative $\frac{d^2 v_p(t)}{dt^2}$ changes sign from

negative to positive, thus we look for

$$\frac{d^3 v_p(t)}{dt^3} > 0 \quad \dots(6.12)$$

Since the derivatives are "a posteriori" function derived from the received signal, they can only be formulated at times $(t+\Delta t)$. Although we require at least a one step memory, for small values of Δt , the process can be considered to operate almost in real time.

6.3 CIRCUIT REALIZATION

The block diagram and the relevant waveform for the speed measuring system is shown in Fig. 6.5.

The circuit basically consists of six main sections. ⁸⁷

6.3.1 Receiver Amplifier

This is a narrow band tuned circuit receiver having a centre frequency $f_0 = 100\text{KHz}$ and a bandwidth $\Delta B = 5\text{KHz}$. The circuit consists of a two stage unity gain power amplifier and provides the matching between the lead-in cable and the demodulator.

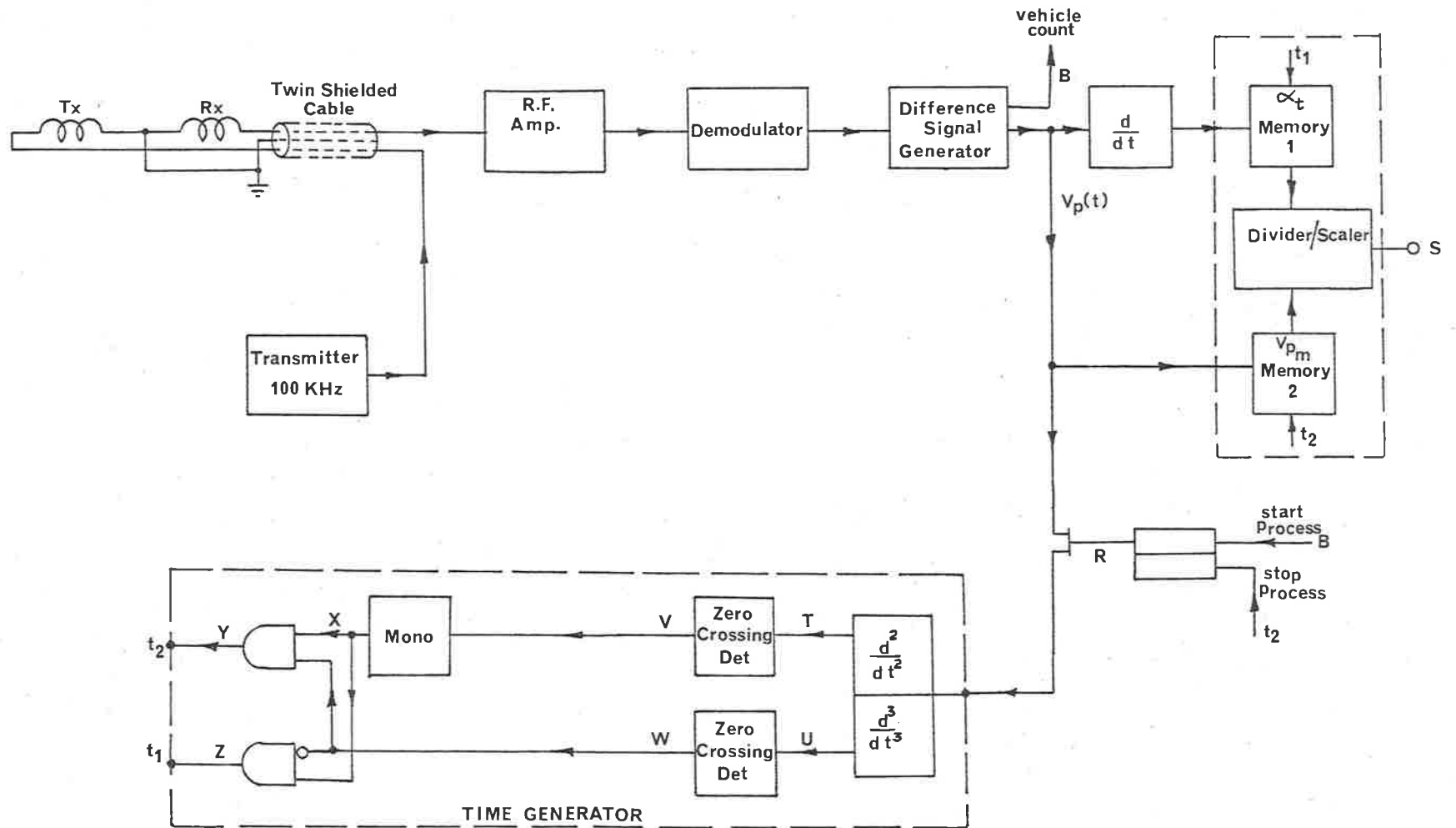


Fig. 6.5(a) Block Diagram for Speed Measuring Circuit

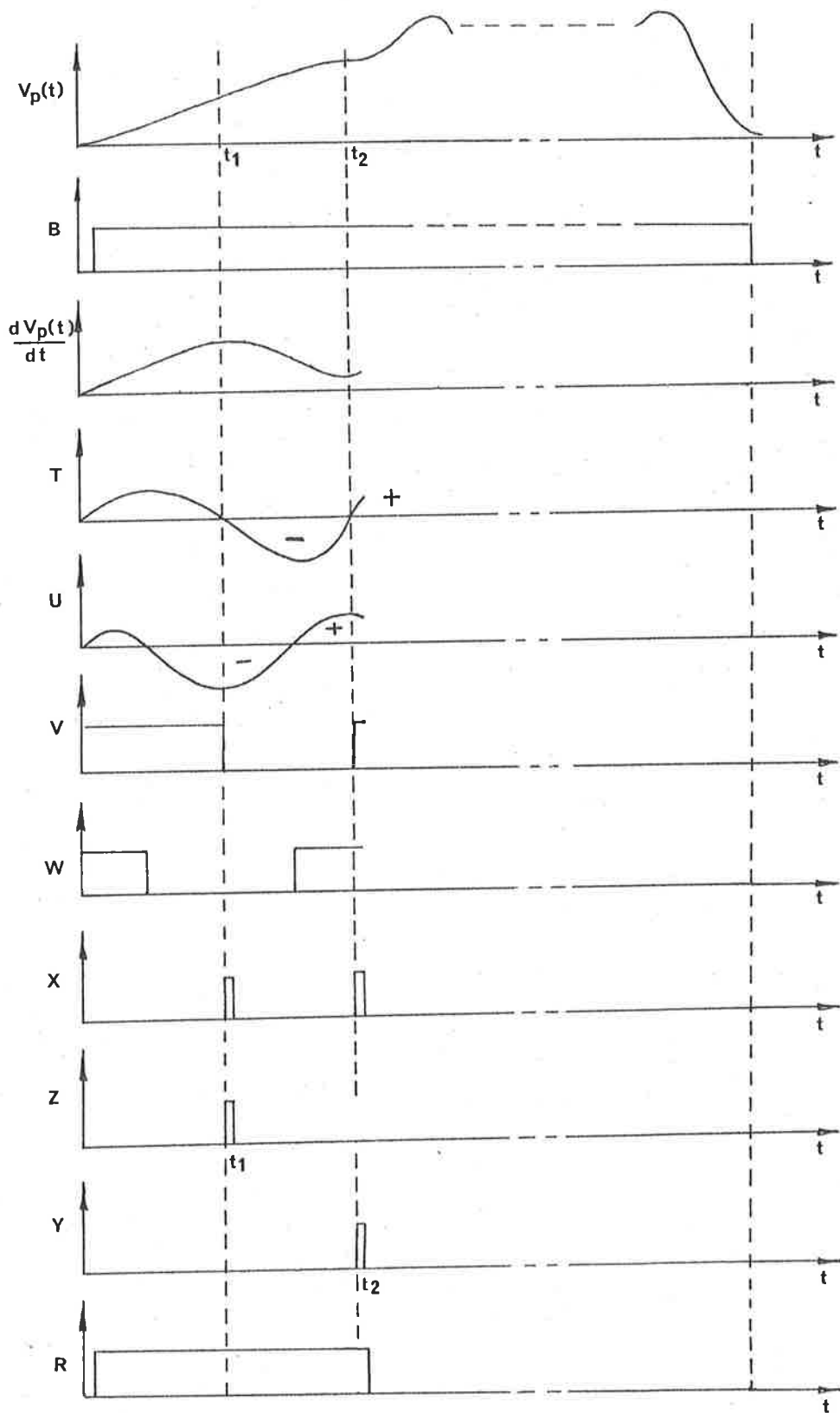


Fig. 6.5(b) Waveforms for Speed Measuring Circuit

6.3.2 Demodulator

The circuit shown in Fig. 6.6 uses a phase-lock loop (PLL) which functions as a synchronous AM detector and lock onto the carrier of the AM signal (100KHz) so that the voltage controlled oscillator (VCO) output, has the same frequency as that of the carrier but no amplitude modulation. The demodulated AM is obtained by multiplying the VCO signal with the modulated input signal and then filtering the output to remove all but the difference frequency components. When the frequency of the input signal is identical to the free running frequency of the VCO, the loop goes into lock with these signals 90° out of phase. If the input signal is now shifted 90° so that it is in phase with the VCO signal and the two signals are mixed in a second phase comparator, the average DC value (difference frequency component) of the phase comparator output will be directly proportional to the amplitude of the input signal. Thus, the method is essentially a coherent detector which involves averaging of two compared signals, and therefore offers a good immunity against ignition noise.*

* Ignition noise covers the range 200KHZ - 30MHZ.

6.3.3 Difference Signal Generator ⁸⁸

The circuit removes the bias which exists due to carrier and produces the image voltage V_p resulting from the presence or the passage of a vehicle. This arrangement is particularly important in compensating for slow changes due to environment. This is shown in Fig. 6.7. The circuit also provides the vehicle count information.

6.3.4 Differentiator

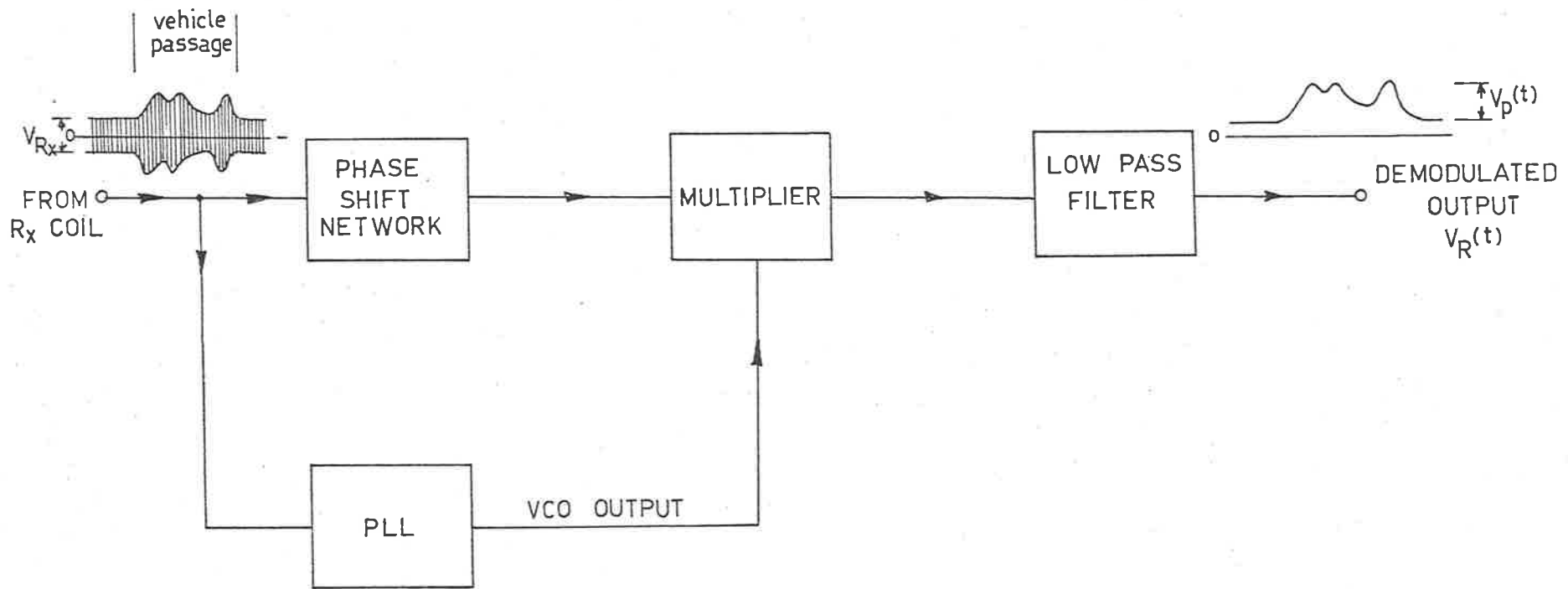
The operation of the circuit shown in Fig. 6.8 is based on the time derivative definition of a time dependent voltage

$$\frac{dV(t)}{dt} = \lim_{\Delta t \rightarrow 0} \frac{V(t+\Delta t) - V(t)}{\Delta t} \quad \dots(6.13)$$

Two sample and hold circuits which sample the input signal at times t and $t+\Delta t$ and subtract one from the other, are used. The value of Δt is set by an external clock and is selected according to the frequency range of the input signal.

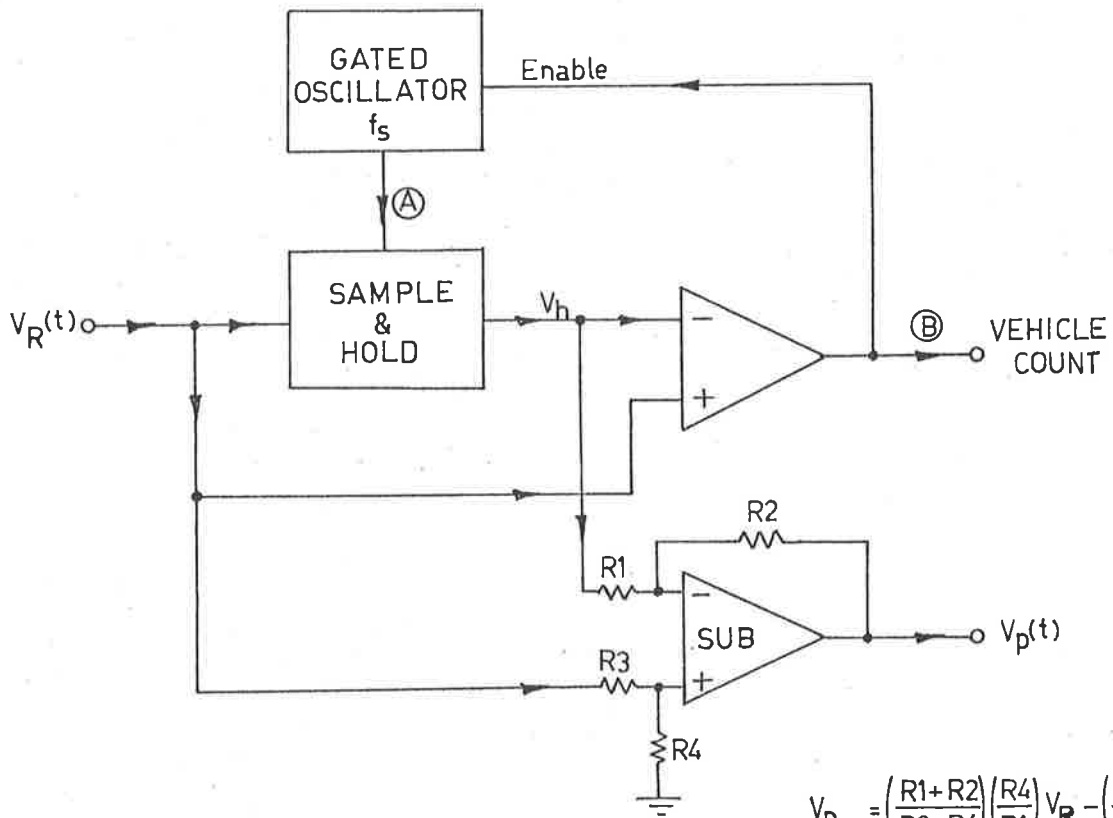
6.3.5 Divider

This technique uses logarithmic converters as shown in Fig. 6.9 for dividing two analogue signals. In addition, the arrangement provides the necessary scaling factor of (0.036P). ⁷⁵



Signetics NE 561 B Integrated cct.

Fig. 6.6 Block Diagram - Demodulator



$$V_p = \left(\frac{R1+R2}{R3+R4} \right) \left(\frac{R4}{R1} \right) V_R - \left(\frac{R2}{R1} \right) V_h$$

for $R1 = R2 = R3 = R4$

$$V_p = \frac{R2}{R1} (V_R - V_h)$$

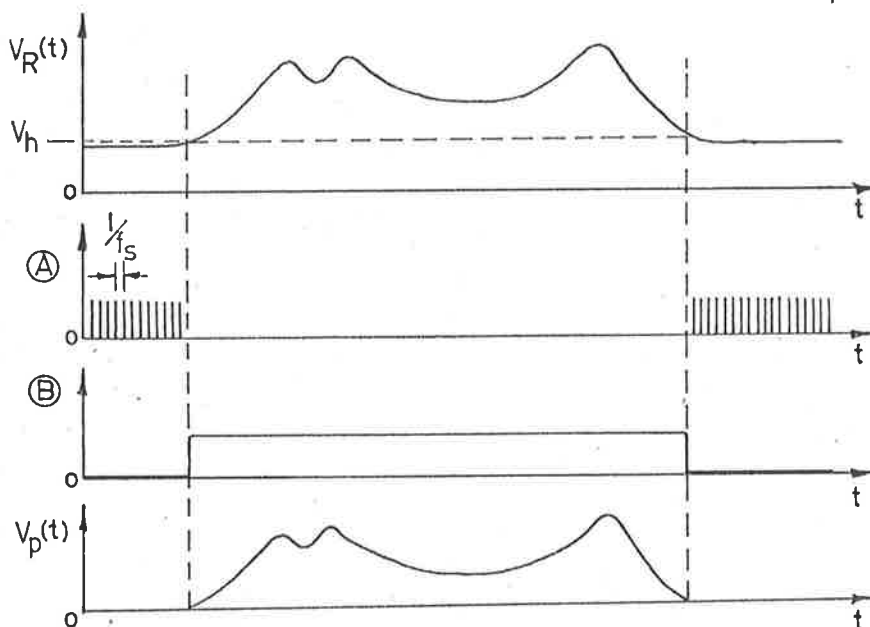
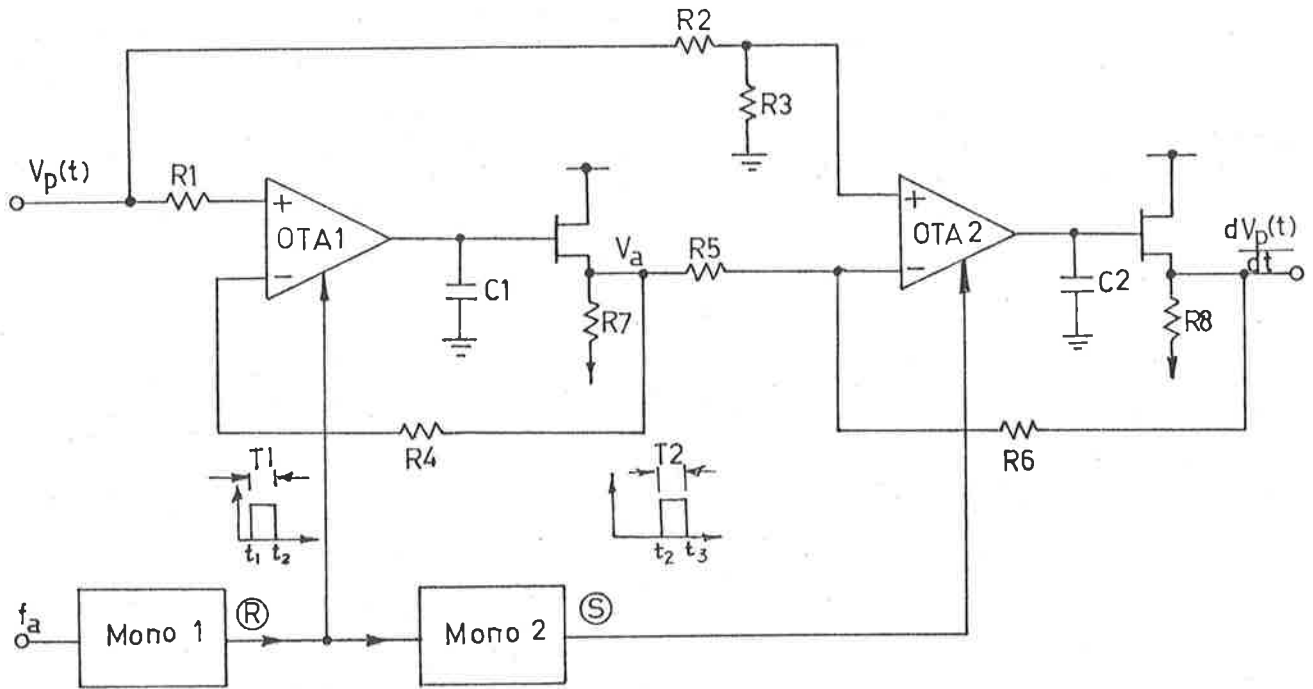


Fig. 6.7 Difference Signal Generator



OTA1, OTA2 = Op. Transconductance Amp.
RCA CA 3060D

$$\begin{aligned} \frac{dV_p(t)}{dt} &= a V_p - b V_a \\ &= \frac{R_3}{R_2 + R_3} \left(1 + \frac{R_6}{R_5} \right) V_p - \left(\frac{R_6}{R_5} \right) V_a \\ \text{for } \frac{R_6}{R_5} = \frac{R_3}{R_2} = 1 \\ &= V_p - V_a \end{aligned}$$

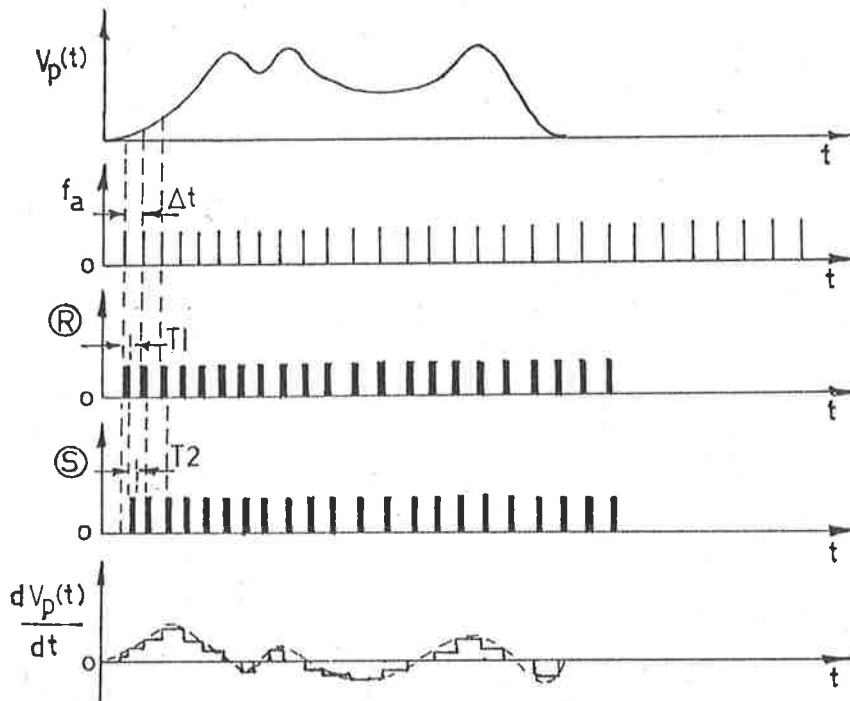
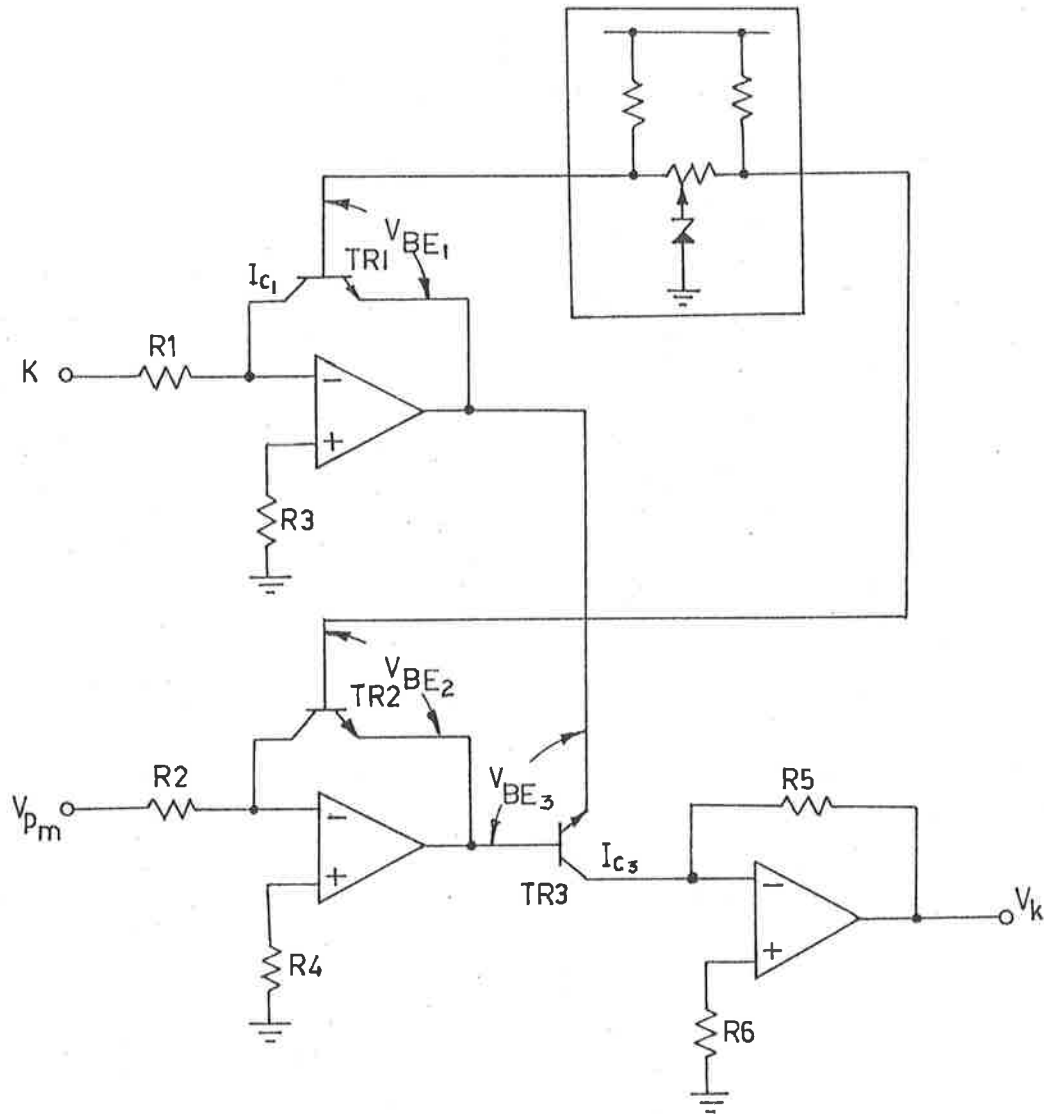


Fig. 6.8 Differentiator



$$V_{BE1} = \frac{q}{kT} \log_e I_{c1}$$

$$I_{c1} = \frac{K}{R1}$$

$$\therefore V_{BE1} \propto \log_e K$$

Similarly

$$V_{BE2} \propto \log_e V_{p_m}$$

I_{c3} varies as exponent of V_{BE3}

$$\therefore I_{c3} \propto \frac{K}{V_{p_m}}$$

$$V_k = \frac{K}{V_{p_m}}, \quad \text{Where } K = 0.036P$$

Fig. 6.9 Divider / Scaler

6.3.6 Time Generator

The time generator provides the clocking information as to the instant when a particular process such as storage of V_{p_m} , division etc., is to commence.

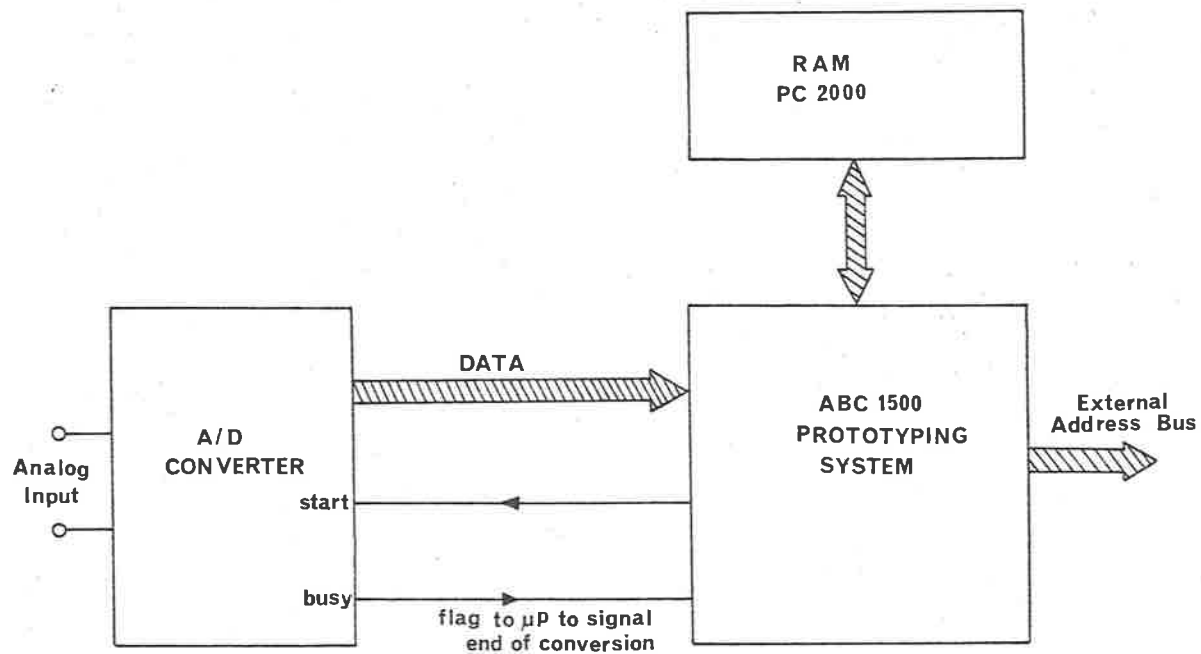
6.4 EXPERIMENTAL RESULTS

Signatures* of several vehicles were recorded by driving the vehicles at constant speed over the sensor situated on the road surface at a controlled experimental site within the Philips area at Hendon, S.A. The block diagram of the data acquisition system using the Signetics microprocessor ABC ⁷⁶⁻⁸⁴ 1500 card and additional memories, is shown in Fig. 6.10. The digitized data was subsequently punched and used as the input to the University's CDC 6400 Computer.

Signatures for 72 Ford Futura, '76 Centura and '76 Datsun 180B are shown in Fig. 6.11, Fig. 6.12 and Fig. 6.13 respectively. In order to obtain the speed, the initial part of the waveforms were analysed using the model defined by Eq.(6.4) in accordance with the identification criteria of section 6.2. The differentiation subroutine used on the data is shown in Appendix V. The results of the procedure are given in Table 6.1.

Table 6.2 shows the comparison between the values

* by this term it is meant the change in the image voltage as the vehicle passes over the sensor



- NOTE: (1) A/D converter type AD7550
(Analog Devices)
- (2) Sampling period of 0.6 mSec
is chosen on the basis of the
available memory capacity and
vehicle speed 20Km/h

Fig. 6.10 Block Diagram - Data Acquisition System

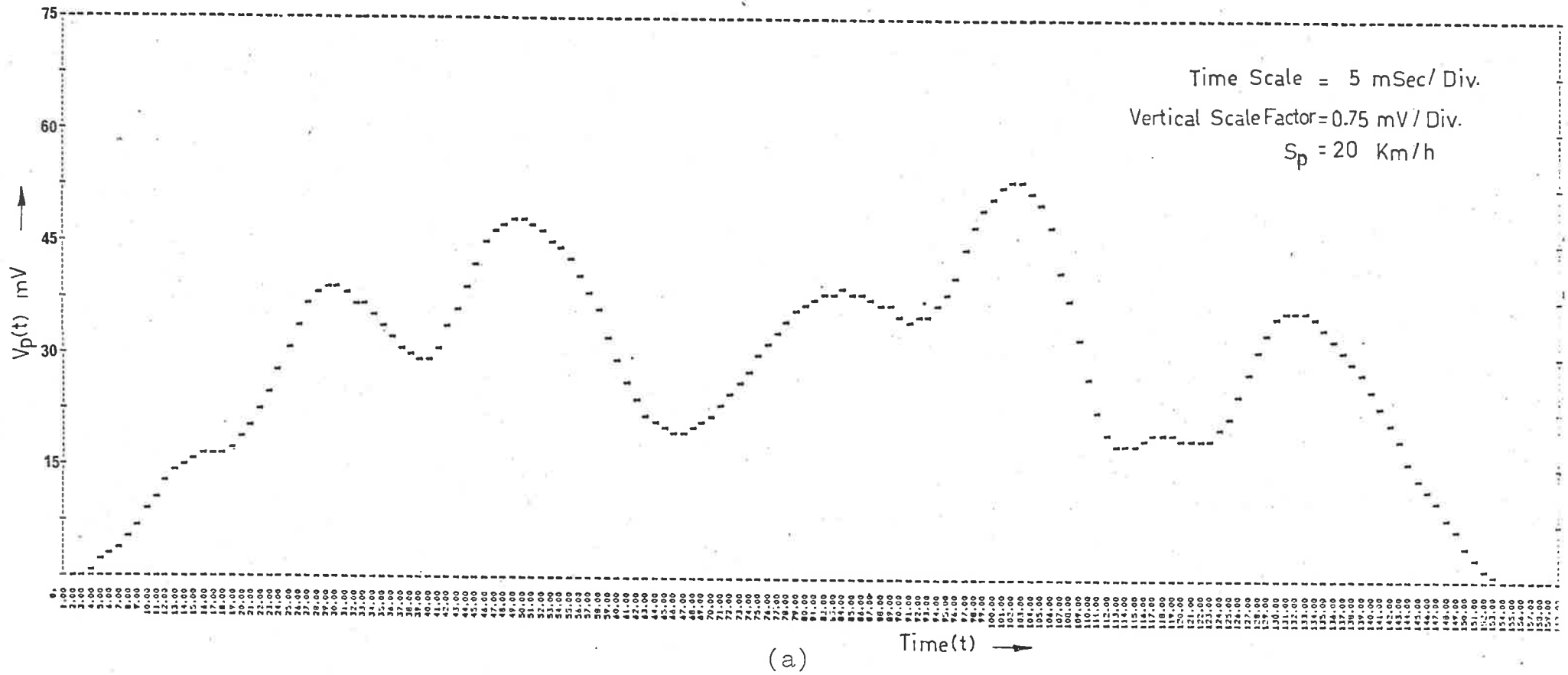


Fig. 6.11 Characteristic Signature for 1972 Ford Futura
 (a) Signature as a Function of Time

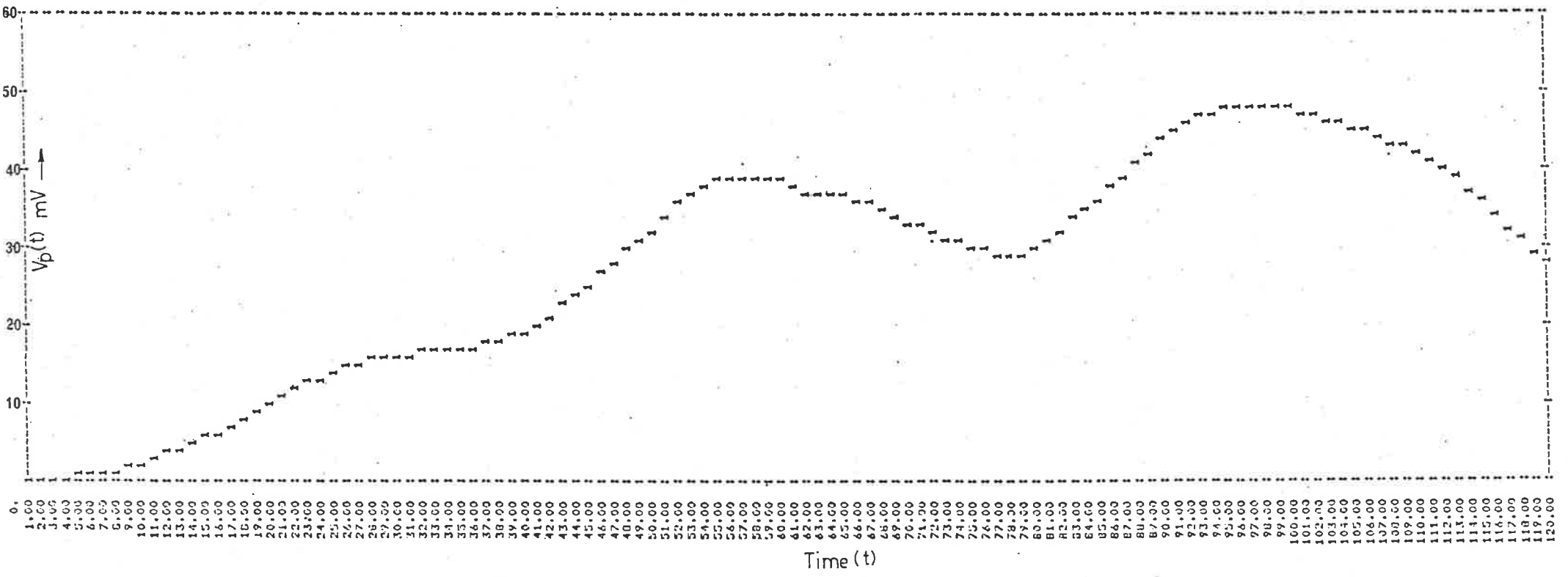
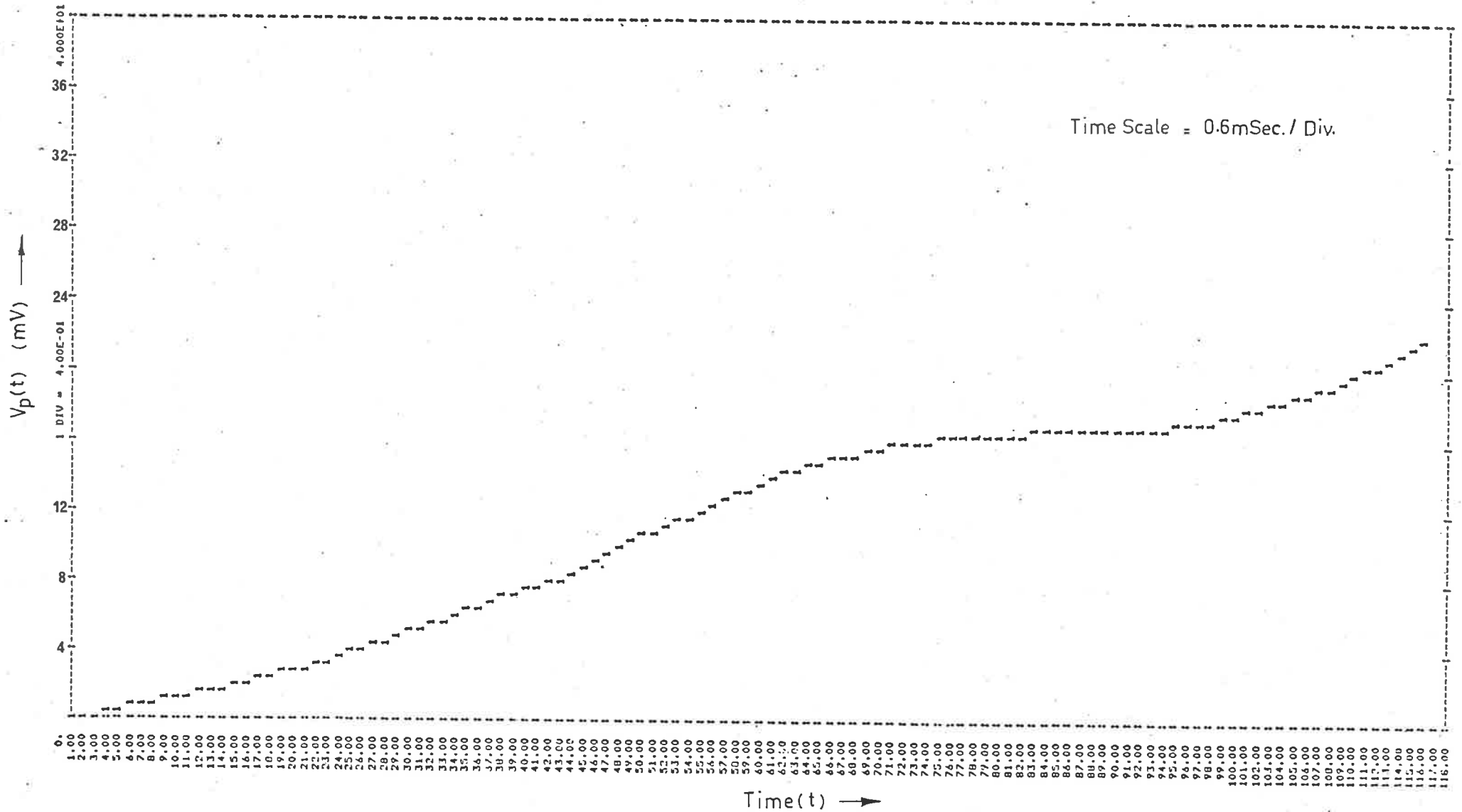


Fig. 6.11(b) Expanded 'Front' Section - Ford Futura



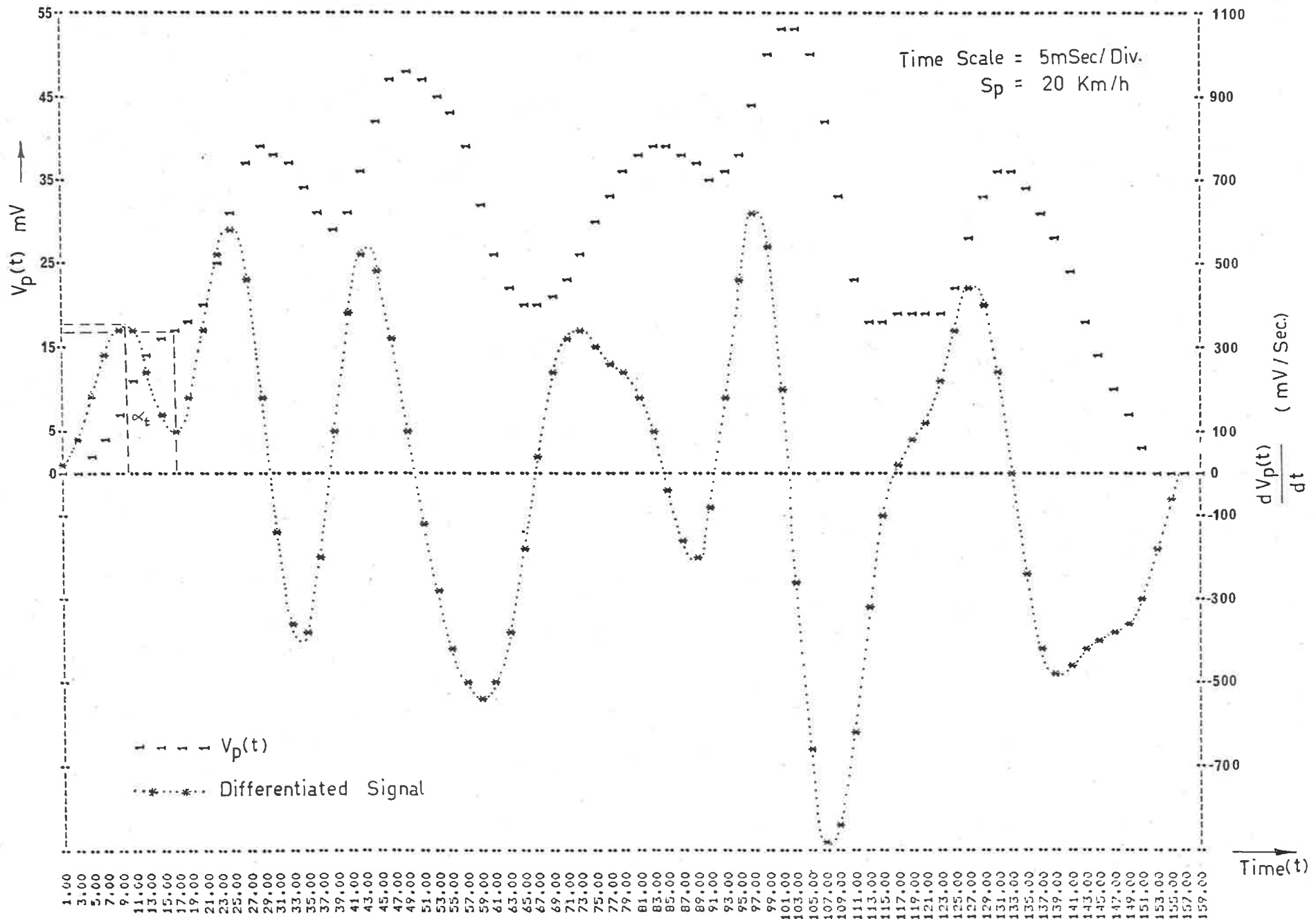


Fig. 6.11 (d) The Signature and the Differentiated Signal for 1972 Ford Futura

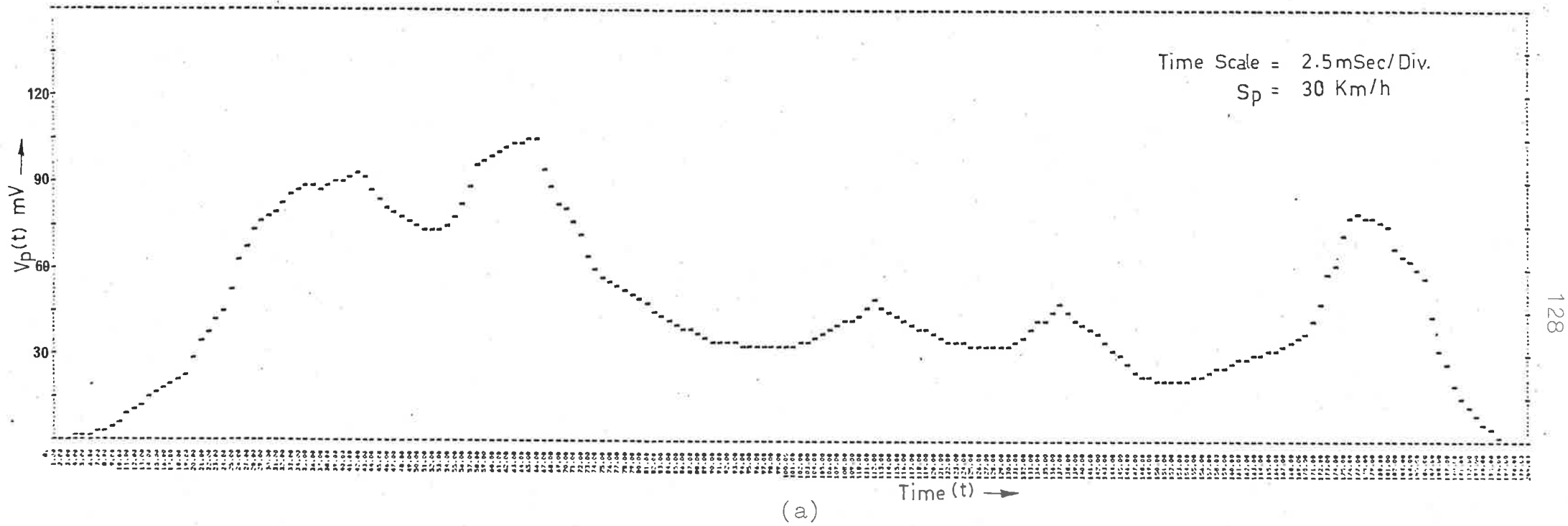


Fig. 6.12 Characteristic Signature for 1976 Chrysler Centura
(a) Signature as a Function of Time

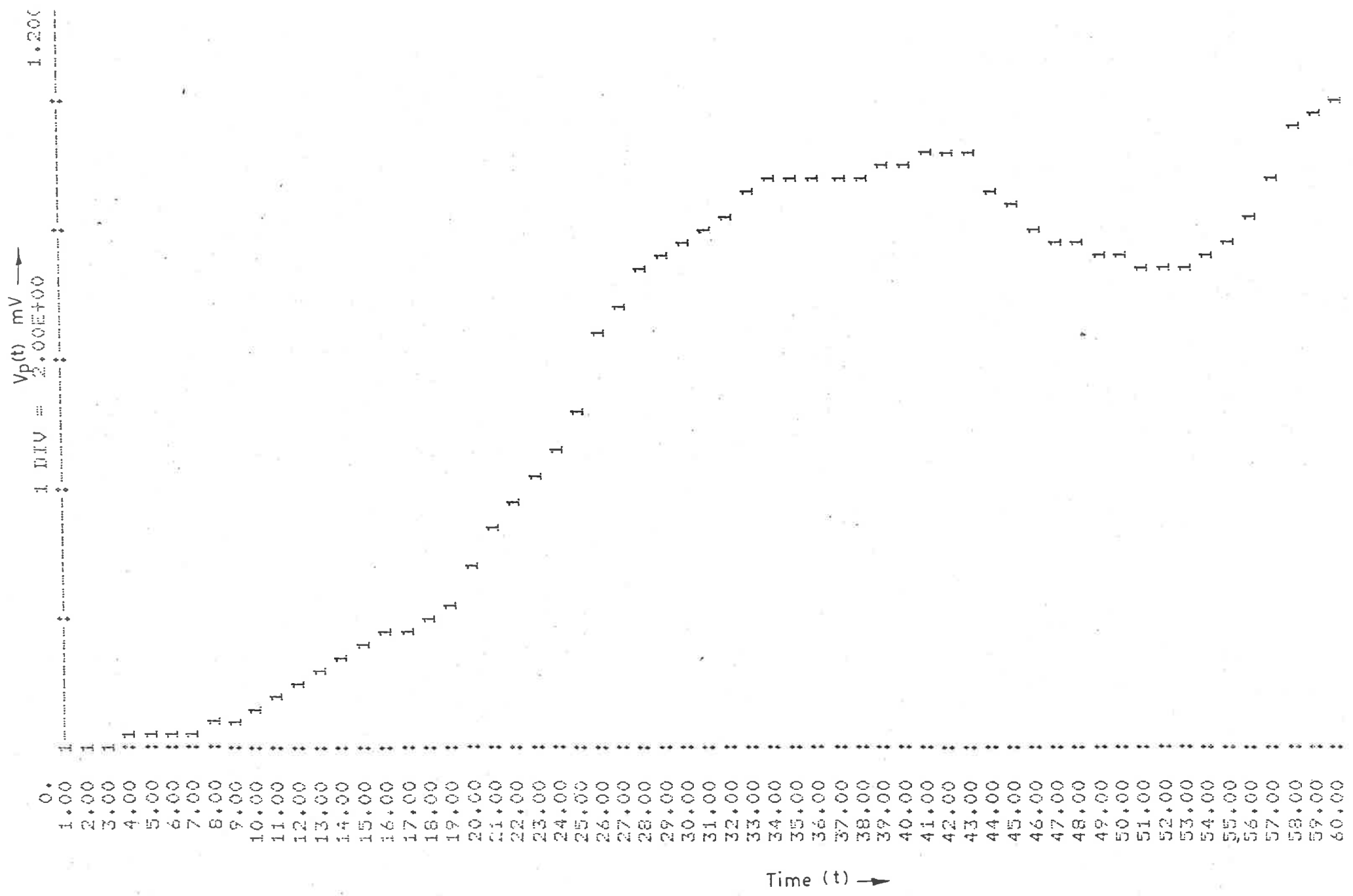


Fig. 6.12(b) Expanded 'Front' Section - Chrysler Centura

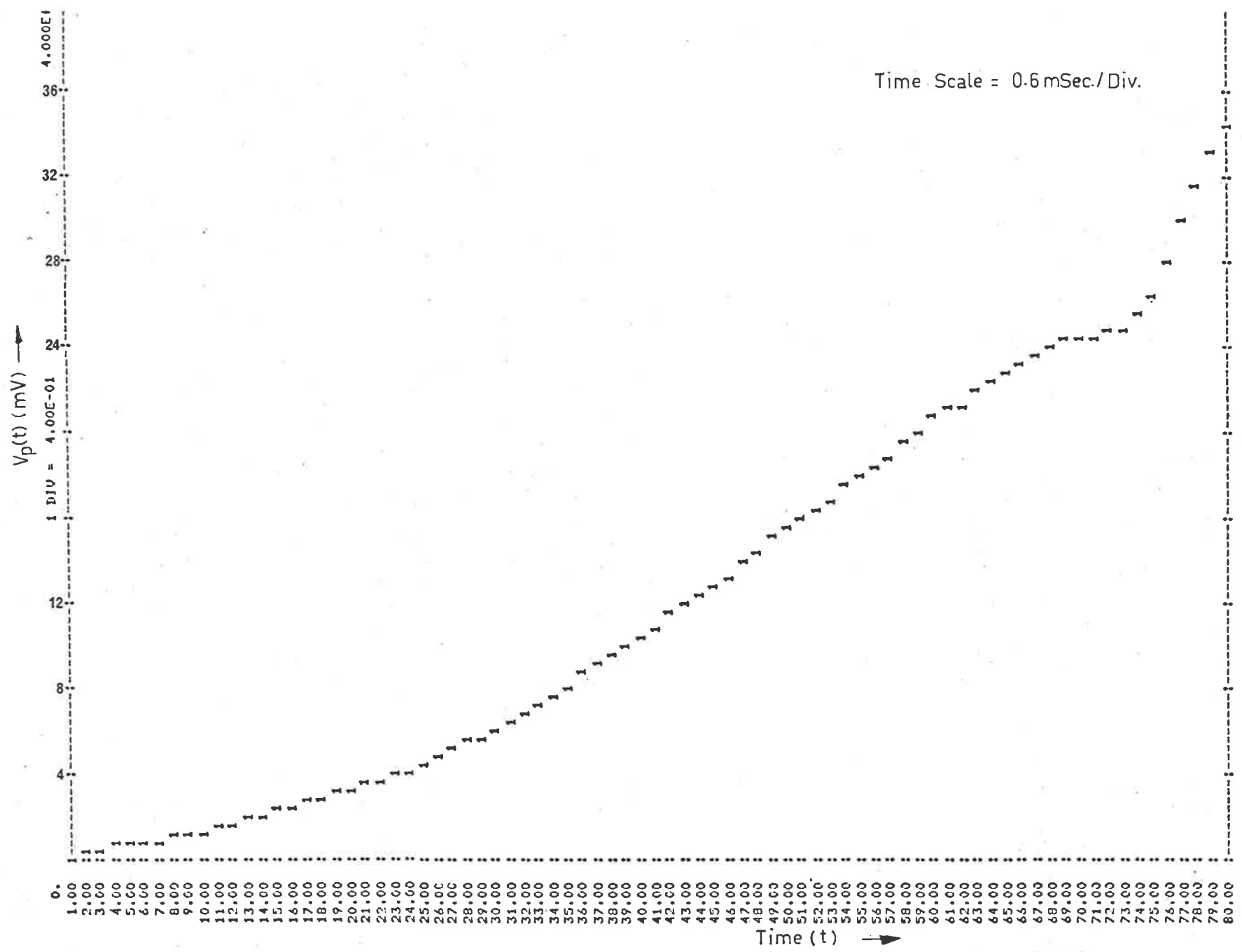


Fig. 6.12(c) Expanded 'Front' section for Determination of V_{p_m} and $\left(\frac{\Delta V_p}{\Delta t}\right)$ - Chrysler Centura

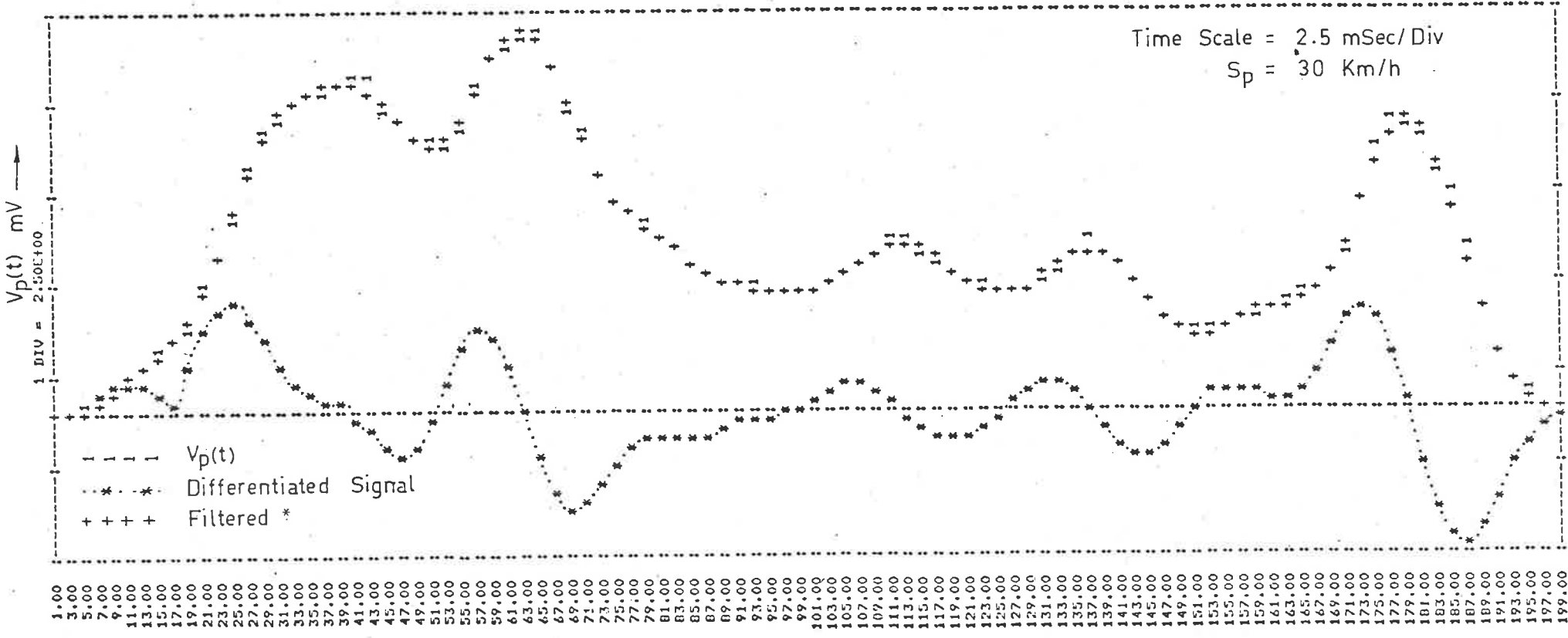


Fig. 6.12(d) The Signature and the Differentiated Signal for Chrysler Centura

* Filtering of data was achieved by observing the signature through a 'window'.

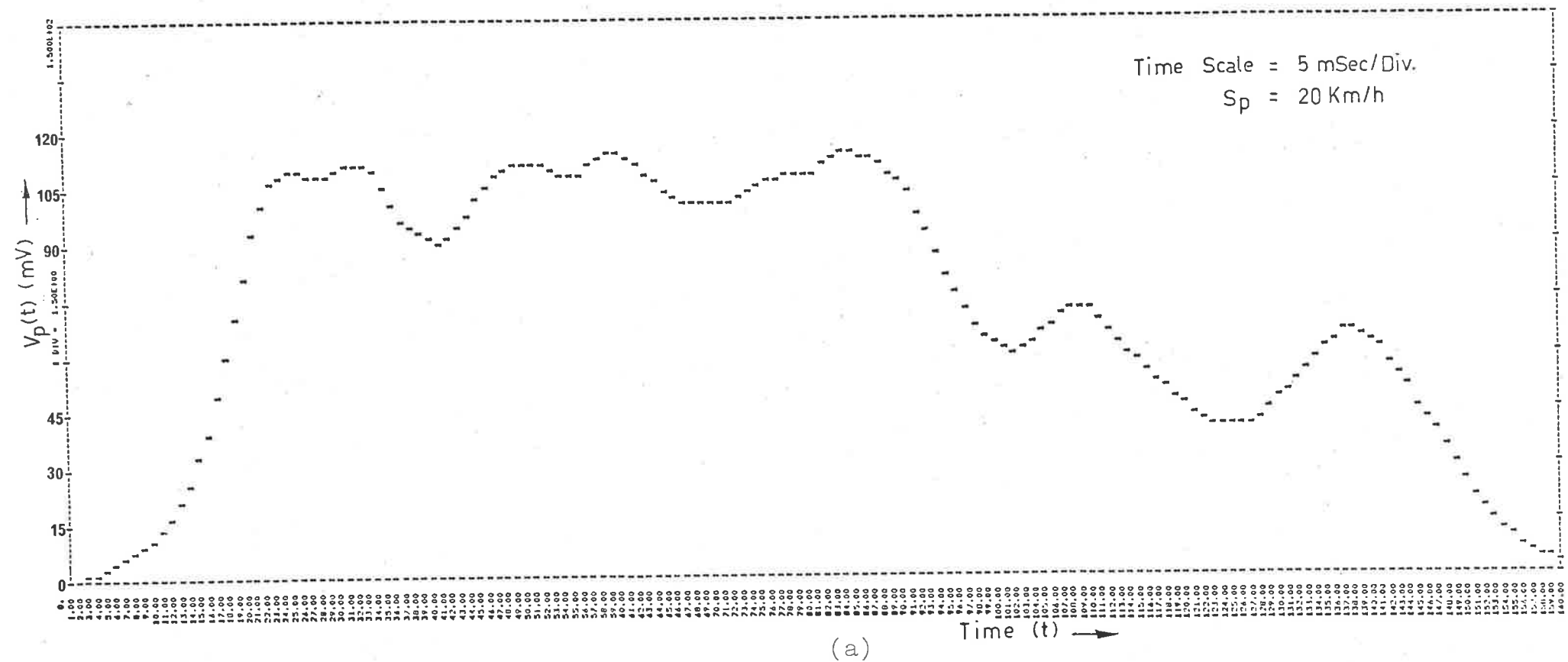


Fig. 6.13 Characteristic Signature for 1976 Datsun 180B
 (a) Signature as a Function of Time

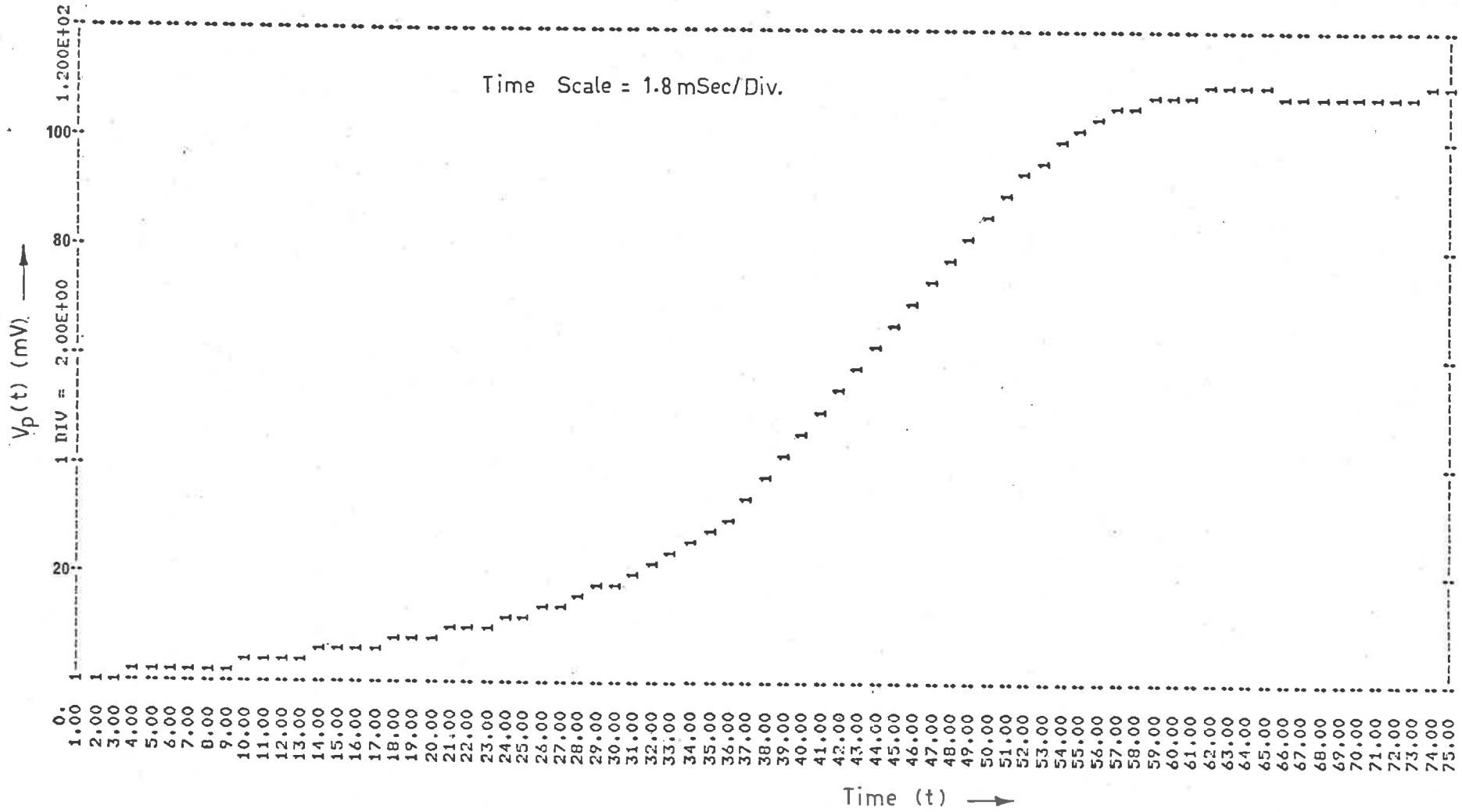


Fig. 6.13(b) Expanded 'Front' Section for Determination of V_{p_m} and $\left(\frac{\Delta V_p}{\Delta t}\right)$ - Datsun 180B

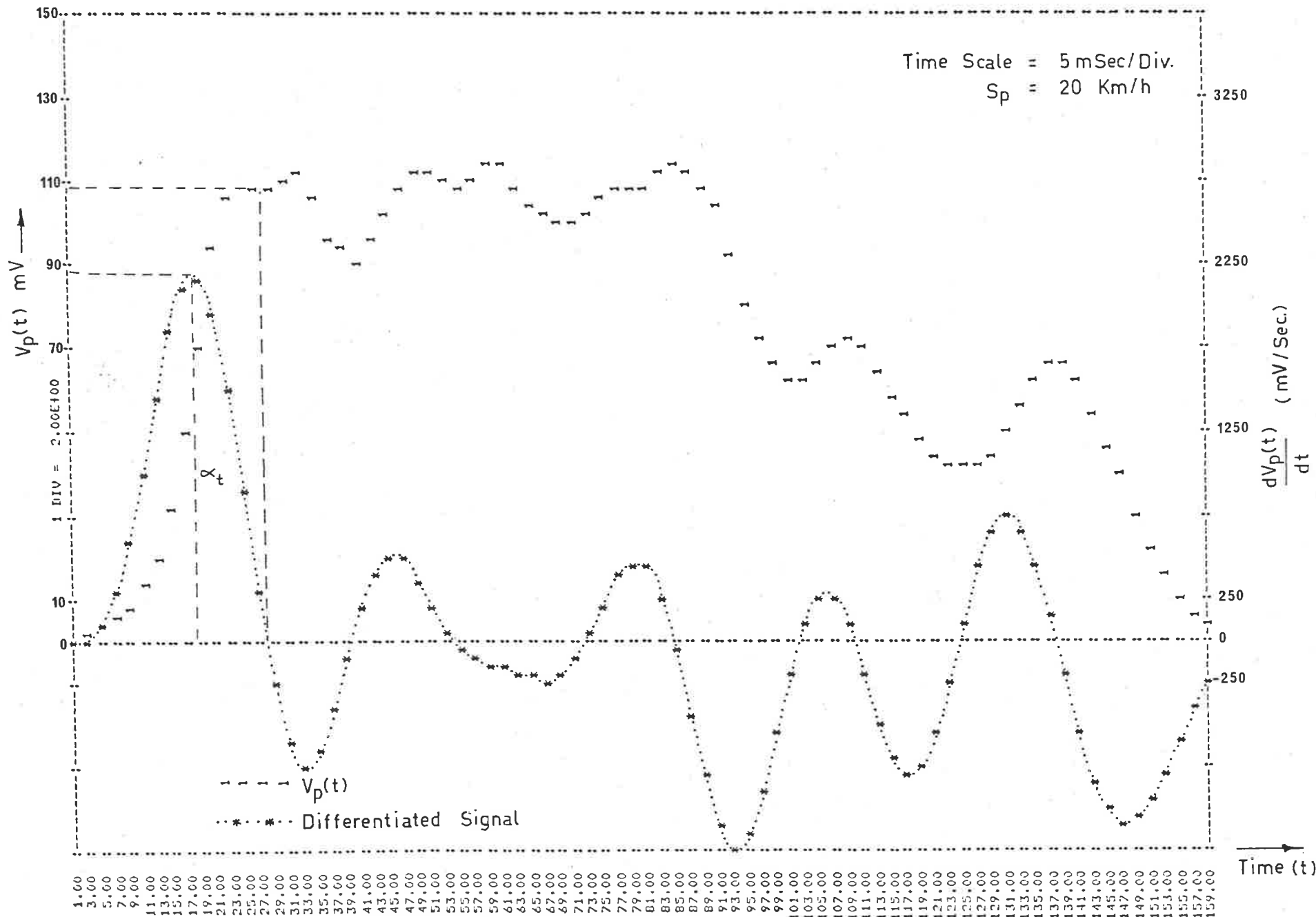


Fig. 6.13 (d) The Signature and the Differentiated Signal for Datsun 180B

Vehicle	$\frac{\Delta V_p}{\Delta t_e}$	$V_{p_{in}}$ (mV)	$S _{P=26}$ Km/h	$S _{P=27}$ Km/h	$S _{P=28}$ Km/h
Ford	358.3	16.51	20.3	21.1	21.9
Centura	799.3	24.82	30.2	31.3	32.5
Datsun	2276.1	110.64	19.3	20.0	20.7

Table 6.1 Value of Speed Using three Values for P

Vehicle	$S _{P=27}$ Km/h	Speed using Vehicle Length		
		t_w (Sec)	l_m (cm)	S_l (Km/h)
Ford	21.1	0.78	469	21.6
Centura	31.3	0.499	458.5	32.9
Datsun	20.0	0.815	419	18.5

Table 6.2 Comparison of the Vehicle Speeds using the Vehicle Length and the Speed Model with P = 27

of speed derived from the speed model and that obtained using the vehicle length l_m and period t_w given by

$$S_1 = \frac{l_m}{t_w} \cdot 0.036 \quad (\text{Km/h}) \quad \dots(6.14)$$

where

l_m = vehicle length specified by manufacturer
in (cm)

t_w = period during which the sensor is occupied
by the vehicle (seconds).

The values of t_w for the three vehicles are obtained from figures 6.11(a) - 6.13(a) respectively.

To check the speed information derived from the model, two additional speed measuring techniques were also implemented.

The first used the transit time of the vehicle over a known distance.⁸⁵ Using Eq.(2.4) the speed S_v was then calculated. The second method used the vehicle's speedometer reading to give an approximate speed indication S_p . In addition the Ford Futura was fitted with a fully styled digital dashboard.⁸⁶ The error associated with this arrangement was $\pm \frac{1}{2}$ digit. Table 6.3 provides a comparison between the three techniques. The speed error is referenced with respect to S_v , and was found to be in the order of 5% with P=27.

Vehicle	S _v Km/h	S _p Km/h	S _{P=27} Km/h	Error
Ford	20.4	20	21.1	3.4
Centura	30.3	30	31.3	3.3
Datsun	19.2	20	20.0	4.2

$$\text{Percent Speed Error} = \frac{|S_v - S_{|P=27}|}{S_v} \times 100\%$$

Table 6.3 Comparison Between the Speed Values using the Three Different Measuring Techniques

6.5 CONCLUSIONS

The modelling technique adopted has provided a relatively simple technique for estimating the vehicle's speed in real time using a single vehicle sensor. Although the recording of data and the subsequent analysis were carried out for only three vehicles, the results using the speed model were consistent with those obtained from conventional techniques, from which it can be deduced that the speed model may be used as an alternative speed measuring procedure with an accuracy of $\pm 5\%$.

Since the errors associated with the identification and the measurements of the V_{p_m} and α_t are circuit orientated, their effects have been excluded in the error assessment. The notable feature of the proposed circuit is the ability of the difference signal generator to vary its reference level continuously so that automatic compensation is achieved for slow environmental changes.

Although some drift problems were encountered with the analog sections, the circuit has provided the basis for future approach in the development of the integrated circuit using I^2L (Integrated Injection Logic) technology.

CHAPTER 7

VEHICLE IDENTIFICATION

7.1 INTRODUCTION

The basic concepts associated with non contact identification of vehicles and their subsequent classification involve the detection of some form of radiated or reflected energy from the vehicle. When a vehicle moves over the vehicle sensor described in Chapter 3 the irregularities in the undercarriage height, is reflected in terms of a time varying voltage $V_p(t)$ known as the "signature" of the vehicle. This characteristic has been demonstrated in Chapter 6 by Fig. 6.11, Fig. 6.12 and Fig. 6.13.

Therefore in this section, the suitability of the coupled coils vehicle sensor is investigated for the purpose of vehicle identification in terms of vehicle grouping and classification.

Although at first sight, processing of the signature in frequency domain seems to be the obvious approach, due to the cost and complexity of the hardware, the technique was not used. The alternative method

adopted for investigation looks for a suitable criteria using the amplitude characteristic of the signature.

7.2 VEHICLE LENGTH MEASUREMENT

One of the parameters required for the identification process is the vehicle length l_m . From Eq.(2.5) and Eq.(6.3) we obtain an expression for the vehicle length l_{m_e} given by

$$l_{m_e} = \left(\frac{\Delta V_p}{\Delta t_e} \right) \left(\frac{P}{V_{P_m}} \right) \cdot t_w \quad (\text{cm}) \quad \dots(7.1)$$

where

$$t_w = \text{period the sensor is occupied}$$

It has been demonstrated in Fig. 4.2 (Chapter 4) that the magnitude of the image voltage V_p as a function of approach distance D is dependent on height h and commences to increase when the plate is several centimeters from the sensor. Therefore, the measurement of the interval at the instant in which voltage change occurs results in a vehicle length which is slightly larger than the actual "mechanical" length of the vehicle. This is known as the "Electrical" length l_{m_e} and deviates from the actual length l_m by an amount given by

$$l_e = l_{m_e} - l_m \quad \dots(7.2)$$

The similarity of shapes of the V_p vs D graphs on which the constancy of P depends as discussed in Chapter 5, results also in an approximately constant ratio given by

$$\gamma_e = \frac{V_{p_m}}{V_{d_0}} \quad \dots(7.3)$$

where

γ_e = length constant

V_{d_0} = image voltage at $D = 0$

From the V_p vs D characteristics shown in Chapter 5, Tables 7.1 - 7.4 are derived showing the value of γ_e as a function of the various parameters such as V_{R_x} , δ and θ_p . If we consider Table 7.4 and assume that the L - Shaped plate corresponds to the front section of the vehicle and for practical values of the undercarriage we neglect $h < 12\text{cm}$, then we obtain a value for γ_e which can be approximated by

$$\gamma_e \doteq 2 \quad \dots(7.4)$$

Therefore

$$V_{d_0} \doteq 0.5 V_{p_m} \quad \dots(7.5)$$

Thus vehicle length may be estimated from the time interval between the initial rise of voltage through the value of $0.5V_{p_m}$ and its subsequent fall through this value combined with Eq.(7.1)

δ (deg) \ h (cm)	0	20
6	3.48	3.60
12	2.78	3.03
18	2.55	2.73

(a)

δ (deg) \ h (cm)	0	20
6	3.33	3.53
12	2.84	3.09
18	2.41	2.53

(b)

Table 7.1 Value of χ_e as a function of Plate Height h (cm) and Approach Angle δ (deg.)

(a) $V_{R_x} = 250\text{mV}$

(b) $V_{R_x} = 500\text{mV}$

θ_p (deg) \ h (cm)	0	5	10	15
6	3.48	3.30	3.75	3.70
12	2.78	3.13	3.56	3.50
18	2.55	2.90	3.28	3.30

Table 7.2 Value of γ_e as a function of Plate Height h (cm) and Incline Angle θ_p (deg.) with $V_{R_x} = 500\text{mV}$

V_{R_x} (mV) \ h (cm)	250	500	1000	2000
6	2.41	2.38	2.27	2.70
12	2.30	2.11	2.26	2.21
18	2.12	2.00	2.00	2.07

Table 7.3 Value of γ_e as a function of Plate Height h (cm) and Initial Induced Voltage V_{R_x} (mV) for an L - Shaped Steel Plate.

δ (deg) \n h (cm)	0	5	10
6	2.40	2.89	2.31
12	2.30	2.30	2.25
18	2.10	2.00	2.00

(a)

δ (deg) \n h (cm)	0	5	10
6	2.38	2.38	2.53
12	2.11	2.10	2.18
18	2.00	2.01	2.09

(b)

Table 7.4 Value of γ_e as a function of Plate Height h (cm) and Approach Angle δ (deg.) for an L - Shaped Steel Plate

(a) $V_{R_x} = 250\text{mV}$

(b) $V_{R_x} = 500\text{mV}$

The determination of the time at which the image voltage reaches $0.5V_p$ implies short term memory of the rise; this can be achieved with the available charge coupled stores.

The measuring technique described in Chapter 5, particularly the relationship between the point of measurement on the vehicle and the sensor shown in Fig.5.16, provides a vehicle length which is different to that specified by the motor vehicle manufacturers. The discrepancy is mainly due to the variations in the position of the "front" and "rear" bumper bars. However, this approach provides a more stable measuring technique due to the mechanical uniformity associated with this region of the vehicle.

The expression showing the modified length l_{m_a} is given by

$$l_{m_a} = \left(\frac{\Delta V_p}{\Delta t_e} \right) \left(\frac{P}{V_{p_m}} \right) (t_{r_o} + t_{f_o} + t_v) \quad (\text{cm}) \quad \dots(7.6)$$

where

t_{r_o} = interval corresponding to $(V_{p_{m_1}} - V_{d_{o_1}})$
for "front" section of a vehicle

t_{f_o} = interval corresponding to $(V_{p_{m_2}} - V_{d_{o_2}})$
for the "rear" section of a vehicle

t_v = interval corresponding to $(V_{p_{m_1}}$ and $V_{p_{m_2}})$

The definitions of these parameters are illustrated in Fig. 7.1. and Fig. 7.2.

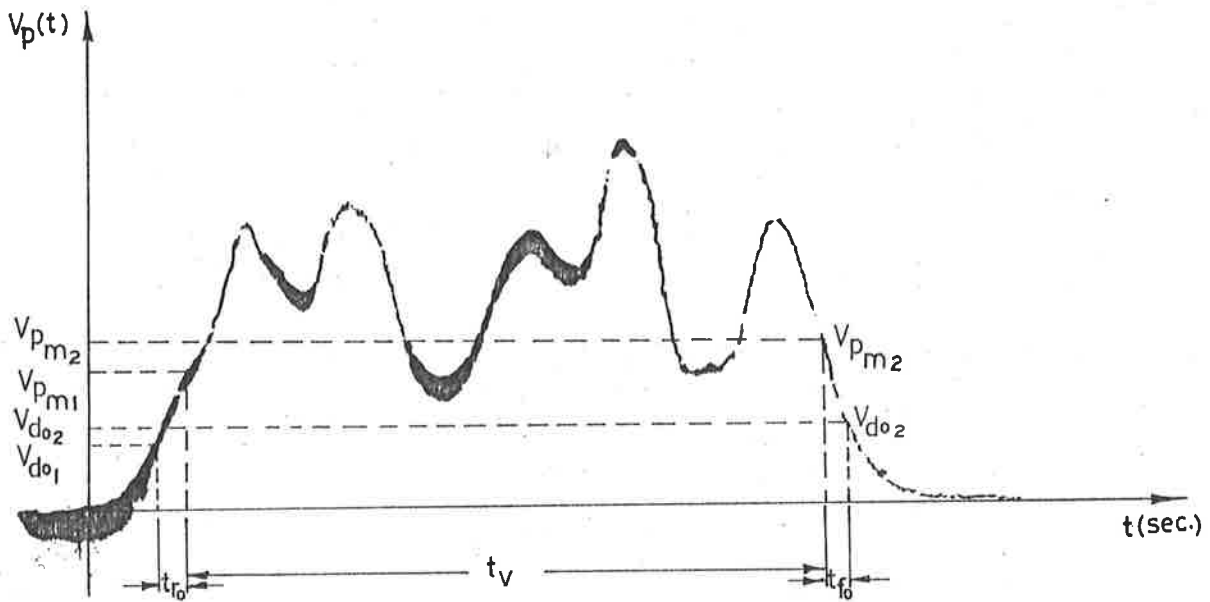


Fig. 7.1 Vehicle Signature Indicating the Parameters for Length Measurement

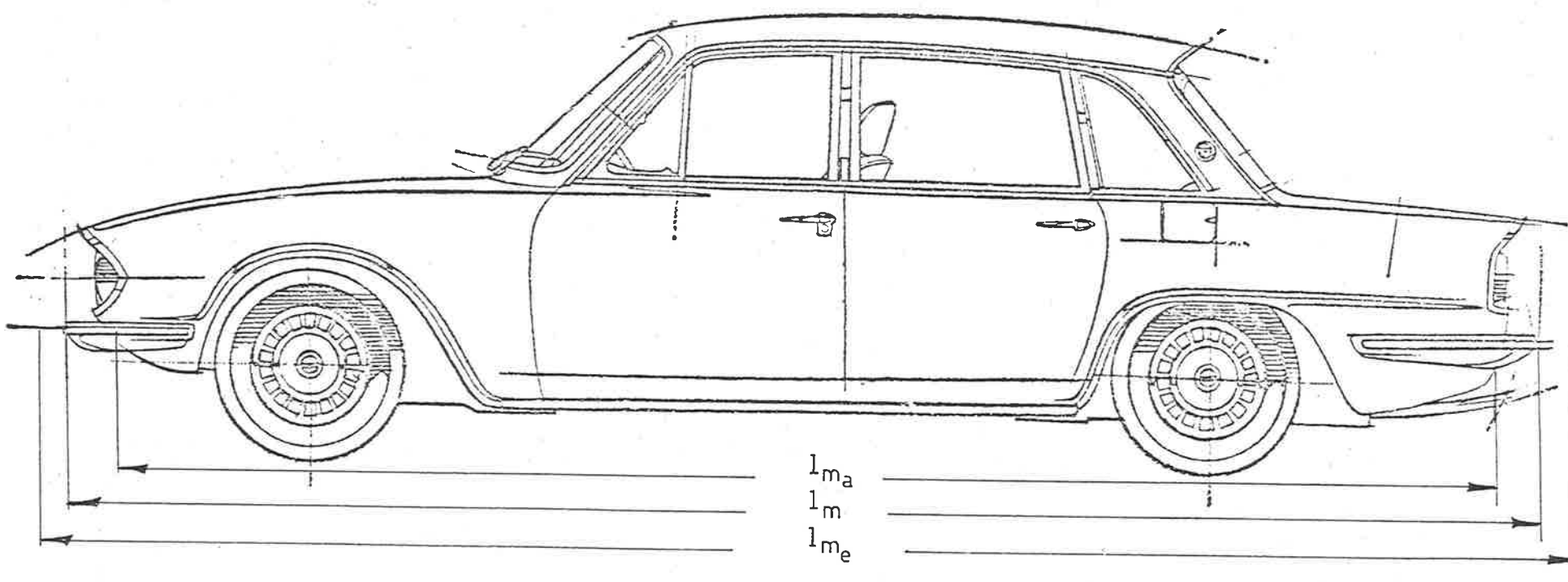


Fig. 7.2 Vehicle Length Definition for Identification in terms of "Mechanical" and "Electrical" Lengths

Table 7.5 shows values of l_{m_a} for the three experimental vehicles derived from Eq.(7.6) and Figures 6.11(a), 6.12(a) and 6.13(a). The corresponding values of vehicle length as specified by the vehicle manufacturers are also included for comparison. Since l_{m_a} is insensitive to changes in the magnitude of V_{R_x} , it is used as the first parameter for vehicle identification.

7.3 VEHICLE SIGNATURE

The second parameter considered for investigation is the ratio $\mathcal{E}(n)$ obtained from the time derivative of the vehicle's signature defined as

$$\mathcal{E}(n) = \frac{k'_n}{k'_{n+1}} \quad n = 1, 2, 3, \dots (7.7)$$

where

k'_i = interval corresponding to the i^{th} positive section of the differentiated signal

This is illustrated in Fig. 7.3. The obvious feature of $\mathcal{E}(n)$ is that it is independent of the variations of V_{R_x} and the vehicle speed, and can be obtained from the vehicles' signature using simple logic design procedures.

In addition, the number of "peaks" appearing in the signature may be derived from

$$N_p = n+1 \quad \dots (7.8)$$

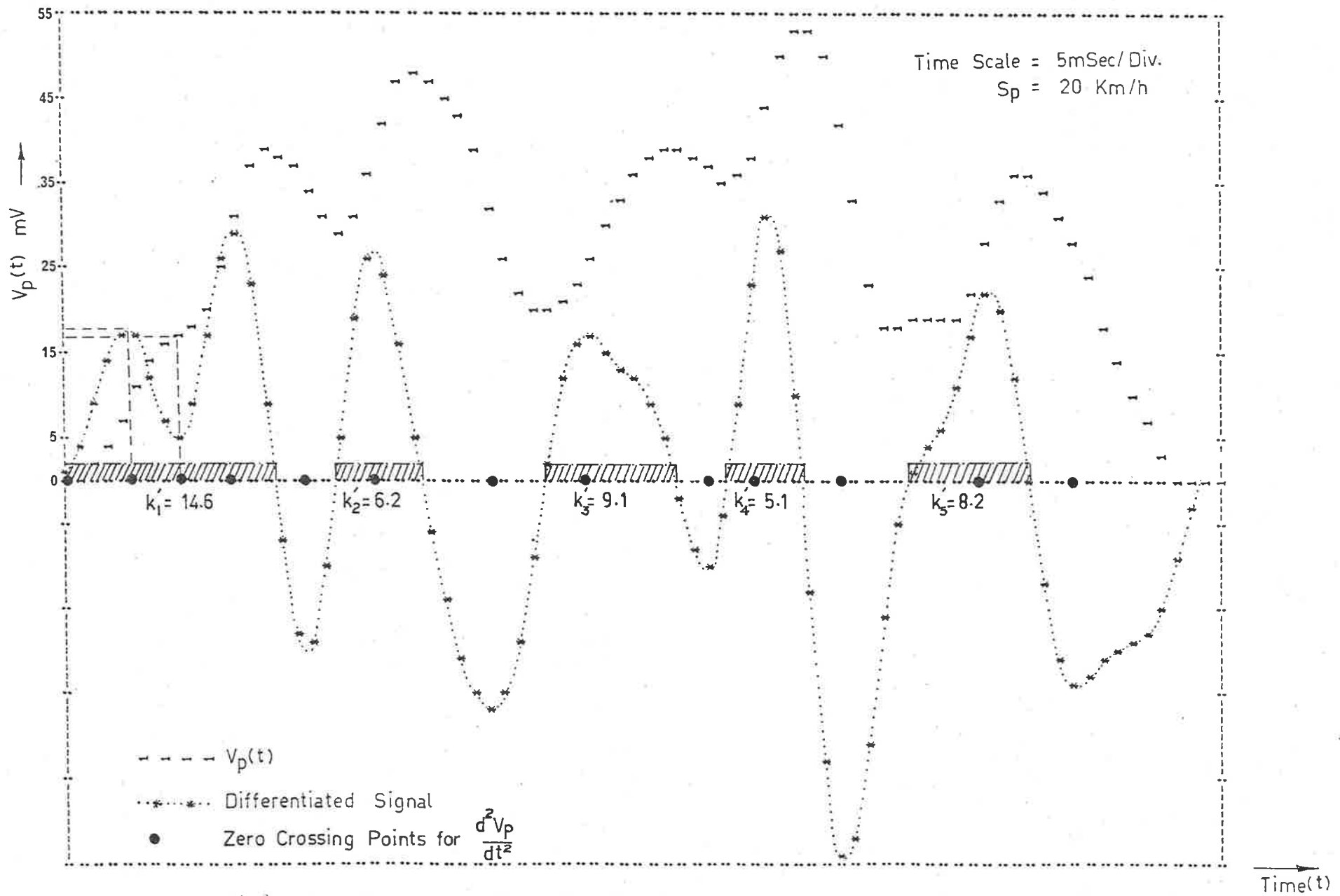


Fig. 7.3(a) The Signature for 1972 Ford Futura showing the Parameters for Derivation of $\mathcal{E}(n)$ and ϕ

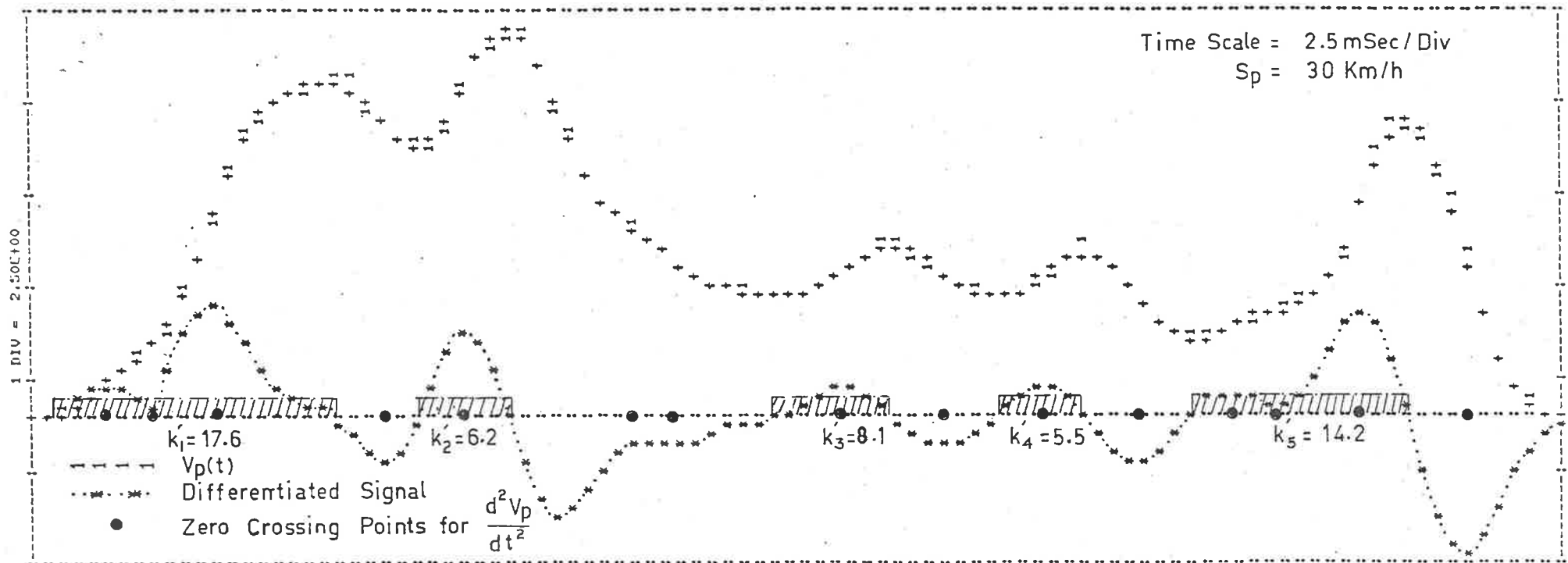


Fig. 7.3(b) The Signature for 1976 Chrysler Centura showing the Parameters for Derivation of $\mathcal{E}(n)$ and ϕ .

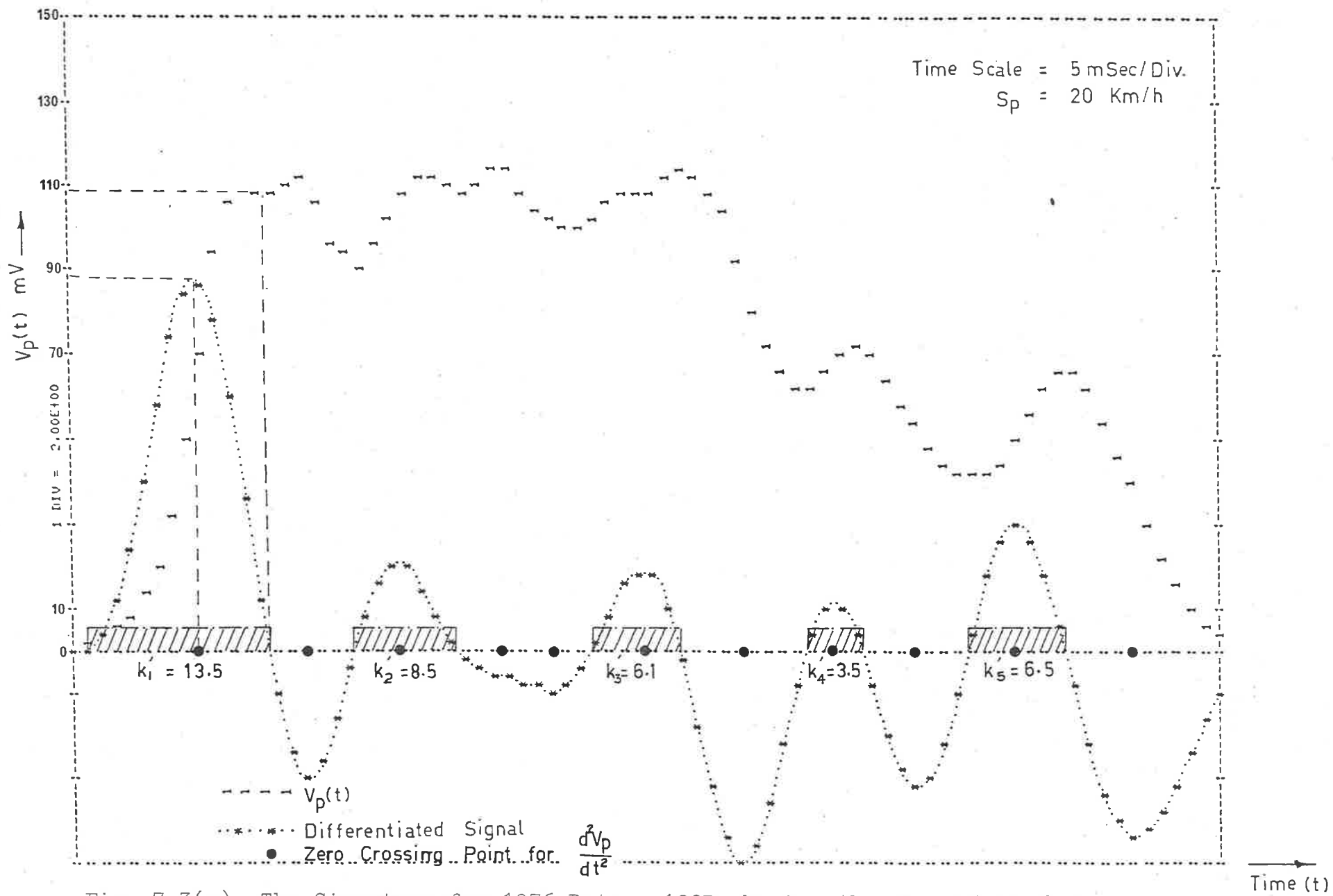


Fig. 7.3(c) The Signature for 1976 Datsun 180B showing the Parameters for Derivation of $\mathcal{E}(n)$ and Φ .

1 DIV = 8.00E-01

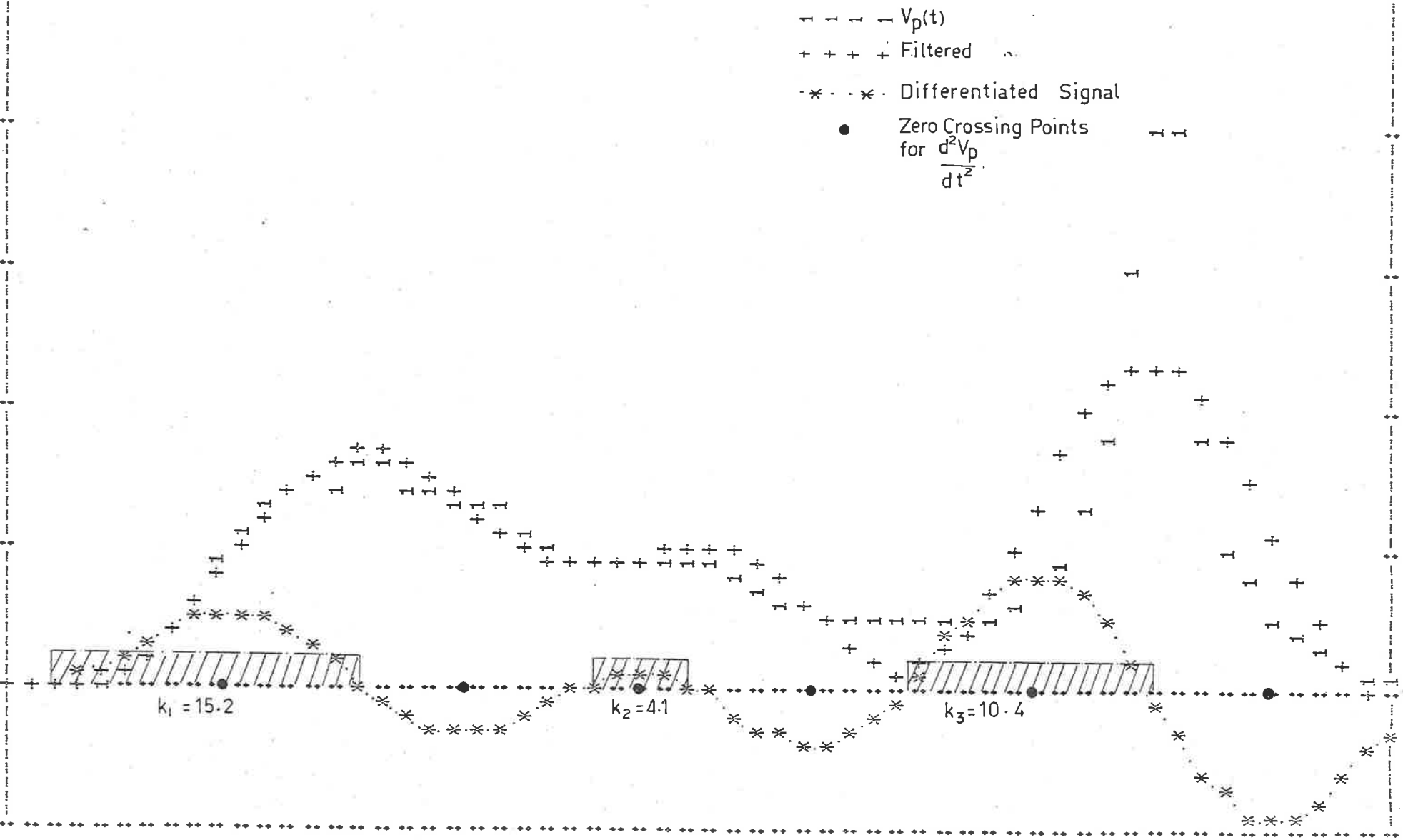


Fig. 7.3(d) The Signature for Bedford Truck showing the Parameters for Derivation of $\mathcal{E}(n)$ and ϕ .

VEHICLE	l_m (cm)	Time Parameters(ms)			l_{ma} (cm)
		t_{ro}	t_{fo}	t_v	
FORD	469	35	20	710	448
CENTURA	458.5	5	7.5	425	380
DATSUN	419	30	15	600	358

Table 7.5 Comparison between the "Mechanical" Length l_m and the Length l_{ma} used for Identification

Examination of the waveforms in Appendix IV (although not analysed) indicate that N_p may be as high as 6, and therefore five separate values of $\mathcal{E}(n)$ may be expected. Table 7.6 shows values of $\mathcal{E}(n)$ for four vehicles including a 1976 Bedford truck.

Since the elements of $\mathcal{E}(n)$ are directly related to the number of peaks, N_p appears redundant and can be neglected.

The final parameter which enables further refinement of the identification process is designated by Φ which is defined by the logic state.

$$\Phi = \begin{cases} '0' & \text{absence of the point of inflection} \\ '1' & \text{presence of the point of inflection} \end{cases} \dots(7.9)$$

This is referred to the initial section of the signature and is determined in accordance with the criteria developed in Chapter 6, using the second and third derivatives. Table 7.7 shows values of Φ for four vehicles.

7.4 IDENTIFICATION PROCESS

For the identification process, each group of similar vehicles (vehicles of same make and model) are assigned a classification code G defined by

$$G = f(\Phi, \mathcal{E}(n), l_{m_a}) \dots(7.10)$$

$\mathcal{E}(n)$	$\mathcal{E}(1)$	$\mathcal{E}(2)$	$\mathcal{E}(3)$	$\mathcal{E}(4)$	$\mathcal{E}(5)$
Vehicle	n = 1	n = 2	n = 3	n = 4	n = 5
FORD	2.3	0.7	1.6	0.7	0
CENTURA	2.8	0.8	1.6	0.4	0
DATSUN	1.6	1.4	1.7	0.5	0
BEDFORD TRUCK	3.8	0.4	0	0	0

Table 7.6 Identification Parameters $\mathcal{E}(n)$ for Four Different Vehicles

VEHICLE	Φ
FORD	1
CENTURA	1
DATSUN	0
BEDFORD TRUCK	0

Fig. 7.7 Identification Parameter Φ for Four Different Vehicles

The number of elements used from \mathcal{E} can be tailored to meet the required "false alarm" rate.

The classification codes for the vehicles are then derived from Tables 7.5, 7.6 and 7.7. For example, G for 1972 Ford Futura, 1976 Chrysler Centura and 1976 Datsun 180B group of vehicles are

(1, 2.3, 0.7, 1.6, 0.7, 0, 448)

(1, 2.8, 0.8, 1.6, 0.4, 0, 380)

(0, 1.6, 1.4, 1.7, 0.5, 0, 358)

respectively.

7.5 DISCUSSIONS

Although the overall system implication of the identification process has not as yet been fully explored in regards to broad class of vehicles, the concept appears simple and more importantly it can be implemented in real time. The manner in which the classification codes for the various vehicles are stored and the procedure for signature matching are the subject of future investigations.

Although at this stage detailed analysis of the signature due to the vehicle lateral displacement has not been made, observation of several signatures as shown in Appendix IV have indicated that both ϕ and l_{ma} appear reasonably stable. Moreover, only one or two

elements of $\mathcal{E}(n)$ seem to deviate slightly from the specified values. However it is expected that in the search procedure for signature matching these deviations can be taken into account.

CHAPTER 8

CONCLUSIONS AND FUTURE DEVELOPMENTS

8.1 INTRODUCTION

Experimental observations associated with the behaviour of the change in the induced voltage of two inductively coupled coils in the presence of a conducting surface provided the basis for the derivation of a constant parameter. This was designated by P and was found to have value of $27 \pm 5\%$ for an L-shaped plate. A theory based on this parameter, was subsequently developed which enabled the estimation of the vehicle speed with an accuracy in the order of $\pm 5\%$ for most vehicles.

It has been further demonstrated that using the characteristic signature of a vehicle derived from a single passive sensor embedded under the road surface, it is possible to obtain the three traffic parameters; count, speed and identification (in terms of vehicle grouping). Although the evaluations were restricted to three vehicles, the observation of the signatures for a broader class of vehicles, shown in Appendix IV, has provided further assurance regarding the validity of the experimental results. It is also noted that

the initial rise of signatures of these vehicles falls within the two identification criteria as defined in Chapter 6, for speed measurement.

Although further research is still required for the vehicle "group" identification technique, the stability of the signature shown in Appendix IV for various vehicle displacements, are encouraging. The parameters used in the vehicle's classification code have been found to be insensitive to many of the changes encountered in real traffic situations and environment.

Finally, in situations where P lies outside the expected range, after the identification process, it is envisaged that a correction factor can be incorporated so that the speed is within the $\pm 5\%$ accuracy.

8.2 ACCELERATION MEASUREMENTS

A further parameter which has been found to provide useful information in the control of traffic signals at an intersection is the vehicle's acceleration. This parameter becomes particularly important when semi-trailers, caravans or commercial vehicles are involved. When one of these vehicles is approaching or crossing a controlled intersection, the knowledge of speed, classification code and acceleration enables the traffic signals to be adjusted so that the vehicle clears the intersection before the traffic signals are changed.

It should be noted that in the absence of such information, a complete cycle change of the traffic signals is possible while the vehicle is progressing through the intersection. In order to obtain the vehicle's acceleration, the section of the signature corresponding to the "rear" bumper-bar can be processed in the same manner as that shown in Chapter 6. However in this instance, short term storage of waveform is necessary. The acceleration information may be computed using the two speed informations.

8.3 CONCLUSIONS

The magnitude of the research and the experimental work were found to be beyond that foreseen at the commencement of the feasibility study and the scope of this thesis. Limitations of the approach as related to actual highway traffic can only be assessed through further experimental studies focused on a variety of vehicles and traffic conditions. However it is concluded that this development fulfils many of the requirements of the modern traffic monitoring and control systems, as discussed in Chapter 1.

APPENDIX I

DERIVATION OF INDUCED VOLTAGE IN RECEIVER COIL

I.1 Derivation of the Magnetic Field Component

To obtain an analytic solution for the modified field pattern and hence the induced voltage in the receiving coil in the presence of a vehicle, the undercarriage can be represented by an infinite conducting plane.

We can apply the image theory concept and derive expressions for the magnetic field components.

The magnetic vector potential \bar{A} ⁷⁰ at a distant point from an elemental current loop can be derived with reference to Fig. I.1

For any point $P(r, \theta, \phi)$ at which \bar{A} is to be found, some current elements Idl' are oriented such that they produce components of \bar{A} in directions other than the ϕ direction. This is shown in Fig. I.1

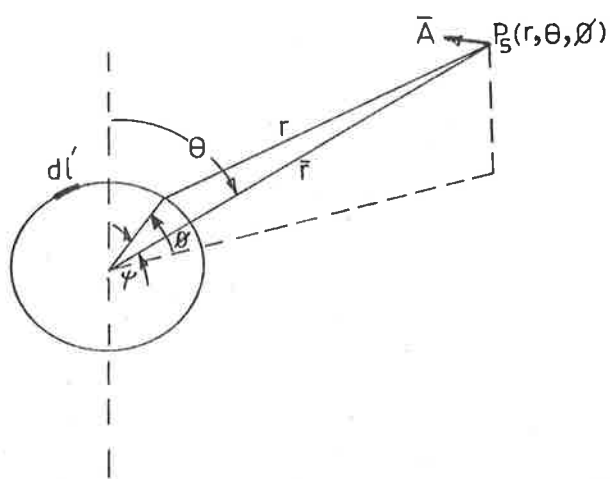
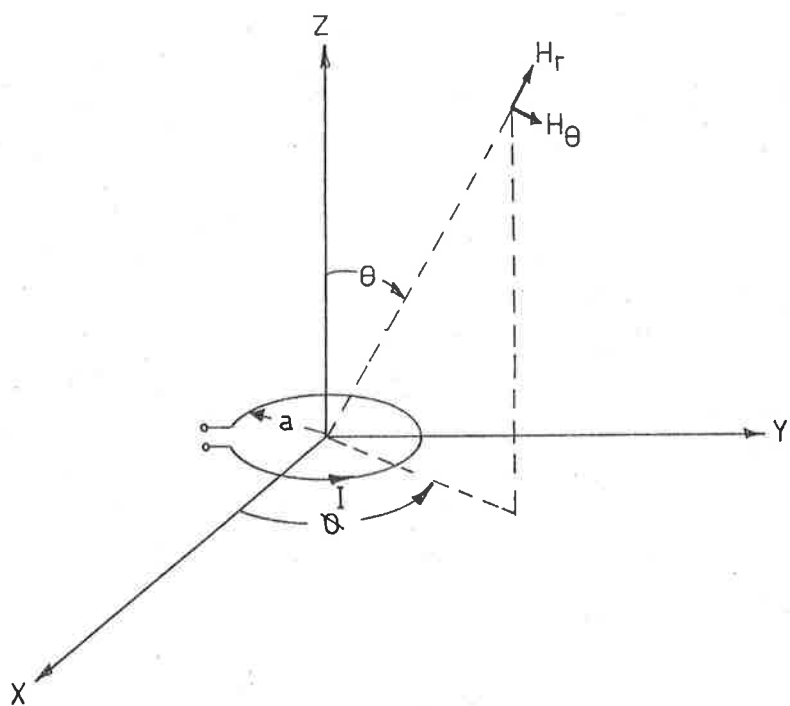


Fig. I.1 Magnetic Vector Potential Representation at a Distant Point from an Elemental Current Loop

By the symmetry of the loop, equal and opposite amounts of such components exist. As a result \bar{A} is ϕ directed and is independent of the value of ϕ at which it is to be found. For convenience, we choose to calculate \bar{A} at the point $(r, \theta, 0)$.

The ϕ - directed contribution of a differential element of current is

$$dA_{\phi} = \frac{\mu dl' \cos\phi}{4\pi R} \quad \dots(I.1)$$

Where R is the distance $|\bar{r}-r|$ from the element dl' to $(r, \theta, 0)$, the total is found as the integral around the loop.

$$A_{\phi} = \frac{\mu I}{4\pi} \oint \frac{dl \cos\phi}{R} \quad \dots(I.2)$$

$$= \frac{\mu Ia}{4\pi} \int_0^{2\pi} \frac{\cos\phi}{R} d\phi \quad \dots(I.3)$$

The distance R can be expressed as

$$R^2 = (r^2 + a^2 - 2ra\cos\psi) \quad \dots(I.4)$$

Now $r\cos\psi$ is the projection of r onto the radius line dl'

$$\therefore r\cos\psi = ra\sin\theta\cos\phi \quad \dots(I.5)$$

For $r \gg a$ we can approximate

$$R \doteq r \left(1 - 2 \frac{a}{r} \text{Sine} \cos \phi \right)^{\frac{1}{2}} \quad \dots(\text{I.6})$$

Substituting for R we have

$$\begin{aligned} A_{\phi} &= \frac{\mu I a}{4\pi r} \int_0^{2\pi} \left(\cos \phi + \frac{a}{r} \text{Sine} \cos^2 \phi \right) d\phi \quad \dots(\text{I.7}) \\ &= \frac{\mu I a \text{Sine}}{4\pi r^2} \end{aligned}$$

The components of magnetic flux density may be found from

$$\nabla \times \bar{A} = \bar{B} \quad \dots(\text{I.8})$$

giving

$$B_r = \frac{\mu I A}{2\pi r^3} \text{Cos} \phi \quad \dots(\text{I.9})$$

$$B_{\theta} = \frac{\mu I A}{4\pi r^3} \text{Sine} \quad \dots(\text{I.10})$$

$$B_{\phi} = 0. \quad \dots(\text{I.11})$$

Now we can obtain directly the magnetic field components H_r and H_{θ} from the relation

$$B = \mu H \quad \dots(\text{I.12})$$

$$\therefore H_{\theta} = \frac{m}{4\pi r^3} \text{Sine} \quad \dots(\text{I.13})$$

$$\text{and } H_r = \frac{m}{2\pi r^3} \text{Cose} \quad \dots(\text{I.14})$$

where

$$m = NIA_c \mu_r$$

μ_r = effective permeability of material

Now the x component of the magnetic field can be written as

$$H_x = H_r \text{Cose} - H_{\theta} \text{Sine} \quad \dots(\text{I.15})$$

$$= \frac{m}{2\pi r^3} \text{Cose} \text{Cose} - \frac{m}{4\pi r^3} \text{Sine} \cdot \text{Sine} \quad \dots(\text{I.16})$$

$$= \frac{m}{4\pi r^3} (3\text{Cos}^2\theta - 1) \quad \dots(\text{I.17})$$

When a conducting surface is brought above the coils to satisfy the boundary conditions we can remove the interface and replace it with an image coil as shown in Fig. I.2.

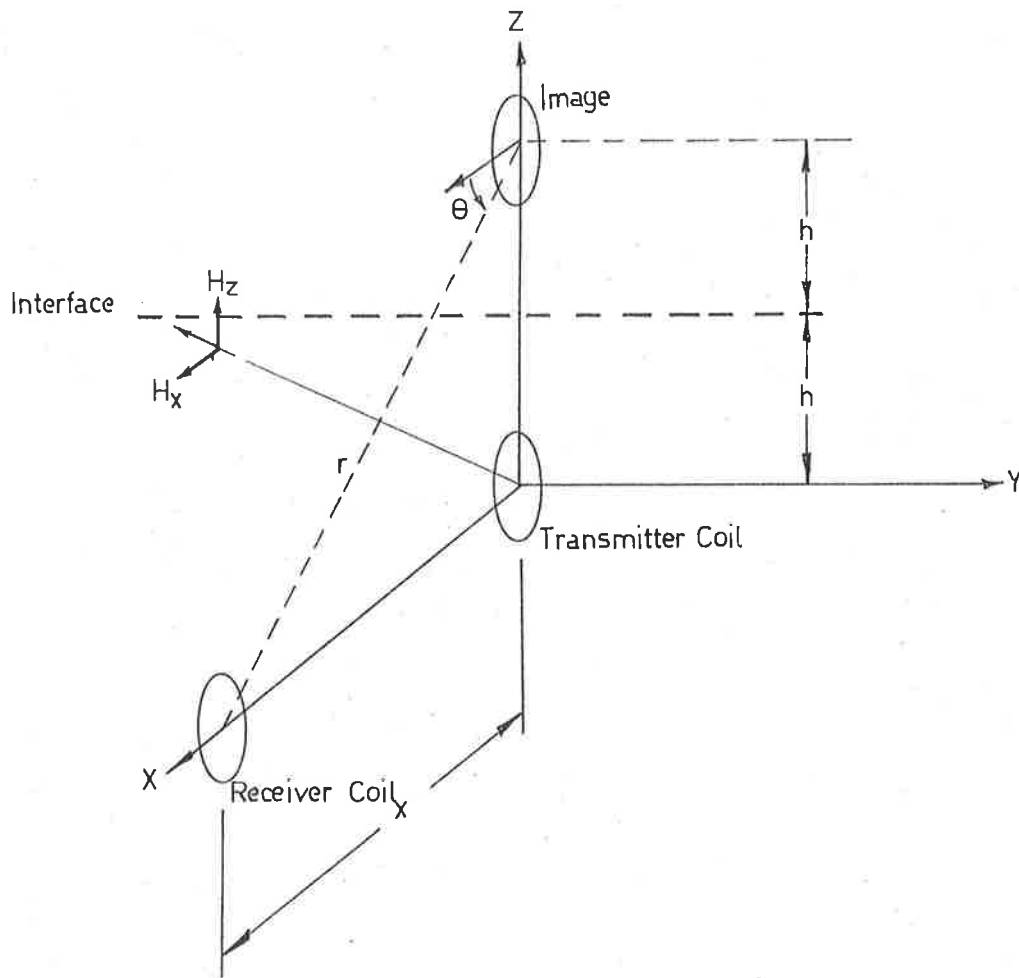


Fig. II.2 Representation of the Image Coil in Terms of the Co-ordinate System

The field at receiver coil due to image is obtained by considering

$$\cos\theta = \frac{x}{r} \quad \dots(\text{I.18})$$

and

$$r = \sqrt{4h^2 + x^2} \quad \dots(\text{I.19})$$

$$H_{xi} = \frac{m}{4\pi r^3} \left[3 \left[\frac{x^2}{r} \right] - 1 \right] \quad \dots(\text{I.20})$$

$$= \frac{m}{2\pi} \cdot \frac{x^2 - 2h^2}{[4h^2 + x^2]^{5/2}} \quad \dots(\text{I.21})$$

The magnetic field due to the transmitter coil at the receiver coil in the absence of the interface can be determined by putting $\theta=0^\circ$. Thus

$$H_{xt} = \frac{m}{2\pi x^3} \quad \dots(\text{I.22})$$

DERIVATION OF P BASED ON "SCATTERED" POINTS

In order to obtain a straight line of best fit the least-squares linear regression method is used.

The equation for the linear section of the V_p versus D curve is shown in Fig.(4.2) and is given by

$$V_p = \alpha D \quad \dots(\text{II.1})$$

The slope in terms of a line of best fit which minimizes the sum of the squares of the deviation of the data points can be written as ⁷¹

$$\alpha_m = \frac{\frac{\sum_{i=1}^N D_i V_{p_i}}{N} - \bar{D} \bar{V}_p}{\sigma_d^2} \quad \dots(\text{II.2})$$

where

$$\bar{V}_p = \frac{\sum_{i=1}^N V_{p_i}}{N} \quad \dots(\text{II.3})$$

$$\bar{D} = \frac{\sum_{i=1}^N D_i}{N} \quad \dots(\text{II.4})$$

and

$$\sigma_d^2 = \frac{\sum_{i=1}^N D_i^2}{N} - \bar{D}^2 \quad \dots(\text{II.5})$$

Substituting the modified slope α_m in Eq.(4.1) we obtain

$$P = \frac{V_{p_m} \cdot \sigma_d^2}{\frac{\sum_{i=1}^N D_i V_{p_i}}{N} - \bar{D}_i \bar{V}_{p_i}} \quad \dots(\text{II.6})$$

To determine the degree of association between the variable $(D_i, V_{p_i}) \dots \dots (D_N, V_{p_N})$ the correlation coefficient r_c is examined.

Thus

$$r_c = \frac{\frac{\sum_{i=1}^N D_i V_{p_i}}{N} - \bar{D} \bar{V}_p}{\sigma_d \sigma_v}}{\dots(\text{II.7})}$$

where

$$\sigma_v^2 = \frac{\sum_{i=1}^N V_{p_i}^2}{N} - \bar{V}_p^2 \quad \dots(\text{II.8})$$

Eq.(II.1) can be re-written in terms of Eq.(II.2) and Eq.(II.7) giving

$$\alpha_m = r_c \cdot \frac{\sigma_v}{\sigma_d} \quad \dots(\text{II.9})$$

Therefore the speed constant P can be expressed as

$$P = \frac{V_{P_m}}{r_c} \cdot \left[\frac{\sigma_d}{\sigma_v} \right] \quad \dots(\text{II.10})$$

BEHAVIOUR OF THE IMAGE VOLTAGE IN TERMS OF THE DISTANCE BETWEEN A CONDUCTING SURFACE AND THE SENSOR

In order to have some indications regarding the behaviour of the change V_p in the induced voltage V_R as a conducting plate approaches the coils, a simple model was developed.

The image was assumed to have constant intensity having the co-ordinates shown in Fig. III.1.

The approximate field at the receiver coil due to the moving image is obtained by considering the magnetic field H_ϕ . Thus

$$H_\phi = -H_x' \sin\phi + H_y' \cos\phi \quad \dots(\text{III.1})$$

After rotation of the axis as shown in Fig. III.1 this is re written as

$$H_\phi = -H_y \sin\phi + H_z \cos\phi \quad \dots(\text{III.2})$$

Substituting for H_y and H_z in (III.2)

$$H_\phi = -(H_r \sin\theta \sin\phi + H_\theta \cos\theta \cos\phi + H_\phi \cos\phi) \sin\phi + (H_r \cos\theta - H_\theta \sin\theta) \cos\phi \quad \dots(\text{III.3})$$

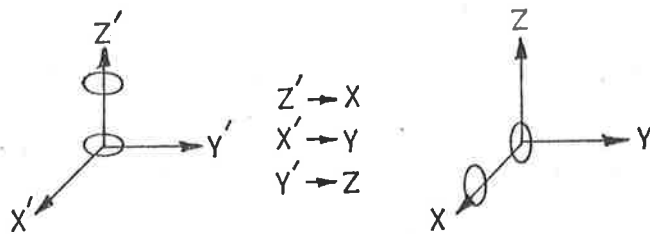
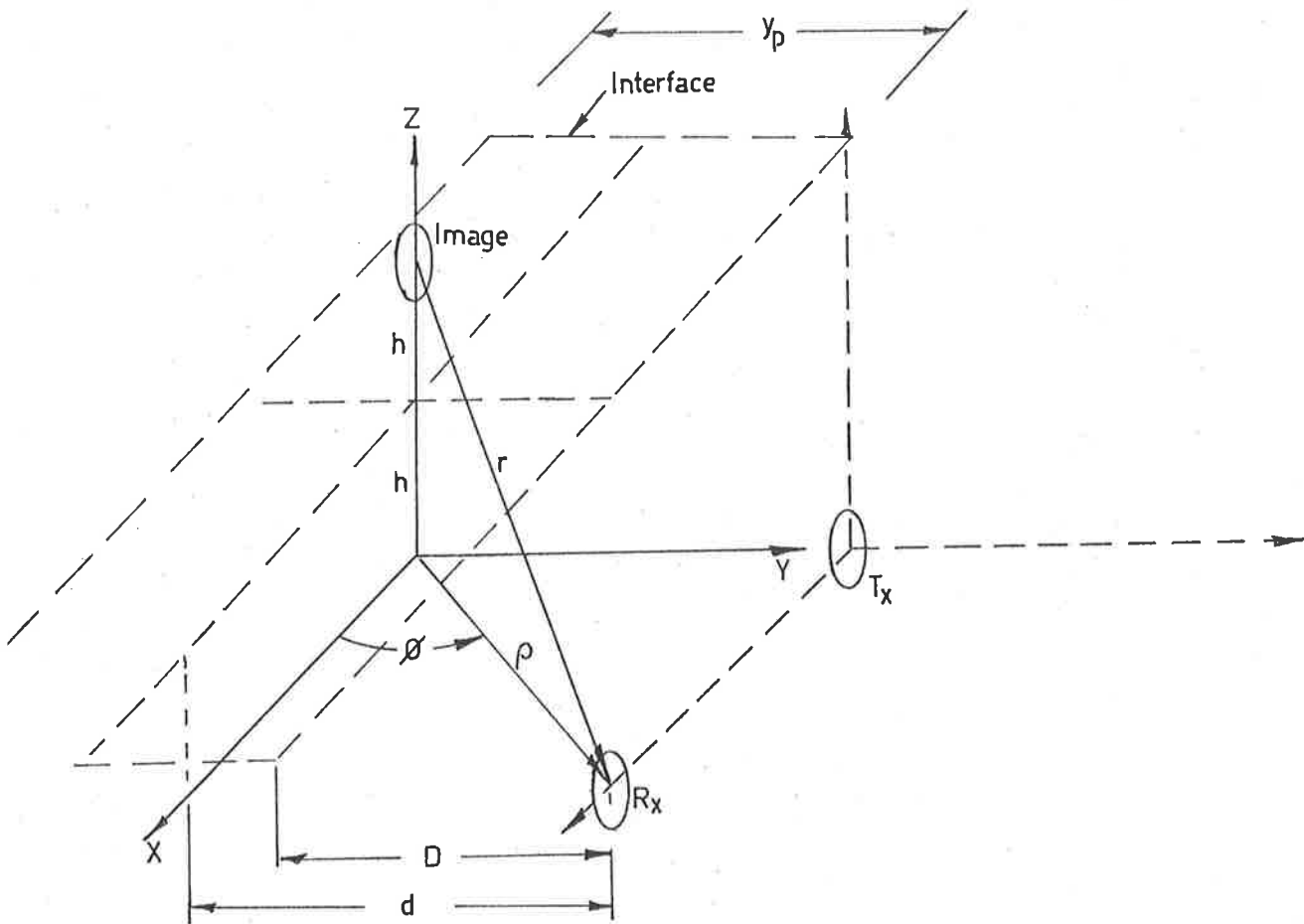


Fig. III.1 Co-ordinates for the Geometry of the Receiver Coil R_x in terms of a Moving Image Coil due to the Presence of a Conducting Plane.

After re-arranging we obtain

$$H_{\phi} = \frac{H_r (\cos\theta \cos\phi - \sin\theta \sin^2\phi) - H_{\theta} (\sin\theta \cos\phi - \cos\theta \sin^2\phi)}{1 + \cos\phi \sin\phi} \quad \dots(\text{III.4})$$

Now

$$\cos\phi = \frac{x}{\rho} \quad \dots(\text{III.5})$$

$$\sin\phi = \frac{d}{\rho} \quad \dots(\text{III.6})$$

$$\rho = \sqrt{x^2 + d^2} \quad \dots(\text{III.7})$$

and

$$\cos\theta = \frac{x}{r} \quad \dots(\text{III.8})$$

$$\sin\theta = \frac{2h}{r} \quad \dots(\text{III.9})$$

$$r = \sqrt{4h^2 + x^2 + d^2} \quad \dots(\text{III.10})$$

$$H_{\phi} = \frac{1}{1 + \cos\phi \sin\phi} \left[\frac{m}{2\pi r^3} \cos\theta (\cos\theta \cos\phi - \sin\theta \sin^2\phi) - \frac{m}{4\pi r^3} \sin\theta (\sin\theta \cos\phi - \cos\theta \sin^2\phi) \right] \quad \dots(\text{III.11})$$

Substituting for r , θ and ϕ we have

$$H_{\phi} = \frac{m}{2\pi} \cdot \left[\frac{x}{[(2h)^2 + x^2 + d^2]^{\frac{5}{2}}} \cdot \frac{1}{(x^2 + d^2 + xd)} \cdot \left((x^3 - d^2x - 2dh) - h[2h(x^2 + d^2)^{\frac{1}{2}} - d] \right) \right] \quad \dots(\text{III.12})$$

If $d = 0$ we have

$$H_{\phi} = \frac{m}{2\pi} \cdot \frac{x^2 - 2h^2}{[x^2 + (2h)^2]^{\frac{5}{2}}} \quad \dots(\text{III.13})$$

which is the same as Eq. 3.11.

The image voltage as a function of distance d using Eq.(3.16) is given by

$$V_p = K_i \left[\frac{x}{[(2h)^2 + x^2 + d^2]^{\frac{5}{2}}} \cdot \frac{1}{(x^2 + d^2 + xd)} \cdot \left((x^3 - d^2x - 2hd) - h[2h(x^2 + d^2)^{\frac{1}{2}} - d] \right) \right] \quad \dots(\text{III.14})$$

The plot of V_p as a function of d for several values of height h is given in Fig III.2. Experimental values for similar conditions are also plotted.

The relationship between D and d is given by

$$D = d - \frac{y_p}{2} \quad \dots(\text{III.15})$$

Where

y_p = Width of the conducting plate

D = Distance between the leading edge of the plate and the coils.

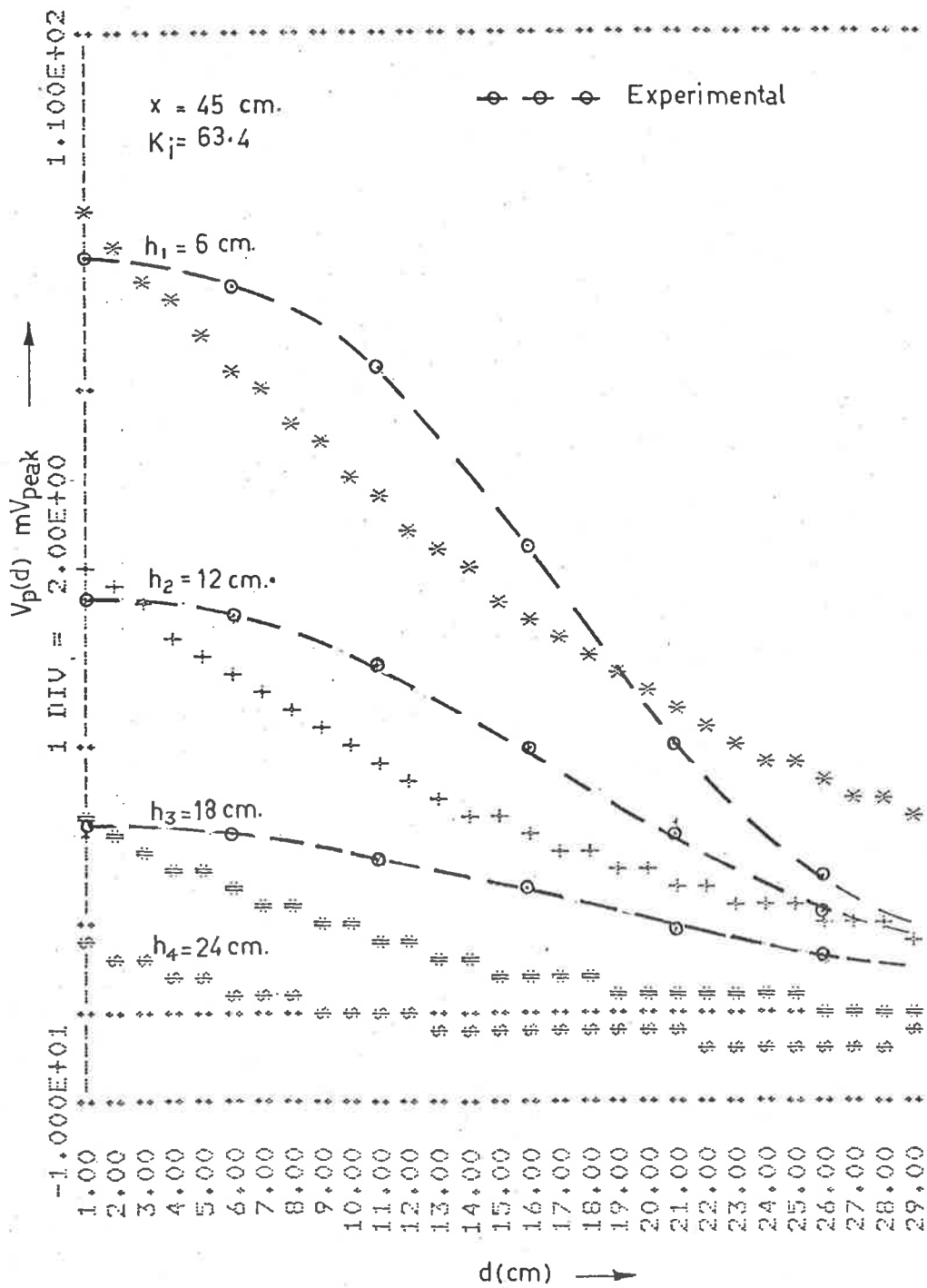


Fig. III.2 Image Voltage Characteristic as a function of Approach Distance d for several values of Height h

CHARACTERISTIC SIGNATURES OF VEHICLES

IV.1 WAVEFORMS

This section is a supplement to Chapter 6 and Chapter 7 and shows the photographs of the signatures for several vehicles. These are demonstrated by Figures IV.1 - IV.11.

IV.2 LATERAL DISPLACEMENT OF VEHICLES FROM CENTRE POSITION

Signatures associated with lateral displacement of several vehicles from centre position as shown in Fig. IV.12, are also illustrated in Figures IV.13 - IV.15.

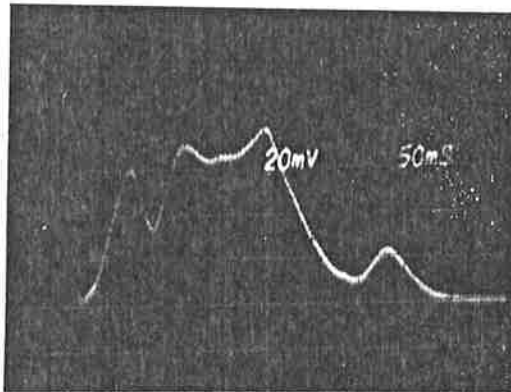


Fig. IV. 1. Signature for Fiat 124

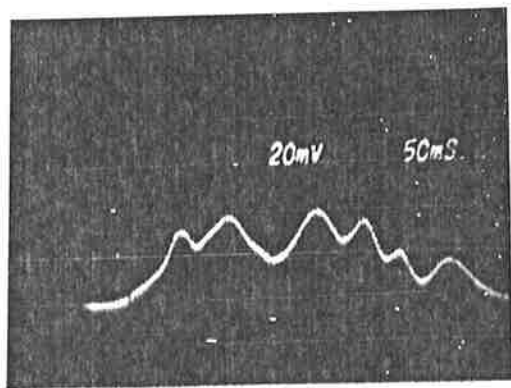


Fig. IV. 2. Signature for 1969 Hillman Hunter

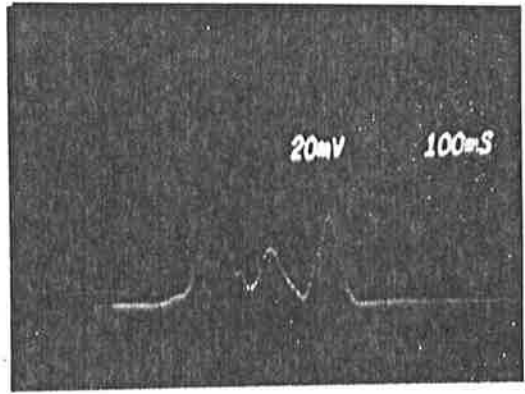


Fig. IV. 3. Signature for H.Q. Holden - Station Wagon

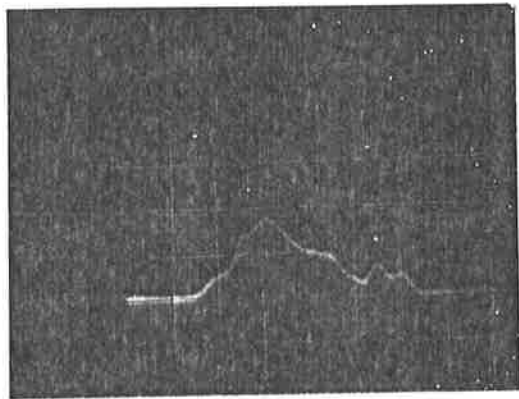


Fig. IV. 4. Signature for 1976 Ford Escort - Panel Van

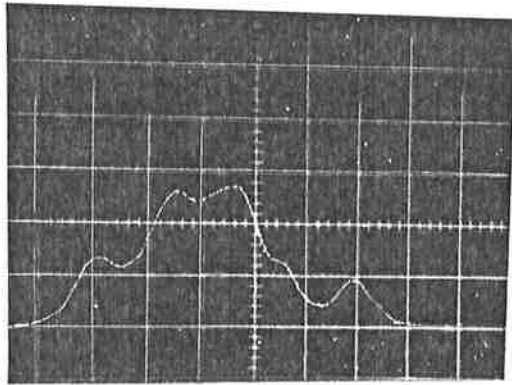


Fig. IV.5. Signature for 1976 VW Passat

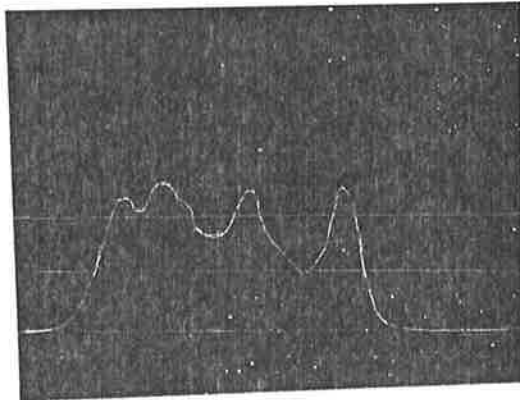


Fig. IV.6. Signature for 1976 Lancer

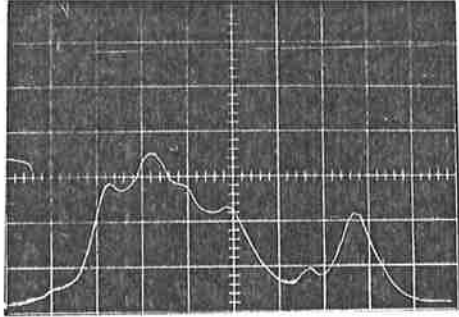


Fig. IV.7. Signature for 1974 Volvo 164

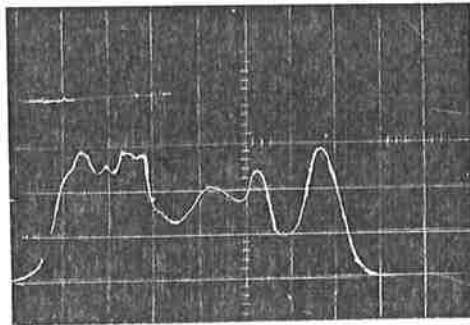


Fig. IV.8. Signature for 1976 Valiant Station Wagon

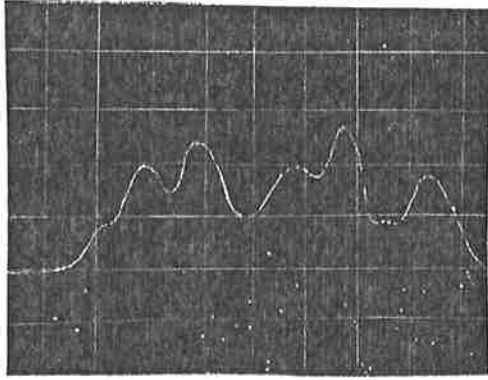


Fig. IV. 9. Signature for 1972 Ford Futura

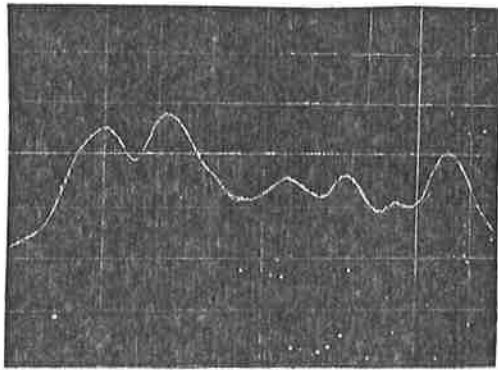
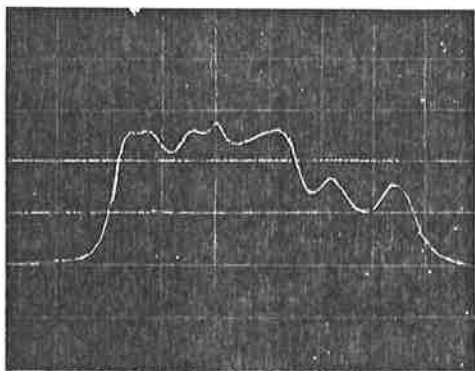
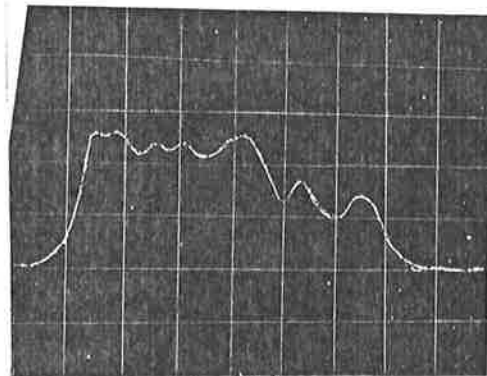


Fig. IV.10. Signature for 1976 Chrysler Centura



(a)



(b)

Fig, IV.11. Signature for 1976 Datsun 180B
 (a) 20 K.p.h.
 (b) 40 K.p.h.

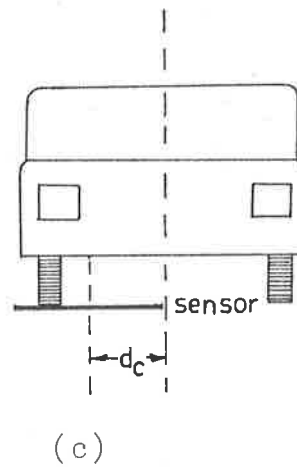
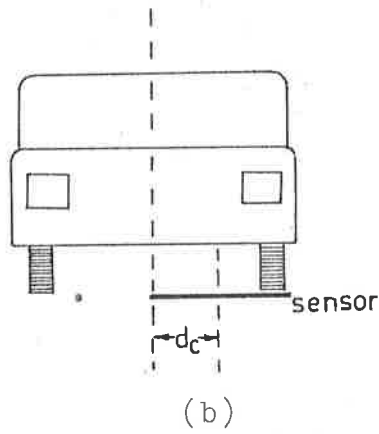
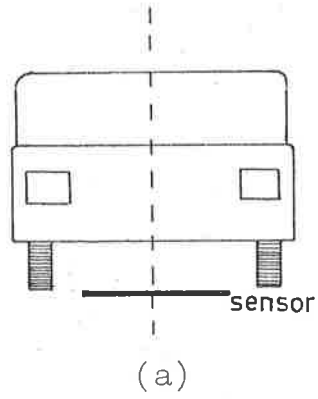
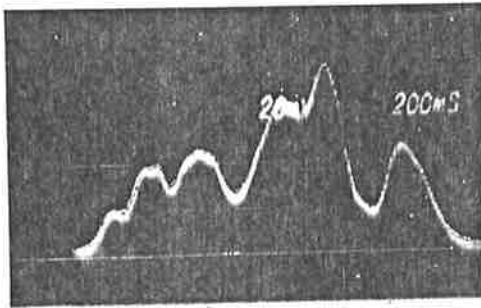


Fig. IV.12 Lateral Displacement of Vehicle in Relation to the Sensor

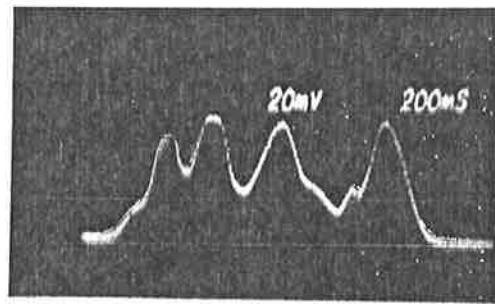
(a) Centre Position

(b) Left Displacement

(c) Right Displacement



(a)

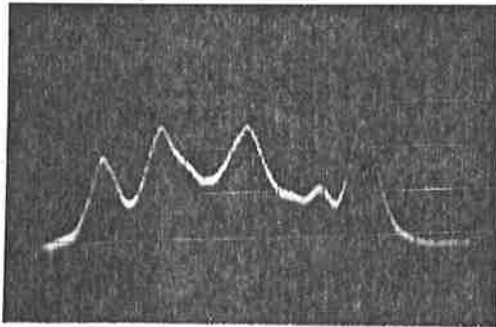


(b)

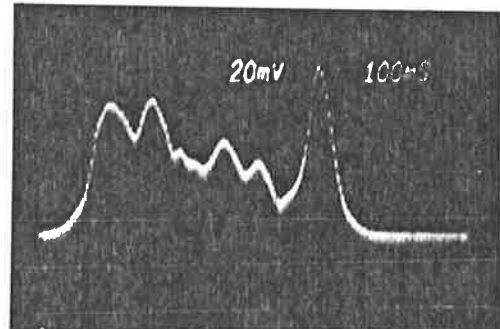
Fig. IV.13 Signature for 1972 Ford Futura

(a) Vehicle Left Displacement, dc = 60 cm

(b) Vehicle Right Displacement, dc = 60 cm



(a)

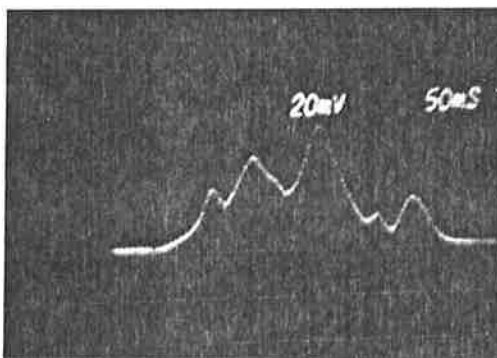


(b)

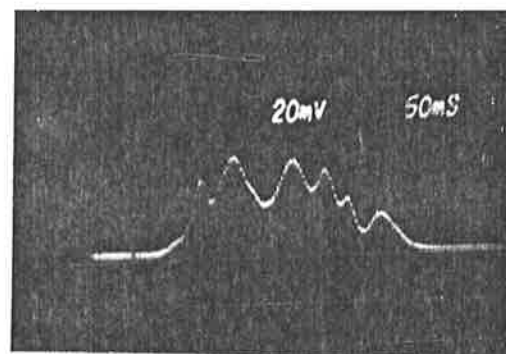
Fig. IV.14 Signature for 1976 Chrysler Centura

(a) Vehicle Left Displacement, dc = 60 cm

(b) Vehicle Right Displacement, dc = 60 cm



(a)



(b)

Fig. IV.15 Signature for 1969 Hillman Hunter

(a) Vehicle Left Displacement, dc = 60 cm

(b) Vehicle Right Displacement, dc = 60 cm

SUBROUTINE FOR DIFFERENTIATION OF DATA

```

FUNCTION DIF(L,M,NP,VARI,VARD)
C THIS FUNCTION SUBPROGRAM FINDS THE DERIVATIVE AT A GIVEN POINT
C L, FOR THE DESIRED X AND Y IN A GIVEN TABLE. THE N-POINT
C LAGRANGIAN FORMULA IS USED WHERE N IS ODD.
*
C L=INTEGER, THE POINT OF X AND Y AT WHICH DERIVATIVE IS FOUND
C M=INTEGER, 1-5, TO DETERMINE THE POINT FORMULA, N, N=2*M+1
C NP=INTEGER, THE NUMBER OF POINTS IN TABLE OF VARIABLES
C VARI=ARRAY OF INDEPENDENT, X, VARI(NP)
C VARD=ARRAY OF DEPENDENT, Y, VARD(NP)
*
DIMENSION VARI(NP), VARD(NP), X(11), Y(11)
*
DIF=01777000000000000000
IF(M,LT,1) RETURN
N=2*M+1
IF (M,GT,5,OR,N,GT,NP)RETURN
M1=M+1
M2=NP-M+1
K=L
IF(L,LE,M1,OR,N,EQ,NP)GO TO 30
K=M1
IF(L,LT,M2)GO TO 30
K=L-(NP-N)
30 MX=L-K
DO 50 J=1,N
MJ=MX+J
X(J)=VARI(MJ)
50 Y(J)=VARD(MJ)
A=1.
B=0.
C=0.
DO 70 J=1,N
IF (J,EQ,K) GO TO 70
F=1.
DO 60 I=1,N
IF(I,EQ,J)GO TO 60
F=P*(X(J)-X(I))
60 CONTINUE
T=X(K)-X(J)
B=B+Y(J)/(P*T)
A=A*T
C=C+1./T
70 CONTINUE
DIF=A*B+Y(K)*C
RETURN
END

```

PUBLICATIONS

- (1) K.Eshraghian and R.E. Bogner, "Traffic Vehicle Monitoring", IREECON . Convention Digest, pp 401-403, August 1977.
- (2) K.Eshraghian and R.E. Bogner, "A Novel Approach to Speed Monitoring and Identifiaction of Road Vehicles", ANZAAS REPORTER, August 1977.

PATENTS

- (1) "Improved Vehicle Detection System", Australian Patent App. No. PDO001.
- (2) "Vehicle Detection System", Australian Patent App. No. PDO008.

BIBLIOGRAPHY

1. H. Wolff, "Electronic Traffic Control: Can it make the Grade ?," *Electronics*, pp 157-161, April 1968.
2. L.A. Yardeni, "Vehicular Traffic Control: A Time - Space Design Model", *Proc. ITE*, pp 60-74, 1964.
3. D.C. Gazis and R.B. Potts, "Route Control at Critical Intersections", *Proc. ARRB*, Vol.3, part 1, pp 354-363 1966.
4. D.J. Buckley, L.G. Hackett, D.J.E. Keuneman and L.A. Beranek, "Optimum Timing for Co-ordinated Traffic Signals", *Proc. ARRB*, Vol. 3, part 1, pp 334-353, 1966.
5. A.D. May, "Experimentation with Manual and Automatic Ramp Control", *Highway Research Record*, No. 59, pp 9-25, 1964.
6. R. Brenner, E. Telford and D. Frisher, "A Quantitative Evaluation of Traffic in a Complex Freeway Network", *Highway Research Board Bulletin*, No. 291, pp 163-206, 1961.
7. A.D. May, "Experimentation with Manual and Automatic Ramp Control", *Highway Research Record*, No. 59, pp 9-38, 1964.
8. E.F. Grevais, "Optimization of Freeway Traffic by Ramp Control", *Highway Research Record*, No. 59, pp 104-118, 1964.
9. J.A. Hillier, "Area Traffic Control by Computer: Equipment in the Glasgow Experiment", *Traffic Eng. & Control*, Vol. 9, pp 496-498, 1968.
10. J.A. Hillier, "Glasgow's Experiment in Area Traffic Control" *Traffic Eng. & Control*, Vol. 7, pp 502-509, 1966.
11. D.I. Robertson, "Transyt method for Area Traffic Control", *Traffic Eng. & Control*, Vol. 11, pp 276-281.
12. W.D. Brooks, "Vehicular Traffic Control - Designing Traffic Progression Using a Digital Computer", *IBM - Data Processing Report*, Kingston, N.Y., 1965.
13. J.T. Morgan and J.D.C. Little, "Synchronizing Traffic Signals for Maximal Bandwidth", *Opns. Res.* Vol. 12, pp 896-912, 1964.
14. A.J. Miller, "Computer Control System for Traffic Network", *Proc. Soc. Internat. Symposium on the Theory of Road Traffic Flow*, J. Almond (Ed.), O.E.C.D., Paris 1965.

15. R. Herman and R. Rothery, "Driver Response to Speed Signs", Traffic Eng. & Control, Vol. 6, pp160, 1964.
16. — "Warning System Monitors Congestion on Autobahn", Electronic Design, Vol. 25, pp 150, April 12, 1977.
17. — "Master Controller with Microcomputer for Road Traffic", Ericsson Rev., No. 1, pp 51, 1976.
18. J. Smith, "Europe Maps Road-Safety Plan", Electronics, pp 82-83, July 22, 1976.
19. R.L. Pera and R.Nenzi, "Tana - An Operating Surveillance System for Highway Traffic Control", Proc. IEEE, Vol. 61, No. 5, pp 542-556, May 1973.
20. W.F. Arnold, "Computers Switch Traffic Signals", Electronics pp 75-76, Feb. 1, 1973.
21. K.W. Mackall, "The History and Development of Modern Traffic Control", Crouse Hinds Bull. 2561, Municipal Signal Engineer, 1940.
22. F.V. Webster, "Traffic Signal Settings", Dept. of Scientific and Industrial Research, Road Research Technical Paper No. 39, London, 1958.
23. T.R. Horton, "Traffic Control: Theory and Instrumentation", Plenum Press, N.Y., 1965.
24. T.M. Matnon, W.S. Smith and F.W. Hurd, "Traffic Engineering" McGraw-Hill, N.Y., 1955.
25. W.V. Braun and D.L. Walker, "Vehicular Location and Information Systems", IEEE Trans., Vol. VT-19, pp 136-143, 1970.
26. D.A. Rosen, F.J. Mammano and R. Favout, "An Electronic Route - Guidance System for Highway Vehicles", Trans. IEEE, Vol. VT-19, No. 1, pp 143-161, Feb. 1970.
27. A.A. Carter, J.W. Hess, E.A. Hodgjins and J. Raus, "Highway Traffic Surveillance and Control Research", Proc. IEEE, Vol. 56, pp 566-576, April 1968.
28. R.L. Gordon, K.W. Dodge and J.E. Scott, "Surveillance Aspects of a Computer Controlled Traffic System", Trans IEEE, Vol. VT-19, No. 1, Feb. 1970.

29. M.J. Lighthill and G.A. Whitham, "On Kinematic Waves II. A Theory of Traffic Flow on Long Crowded Roads", Proc. Roy. Soc., Ser. A., Vol. 229, pp 317-345, 1955.
30. F.A. Haight, "Mathematical Theories of Traffic Flow", Academic Prin., N.Y., 1963.
31. R.T. Underwood, "Some Aspects of the Theory of Traffic Flow", Aust. Road Research, No. 2, pp 35-47, June 1962.
32. J.S. Drake, J.L. Schafer and A.D. May, "A Statistical Analysis of Speed - Density Hypothesis", Highway Res. Board Rec., No. 154, pp 53 -87, 1976.
33. D. Bushnell, "A Merging Control System for the Urban Freeway", IEE Trans., Vol. VT-19, No. 1, pp 107-120 Feb.1970.
34. H.J. Payne, "Models of Freeway Traffic and Control - Mathematical Models of Public Systems", Simulation Council Proc., Vol. 1, No. 1, 1971.
35. R. Herman and R.W. Rothery, "Microscopic and Macroscopic Aspects of Single Lane Traffic Flow", J.Oper. Res. Soc. Japan, Vol. 5, pp 74-93, 1959.
36. D.C. Gazis and C.H. Knapp, "On-line Estimation of Traffic Densities from Time-series of Flow and Speed Data", Trans. Sc. Vol. 5, No. 3, pp 283-302, 1971.
37. B. Mikhalkin, "The Estimation of Roadway Behaviour Using Occupancy Detectors", Ph.D. Dissertation, Department of Industrial and Systems Engineering, University of Southern California, 1971.
38. N.E. Nahi, "Freeway - Traffic Data Processing", Proc.IEEE, Vol. 61, No. 5, pp 537-541, May 1973.
39. N.E. Nahi and A.N. Trevedi, "Recursive Estimation of Traffic Variables : Section Density and Average Speed", Trans. Sc. Vol. 7, No. 3, August 1973.
40. W.M. Brown and L.J. Porcello, "An Introduction to Synthetic Aperture Radar", IEEE Spectrum, pp 52-62, Sept. 1969.

41. A.S. Palastnick and H.R. Inhelders, "Automatic Vehicle Identification Systems - Methods of Approach", IEEE Trans., Vol. VT-19, pp 128-136, Feb. 1970.
42. Special Issue on Highway Electronic Systems, IEEE Trans. Vol. VT-19, Feb. 1970.
43. R.H. Murray, "Traffic Sensor Program", Prepared for the Bureau of Public Roads, Federal Highway Administration, Report No. U1-826602-F, Contract FH-11-6973, Feb. 1970.
44. S.G. Gustafsson and J.F. Marion, "LOCOM - A Vehicular Location and Communication System for Urban Fleets", Urban Technol. Conf., May 24-26, 1971, AIAA paper No. 71-513.
45. H. Staras and S. Honickman, "The Accuracy of Vehicle Location by Trilateration in a Dense Urban Environment", IEEE Trans., Vol. VT-21, pp 38-43, Feb. 1972.
46. J.N. Constant, "Microwave Automatic Vehicle Identification (MAVI) System", IEEE Trans., Vol. VT-23, No. 2, May 1974.
47. S.H. Roth, "History of Automatic Vehicle Monitoring (AVM)", IEEE Trans., Vol. VT-26, No. 1, pp 2-6, Feb. 1977.
48. - Special Issue on "Automatic Vehicle Monitoring", IEEE Trans., Vol. VT-26, No. 1, Feb. 1977.
49. - "Vehicle Identification System - Vetag", Philips Traffic Systems - TDS 2671-2500 E-8-73, 1975.
50. - "Traffic Sensor Program", prepared by the Bureau of Public Roads, Federal Highway Administration by Texas Instruments, Inc., Contract FH-11-6973, Appendix K, Aug. 1969.
51. J.L. Baker, "Radar, Acoustic and Magnetic Vehicle Detectors", Trans. IEEE, Vol. VT-19. pp 30-34, Feb. 1970.
52. "Manual on Uniform Traffic Control Devices for Streets and Highways", Washington D.C. Bureau of Public Roads, U.S. Dept. of Commerce, pp 3E-11-3E-15, 1961.
53. "CL8880 Series Radar Traffic Sensors", Philips Technical Infor. No. 021, Sept. 1976.
54. R.I. Gordon, K.W. Dodge and J.E. Scott, "Surveillance Aspects of a Computer-Controlled Traffic System", IEEE Trans., Vol. VT-19, pp 90-97, 1970.

55. F.P. Ziolkowski and C.K.H. Tsao, "Antennae Buried in a Roadway for Vehicular Traffic Communications", Trans. IEEE Vol. VT-20, No. 4, pp 104-114, Nov. 1971.
56. W.N. Huppert, "Familiarity with loop detectors will aid Application Installation", Traffic Engineering, Aug. 1965.
57. W. Schempers, "Loop Detectors", Traffic Engineering, Sept. 1966.
58. - "Design Consideration for Vehicle Detector Loops", Link Precision Systems, Inc., 1968.
59. L. Isaksen and H.J. Payne, "Freeway Traffic Surveillance and Control", Proc. IEEE, Vol. 61, No. 5, May 1973.
60. S. Ramo and J.R. Whinnery, "Fields and Waves in Communication Electronics", J.Wiley and Son, Inc., N.Y., pp 309-313, 1964.
61. J.A. Stratton, "Electromagnetic Theory", McGraw-Hill Book Company, Inc. New York, pp 264, 1941.
62. R. Plonsey and R.E. Collin, "Principles and Applications of Electromagnetic Fields", McGraw-Hill, New York, pp275, 1961.
63. R.L. Anderson, "Electromagnetic Loop Vehicle Detectors", IEEE Trans., Vol. VT-19, No. 1, pp 23-30, Feb. 1970.
64. V.K. Drebinger and P. Thilo, "Automatisches Unterscheiden Von Fahrgasten bei Verkehrszahlung", Siemens - Zeitschrift 44, 1970.
65. A.F. Malo, H.S. Mika and V.P. Walbridge, "Traffic Behaviour on an Urban Expressway", Highway Res. Board Bull., No. 235, pp 19-37, 1960.
66. G.V. Keller and F.C. Frischkneet, "Electrical Method in Geophysical Prospearity", New York, N.Y. Pergamen, pp 294-295, 1966.
67. - "Magnetic Sensors", Texas Instruments Inc., Contract FH-11-6973, Appendix C (for Bureau of Public Roads - Federal Highway Administration - U.S.) pp C-6 C-14, 1969.

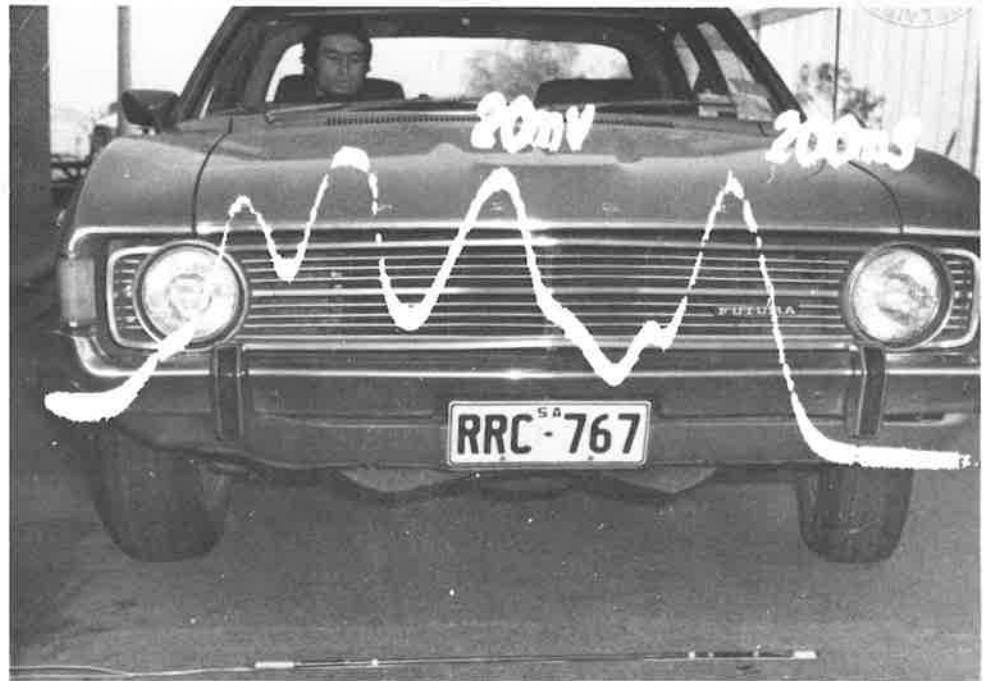
68. C.P. Bean, R.W. de Blois and L.B. Nesbitt, "Eddy-Current Method for Measuring the Resistivity of Metals", Journal of Applied Physics, Vol. 30, No.12, Dec. 1959.
69. J.D. Kraus, "Antennae", New York, McGraw-Hill, pp 303-318, 1950.
70. R.F. Harrington, "Introduction to Electromagnetic Engineering", McGraw-Hill N.Y., pp 123-135, 1958.
71. J. Aitchison, "Statistics II", Oliver and Boyd, Edinburgh, 1971.
72. D.L. Wardelich and C.J. Renken, "The Impedance of a Coil Near a Conductor", Proc. National Electronics Conference, Vol. 12, pp 188-196, 1956.
73. R. Moser, "Low Frequency Shielding of a Circular Loop Electromagnetic Field Source", IEEE Trans., Vol. EMC-9, No. 1, pp 6-18, March 1976.
74. - "Signetics - Digital, Linear and MOS Applications", Signetics, 1974.
75. - "Linear Applications", National Semiconductors, 1973.
76. - "2650 DEMO System", App. Memo SP51, Signetics, 1976.
77. - "2650 Microprocessor Manual", Signetics, 1975.
78. - "The ABC1500 Adaptable Board Computer", App. Memo SP55, Signetics, 1976.
79. R. Malotause, "A Very Simple Interface to Connect an Audio Cassette Tape Recorder to a Serial Binary Data Line", Philips CAB, Lab. Report No. EDP 7705, March 1977.
80. J.M. Bakker, "General Protocol for Data - Exchange between A 2650 Microcomputer and Peripheral Devices", Philips CAB, Lab. Report No. EDP 7604, Sept. 1976.
81. H. Schutte, "Dynamic Memory Interface with the 2650 Microprocessor", Elcoma, Internal Report PRR22-25-493, April 1976.
82. S. Kelly, "Low Cost Data-acquisition Systems", Electronic Design, No.24, pp 152-157, Nov. 1976.

83. - "Advanced Interfacing, A-D Converters", Microprocessor Course, Dept. Elec. Eng., University of Adeliade, 1977.
84. - "2650 PC2000 4K Memory Card", Signetics, 1976.
85. G.P. Banky and A.E. Ferguson, "A Direct Reading Digital Instrument for the Measurement of Speed of Road Vehicles", Dept. Elec. Eng., University of Melbourne, Report No. 3, ISBN 085867 0070, 1971.
86. K. Eshraghian, "Digital Speedometer Aided by Electronic Accelerometer Circuitry", Proc. IREE, pp 268-272, Sept. 1974.
87. K. Eshraghian and R.E. Bogner, "Vehicle Detection System", Australian Patent App. No. PDO008, 1976.
88. K. Eshraghian and R.E. Bogner, "Improved Vehicle Detection System", Australian Patent App. No. PDO0001, 1976.
89. J.A. Stratton, "Electromagnetic Theory", McGraw-Hill Co. Inc., N.Y. 1941

PHILIPS

09LNS
E75
C.2.

24.8.78

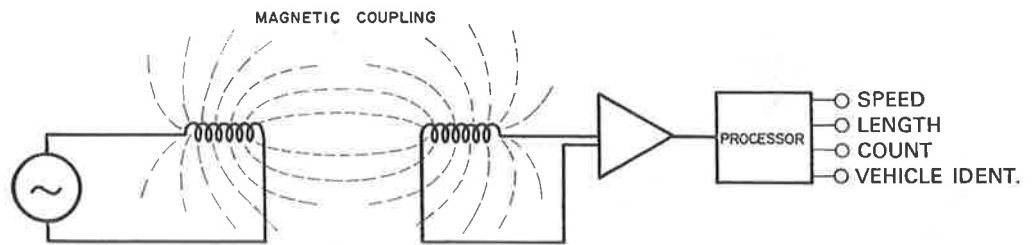


1 VEHICLE SENSOR THAT CAN MEASURE
**SPEED
LENGTH
COUNT & PRESENCE**

It can even identify some types of vehicle crossing it. This has not previously been possible with a single sensor.



Philips
Allied
Industries



APPLICATIONS

Traffic Light Control

Freeway Traffic Monitoring

Vehicle Monitoring on Airports

This device was developed jointly with the University of Adelaide, Department of Electrical Engineering.

For further information contact

Phillips Allied Industries

Box 1. P.O.

Alberton

South Australia 5014

Phone (08) 45 0211

Telex 82230

PHILIPS



PSF1 Traffic Controller Technical Notes

Controller Module Assembly.

The controller, which is completely self-contained, incorporates an 8 bit micro-processor, non-volatile solid state memory, input and output isolation, system monitoring and clock. Solid state circuitry is used throughout, assembled on plug-in cards which mount in an international standard frame.

All outside information required by the processor is presented to the input ports via optical isolators. As well as lantern power switching, the output ports drive 22 control panel light emitting diodes (LED's) which continuously display the operation of the programme. A combination of 8 LED's and an 8 position row selector switch provides a display of 64 bits making a total software information display of 78 bits. An additional 40 LED's continuously monitor the hardware.

Additional hardware is used to monitor correct operation of the system power supplies and time out the main programme. A mains derived clock provides the controller timing.

The processor memory, which has a maximum capacity of 16K/8 words, is made up of a non-volatile Read Only Memory for both the main programme and the intersection strategy. If necessary, the information may be erased by exposure to high level ultra-violet radiation and fresh data permanently implanted. A Random Access Read/Write Memory is provided for all variable data such as timers and stored demands. Up to 92 four bit plug switches set the various time periods and are read by the processor as memory.

The main loop and facility monitors are interrupted every 50 m.sec. by the RTC programme. A full interrupt with "save and restore" technique is utilised and a library of 40 sub-routines is provided. The total slave controller programme occupies 2.5K/8 words and the traffic actuated programme up to 4.5K/8 words.

The programme start-up is fully automatic and the reading of 5 RAM locations ensures an unambiguous start.

Safety Features.

A watchdog timer is used to ensure that key parts of the programme are being executed at a satisfactory rate. A second check detects any accidentally attempted colour change from green to red. These safety features are further enhanced by the complete reassessment of the state of the intersection 4 times per second.

The final level of protection is provided by hard wired conflicting green lock-out.

Intersection Description or Traffic Strategy.

Provision is made in the software for the traffic engineer to present a detailed description of the intersection to the controller without programming knowledge. This description determines the manner in which the following facilities are utilised:

- 4 phases (extendable to 7 by specifying time switch sharing).
- 12 3 colour vehicle aspect groups.
- 4 pedestrian movements.
- 16 detector inputs.
- 12 presence timers.

A general table establishes the common colour sequences, special conditions, indexable special conditions and sequence timers.

Phasing details are described with respect to the total vehicle aspects used, total phases used, aspects nominated as special movements, prohibited phase sequences and time switch sharing.

Pedestrian movements can be described in respect of phases in which they may be introduced, phases in conflict with pedestrian movements, pedestrian introduction/reintroduction requirements, automatic

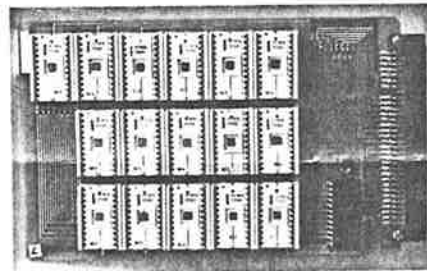
introduction requirements, terminations and flags for pedestrian overlap.

In the case of traffic actuated strategy, the following instructions may be added to the intersection description:

- Correlation of detectors associated with presence timers, phases, aspects and use of variable initial green.
- Specification of conditional detector functions.
- Maximum length of detection signal.
- Headway time range of 100 m.sec. or 200 m.sec.
- Identification of phases with maximum reversion feature.
- Use of maximum variable initial green in the event of maximum reversion.
- Linking instructions.

Each aspect may have a table defining 4 special conditions from an assortment of 80. If all stated conditions are fulfilled, the aspect colour is controlled by the sequence timer and the 4 colour sequences stated in the table.

Provision is also made to define pedestrian movement overlaps between phases when required.



Semiconductor Memory Card - This card, which is illustrative of the size of all logic cards within the controller, measures 111 mm x 178 mm and carries the 4,000 word instruction program necessary for control of all intersections. Each of the 16 semiconductor "chips" carries 2048 bits of information permanently implanted by voltage charge.

Philips Traffic Controller Type PSF1

a joint development project with the
Department of Motor Transport N.S.W.

24-8 78
OGENS
ETS
29



Philips Universal Traffic Controller Type PSF1

The PSF1 Traffic Controller is the result of an eighteen months R. & D. project undertaken for the N.S.W. Department of Motor Transport to develop a universal controller capable of fulfilling the exacting requirements of the Department.

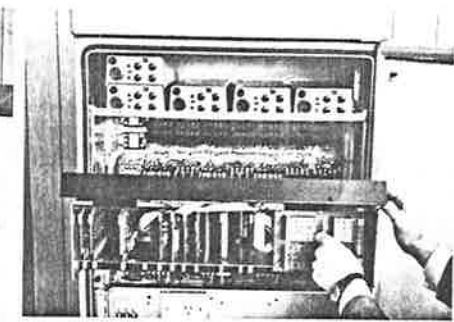
The operational logic, consisting of an 8 bit micro-processor, carries out all logical functions, relates detector inputs and signal lantern outputs including all signal timing, phase demand storage, monitoring and fail-safe override. The instruction description is introduced to the operational logic from look-up tables stored in non-volatile semiconductor memory and the traffic engineering parameters stored in binary coded switches.

Until now, traffic engineering strategies have been limited by the capabilities of the intersection controller. By designing a micro-computer and adapting it to traffic control, the Philips Systems Engineering Centre has removed these limitations, thus making it possible to provide traffic strategies

better suited to the needs of both the motorist and the pedestrian.

A moulded fibreglass housing of reduced size and with single door access allows the controller to be mounted against the building alignment, thus reducing street obstruction.

This new controller, whilst comparable in manufacturing costs with existing types of equipment, promises substantial savings in installation and maintenance cost.



Above Left - After removing the input/output plugs from the rear of the assembly, the complete controller may be removed by simply lifting away from the pivot slots. The field removal operation can be completed in less than one (1) minute.



Above Right - With the control module in the third (90°) position, the front panel may be hinged upwards for access to the plug-in electronic circuit cards. The equipment may be fully operational whilst in this position.

Left - The grey fibreglass cabinet measuring 130 cm x 70 cm x 40 cm is designed to provide a slim, low profile appearance when installed at an intersection. The single door access allows the equipment to be installed at the building or fence alignment, thus improving the kerbside view. The cabinet door is fitted with two locks so that only authorised personnel may have access to the equipment.

PHILIPS

Controller PSF-1

Vehicle Detectors

L1- 1, L1+ 2, L2- 3, L2+ 4, L3- 5, L3+ 6, Z- 7, Z+ 8

1, 2, 3, 4, 5, 6, 7, 8, 9, 10, 11, 12, 13, 14, 15, 16

Supply Monitors: +5V(A), +5V(B), +5V(C), +5V(D), +5V(E), -5V

Systems Status: Normal, Fail, Start Up, Power Fail

Running Phase: A, B, C, D, E, F

Vehicle Detectors: 1-16

Alarm Cancel, Pedestrian Detectors, Six Link, Antenna

	Late Start	Min Green	Var Initial Green	Rest	Early cut-off Green	Early cut-off Amber	Amber	All Red	
A Next	B Next	C Next	D Next	A Dem	B Dem	C Dem	D Dem		
Sp. Mov 1	P. Dem 1	Amber 1	Delay 1	Walk 1	1st Clear 1	2nd Clear 1	T/O 1		
Sp. Mov 2	P. Dem 2	Amber 2	Delay 2	Walk 2	1st Clear 2	2nd Clear 2	T/O 2		
Sp. Mov 3	P. Dem 3	Amber 3	Delay 3	Walk 3	1st Clear 3	2nd Clear 3	T/O 3		
Sp. Mov 4	P. Dem 4	Amber 4	Delay 4	Walk 4	1st Clear 4	2nd Clear 4	T/O 4		
Gap 1	H/Way 1	Waste 1	Gap 2	H/Way 2	Waste 2	Max	M.T. X/ter		
Pres 1	Pres 2	Pres 3	Pres 4	Pres 5	Pres 6	Pres 7	Pres 8		
RPT Pulse	Link GRN	VP Offset	VP Stor	VP Intro	VP Walk	Arrow	BST Exp		

	Late Start	Min Green	ECO Green	Amber	All Red	Interm	Max Var. Gr.		Walk	Clear 1	Clear 2	Red Arrow	Start Walk
A	2	3	6	6	1			1	3	6	3		5
B	3	5	3	0	1			2	6	3	3		
C	4	2	0	0	2			3	5	5	3		
D	0	3	0	0	1			4	6	1	3		
	X1.0	X1.5	X1.8	X1.0	X1.0	X0.2	X0.0		X1.0	X1.0	X1.0	X1.0	X1.0
	X0.5	X0.5	X0.5	X0.5	X0.5	X0.0	X1.0		X0.5	X0.5	X0.5		X2.0
A													
B													
C													0
D													12
	Gap 1	Gap 2	H/W 1	H/W 2	Waste 1	Waste 2	Max		Pres 1-4	Pres 5-8	Pres 9-12		Off Set

The output ports of the micro-processor drive 22 control panel LED indicators displaying 78 software parameters such as phase sequence steps, the current phase, next phase, phase demands and programme timer state. Additionally, 40 LED's provide continuous monitoring of the hardware including power supply. Ninety-two 4 bit time switch plugs are provided on the right hand side of the panel to set-up the intersection strategy.